Impact of Ventilation on Ammonia and Odour Emissions from Pig Housing

Raphael Kubeba Tabase

Thesis submitted in partial fulfilment of the requirements for the degree of Doctor in Bioscience Engineering

May 2020

“True friends challenge us and help us to be faithful on our journey”

Pope Benedict XVI

Members of the Examination Board:

Prof. dr. ir. Wim Soetaert, UGent, Chairman

Prof. dr. ir. Stefaan De Smet, UGent, Secretary

Prof. dr. ir. Jan Pieters, UGent

Prof. dr. ir. Tomas Norton, KU Leuven

Dr. ir. Andre Aarnink, Wageningen University & Research

Prof. dr. ir. Guoqiang Zhang, Aarhus University

Promotors:

Prof. dr. ir. Bart Sonck, UGent & ILVO

Prof. dr. ir. Michel De Paepe, UGent

Dr. ir. Peter Demeyer, ILVO

Dean: Prof. dr. ir. Marc Van Meirvenne

Rector: Prof. dr. ir. Rik Van de Walle

Dutch translation of the title:

Impact van ventilatie op ammoniak en geuremissies uit varkensstallen

This research was funded by the Flanders Innovation & Entrepreneurship (VLAIO LA).

Tabase, R. K. (2020). Impact of ventilation on ammonia and odour emissions from pig housing. PhD Thesis. Ghent University, Belgium

ISBN number: 9789463573108

Summary

Pig farming in Flanders is an important economic sector. However, intensive pig production generates NH_3, odour, greenhouse gases (GHG) and dust emissions which are harmful to the environment, public health and wellbeing. Currently, the Flemish government has the challenging task of adhering to the EU environmental regulations on emissions without hindering the economic growth in pig industry. This is because Best Available Techniques (BAT) for emission reduction are needed to enforce the EU emission regulations. However, many of the BATs in pig buildings are capital-intensive to develop, complicated to manage and can promote undesirable cross pollutant effects. In addition, reducing these pollutants through the approved low-NH_3 emission techniques with a reduction potential of more than 50% in Flanders, may still be insufficient to achieve the environmental targets, especially in regions near Natura 2000 sites. To effectively reduce emissions, also low-cost and easy to manage emission mitigation techniques need to be developed to complement the current high-performance BATs. Therefore, the aim of this PhD research was to investigate the potential of adapted ventilation strategies to complement the BATs and further reduce NH_3 and odour emissions from pig buildings in Flanders.

Field surveys show that pig farmers who are less familiar with the computerised climate controller often poorly tune the settings, resulting in unnecessary high ventilation rates (VR) which can increase NH_3 and odour emissions. In addition, it was previously demonstrated using computer simulations that optimally tuning ventilation control settings (VCS) can reduce NH_3 and odour emissions without additional costs. Hypothesis is that air velocity, turbulence and temperature conditions at the emitting surfaces at pen floor and slurry pit level are closely linked to VR. For this reason, the focus of this PhD research was on VCSs as a potential emission reduction technique. Furthermore, since about two-thirds of newly constructed fattening pig buildings have underfloor air distribution (UFAD) systems, this PhD research aimed to gain a better understanding of their NH_3 and odour transport behaviour at different VCSs. Challenging aspect of this type of pig building is the risk of pit air displacement leading to increased emissions.

To achieve these research objectives, a novel research approach was developed, thereby integrating both mathematical and physical modelling with field measurements. This research approach was chosen because of the synergy

advantages from the modelling and field measurement methods. The modelling methodologies included the development of a steady-state indoor climate simulation model (chapter 2), an experimental test platform (chapter 3) and a Computational Fluid Dynamics (CFD) model (chapter 6). The applied research methodology through experiments in chapters 4, 5 and 7, enabled this PhD research to gain detailed knowledge about the pollutants transport behaviour from the emitting source in the pig building and assessed emission reduction potential of the ventilation control settings/design techniques.

In chapter 4, measurements were performed in the test platform aimed at confirming the impact of 3 ventilation set-points (T_{set} = 21, 23 & 25 °C) selected from the steady-state indoor climate simulation model. Experiments were carried out in the pig fattening facility at the “pig campus” of ILVO-UGent-HoGent. Therefore two pig compartments were equipped with artificial pigs and a spray system for urea. The artificial pigs simulated heat production and the pig urination was mimicked by spraying urea solution instead of pig urine on the fully slatted pen floors. In chapter 5, field measurements were carried out with real pigs at the ILVO-UGent-HoGent “pig campus” as an additional test to confirm the findings on the NH_3 emissions from the test platform and to check for the impact on pig performance. The field measurement compared NH_3, odour and GHG (CO_2, CH_4, and N_2O) emissions, including pig performance during three fattening rounds between the reference and three other VCSs (T1, T2 and T3). The T_{set} in T1 was +2 °C higher than the reference strategy (CON). In T2, the minimum (VR_{min}) and maximum (VR_{max}) ventilation settings were 75% and 90% of the CON, respectively. For T3, the T_{set} was + 1 °C higher than the CON, while the VR_{min} and VR_{max} settings were initially set at 25% and 80% of the CON and gradually increased during the fattening round.

To better understand the NH_3 transport behaviour from the slurry pit in the pig building with UFAD system, a validated CFD model was developed (chapter 6) with an advanced NH_3 emission model capable of simulating NH_3 generation in the slurry pit and pen floor. Later, CFD simulations were performed in chapter 7 at different inlet and exhaust configurations and varying VRs and inlet air temperatures.

Results in chapters 4 and 5 showed the potential for reducing NH_3 and odour emissions through the VCSs. However, both investigations identified ground channel temperature (T_{GC}) as a key factor affecting NH_3 emissions in the pig buildings with UFAD system. For instance, in the test platform measurements, the increase in the T_{set} by +2 °C compared to the reference temperature of 23 °C, decreased the hourly average NH_3 emission by 29 - 43% at T_{GC} below 18 °C due to the relative reduction in VR. However, at T_{GC} above 18 °C, the NH_3 emission did not differ between T_{set} (23 °C) and T_{set} (25 °C). The field measurement results in chapter 5 imply T1 as the best VCS, as T1 significantly lowered the odour emission compared to the CON by 34%. Despite the significant decrease in VR, the overall hourly average NH_3 emissions did not differ between T1, T2, T3 and the CON. However, based on the Verification of Environmental Technologies for Agricultural Production (VERA) protocol approach, annual NH_3 emission factors were calculated and demonstrated the potential of T1 to decrease NH_3 emissions by 11% compared to the CON. The lack of the significant difference in the overall hourly average NH_3 emissions between T1, T2, T3 and the CON was in part due to the diurnal and seasonal variation in air exchange rate of the slurry pit caused by the effect of T_{GC} and the temperature difference between the room and T_{GC} (ΔT), which was observed in chapter 4. The findings indicate that, despite the importance of the VR on emissions, the effect of the indoor airflow pattern on the gaseous release from the slurry pit into the building is likewise crucial.

This PhD research evaluated the VERA test protocol's, case-control sampling strategy for calculating the average of NH_3 emission reduction over 1 year from T1, T2 and T3 compared to CON (chapter 5). Thereby 20 different VERA compliant sampling sequences of six 24-hour measurement days were selected. The results showed large variations in the calculated respective yearly average NH_3 emission reductions (T1: -23 to 8%; T2: -6 to 23%; T3: -6 to 14%). Based on all available measurement days, the NH_3 emission reduction was -11%, 0% and +2%, for respectively T1, T2, T3 compared to the CON. Therefore it was concluded that the VERA sampling strategy can result in unreliable estimations of the performance of NH_3 emission reduction technologies, especially since the technology studied in this PhD only concerned the ventilation control settings. Note that the case-control sampling strategy of the VERA protocol require that measurements are performed in at least two different farm locations. Therefore, ideally additional measurements should be taken at another farm location to improve the applicability of the results in this PhD work.

The CFD simulation results in chapter 7 confirmed the effect of the (ΔT) and the VR on the air exchange rate of slurry pit and the NH_3 emission in pig buildings with UFAD system. Reducing the slatted floor inlet porosity at the service alley (from 15% to 4% and 8%) and lowering the exhaust duct opening height (from 3.6 to 2.0 m) had minor effect on the NH_3 emissions and the air distribution at the animal occupied zone (AOZ).

At the service alley, covering half of the slatted floor inlet towards the pens, significantly increased the NH_3 emission from 0.57 to 15.34 g h^{-1}. This was due to the increase in slurry pit air exchange rate and the significant increase in the air velocity and turbulence intensity above the pit slurry surface, which increased the NH_3 mass transfer coefficient. Reducing the slatted floor inlet porosity at the service alley (from 15% to 4% and 8%) at inlet air temperature of 0 °C and VR of 14.0 m^3 h^{-1} pig^{-1} did not affect the CO_2 concentration between the pens in the compartment. However, lowering the exhaust duct opening height (from 3.6 to 2.0 m) at inlet air temperature of 0 °C and VR of 14.0 m^3 h^{-1} pig^{-1} decreased the CO_2 concentration at the AOZ and improved the air quality at the service alley.

In conclusion, the field measurements guaranteed acceptable pig performance for the tested ventilation set-points and generated potentially useful NH_3, odour and GHG emission data. Results showed also that strategies are required to reduce the slurry pit air exchange in pig buildings equipped with UFAD systems. It is recommended that additional tests should be performed at other farm locations especially in commercial pig houses to improve the wider applicability of the results in the present investigation. The developed TP compartments and the validated CFD model in this PhD research can be used as cost-effective modelling tools for a first evaluation of NH_3 emission mitigation techniques in buildings equipped with UFAD system. Thereby expensive animal experiments are not needed from the start.

Samenvatting

De varkenshouderij is een belangrijke economische sector in Vlaanderen. Intensieve varkensproductie geeft echter aanleiding tot emissies van NH_3, geur, broeikasgassen en fijn stof, welke schadelijk kunnen zijn voor de omgeving, de volksgezondheid en het algemeen welzijn. Het is ook de taak van de Vlaamse overheid om EU-richtlijnen in dit verband te implementeren, rekening houdend met de economische groeimogelijkheden voor de varkensindustrie. Daarom zijn ook Best Beschikbare Technieken (BBT) voorhanden om de Europese emissieregelgeving te kunnen afdwingen. Veel van deze BBT zijn echter kostelijk om te ontwikkelen, complex om te beheren en bevorderen soms ongewenst kruiseffecten op polluenten. Bovendien kunnen de emissiereducties die in Vlaanderen reeds gerealiseerd worden via de NH_3-emissiearme stalsystemen (met een reductiepotentieel vanaf ongeveer 50%), mogelijks nog onvoldoende zijn om bepaalde milieudoelstellingen te bereiken, vooral in regio's nabij de Natura 2000 zones. Daarom is er nood aan de ontwikkeling van goedkopere en gemakkelijk te beheersen emissiereductietechnieken die de reeds bestaande performante BBT kunnen aanvullen. Het doel van dit doctoraatsonderzoek is om na te gaan in hoeverre aangepaste ventilatiestrategieën in Vlaanderen een aanvulling kunnen zijn op de BBT's om de ammoniak-en geuremissie uit varkensstallen verder te verlagen.

Veldonderzoek toont aan dat varkenshouders die minder vertrouwd zijn met geautomatiseerde klimaatregelaars, dikwijls de controle-instellingen onvoldoende precies kunnen afstellen wat tot 'overventilatie' en meer NH_3- en geuremissies kan leiden. Eerder onderzoek met gebruik van computer simulaties, heeft daarenboven aangetoond dat het optimaal instellen van de ventilatiecontrole (VCS, Ventilation Control Settings), NH_3-en geuremissie kan verlagen zonder bijkomende kosten. Ventilatie is immers nauw gelinkt met belangrijke invloedparameters van emissieprocessen op de roostervloer en in de mestput (luchtsnelheid, turbulentie en temperatuur). De focus van dit doctoraatsonderzoek lag dan ook op VCS als emissiebeperkende techniek. In Vlaanderen heeft ongeveer twee derden van de nieuwbouwvarkensstallen kanaalventilatie (UFAD, Underfloor Air Distribution systemen). In varkensstallen met dergelijke systemen wordt het risico op NH_3-transport vanuit de mestput naar het gebouw vergroot, waardoor NH_3-emissies kunnen stijgen. Een bijkomende doelstelling van dit doctoraatsonderzoek is dan ook het verkrijgen van meer inzicht in het transportgedrag van NH_3 en geur bij verschillende

instellingen van de ventilatie-controle.

Om de onderzoeksdoelstellingen te kunnen bereiken, werd een vernieuwende aanpak ontwikkeld door mathematische en fysische modelleringstechnieken te combineren met praktijkmetingen. De ontwikkelde modeleringstechnieken behelsden een steady-state simulatiemodel voor het binnenklimaat (hoofdstuk 2), een experimenteel testplatform (hoofdstuk 3) en een CFD (Computational Fluid Dynamics) model (hoofdstuk 6). Deze onderzoeksbenadering werd gekozen omwille van de grote synergie die kan bereikt worden tussen modellering en praktijkmetingen. Het experimenteel luik binnen dit doctoraatsonderzoek (hoofdstukken 4, 5 en 7) liet toe om gedetailleerde kennis te vergaren over polluenttransport vanuit de emissiebronnen in de varkensstal en om het emissiereductiepotentieel te begroten van verschillende ventilatiestrategieën.

Hoofdstuk 4 beschrijft de metingen uitgevoerd in het testplatform om de impact te bevestigen van 3 ventilatie set-points (T_{set} = 21, 23 & 25 °C) die werden geselecteerd door simulaties met het binnenklimaatmodel. De experimenten werden uitgevoerd in de vleesvarkensstal op de “varkenscampus” van ILVO-UGent-HoGent. Er werden 2 varkenscompartimenten uitgerust met varkensmodellen en een ureumsproeisysteem. De kunstmatige varkens simuleerden de hitteproductie en het urineren van de varkens werd nagebootst door een ureumoplossing te sproeien op de volle roosters. In hoofdstuk 5 werden praktijkproeven uitgevoerd met echte varkens om de bevindingen van het testplatform te bevestigen en om de impact op de varkensprestaties te controleren. Gedurende drie mestrondes werden 3 alternatieve ventilatieregimes (T1, T2 en T3) getest ten opzichte van de referentie-instellingen (CON). Er werden continue emissiemetingen van NH_3, geur en broeikasgasen (CO_2, CH_4 en N_2O) uitgevoerd, samen met de opvolging van de varkensprestaties. De insteltemperatuur (T_{set}) van T1 was +2 °C hoger dan de CON. In T2 waren de minimum (V_{min}) en maximum (V_{max}) ventilatie-instellingen respectievelijk 75% en 90% van de CON. Voor T3 was de Tset +1 °C hoger dan de CON, terwijl de V_{min} en V_{max} settings initieel ingesteld waren op 25% en 80% van de CON en gradueel stegen gedurende de mestronde. Er werd een gevalideerd CFD-model ontwikkeld (hoofdstuk 6) om het NH_3-transport uit de mestput van het varkenscompartiment met UFAD-systeem beter te kunnen begrijpen. Dit model werd gekoppeld met een geavanceerd NH_3-emissiemodel dat in staat is om de NH_3-productie in de mestput en vanop de roostervloer te simuleren. Ook in hoofdstuk 7 zijn CFD-simulaties uitgevoerd voor verschillende inlaat- en uitlaatconfiguraties en bij variërende ventilatiedebieten en luchtinlaat- temperaturen.

De resultaten in hoofdstuk 4 en 5 tonen het potentieel van VCS om emissies van NH_3 en geur te reduceren. Beide onderzoeken identificeerden de luchttemperatuur in het grondkanaal (T_{GC}) als een bepalende factor voor de grootte van de NH_3-emissies in varkensstallen met UFAD- systeem. Experimenten met het testplatform bij een T_{GC} onder de 18°C, toonden bv. dat de verhoging van T_{set} +2°C in vergelijking met de referentietemperatuur van 23°C, leidde tot een afname met 29 - 43% van de gemiddelde NH_3 emissie per uur. Dit ten gevolgen van de relatieve afname in ventilatiedebiet (VR, ventilation rate). Nochtans wijzigde de NH_3 emissie niet tussen T_{set} (23 °C) en T_{set} (25 °C) bij T_{GC} boven de 18 °C. De meetresultaten in hoofdstuk 5 impliceren T1 als de beste VCS, aangezien deze de geuremissie deed dalen met 34% in vergelijking met de CON. Ondanks de significante daling in ventilatie, verschilden de gemiddelde NH_3-emissies per uur niet tussen de T1, T2, T3 en de CON. Berekeningen van de NH_3-emissiefactoren (kg N/year/animal place) op basis van het VERA-protocol (Verification of Environmental Technologies for Agricultural Production), tonen echter het potentieel aan van T1 om NH_3-emissies te doen afnemen met 11% in vergelijking met de CON. Het gebrek aan significant verschil tussen de gemiddelde NH_3 -emissies per uur van T1, T2, T3 en CON, was gedeeltelijk te wijten aan dagelijkse en seizoensgebonden variaties in de luchtuitwisselingsnelheid van de mestput. In hoofdstuk 4 werd geobserveerd dat deze variaties werden veroorzaakt door het effect van T_{GC} en het temperatuurverschil tussen de binnentemperatuur en T_{GC} (ΔT). Ondanks het belang van VR voor emissies, wijzen deze bevindingen erop dat het effect van het luchtstromingspatroon in de stal op gasemissies vanuit de mestput evenzeer cruciaal is.

Dit doctoraatsonderzoek heeft de case-control meetstrategie van het VERA-testprotocol geëvalueerd door de NH_3-emissiereducties van T1, T2 en T3 te berekenen ten opzichte van de CON via willekeurige selectie van 20 verschillende sets van zes 24-uren meetdagen die voldeden aan de criteria (hoofdstuk 5). Daarnaast werden de 20 sets ook gebruikt om de NH_3-emissiefactoren te berekenen voor elke behandeling en werden deze vergeleken met de jaargemiddelde NH_3-emissie op basis van alle beschikbare meetdagen. De resultaten toonden variaties in de jaarlijks gemiddelde NH_3-emissiereducties tussen T1, T2, T3 en de CON met respectievelijk 8% tot -23% (T1) , 23% tot -6% (T2) en 14% tot -6% (T3) op basis van de 20 sets. Vergeleken met de jaargemiddelde NH_3-emissie op basis van alle beschikbare meetdagen bedroeg het NH_3-emissieverschil tussen T1, T2, T3 en de CON respectievelijk -11%, 0% en +2%. Er kon worden besloten dat de VERA bemonsteringstrategie kan resulteren in onbetrouwbare schattingen van de efficiëntie van emissiereductietechnieken, dit vooral omdat de geteste techniek beperkt was tot verschillende ventilatie-instellingen. Er wordt opgemerkt dat de case-control setup van VERA voorschrijft om op minstens 2 locaties te meten. Daarom is het aangewezen om deze experimenten te herhalen op een andere locatie.

De resultaten van de CFD simulatie in hoofdstuk 7 bevestigen het eerder vermelde effect van ΔT en de VR op de luchtuitwisseling met de mestput en de NH_3-emissies in varkensstallen met UFAD systeem. Het verminderen van de porositeit van de luchtinlaat in de dienstgang (van 15% tot 4% of tot 8%) en het verlagen van de hoogte van de ventilatie-uitlaat (van 3.6m tot 2.0m), hadden een gering effect op de NH_3-emissies en de luchtverdeling ter hoogte van de dieren (AOZ, animal occupied zone). De NH_3 -emissies stegen daarentegen significant van 0.57 tot 15.34 g h^{-1} wanneer de helft van de luchtinlaat (roostervloer in de dienstgang) aan de hokzijde werd afgesloten. Dit was te wijten aan een verhoogde mestputventilatie en aan een significante verhoging van de luchtsnelheid en turbulentie-intensiteit boven het mestoppervlak in de mestput waardoor de NH_3-massatransfercoëfficiënt toenam. De CO_2-concentratieverdeling tussen de hokken werd niet beïnvloed door het verminderen van de inlaatporositeit (van 15% tot 4% en 8%) en bij een inlaat-luchttemperatuur van 0°C en een VR van 14.0 m^3 h^{-1} varken^{-1}. Dit in tegenstelling tot het verlagen van de ventilatie-uitlaatopening (van 3.6 naar 2.0m), wat leidde tot verminderde CO_2 concentraties in de AOZ en ook een betere luchtkwaliteit in de servicegang.

Tot besluit kan gesteld worden dat veldmetingen aanvaardbare varkensprestaties toonden voor de geteste ventilatiestrategieën en aanleiding gaven tot potentieel nuttige emissiedata voor NH_3, geur en broeikasgassen. De resultaten wezen ook op de nood aan maatregelen om luchtuitwisseling met de mestput te verminderen in varkensstallen die uitgerust zijn met UFAD-systemen. Voor een bredere toepasbaarheid van de resultaten is het aangewezen om bijkomende experimenten uit te voeren op andere locaties, en dan vooral bij praktijkbedrijven. De in dit doctoraatsonderzoek ontwikkelde TP-compartimenten en het gevalideerde CFD-model kunnen gebruikt worden als kosteffectieve modelleringsinstrumenten voor een eerste evaluatie van technieken voor NH_3-emissiereductie in stallen met UFAD-systeem. Hierdoor kunnen kostelijke dierenproeven in eerste instantie vermeden worden.

List of abbreviations

AOZ	animal occupied zone
CFD	computational fluid dynamics
CON	reference (Control)
C-R ratio	convective to radiation ratio
CUAC	central underground air channel
G:F	gain and feed ratio
GC	ground channel
GCI	grid convergence index
HBZ	human breathing zone
HS	headspace
LW	live weight (kg)
NUSE	no-urea spray experiment
RANS	Reynolds-Averaged Navier–Stokes
T	treatment
T_{ref}	reference ventilation control settings
TP	test platform
T_{Prof}	temperature profile
UDF	user defined function
UFAC	underfloor air channel
UFAD	underfloor air distribution
USE	urea spray experiment
VCS	ventilation control setting

$\left\|u_y\right\|$	absolute y-direction velocity at the slatted floor $(m\,s^{-1})$
A_{act}	animal activity
B_0	initial specific jet buoyancy flux (m^4 s^{-3})
EOA	effective opening area (m^2 pig^{-1})
F_s	safety factor
K_a	acid dissociation constant (dimensionless)
K_t	proportional constant of T_H (dimensionless)
M_0	initial specific jet momentum flux (m^4 s^{-2})
T_{AOZ}	temperature in the animal occupied zone (AOZ) (°C, K)
T_H	supply air throw height (m)
T_{in}	supply air temperature at the service alley (°C, K)

l_m	thermal length scale (m)
ΔP	pressure drop through porous zone (Pa)
A	area (m^2)
C	concentration (ppm; g m^{-3}; OU_E m^{-3})
C_p	specific heat capacity of air (J kg^{-1} K^{-1})
DFI	daily feed intake (kg d^{-1})
DG	daily gain (kg d^{-1})
ER	emission rate (g h^{-1}; g d^{-1} kg-LW^{-1}; kg pig^{-1} yr^{-1}; OU_E s^{-1} pig^{-1})
g	gravitational acceleration (m s^{-2})
m	mass (kg)
Q	heat loss (W)
RH	relative humidity (%)
T_{ex}	exhaust temperature (°C)
T_{GC}	ground channel temperature (°C)
T_i	room temperature (°C)
T_{out}	outside temperature (°C)
T_{set}	set-point temperature (°C)
U	U-value (W m^{-2} K^{-1})
V	volume (m^3)
VR_{max}	maximum ventilation requirement (m^3 h^{-1} pig^{-1})
VR_{min}	minimum ventilation requirement (m^3 h^{-1} pig^{-1})
V_{phase}	ventilation phase (day)
VR	ventilation rate (m^3 s^{-1}, m^3 h^{-1}, m^3 h^{-1} pig^{-1})
ΔT	temperature difference between T_{AOZ} , T_i and T_{in} (°C, K)
AER	air exchange rate (h^{-1})
D	viscous resistance coefficient (m^{-2})
F	initial resistance coefficient (m^{-1})
H	Henry's law constant (dimensionless)
f	fraction of the un-ionised total ammoniacal nitrogen (TAN concentration (dimensionless)
k_c	mass transfer coefficient $(m\ s^{-1})$
l	porous material thickness (m)
p	order of convergence
r	grid refinement ratio
u	velocity (m s^{-1})

Greek symbols

μ	air viscosity (N s m^{-2})
ρ	air density (kg m^{-3})
ε	relative error
ϕ	solution variable of interest
θ	Dimensionless temperature difference

Subscripts

comp	compartment
ex	exhaust
i	indoor
in	incoming
out	outside
pit	slurry pit
s	sensible heat
set	set-point
tot	total

Table of contents

Chapter 1: General introduction

1.1. Pig production in Flanders

Pig production is important for food security and nutrition in the world, as over one-third of the global meat consumed is pork (Alexandratos & Bruinsma, 2012). By 2050 the current level of pork consumption is projected to double due to the increase in the world population from 6.9 billion today to 9.2 billion by 2050 (Herrero et al., 2009; Kearney, 2010). Other reasons for the growing demand for pork are rapid urbanisation, rising incomes, and growing food and dietary preferences for meat products in developing countries (Herrero et al., 2009; Kearney, 2010; Alexandratos and Bruinsma, 2012).

In 2018, the total global pork production was 113,081,000 metric tonnes (carcass weight equivalent), out of which China (48%), the EU (21%) and USA (11%) produced 80% of the total pork all together (USDA, 2019). The EU's major pork producers are Germany (22.4%), Spain (19.0%), France (9.1%), Poland (8.7%), Denmark (6.6%), The Netherlands (6.4%), Italy (6.2%), and Belgium (4.5%), which together produced 83% of the total pork output (23,846,350 metric tonnes, carcass weight equivalent) in 2018 (Eurostat, 2019). Among the top eight pork producers, the relative share of pig production to total agricultural output in Denmark (29%) was highest, followed by Belgium (20%), Spain (14.7%) and Germany (14.5%) (Marquer et al., 2014).

Belgium as a leading exporter of pork in the EU, slaughtered 11,231,000 pigs in 2018 (Eurostat, 2019). In 2018, the total number of live pigs in Belgium was 6,209,130 with the Flemish region accounting for 94% of the total pigs and the remaining 6% in the Wallonia region (Platteau et al., 2018; Eurostat, 2019). The Flemish pig farms are especially concentrated in West-Flanders, which hosts 57% of the total pig population in Flanders. The number of pig farms in Flanders decreased by 38% in 2017 compared to 2007 (Platteau et al., 2018). Nonetheless, in 2017, the average number of pigs per farm increased by 36% compared to 2007. This was because the number of pigs in the larger farms increased more during the decade than in the smaller farms (Platteau et al., 2018).

1.2. Aerial emissions from pig buildings

Pig production via intensive animal housing enables farmers to maximise production efficiencies by controlling their management practices. However, intensively housed pigs generate pollutants such as NH_3, odour, greenhouse gases (GHGs), dust and surplus manure, which are detrimental to animals, the environment, public health and wellbeing. In Flanders, pig production contributes significantly to environmental pollution due to the higher concentration of pig farms than in other EU countries (Marquer et al., 2014). Only NH_3, odour and GHG emissions are discussed in this section of the thesis, in line with the focus of this PhD research. In addition, this section gives a detailed description of NH_3 emissions in the nitrogen chain of fattening pigs and the NH_3 release mechanism from pig manure. This is because there is extensive research and understanding on the NH_3 release mechanism from animal manure compared to the other pollutants (Arogo et al., 1999; Ni, 1999; Sommer et al., 2006).

1.2.1. Ammonia emission and influencing factors

Ammonia emissions from agriculture are associated with environmental degradation through acidification and eutrophication of ecosystems, as well as a precursor for atmospheric secondary particulate matter (PM) formation (Erisman and Schaap, 2004; Santonja et al., 2017). The main sources of NH_3 emission in pig production are from pig buildings, manure storage and during/after manure application to soil (Fig. 1.1). In 2014, the agricultural sector accounted for 94% of Flanders' total NH_3 emissions, with two-thirds of the emissions from intensive livestock production, primarily from animal housing and manure storage (MIRA, 2017). According to MIRA (2017), pig production alone accounted for more than 50% of the total livestock NH_3 emissions from housing and manure storage.

Ammonia is produced in pig manure following urea degradation and the rate of NH_3 formation is a function of the urease activity (Sommer et al., 2006). Urine is the main source of NH_3. Urine is primarily in the form of urea, which is easily converted to NH_4^+ by urease enzyme. Conversion of urea to NH_3 happens only after urine mixes with faeces, as the urease enzyme is not present in pure urine (Braam et al., 1997a). The contribution of faeces to NH_3 is small. This is because the excreted nitrogen in animal faeces is mainly proteins, which are less prone to rapid decomposition (Van der Peet-Schwering et al., 1999). Fig. 1.1 illustrates NH_3 emission in a nitrogen chain of a fattening pig. The figure shows that about 45% of the total nitrogen excretions from pigs can be emitted during manure storage and application, indicating significant loss of N-fertilizer.

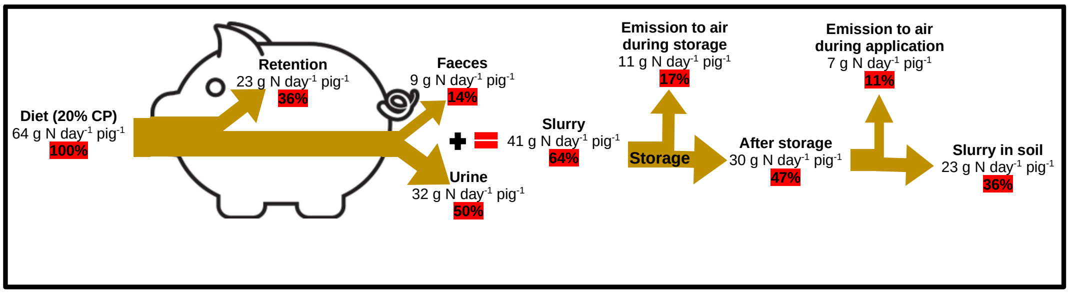

Fig. 1.1 — Emission of NH_3 in nitrogen chain of fattening pigs fed 20% crude protein (CP) diet (Portejoie et al., 2004).

Pig excretions (urine + faeces) on the pen floor and slurry in the pit are the two main sources of NH_3 emission in pig buildings. Although animal wallowing and excretion on the pen walls may also contribute to the total NH_3 emissions. Their contributions to the total NH_3 emissions are less significant compared to pen floor and the slurry pit (Aarnink et al., 1996). The contribution of the slurry pit to the total NH_3 emissions ranges from 30% up to 50% and the remaining emissions are from the pen floor. Additionally, the relative contribution of the pen floor or the slurry pit to the total NH_3 emissions in pig buildings depends on the type of ventilation system, the pen floor type, area of the floor wetted by pig excretion, manure management technique, weight of the pigs etc. (Hoeksma et al., 1992; Aarnink et al., 1997; Kai et al., 2006; Ni et al., 2000). Fig. 1.2 shows the NH_3 release mechanism from liquid slurry. Equation 1.1 provides the general description of the NH_3 volatilisation process from pig excretions to the ambient air (Olesen and Sommer, 1993).

$$ER'_{NH_3} = k_c([NH_3]_g - [NH_3]_a) \quad (1.1)$$

where ER'_{NH_3} is NH_3 volatilisation from the emitting surface (kg m^{-2} s^{-1}), k_c is the convective mass transfer coefficient of NH_3, $[NH_3]_g$ and $[NH_3]_a$ are NH_3 concentrations (kg m^{-3}) at emitting surface and ambient air, respectively.

Equation 1.1 and Fig. 1.2 basically suggest that NH_3 volatilisation is a function of k_c at the emitting surface. The k_c is often described in theoretical terms using either the "two-film" or "boundary layer" theory (Ni, 1999). The two-film theory is based on the assumption that at the interface between liquid and gas phases there are two static fluid layers/films. The films can be assumed to have a thickness and allow the diffusion of compounds from the liquid to gas phase and vice versa without interface resistance. Thus, the diffusion rate through the films controls k_c. The boundary layer theory assumes that airflow above the NH_3 emitting surface can generate a concentration boundary layer, and that the boundary layer thickness determines the convective mass transfer rate (Ni, 1999). The k_c of NH_3 can be derived from either the "two-film" or the "boundary layer" theory. In both cases, k_c closely relate to the air velocity above the emitting surface due to the influence of the airflow condition on the boundary layer thickness (Table 1.1). Table 1.1 illustrates the other variable that influence the NH_3 k_c. It is important to note that the influence of air velocity on k_c is limited by NH_3 generation rate, free NH_3 concentration and diffusivity of free NH_3 in pig manure/urine (Zhang et al., 1994). The above factors are influenced by urease activity, slurry pH, TAN concentration, temperature etc (Zhang et al., 1994; Braam et al., 1997a; Aarnink and Elzing, 1998; Arogo et al., 1999). It is for these reasons that slurry acidification, cooling, feed manipulation etc. are used as mitigation techniques to reduce NH_3 emission in pig houses (Petersen et al. 2016; Santonja et al., 2017; Vlaamse Landmaatschappij, 2019).

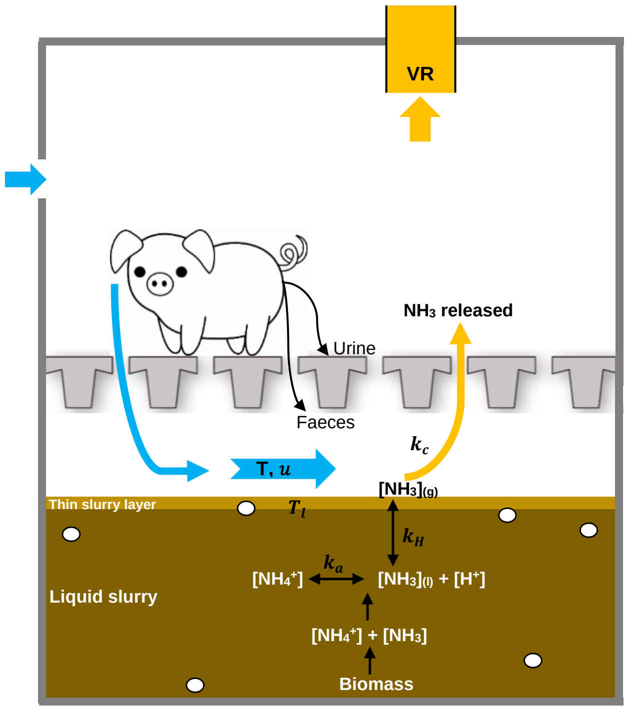

Fig. 1.2 — Ammonia release mechanism from liquid slurry in the pit (Ni, 1999).

Table. 1.1. Ammonia mass transfer coefficient equations from literature

Reference	Equation	Description
Bliss et al. (1995)[a]	$k_c = 3.488 \times 10^{-3} \times u^{0.5}$	Derived from theoretical analysis and experimental data of a wind tunnel study with NH_3 solution
Aarnink and Elzing (1998)	$k_c = 50.1 \times u^{0.8} \times T^{-1.4}$	Revision of the equation of the k_c from Haslam et al. (1924)[b] using experimental data
Arogo et al. (1999)[b]	$k_c = 3.7 \times D^{0.58} \times \mu^{0.33} \times u^{0.10} \times T_L^{0.97} \times L^{-0.90} \times \rho^{-0.33} \times T^{-0.97}$	Derived from wind tunnel study using pig slurry at T and T_L from 15 - 35 °C and u from 0.1 - 0.6 m s^{-1}
Ni (1999)[b]	$k_c = 4.78 \times 10^{-7} \times T_L^{0.8} \times VR^{0.7}$	Derived using field measurement data in a real pig house at T_L from 8 - 22 °C and VR from 200 - 5500 m^3 h^{-1}
Cortus et al. (2008)[a]	$k_c = 0.0821 \times D^{0.667} \times u^{0.5} \times T^{0.7} \times L^{-0.5}$	Developed using theoretical analysis
Ye et al. (2008b)[a]	$k_c = 3.4 \times 10^{-3} \times u^{0.33} \times Ti^{0.33} \times VR^{0.19}$	Derived from a scale model pig house with NH_3 solution at Ti from 5 - 20% and VR from 0.0014 - 0.0081 m^3 s^{-1}
Montes et al. (2009)[b]	$k_c = 1.62 \times 10^{-4} \times u^{0.8} \times T^{0.382} \times L^{-0.2}$	Developed from cow manure or NH_3 solution in a wind tunnel based on theoretical analysis
Saha et al. (2010)[a]	$k_c = 0.00126 \times u^{0.34} \times Ti^{0.21}$ or $0.00232 \times u^{0.33}$	Derived from a wind tunnel study with NH_3 solution at u and Ti from 0.1 - 0.4 m/s and 11 - 30%, respectively
Vaddella et al. (2013)[b]	$k_c = 4.85 \times 10^{-11} \times T_L^{9.7} \times u^{0.34} \times T^{-8.02} \times TS^{0.26}$	Derived from wind tunnel study with cow manure at T, T_L, u and TS from 15 - 35 °C, 5 - 35 °C, 0.5 - 4.0 m s^{-1} and 0.5 - 2.5%, respectively
De Paepe et al. (2015)[a]	$k_c = 0.0096 \times u^{0.96}$	Derived from wind tunnel study with NH_3 solution and full-scale slatted floor at u from 0 - 0.65 m s^{-1}
Ding et al (2020)[a]	$k_c = 1.707 \times 10^{-6} \times u^{0.337} \times VDP^{0.1471}$	Derived from a wind tunnel study using cow manure at u, T and RH ranged from 0.6 - 2.2 m s^{-1}, 15 - 35 °C and 20 - 60%, respectively.

Notations: k_c = mass transfer coefficient (m s^{-1}), u = air velocity (m s^{-1}), T = air temperature (°C), T_L = liquid/slurry temperature (°C), D = diffusivity of air (m^2 s^{-1}), μ = air viscosity (kg m^{-1} s^{-1}), ρ = air density (kg m^{-3}), VR = ventilation rate (m^3 s^{-1},[Ye et al. (2008b)] and m^3 h^{-1} [Ni (1999)]), L = characteristic length (m), Ti = turbulence intensity (%), TS = total solids content of manure (%), VDP = air vapour pressure deficit (Pa) is a function of the T and relative humidity (RH) at emitting surface. k_c derived using [a] boundary layer and [b] two-film theory.

The NH_3 concentration ($[NH_3]_g$) at the emitting surface is influenced by the dimensionless Henry's law (k_H, equation 1.2) and the dissociation (k_a, equation 1.3) constants. The Henry's law is a function of the emitting surface temperature, while the dissociation constant is influenced by manure pH, TAN concentration, temperature etc. (Ni, 1999). The ambient air NH_3 concentration ($[NH_3]_a$) in the pig building depends on ventilation rate, air exchange in the slurry pit, inlet NH_3 concentration and emission rate (Ni, 1999).

$$k_H = \frac{[NH_{3_l}]}{[NH_{3_g}]} \tag{1.2}$$

$$k_a = \frac{[NH_{3_l}][H^+]}{[NH_4^+]} \tag{1.3}$$

where NH_{3_l} is the ammonia concentration in the slurry/urine liquid film.

Slurry pit air exchange may also contribute to NH_3 emissions in livestock buildings (Braam et al., 1997a; Braam et al., 1997b; Zong et al., 2015). The type of airflow pattern in the buildings influences this phenomena (Zong et al., 2015, Botermans and Jeppsson, 2008). The driving factors for slurry pit air exchange are type of ventilation inlet, animal behaviour, season of the year, slatted floor design, temperature differences between the air inside the slurry pit and outside the building etc.(De Praetere and Van Der Biest, 1990; Braam et al., 1997a; Botermans and Jeppsson, 2008 ;Ye et al., 2009; Zong et al., 2015). In a cow barn, Braam et al. (1997b) observed that air exchange between the pit and the house was caused by cold incoming air that entered the slurry pit, which forced the emission of NH_3 formed in the pit. Highest NH_3 emissions were seen at positive indoor and outside temperature difference and sharply declined when the temperature difference was negative. Later, the NH_3 emission from the cow barn was reduced by 37% after covering the slurry pit. Thus, more research is needed to acquire knowledge about the effect of ventilation design and control settings on slurry pit exchange and its effect on NH_3 emissions.

1.2.2. Odour and greenhouse gas emissions

Odour emissions from pig production can cause nuisance and complaints. Odour decreases human wellbeing and cause disputes between farmers and neighbours (Wing et al., 2008; Juska, 2010). Consequently, the issue of odour nuisance has received high attention lately, particularly in regions with large pig farms and decreasing proximity between the pig farms and human dwellings (Wing et al., 2008; Juska, 2010). Odour from pig farms contain a complex mixture of compounds such as sulphur-containing compounds (e.g. hydrogen sulphide, methanethiol and dimethyl sulphide), nitrogen-containing compounds (e.g. NH_3 and methylamine), volatile fatty acids (e.g. acetic acid, propionic acid), indoles, and phenols (e.g. skatol) (O'Neil and Phillips, 1992; Mackie et al., 1998; Feilberg et al., 2010). Most of the odorants in pig buildings are produced during the digestion of proteinaceous feed in pig guts as wells as from decomposition of waste products such as faecal, urine, skin, hair, and spilled feed on the pen floors and the slurry pit (O'Neil and Phillips, 1991, Mackie et al., 1998).

The significance of GHG emissions from pig production is their long-term effect on global warming through greenhouse effect. GHG emissions associated with intensive pig farming are carbon dioxide (CO_2), methane (CH_4) and nitrous oxide (N_2O) (Van Ransbeeck et al., 2013; Philippe and Nicks, 2015). However, since plants use manure-generated CO_2 and exhaled CO_2 from livestock to produce animal feed during photosynthesis, the contribution of this CO_2 to the greenhouse gas effect is usually excluded (Philippe and Nicks, 2015). As a result, GHG emissions from pig production are mainly attributable to CH_4 and N_2O. In pig production, enteric fermentation from pigs produces CH_4, whereas manure management produces CH_4 and N_2O (Philippe and Nicks, 2015). The agricultural sector contributes approximately 10% of GHG emissions annually in Flanders (Platteau et al., 2018). In 2017, intensive livestock production was responsible for 18% of the total GHG emissions from the agricultural sector (Platteau et al., 2018). In the livestock sector, pig and poultry production all together produced 18% of the GHG emissions (Platteau et al., 2018).

1.2.3. Environmental regulations and emission reduction techniques

Increasing public concerns regarding the detrimental effects of emissions from intensive livestock production on air quality, public health and the environment continue to generate environmental legislations in the EU and Flanders. For example, the National Emission Ceiling (NEC) Directive of the EU sets and enforces emission reduction commitments for NO_x, non-methane volatile organic compounds, SO_2, NH_3 and PM2.5. The new NEC Directive (2016/2284/EU) which replaces the old Directive (2001/81/EC) came into force on 31 December 2016. The NEC Directive (2016/2284/EU) enforces the emission reduction obligations for 2020 under the 2012 Gothenburg Protocol and the Long-range Transboundary Air Pollution Convention for the EU Member States. Belgium reached the five pollutants' emission targets in 2017.

The Directive 2010/75/EU of the European Parliament and the Council on Industrial Emissions (Integrated Pollution Prevention and Control) is also aimed at reducing NH_3, odour and dust emissions from the pig and poultry industry (EC, 2017). The directive requires farmers to implement Best Available Techniques (BAT) if they have more than 2000 fattening pigs or 750 sows. This directive also apply to farmers seeking new licenses to increase their farm size. The BATs are low emission methods in pig buildings through efficient nutritional management, improved manure collection, storage and processing techniques. The latest Best Available Techniques Reference Document (BREF) for the Intensive Rearing of Poultry or Pigs (Santonja et al., 2017) includes detailed descriptions of the various BATs.

A ministerial decree to restrict NH_3 emissions from pig and poultry housing was adopted by the Flemish government in 2004. This decree involves introducing new officially approved low NH_3 emission pig housing systems. The list of these systems includes manure collection, storage and processing techniques that limit the area of contact/time of manure with the air in pig houses (Vlaamse Landmaatschappij, 2019). Low NH_3 emission techniques in pig housing include slatted floor/manure pit designs with reduced emitting surface area, frequent manure flushing, manure cooling, pig urine and faeces separation systems and manure drainage/storage in air-tight systems. New techniques can be added to the approved list if they can reduce NH_3 emissions by about 50% compared to traditional pig houses in Flanders. Vlaamse Landmaatschappij (2019) provides a list of licensed low-emission housing systems for fattening pigs.

To promote economic development in the livestock sector while implementing EU's general emission abatement regulations, the Flemish government recently introduced the Programmatic Approach to Nitrogen (PAN) (De Pue & Buysse, 2019). This programme restricts intensive livestock production in farms that emit NH_3 above a certain critical load near Natura 2000 habitats. The aim of the PAN is to create room for nitrogen deposition that could be used to permit livestock farming. In the PAN programme, if the deposition of nitrogen from a farm exceeds 50% of the specified critical load for a habitat, the production license is withdrawn. While farms whose nitrogen deposition is between 5% and 50% acquire conditional permits not to increase their NH_3 emissions (De Pue et al., 2017, De Pue & Buysse, 2019).

The Flemish odour policy is regulated by various environmental laws and decrees aimed at achieving an acceptable odour nuisance from livestock production (Hove, 2018). The acceptable odour nuisance level is between a given odour target and odour limit value. The odour target and limit values indicate the perceived level of discomfort from a group of respondents who are exposed to odour concentrations. The odour target value is lower than to the limit value. In Flanders, the above odour values are determined using odour dispersion models prior to issuing pig housing permits. Hove (2018) presented the comprehensive odour nuisance testing framework for livestock housing in Flanders. Hove (2018) also indicated actions to be taken by the farmer if the odour emissions exceed the target and limit values. Sections 1.5.1 and 5.2.3 describe odour concentration measurements from animal housing and the odour units.

In Belgium, the Kyoto Protocol of the United Nations Framework Convention on Climate Change regulates the emission of GHGs. Belgium achieved the GHG emission reduction target of 7.5% compared to the reference year (1990) level in the first commitment period (2008 – 2012). The second commitment period of the Kyoto Protocol runs from 2013 – 2020. Belgium commits a 20% GHG emission reduction target compared to the base year by 2020 although it is currently not legally binding.

1.3. Ventilation in pig buildings

1.3.1. Role and concept of ventilation

The main objective of ventilation inside pig buildings is to maintain an optimum microclimate around pigs to maximise the production of meat. This goal is accomplished by providing a microclimate within the thermoregulatory tolerance limits of pigs. The latter is also known as the thermo-neutral zone (TNZ), characterised by a temperature zone in which the minimum metabolic heat production from pigs equal the thermal demand from the environment around the pigs (Baxter, 1984). TNZ is a function of pig weight, stocking density, feed intake, type of floor etc.

The Lower Critical Temperature (LCT) is the lower limit of TNZ where pigs must increase their metabolic heat production to maintain their deep body temperature due to the high environmental thermal demands, as the environmental temperature declines. The Upper Critical Temperature (UCT) on the other hand is the upper limit of the TNZ where pigs try to lose heat to maintain their deep body temperature because of the rise in environmental temperature. At the UCT, heat loss by sensible means declines with a significant increase in the evaporative means of heat loss. Outside the TNZ, pigs adapt to either physiological or behavioural means to maintain their deep body temperature e.g. by increasing/decreasing feed intake, huddling, wallowing, divert feed energy for heat production rather than for growth etc. The LCT ranges between 20 - 25 °C for fattening pigs (Baxter, 1984). The exact temperature (UCT) at which fattening pigs begin to experience heat stress is not so clear. Huynh et al. (2005) reported that 60 kg pigs already show signs of heat stress at 22 °C, while Nienaber et al. (1997a; 1997b) and Brown-Brandl et al. (2004) noted that new genetic lines of pigs may be more vulnerable to heat stress than their older counterparts due to higher levels of lean tissue. Apart from maintaining optimum thermal microclimate around pigs, another role of ventilation is to provide acceptable indoor air quality by extracting aerial pollutants generated by pigs which are detrimental to the animals and farmers' health and welfare. Consequently, the type of ventilation design/performance can affect the health, welfare, behaviour, feed consumption, as well as pollutant emissions from pig buildings (Sällvik and Walberg, 1984; Scheepens et al., 1991a; Scheepens et al., 1991b; Aarnink et al., 2006; Nimmermark and Gustafsson, 2005; Aarnink et al., 2006; Ngwabie et al., 2011; Schauberger et al., 2013). Table 1.2 illustrates recommendations for maximum CO_2, NH_3, RH and air speed inside pig buildings.

Table. 1.2. Recommendations for maximum CO_2, NH_3, RH and air speed inside pig buildings.

Reference	NH_3 (ppm)	CO_2 (ppm)	Air speed (m s^{-1})	RH (%)
[1]	25 (LTEL);35 (STEL)	5000 (LTEL); 15000(STEL)		
[2]	7 (Humans); 11(Pigs)	1540 (Humans & Pigs)		
[3]	25 (LTEL); 25 (STEL)		0.15	40-80
[4]	20	3000		

Long Term Exposure Limit for humans over 8-hour period (LTEL)

Short Term Exposure Limit for humans over 15-minute period (STEL)

[1] HSE (2018); [2] Donham et al. (2002); [3] ASAE (1986); [4] CIGR (1984)

1.3.2. Common ventilation designs in Flanders

In Flanders, most pigs are housed indoors in mechanically ventilated buildings. In these buildings, the climate control computer automatically controls the ventilation rate to achieve the set-point temperature and acceptable indoor air quality. The set-point temperature often falls within the TNZ of pigs. Furthermore, the minimum and maximum ventilation requirement for the pig building is set-up in the climate control computer. The minimum ventilation is the airflow expected to maintain an acceptable indoor air quality during winter, while the maximum ventilation is expected to limit the rise in the air temperature inside the building to 3 °C more than the outside air temperature during summer (CIGR, 1984). The set-point temperature (T_{set}), minimum (VR_{min}) and maximum (VR_{min}) ventilation settings vary depending on the country and the ventilation air inlet type in the pig building. Table 1.3 shows the ventilation settings for fattening pig buildings in the Netherlands that was adopted in Flanders (Van Gansbeke et al., 2009). Table 1.4 also show seasonal variation in indoor temperature, exhaust NH_3 and CO_2 concentrations in mechanically ventilated fattening pig buildings in different countries with different air inlets. Jet, porous ceiling, door and underfloor air distribution (UFAD) designs are common types of ventilation air inlet in Flanders. Jet and porous ceiling air inlet designs operate by the principle of air mixing, while the door and underfloor air inlet designs operate by the principle of air displacement. Detailed description of the air inlet types are given below.

Table. 1.3. Ventilation settings at the climate controller for fattening pig buildings with UFAD and diffused ceiling inlet systems (Klimaatplatform varkenshouderij, 2008)

		UFAD		Porous ceiling air inlet[a]	
Day number	T_{set} (°C)	VR_{min} (m^3 h^{-1} pig^{-1})	VR_{max}(m^3 h^{-1} pig^{-1})	VR_{min} (m^3 h^{-1} pig^{-1})	VR_{max}(m^3 h^{-1} pig^{-1})
1 (at 23 Kg)	25	6	20	8	30
5	23	6	20	8	30
50	22	11	40	15	55
100	21	14	60	20	80

VR_{min} and VR_{max} are the minimum and maximum ventilation settings respectively

Table. 1.4. Overview of seasonal room temperature, exhaust NH_3 and CO_2 concentrations, VR and emissions in mechanically ventilated fattening pig buildings with different air inlets and pen floor types.

Country	Season	Inlet	Floor	T_{out} (°C)	VR (m^3 h^{-1} pig^{-1})	T_i (°C)	CO_2 (ppm)	NH_3 (ppm)	NH_3 (g h^{-1} pig^{-1})
Denmark [1]	Summer	DC	FS	14.3	83	20.3	800	2.1	0.121
	Winter	DC	FS	5.1	28	19.4	1542	4.3	0.092
	Summer	SW	FS	14.3	68	20.8	966	3.4	0.158
	Winter	SW	FS	5.1	24	19.4	1491	4.2	0.071
Belgium [2]	Winter	SW	FS		30		1846	18.1	0.431
	Summer	SW	PS	14.9	28	29.2	1944	15.5	0.292
	Summer	SW	FS		19		2024	16.7	0.228
	Summer	UFAD	FS		25	23.7	1769	21.9	0.444
Sweden [3]	Spring	DC & SC	PS	14.6	80	19.7	1050	4.5	0.180
	Autumn	DC & SC	PS	9.4	75	16.8	950	3.9	0.190
	Summer	DC & SC	PS	17.4	65	22.8	1140	5.4	0.200
USA [4]	Winter			5.5	23	19.7		10.8	0.196
	Spring			13.7	52	22.3		10.2	0.272
	Summer			22.3	69	26		3.0	0.093
	Autumn			9.1	17	19		5.2	0.051
Canada [5]	Summer	SC	PS	19.4	161	23.1	508	5.0	0.513
	Autumn	SC	PS	-1.6	25	18.8	1966	11.0	0.209
	Winter	SC	PS	-9.7	22	16.4	3647	27.0	0.450
	Summer	SC	FS	19.4	161	23	544	9.0	1.031
	Autumn	SC	FS	-1.6	36	17.9	2225	22.0	0.577
	Winter	SC	FS	-9.7	22	16.7	4030	32.0	0.503
Belgium [6]			FS	10.9	79	20.8			0.320
			FS	19.2	118	20.2			0.355
			FS	0.9	45	19.4			0.167
			FS	11.8	83	21.2			0.234
			FS	11.8	81	21.1			0.221

[1] Zong et al. (2015) [2] Van Ransbeeck et al. (2013) [3] Ngwabie et al. (2011) [4] Blunden et al. (2008) [5] Sun et al. (2010) [6] Philippe et al. (2007).DC [Diffused Ceiling]; SW [Sidewall]; UFAD [Underfloor Air Distribution]; SC [Slotted ceiling]. FS [Fully slatted]; PS [Partly slatted]; T_{out} [Outside temperature]; T_i [Room temperature]; VR [Ventilation rate]; ER [Emission rate]. Note that partial pit ventilation was applied in Zong et al. (2015). The buildings in Table 1.4 had different manure handling systems and measurements were taken at different pig weights other than the average weight during the entire fattening period.

1.3.2.1. Jet and porous ceiling air inlet designs

Jet air inlet designs supply the air via valves, slots or diffusers from either the ceiling or walls of the building (Fig. 1.3) at relatively high air velocities. The air jets formed at the inlet entrain the air in the building, mixing it before reaching the Animal occupied zone (AOZ). The air mixing reduces draught on the pigs (Albright, 1990). In jet air inlet designs, the inlet location and configuration determine the airflow pattern in the building with minimal effect of the outlet

(Randall, 1975). The outlet can therefore, be found at the roof, wall or the floor of the building (Wang and Zhang, 2005; Jeppsson and Botermans, 2014).

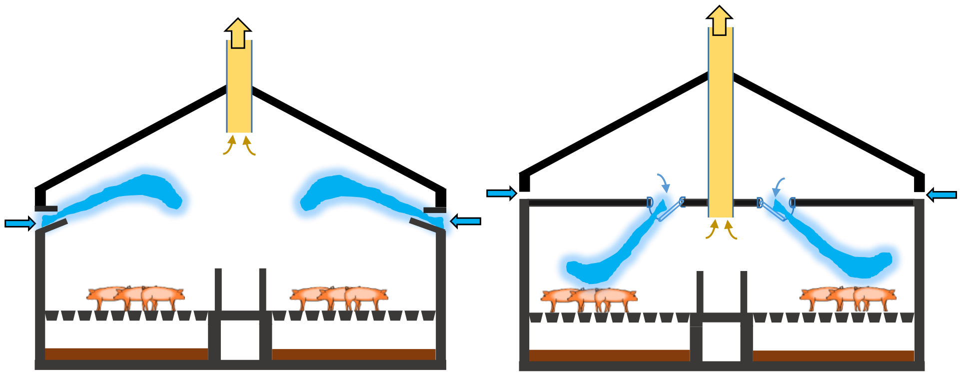

Fig. 1.3. — Pig building ventilation design with jet air inlet at the (a) wall and (b) ceiling.

Jet air inlet designs operate based on the negative pressure principle, driven by an exhaust fan and the inlet openings, which are normally equipped with baffles to control the inlet air jet to attain the suitable indoor air distribution (Albright, 1989). The inlet opening characteristics, the building dimensions, the inlet jet velocity as well as buoyancy force from the AOZ determines the air jet travel distance before the air mixing. The Archimedes number, which expresses the relative ratio of the buoyancy forces to the inertia forces acting on a fluid (Etheridge and Sandberg, 1996), determines the stability of the airflow pattern in jet inlet systems (Randall and Battams, 1979; Leonard and McQuitty, 1986; Albright, 1989). The Archimedes number is therefore, often used as the design criterion for the control of the airflow pattern in pig buildings equipped with jet air inlet systems (Zhang et al., 1996; Zhang and Strøm, 1999).

The airflow patterns in jet air inlet systems are rotational and normally do not achieve the desired uniform air distribution (Randall, 1975; Wang and Zhang, 2005). At lower ventilation rates in colder seasons, the incoming air drops immediately due to buoyancy effect from the pigs. Praetere & Van Der Biest (1990) observed two airflow patterns in a slotted air inlet pig building with a fully slatted pen floor. There was a primary flow above the slatted floor and a secondary flow pattern underneath the slatted floor. The airflow pattern affected the slurry temperature in the pit and promoted the backdraught of NH_3 to the animal occupied zone. Zong et al. (2014) observed a similar airflow pattern in a pig building with a wall jet air inlet, which resulted in higher indoor NH_3 concentration and emission than the building with the porous ceiling air inlet. The main advantage of jet air inlet ventilation design is that they are easy to construct compared to the UFAD systems. They however, have higher ventilation requirements than UFAD systems. In the comparative study of the air quality at the farmer's height between a ceiling air jet and UFAD system, the ventilation requirement in the pig building with the ceiling air jet design was 40% greater than the underfloor air inlet design (Jeppsson and Botermans, 2014).

Porous ceiling air inlet designs are known for the ability to eliminate draught in the AOZ. As a result, they are common in buildings with draught sensitive pigs such as piglets and weaners. The ventilation principle with this design is based on the negative pressure from the exhaust fan which forces the incoming air to pass through porous or perforated materials at the ceiling (Fig. 1.4). Because of the low porosity and high specific surface area of the porous material, the inlet air enters the pig building at air speeds below 0.05 m s^{-1} (Randall, 1975; Bjerg et al., 2011). Here, the buoyancy force in the AOZ or heat from another source controls the airflow pattern. Thus, the animal distribution in the pen can cause the airflow pattern in the building to be rotational and random (Randall, 1975; Kuczyński and Przybyła, 2002). Common porous ceiling materials applied in pig buildings are mineral wool, glass fibre, glass wool and perforated plastic plates. In porous ceiling buildings, the exhaust duct can be installed at the roof, sidewall or the floor (Aarnink and Wagemans, 1997; Bjerg et al., 2011). The main advantage is that greater promotion of the inlet air is mixed with the air inside the building, causing it to warm up before reaching the AOZ. This reduces draught on the pigs in colder seasons. Furthermore, supplying the inlet air at lower momentum from the ceiling to the floor reduces PM dispersion and promotes the settling of PM compared to UFAD systems (Tan and Zhang, 2004).

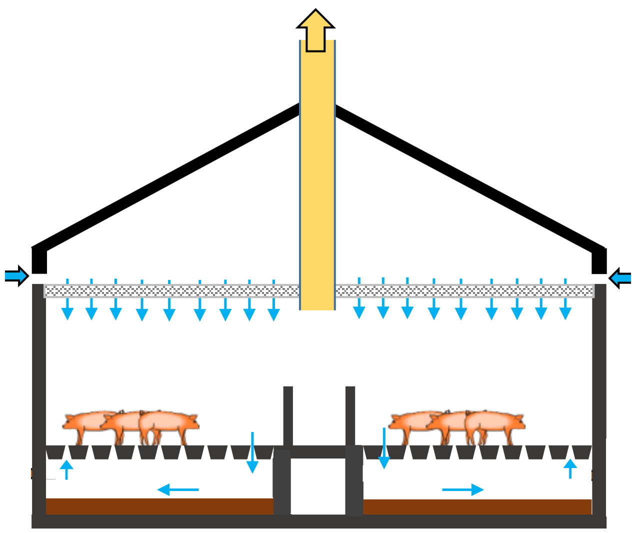

Fig. 1.4 — Cross-section view of a fattening pig building with a porous ceiling inlet.

However, the ventilation rates in pig buildings with porous ceiling inlet can be 35% higher than other air inlet designs. This is because of the high pressure drop of the inlet air through the porous ceiling material. As a result, energy consumption associated with ventilation can be 27% more than other air inlet designs (Kuczyński and Przybyła, 2002; Threm et al., 2012; Zong et al., 2014). Porous ceiling inlet systems also have inlet clogging problems due to dust. In addition, during winter, it is difficult to control and maintain the desired airflow pattern due to the lower momentum of the inlet air and the interference from the buoyant forces at the AOZ (Kuczyński and Przybyła, 2002). The thermal plumes from the pigs in the pen could also lower the contaminant removal effectiveness in porous ceiling air inlet buildings compared to pig buildings with UFAD systems due to the up draught of the air at the AOZ (Aarnink and Wagemans, 1997; Van Wagenberg et al., 2002). This could lead to higher concentrations of bio-aerosols, NH_3 and CO_2 contaminants in porous ceiling air inlet buildings and expose farmers to higher risks of respiratory diseases compared to the other inlet designs (Radon et al., 2001). In addition, during summer the ceiling attic can act as a solar collector and affect the inlet air temperature resulting in short-circuiting of the incoming air to the exhaust, especially at higher ventilation rate without removing the heat from the AOZ (Van Wagenberg et al., 2002).

1.3.2.2. Door and underfloor air distribution (UFAD) inlet designs

Door air inlet pig buildings are common in Flanders because their inlets are simple and cheaper to construct (Van Gansbeke et al., 2009). Furthermore, the long travel distance of the supply air at the service alley encourages preheating of the supply air during winter. Door air inlet buildings operate with the negative-pressure principle, using the solid floor at the service alley as the supply air channel. Pig buildings with door air inlets admit the supply air via a lower opening under the door of the building and extract the air in the ceiling (Van Wagenberg, 2005). In order to allow adequate air mixing at the service alley before entering the AOZ and to prevent the inlet air from flowing directly to the end of the service alley, the inlet air speed is often less than 2.0 m s^{-1}. For efficient ventilation performance, pig buildings with door air inlets have wider service alleys compared to other air inlet designs (Van Wagenberg, 2005; Van Gansbeke et al., 2009).

In a comparative study, Van Wagenberg (2005) reported that the airflow pattern in a pig building with door air inlet was by displacement and air mixing and that the ventilation effectiveness was higher in the pig building with the UFAD system than the door air inlet building. This was because of the non-homogeneous air distribution within pens and large temperature gradients between the pens due to single inlet location at the door that promoted cross pollutant contamination between pens. However, the low air resistance at the inlet can reduce the ventilation requirements in pig buildings with door air inlet by 25% compared to porous ceiling air inlet systems (Van Wagenberg, 2005; Van Gansbeke et al., 2009).

Pig buildings with UFAD system displace the warmer air in the animal area with the cool supply air from the lower level of the building (Fig. 1.5). The shorter travel distance of the supply air to the animal area therefore, enables pig buildings with UFAD systems to deliver better air quality and efficient cooling at the AOZ than jet and porous ceiling air inlet systems (Aarnink and Wagemans, 1997; Van Wagenberg and Smolders, 2002; Tong et al., 2019). In Flanders, about two-thirds of newly constructed fattening pig buildings have UFAD systems (DLV-Belgium, 2014). Pig buildings with UFAD systems are also used in The Netherlands (Aarnink and Wagemans, 1997; Van Wagenberg and Smolders, 2002), Sweden (Botermans and Jeppsson, 2008) and Germany (Threm et al., 2012; Adrion et al., 2013).

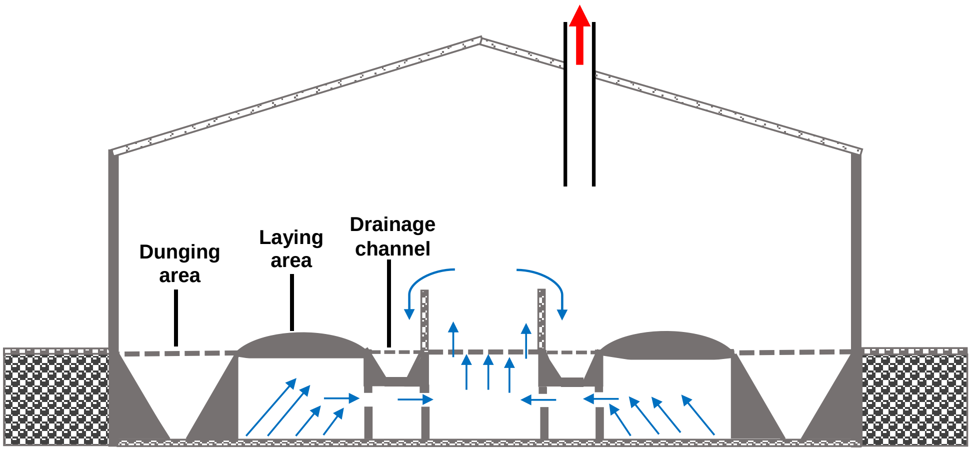

Fig. 1.5 — Cross-sectional view of a pig building with an underfloor air inlet

Pig buildings with UFAD systems use negative-pressure ventilation principle. In addition, the ventilation inlets are often located at the slatted floor of the service alley and the exhaust duct at the ceiling (Fig. 1.5). Due to the large inlet openings and the low resistance to the supply air at the inlet, the incoming air enters the pig building at very low air speeds, less than 1.0 m s^{-1}. The location of the inlet at the floor also makes it easy to incorporate earth to air heat exchangers in pig buildings with UFAD systems. Hence, it allows the incoming air to first pass through the underground air channel at about 2 m below ground level before being delivered into the building. Doing so, the concrete walls in the underground air channel cools the incoming air when the ambient air is warm (Deglin et al. 1999; Threm et al., 2012). The underground air channel also warms the incoming air when the ambient air is cold. Because of the underground cooling and low resistance of the air supply at the inlet, the ventilation requirements and ventilation electricity consumption in pig buildings with UFAD can be 40% and 36% lower than diffused ceiling and/or jet inlet designs, respectively (Van Gansbeke et al., 2009; Threm et al., 2012).

Nonetheless, pig buildings with UFAD systems are expensive to construct, compared to mixing ventilation systems (Threm et al., 2012). Additionally, there is the risk of draught on pigs during winter due to the displacement of air at the AOZ. This can influence pig performance and indirectly affect odour and NH_3 emissions as the pigs would prefer to dung close to the supply air inlet and lie in the opposite section of the pen (Sällvik and Walberg, 1984; Scheepens et al. 1991a; Scheepens et al. 1991b, Aarnink et al., 2006; Botermans and Jeppsson, 2008). Furthermore, there is the risk of NH_3 transport from the slurry pit into the building, thereby increasing NH_3 emissions (Botermans and Jeppsson, 2008). Therefore, the type ventilation inlet studied in this PhD research is the UFAD system because they are popular in Flanders, and they have problems with slurry pit air exchange.

1.4. Effect of ventilation settings/control on emissions from pig buildings

Many of the BATs (e.g. manure flushing, cooling, urine and faeces separation systems, air scrubbing etc.) in the BREF report and the list of Flanders approved low NH_3 emission systems, are capital-intensive to develop (section 1.2.3). In addition, some of these methods are expensive to implement and/or complex to manage while others have undesirable cross pollutant effects (Santonja et al., 2017). According to Vranken (1999) and Zhang et al. (2009), however, optimising the climate control settings in mechanically ventilated pig buildings could reduce ventilation rate and decrease NH_3 and odour emissions without extra costs, since the air velocity in the NH_3 mass transfer coefficient equations (Table 1.1) are linked to the ventilation rate (Kavolelis, 2003; De Paepe et al., 2015).

Vranken (1999) demonstrated in a dynamic mathematical model that fluctuations in indoor temperature and ventilation rate could be reduced through optimising the climate control settings in a fattening pig building by adapting the set-point temperature and the minimum/maximum ventilation settings by pig weight, and using a proportional bandwidth setting regulated by the outside temperature. Doing so, Vranken (1999) estimated 8% reduction in NH_3 emissions on yearly basis compared to the traditional settings in Flanders. Zhang et al. (2009) also stated using computer simulations that it was feasible to reduce 50% of odour emissions from a fattening pig building by gradually increasing the maximum ventilation settings based on pig weight compared to the traditional setting in Denmark. These investigations were however, not validated in a real pig house.

Häussermann et al. (2006) also demonstrated the potential of reducing ventilation rate in pig house by combining traditional ventilation control based on indoor air temperature with pig activity and CO_2 concentration as additional ventilation control parameters. They also explored automatic fogging and ventilation control in the pig building by combining traditional control parameters of indoor temperature and relative humidity with animal activity and CO_2 concentration. Compared to the temperature control strategy alone, their strategy resulted in a 20% reduction in ventilation rate through the CO_2 control strategy.

Zhang et al. (2008) also proposed that adjusting the inlet opening in pig buildings as a control strategy to maintain constant inlet air velocity and/or jet momentum could reduce NH_3 emissions. This is because the airflow at the inlet opening influences NH_3 emissions due to the effect on the airflow characteristics at pen floor and the slurry surface in the pit (Ye et al., 2008a; Ye et al., 2008b; Ye et al., 2009). Currently, the proposed strategy still requires validation in a real pig house since the test was only limited to reduced-scale modelling.

1.5. Assessment of emission levels in pig buildings

Designers of animal houses frequently use field measurements, full-scale, reduced-scale and mathematical modelling techniques to design and evaluate ventilation performance because of the following reasons. First, evaluating ventilation performance with respect to the thermal comfort of animals and indoor air quality can be very expensive and impractical under real conditions. Furthermore, existing and novel ventilation systems and emission reduction techniques require tools that can easily monitor and analyse their performance before being implemented in real animal houses. Similarly, there is a need for understanding adequately pollutant transport behaviour at the emitting source and to study the key factors influencing the emissions in detail.

1.5.1. Field measurements

Field measurements are the most popular method employed to assess ventilation performance and emission in livestock buildings, because they are performed under actual production conditions. Field studies typically measure ventilation rate, indoor temperature, relative humidity, gaseous concentration and emission rate (Van Ransbeeck et al., 2013; Ngwabie et al., 2011). However, explicit studies on the influence of specific factors on emissions are usually absent due to the lack of control of external climatic factors and the presence of animals (van Wagenberg and de Leeuw, 2003). Field studies are further noted as expensive, difficult to set-up, time consuming, lack repeatability and are liable to high experimental error compared to reduced scale and mathematical modelling. The lack of repeatability and the higher experimental error in field measurements are due to animal interference, husbandry management practices, measurement set-up and strategy, indoor climatic conditions, uncertainty in ventilation rate measurement, instrumental error etc. (Ni and Heber, 2001; Van Buggenhout et al., 2009; Rom and Zhang, 2010).

Nonetheless, because of the harmful effects of NH_3, GHG and odour emissions, concentrations of these pollutants are often measured in animal buildings in order to assess indoor air quality, to quantify the emission rate of the pollutants and to evaluate the performance of new low-emission techniques for policy makers. In addition, field measurements enables researchers to obtain detailed knowledge about the production processes of the pollutant in order to improve emission abatement techniques in livestock buildings.

There are a wide range of measuring devices for NH_3 and GHGs in livestock buildings. The choice of a measuring device depends on the sampling strategy (on-the-spot, continuous, multiple or single concentration measurement), cost, simplicity, accuracy and measuring range of the measurement method (Ni and Heber, 2001; Phillips et al., 2001). Some of the common NH_3 and GHGs measuring devices are the wet chemical method, gas detector tubes, Fourier Transform Infrared (FTIR) Spectrometers, Non-Dispersive Infrared (NDIR) analysers, NO_x-chemoluminescence monitors etc. Only the wet chemical method, gas detector tubes and the FTIR spectrometer techniques are described in this section of the PhD thesis. This is because, the wet chemical approach is considered the "standard reference method" for validating other NH_3 measurement techniques (EN 14793, 2017), whereas the gas detector tube and the FTIR measurement techniques were applied during this PhD research.

The wet chemical method is a simple and cheap method for determining NH_3 concentration (Phillips et al., 2001). During the measurement, a known volume of air is passed through a dilute acid solution in Dreschel bottles. Since NH_3 is a basic compound, it dissolves in the solution forming NH_4^+ ions, which is later analysed in the laboratory by colorimetric or analytical techniques (Ni & Heber, 2001; Phillips et al., 2001). Due to the high measuring precision, accuracy, reliability and ability to measure very low NH_3 concentrations, the wet chemical method is used as the “standard reference method” for validating other NH_3 measuring techniques in the Verification of Environmental Technologies for Agricultural Production (VERA, 2018) protocol. Using the wet chemical method however, is laborious and only takes non-continuous measurements (Phillips et al., 2001).

Measuring gaseous concentration with gas detector tubes is more portable, simple and inexpensive than the wet chemical method (Phillips et al., 2001). The measurement method uses an active (with pump) or passive (without pump) single-use graduated sampling glass tube, packed with a gas detection reagent that changes colour when an air sample is drawn through the glass tube (Ni & Heber, 2001). In the glass tube, the length of the colour change of reagent shows the gas concentration level. The sampling strategy is on-the-spot, either for short (less than 15 minute) or long-term (greater than 2 hours) measurement basis (Phillip et al., 2001). There are a number of gas detector tubes from various measurement ranges for measuring NH_3, H_2S, CO_2 etc.

FTIR spectroscopy is a more advanced gas measurement technique than wet chemical and gas detector tube methods that can monitor multiple gases simultaneously. In FTIR analysis, the interaction of infrared radiation with an air sample in an interferometer produces an output signal known as the interferogram. The interferogram (i.e. raw signal) is then Fourier transformed using computer software to produce a spectrum that can be correlated with known spectra of chemical samples. The concentration of each gas in the air sample can be determined depending on the spectrum or peak characteristic (Ni & Heber, 2001; Phillips et al., 2001; Hu et al., 2014). The advantage of FTIR analysers is the very low detection limits and the ability to continuously measure gas concentrations at very high temporal resolutions. FTIR gas analysers, however, have a high capital cost, are expensive to maintain and require skilled operators compared to the chemical and gas detector tube methods. Reviews can be found in Ni and Heber (2001), Phillips et al., (2001) and Hu et al. (2014) on other NH_3 and GHG measurement techniques/devices used in animal houses.

Odour measurements in animal production apply a completely different approach compared to the NH_3 and GHG concentration measurement. In Europe, dynamic olfactometry, which uses human panellists, is the standard way to measure odour (CEN, 2003; Hansen, 2011; Hove, 2018). The odour unit in the dynamic olfactometry is referred to as the European odour unit per cubic meter (OU_E m^3), which is the amount of odorants that, when diluted in cubic meter of clean air, give a physiological response from half of the panellists (CEN, 2003). The European standard (CEN, 2003) specifies how to perform an odour analysis. In addition, Hansen (2011) and Hove (2018) have described the experimental challenges of air sampling, storage and human panel selection during the odour sampling and olfactometry measurement.

The emission rate of NH_3, GHG or odour is often calculated as the product of the difference in the pollutant concentration between the background and exhaust air sample, and the ventilation rate in the animal house. The emission rate of gases from livestock buildings are typically reported as the emission factor, which defines the mass of a specific gas emitted over a year per animal place (kg year^{-1} animal^{-1}). Odour emission rates are reported as the amount of European odour units emitted per second per animal place (OU_E s^{-1} pig^{-1}). The ideal approach for determining gaseous and odour emissions from livestock housing requires continuous emission measurements throughout the year (Mosquera and Ogink, 2011; Kafle et al., 2018).

However, due to the high measurement and labour costs in such a sampling strategy, several protocols with reduced sampling days have been proposed in literature (Vranken et al. 2004; Dekock et al., 2009; Mosquera and Ogink, 2011; Kafle et al., 2018). The VERA standardised measurement protocol (2018) is one of the popular emission assessment tools for livestock housing. The VERA protocol suggests that field measurements must be carried out in at least two pig farms for an accurate estimate of the emission rate (factor). Furthermore, measurements must be performed in at least six sampling days over the year per farm, taking into account the between and within farm variations, diurnal and seasonal variations and the linear increase of fattening pig weight to calculate the emission rates. The case-control approach of VERA protocol was adopted in this PhD research (Chapter 3) during the field measurements of the gaseous and odour emissions.

1.5.2. Full- and reduced-scale models

Full-scale studies are considered comparatively convenient to evaluate the effect of ventilation and climate control strategies on indoor climate and emissions in livestock buildings, mainly because full-scale models offer relatively better control of external climatic factors and eliminate disturbance by animals (Puma et al., 1999; Ye et al., 2011) and do not have to satisfy many similarity criteria in reduced-scale models (Saha et al., 2011a; Saha et al., 2011b). Full-scale models are developed by designing simplified animal house configurations that can be easily altered and artificially mimic animal heat and pollutant production (Puma et al., 1999; Ye et al., 2011). To enhance repeatability, full-scale models are developed in a larger climate chamber with incoming air conditioners or perform measurements on stable days. For example, Ye et al. (2011) used two empty full-scale fattening pig buildings equipped with floor heating cables and slurry (as NH_3 production source) in the pit to investigate the effect of ventilation and different building design features on NH_3 emission. The study, however, did not simulate NH_3 production on pen floor.

In contrast, reduced-scale models are scaled-down models of livestock buildings. The objective of reduced-scale modelling is to control and explicitly investigate the effects of different ventilation control strategies, housing designs and management strategies (e.g. slurry depth, temperature etc.) on airflow and emissions under laboratory conditions (Zhang et al., 2008; Saha et al., 2011c; De Paepe et al., 2016). However, the prerequisite to produce: (1) similar pollutant emission and air velocities at boundary layers of emitting surfaces and (2) similar geometrical configurations (e.g. ventilation openings, slatted floors etc.) and dimensionless parameters such as, Reynolds number, Grashof number etc. as in real buildings makes reduced scale models unattractive (Saha et al., 2010; Saha et al., 2011a; Saha et al., 2011b; Saha et al., 2011c). Nonetheless, results from these studies are very useful in validation studies of CFD models (Norton et al., 2009; Saha et al., 2011b; Rong et al., 2015). In the NH_3 emission studies, Ye et al. (2008a) and Saha et al. (2011b) used aqueous ammonia solutions, while Ye et al. (2008b) used liquid pig slurry to simulate NH_3 production in the slurry pit of the reduce-scale pig house.

1.5.3. Mathematical modelling

Mathematical modelling is an alternative to the real measurement in sections 1.5.1 and 1.5.2, as a result of the ease to perform multiple simulations in short time. Mathematical models are also used to make quick management decisions on new climate control strategies, best building insulation and effective emission mitigation techniques in livestock buildings without real measurements (Schauberger et al., 2000; Zhang, et al., 2005; Haeussermann, et al., 2007; Park et al., 2013; Zhao et al., 2013; Menconi et al., 2014; Mendes et al., 2017). Examples of mathematical modelling techniques in livestock housing are the steady-state or dynamic (time-dependant) balance and Computational Fluid Dynamics (CFD) modelling tools.

1.5.3.1. Steady state and dynamic models

The steady-state balance model uses the control volume concept with the energy and mass conservation laws to simulate the climatic conditions inside livestock buildings. To simplify the calculation process, zero energy and mass storage are assumed to eliminate the time dependency in the energy and mass balance equations. Calculated variables include temperature, relative humidity (RH), gaseous concentration and ventilation rate. Due to the simplicity of the steady-state balance models, studies that involve design of heating, cooling, ventilation, insulation etc. systems and the verification of the effect of climate control systems on the indoor climate in livestock housing use this type of model.

For example, Berckmans & Goedseels (1986) used the steady state sensible energy balance equation to evaluate the climate controller action on indoor temperature in a mechanically ventilated pig house based on proportional control and the on/off heating control at a fixed fattening pig weight, and used the mean frequency of outdoor temperature in Belgium. Cooper et al. (1998) included the steady moisture balance equation to the sensible energy balance equation of Berckmans and Goedseels (1986) to calculate indoor temperature and relative humidity in a fattening pig house and validated it with hourly measured data. The study of Schauberger et al. (2000) further included CO_2 and odour production equations to the sensible energy and moisture balance equation to calculate indoor climatic conditions in the mechanically ventilated pig house. The effect of the climate control settings on animal/stockmen health and welfare were also investigated. Their model used the time series data of the outdoor temperature and humidity for 2 years at a sampling interval of 30 minutes, proportional band setting and a fixed pig weight in the calculation. Zhao et al. (2013) on the other hand, used a validated steady state heat and moisture balance model to compare ventilation and heating requirements including energy use and costs between an alternative and conventional house for layer hens in winter. Sensitivity tests on animal stocking density, target indoor set-point temperature and relative humidity, building insulation and time of the day on building performance were also performed. Chepete & Xin (2004) previously used steady state heat and moisture balance equations to evaluate the effect of old and new, heat and moisture production data for laying hens on ventilation rate calculation for temperature and moisture control in a modern high−rise layer house in the USA.

Although steady state models are simple to use, their prediction accuracy depends on the input data on animal and house level heat, moisture and gaseous generation rate. Most importantly, the neglect of wall heat storage in the energy balance equations limits their application to evaluate indoor temperature and ventilation rate in short time intervals when indoor and outdoor temperature difference are low and there is a high diurnal variation in outdoor temperature (Albright & Scott, 1974). Panagakis & Axaopoulos (2004) and Zhang & Barber (1993) have both noted that the use of steady state models to size heating and ventilation equipment under these limitations can lead to climate control malfunctioning in real livestock buildings and recommends the use of dynamic models.

Dynamic balance modelling is applied in studies that involve the design/evaluation of indoor climate control systems, building design and material properties. However, in contrast to the steady-state models, the dynamic balance models use the time-dependant mass and energy balance equations to simulate the evolution of the indoor climatic parameters over time. Therefore, by accounting for this time-dependency, the dynamic balance model is a more realistic tool to evaluate indoor climate control systems in livestock housing compared to steady-state models (Zhang et al., 1992). However, the numerical solution of the time-dependent equations in dynamic models needs more advanced software compared to the steady-state models. The main drawback of the dynamic balance model is that they assume the simulated spaces as a single perfectly mixed zone, which does not exist in reality. This assumption also exists in the steady-state balance model. Additionally, the dynamic balance models need models that can accurately predict dynamic behaviour of the animal on heat, moisture and contaminant production rate at the house level. The lack of these sub-models often results in poor model predictions (Fabrizio et al., 2014).

As climatic control systems in livestock buildings operate dynamically to maintain optimal indoor climatic conditions, dynamic models are an important tool to assess and optimise climate control algorithms and strategies (Zhang and Barber, 1995; Yang et al., 2009). Zhang and Barber (1995) investigated the effect of a temperature controller versus a temperature-humidity climate controller on indoor thermal response and supplementary heat consumption using a dynamic model. In Menconi et al. (2014) a simple dynamic model was developed to assess the optimal insulation level for an animal house. Vranken (1999) developed a more complicated dynamic model to investigate the influence of different climate control settings (set-point temperature curves over entire growth period of pigs, optimal set-point curve bandwidth and selected minimum ventilation requirement) on NH_3 emission from a fattening pig house. Vranken (1999) calculated the Archimedes number and used it to predict airflow pattern in the pig building.

Haeussermann et al. (2007) evaluated the effect of different ventilation, heating and fogging control strategies and different control settings on the thermal comfort of pigs in a fattening pig house, in addition to their operation costs using a dynamic mathematical model. Panagakis & Axaopoulos (2006) and Panagakis & Axaopoulos (2008) also used a dynamic model in a similar application. Park et al. (2013) and Anthony et al. (2014) applied the dynamic modelling approach to investigate the potential use of recirculation exhaust air devices in a pig house. As previously noted the main drawback in dynamic models is that they assume simulated buildings as perfectly mixed single zones, which does not exist in reality. Therefore, for detailed investigations on the spatial distribution of air velocity, temperature, moisture and gaseous concentration distributions in livestock housing, Computational Fluid Dynamics (CFD) is the alternative.

1.5.3.2. Computational fluid dynamic models

Computational Fluid Dynamics (CFD) is an advanced modelling tool for studying 2 and 3-dimensional flow and temperature fields in animal buildings. In order to do this the space is discretized in small volumes (cells) in which the conservation laws are solved using the Navier-Stokes equations (RANS) (Versteeg, and Malalasekera, 2007). For flows with a high Reynolds number, which are called turbulent, the solution can only be obtained with a relatively coarse grid if a turbulence model is introduced. There are several turbulence models (e.g. Standard k-ε, Renormalisation Group k-ε, Realisable k-ε etc), of which RANS is commonly used for large volumes and internal flows. The choice of the selected turbulence model depends on the type of simulated problem. The main advantage of CFD modelling is that it simulates the spatial indoor air temperature, velocity and gaseous concentration distribution, which can be visualised at a high resolution. CFD simulations are also cheap to perform compared to full-scale and reduced-scale modelling because different building designs can be simulated for different climatic scenarios. As a result, CFD is becoming a very important modelling tool for ventilation design and emission studies in livestock housing (Sun et al., 2004; Norton et al., 2007; Sapounas et al., 2009; Seo et al., 2012). The challenges in CFD investigations are that simulated results are often treated with low confidence until they are validated with experimental results. In addition, accurate CFD simulations often require proficient users who can deal with issues related to grid refinement, selecting appropriate computational domain and physical boundary conditions.

1.6. Problem statement

Most pig buildings in Flanders are mechanically ventilated with climate control computers, which use fans to extract waste air and air inlet systems to supply fresh air into buildings. Furthermore, two-thirds of newly built fattening pig buildings in Flanders are underfloor air distribution (UFAD) systems (DLV, 2014). Ventilation affects NH_3 and odour emission in pig buildings due to the role of ventilation as the channel for transporting heat and pollutants to the ambient environment. The air velocity near the emitting surfaces is an important driving force for NH_3 volatilisation and is closely linked to the ventilation rate (Aarnink and Elzing, 1998; Kavolelis, 2003; De Paepe et al., 2015). Aarnink and Elzing (1998) showed that increasing the air velocity in the slurry pit of a fattening pig house from 0.3 to 0.9 m s^{-1} can increase the NH_3 emission rate by 80%. This is because the thickness of the boundary layer at the emitting surface is reduced by an increase in air velocity, thereby reducing NH_3 mass transfer resistance from the emission surface to the air in the building (Rong et al., 2010). The air displacement ventilation process in pig buildings with UFAD systems also increases the risk of pollutant transport from the slurry pit into the building, consequently increasing NH_3 and odour emissions. Ammonia emissions are a major public concern as NH_3 is a precursor for secondary PM formation and a source of acidification and eutrophication in ecosystems (Erisman and Schaap, 2004; Santonja et al., 2017). Odour emissions are also an important social and environmental concern in view of their potential effects as a public nuisance (Wing et al., 2008; Juska, 2010).

Studies on the optimisation of climate control settings (VCS) as a strategy to reduce NH_3 and odour emissions are limited and unclear. Furthermore, the effect of VCSs on pollutant transport behaviour in pig buildings equipped with UFAD system is still not entirely clear. For instance, Vranken et al. (2003) demonstrated using a dynamic simulation model that adjusting ventilation settings (set-point temperature, bandwidth and minimum /maximum ventilation) at the climate control computer based on pig weight could reduce the annual NH_3 emissions by 8% compared to traditional settings in Flanders. Zhang et al. (2009) also stated using computer simulations that it was feasible to reduce 50% of odour emissions from a fattening pig building by gradually increasing the maximum ventilation settings based on pig weight compared to the traditional setting in Denmark. However, these investigations were not validated in a real pig building. In a related study, Pouliot et al. (2011) assessed the impact of three climate control set-point temperatures on NH_3 emission in an environmental chamber with real pigs but found no clear impact on NH_3 emission.

To address the knowledge gap mentioned above, this PhD used an integrated modelling and experimental approach by first developing mathematical and experimental (test-platform) tools to study the effect of different ventilation control settings on the indoor climate, pollutant transport behaviour, and emissions in pig housing (Fig. 1.6). This was followed by field experiments using real pigs in a building equipped with a UFAD system to assess the effect of the selected ventilation strategies in the mathematical and test-platform on the indoor climate, NH_3, odour emission and pig performance. This PhD also developed a CFD model with an advanced NH_3 emission model to better understand the NH_3 transport behaviour from the slurry pit and the pen floor in the pig building with UFAD system.

1.7. General research objectives, questions and hypothesis

The general objectives of this PhD work are to:

1. Acquire knowledge on the effect of ventilation on NH_3 and odour transport behaviour in pig buildings with UFAD systems.
2. Test and optimise ventilation control settings in order to promote optimal indoor climate and animal production, and to reduce NH_3 and odour emissions in pig buildings with UFAD systems.
3. Apply and evaluate the VERA test protocol's sampling strategy for calculating NH_3 and odour emission factors for fattening pig buildings.
4. Derive NH_3 and odour emission factors for fattening pig buildings at different ventilation control settings.

The main research questions are:

1. What is the behaviour of indoor climate, NH_3 and odour at different ventilation control settings in fattening pig houses with UFAD systems?
2. What ventilation control settings can promote optimal indoor climate and reduce NH_3 and odour emission without affecting pig performance?
3. What are the uncertainty levels on calculated NH_3 and odour emission factors for fattening pig buildings when applying the sampling strategy of the VERA test protocol?

The general research objectives/questions enabled the research to test the following hypotheses:

1. Optimising the ventilation control settings in mechanically ventilated fattening pig buildings with UFAD systems can reduce ventilation rate and air velocity near the emitting surfaces, thereby minimising NH_3 and odour emissions at no extra cost.
2. The air displacement ventilation process in fattening pig buildings with UFAD systems can cause elevated NH_3 transport from the slurry pit into the building.
3. Applying the VERA sampling strategy for fattening pig houses can result in emission factors with high uncertainty levels.

1.8. Thesis outline

The present PhD thesis is made up of three parts (Fig. 1.6). The first part (chapter 1) gives the context to the significance of pig production in Flanders in terms of economy, aerial emissions and the existing environmental regulations in pig production. Chapter 1 also gives a background to the role of ventilation in pig buildings, the most common ventilation designs in Flanders, and ventilation control strategies and emission reduction techniques. Chapter 1 also includes a review on ventilation design and performance assessment methods in livestock buildings, the problem statement, the general research questions and objectives of this PhD research.

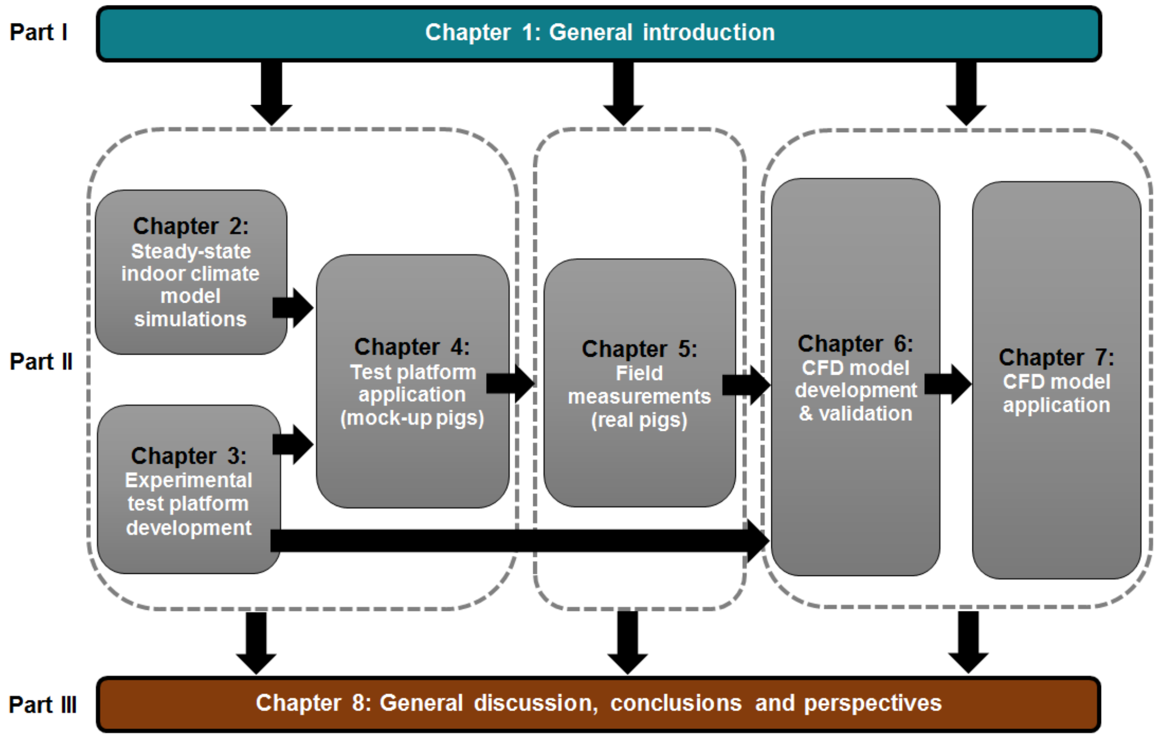

Fig. 1.6 — Outline of the PhD thesis showing the integrated modelling and experimental approach applied during the research.

The second part of this dissertation gives the experimental and mathematical simulation results that were obtained during the PhD research (chapters 2 – 7). The experimental and modelling activities conducted in chapters 2 – 4 were to attain general research objectives 1 and 2. In chapter 2, entitled “Effects of ventilation control settings on ventilation rate and indoor climate: a steady-state simulation approach”. A steady-state indoor climate mathematical model was developed for predicting indoor temperature, RH, CO_2 concentrations and ventilation rate. The validated mathematical model was later used to select three ventilation strategies from nine others that were tested in a pig rearing house (chapters 4 and 5).

In Chapter 3, entitled “Developing an experimental test platform equipped with artificial pigs and automatic urea spraying installation”, the PhD study developed an experimental test platform (physical model) that contains mock up pigs as heat source and an automatic urea spraying installation to mimic pen fouling/NH_3 production in the experimental pig compartment. Chapter 4 is entitled “Effect of ventilation settings on ammonia emission in an experimental (test platform) pig house”. In this chapter, the PhD study used the experimental test platform to investigate the effects of three different ventilation control settings on NH_3 transport behaviour and emission. Another objective of chapter 4 was to verify the effect of the selected ventilation control settings in chapter 2 on NH_3 emissions in the test platform pig house.

Chapter 5 entitled “Effect of ventilation settings on ammonia and odour emissions from a pig rearing building” contains the experiment that was conducted in eight pig compartments during three fattening rounds from 2016 – 2017. The objective of the experiment was to verify whether adjusting the ventilation control settings that were identified in chapter 2 can fulfil the recommended indoor climatic requirements for pig production under practical conditions. Another objective was to verify under practical conditions whether ammonia and odour emissions can be reduced by adjusting the identified ventilation control settings in chapter 2. Thus, the experiment in chapter 5 was conducted to attain objectives 1, 2 and 3 of this PhD's main research objectives.

Chapters 6 and 7 involve the CFD simulations on the effects of ventilation, inlet and exhaust configurations on air distribution and NH_3 emission in a pig building with a UFAD system. These two chapters address research objective 1 and answers research question 1. Chapter 6 includes the development and validation of a CFD model of a pig building with a UFAD system for predicting indoor air temperature, velocity, CO_2, NH_3 distribution and emission. Chapter 7 presents an investigation on the effect of inlet and exhaust configurations on airflow, temperature, CO_2, NH_3 distribution and emission in the validated CFD model. Chapters 6 and 7 present the specific objectives of each task.

The main results of the PhD research are discussed in the last part (chapter 8) of this PhD thesis and their implications for practice and future research are described. The main conclusions of this thesis are also presented in chapter 8.

Chapter 2: Effects of ventilation control settings on ventilation rate and indoor climate: a steady-state simulation approach

2.1. Introduction

The objective in this chapter was to develop a validated steady-state model for predicting the evolution of indoor temperature, relative humidity (RH), CO_2 concentration and ventilation rate (VR) over time in the ILVO/UGent/HoGent fattening pig building. The validated model would then be used as an evaluation tool to select three ventilation settings (from nine) to be tested at the ILVO/UGent/HoGent building (chapters 4 and 5). The selection criterion was based on the ventilation control settings (VCS) with relatively low VRs compared to a reference ventilation setting (T_{ref}). It was assumed that VCSs with lower VR result in lower NH_3 and odour emissions (Vranken et al., 2003; Zhang et al., 2009). This is because lower VR minimises NH_3 volatilisation from slurry in the pit and pen floor in pig buildings since air velocity above the emitting surface that derives NH_3 volatilisation is closely linked to VR (Aarnink and Elzing, 1998; Kavolelis, 2003; Ye et al., 2009; De Paepe et al., 2015). Lowering the VR reduces indoor quality. Hence, an additional selection criterion was used as CO_2 concentration limit of 3500 ppm (CIGR, 1984). Instead of using a dynamic balance or CFD model (Section 1.5.3) at this stage of the PhD research, a steady-state balance model was selected. This is because it is an easy and fast modelling approach for selecting the VCSs that will later be experimentally tested in chapters 4 and 5.

2.2. Materials and methods

2.2.1. Simulated pig house

This study used the fully-slatted compartment (Fig. 2.1) at the ILVO/UGent/HoGent fattening pig building, Merelbeke (Belgium) for the case study simulations. The simulated compartment was part of the 16 separate compartments at the pig campus, which was constructed in 2015. The compartment housed 48 pigs in 8 separate pens (i.e. 6 pigs per pen) at a stocking density of 0.83 m^2 pig^{-1}.

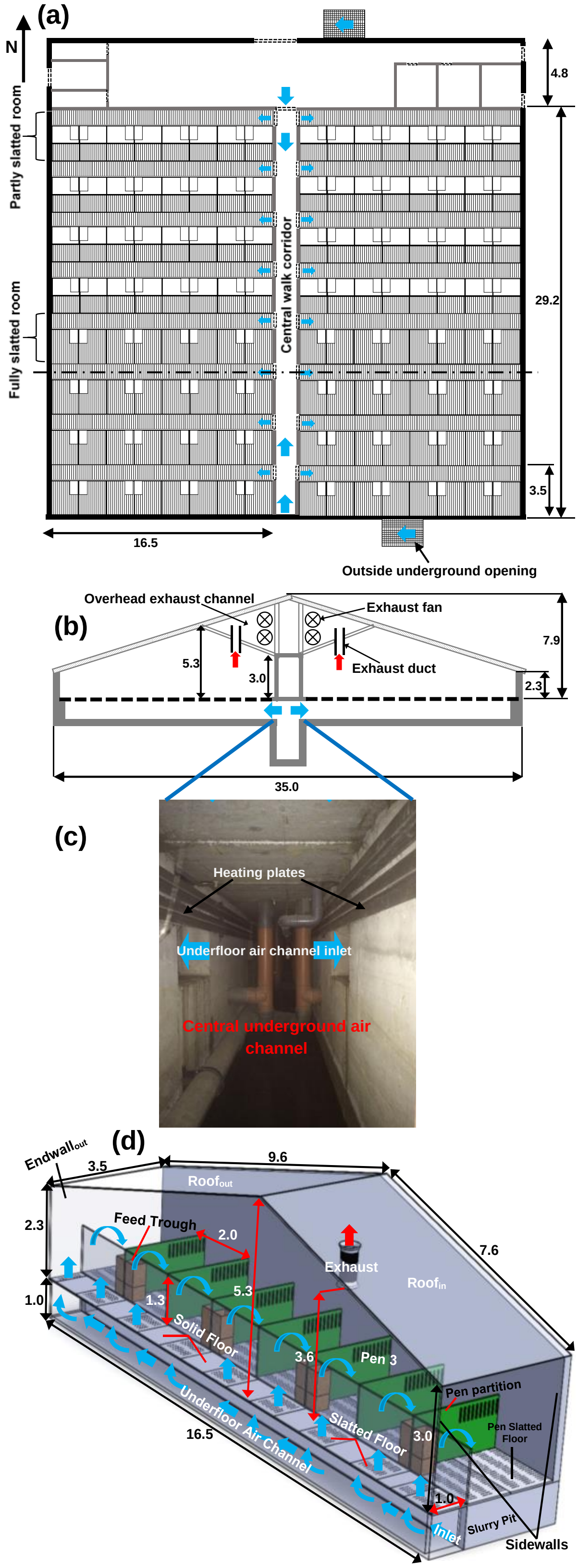

Fig. 2.1— ILVO/UGent/HoGent fattening pig building (a) plan view (b) cross sectional view (c) photo showing the central underground air channel and underfloor air inlets to compartments and (d) the dimensions and the airflow pattern in the compartment (all dimensions are in meters).

The compartment was equipped with an underfloor air distribution (UFAD) system where the incoming air enters the compartment via the slatted floor at the service alley and removes the ventilated air via the exhaust duct at the ceiling (Fig. 2.1d). Table 2.1 provides details of the material and the corresponding overall heat transfer coefficients (U) of the walls in the compartment. The U values were obtained from the building company (DLV cvba, Wetteren, Belgium), and it was not clear how the values were calculated.

Table 2.1. Material descriptions and the overall heat transfer coefficients (U) of the ILVO/UGent/HoGent pig compartment

Building	**Material description**	**Area (m^2)**	**U ($W\ m^{-2}\ K^{-1}$)**
Sidewalls	PVC sandwich air panel	64.65	0.56
$Endwall_{in}$	Fabricated reinforced concrete	10.50	0.39
$Endwall_{out}$	Fabricated reinforced concrete	6.10	0.39
$Roof_{in}$	Polyurethane + corrugated cement sheet	26.50	0.58
$Roof_{out}$	Polyurethane + corrugated cement sheet	33.70	0.25
Window	Double glazed glass	1.99	1.11
Floor	Concrete	40.88	4.50

2.2.2. Weather data

The developed model used the 8 months of the 2.5-year weather dataset to simulate the indoor climate and ventilation rate in the pig compartment. The weather dataset was collected from 3 June 2011 to 22 January 2014 at ILVO, Merelbeke (latitude 50°59'1''N, longitude 3°46''49''E), Belgium. A Campbell Scientific BWS200 weather station (Campbell Scientific Inc., Logan, UT, USA), placed in the open field, measured the outside temperature, RH, solar radiation, wind speed and direction every 15 minutes. The simulations were performed in two fattening periods. The first simulation was from 16 November 2011 to 14 March 2012 (winter fattening period), followed by the second simulation (summer fattening period) from 16 June 2012 to 12 September 2012.

2.2.3. Model description

The steady-state indoor climate model was developed in MATLAB R2011b (MathWorks Inc., Massachusetts, USA) with Simulink (version 7.8). Simulations were performed at a 15-minute time step. For lack of experimental data, this model did not include supplementary winter heating at the underfloor air channel (Fig. 2.1c). Thus, outside air temperature (T_{out}) was assumed to be the air temperature at the inlet (Fig. 2.1d). In addition, the slurry pit and underfloor air channel at the service alley (Fig. 2.1d) were excluded from the total volume of the simulated compartment. It is noted that urine and faeces deposited on floors and slurry in the pit contribute to heat and moisture exchange in pig buildings but for simplicity they were not included in this model.

The simulated compartment housed 48 pigs and the pig growth was calculated from 9 – 17 weeks using Eq. 2.1 (Braig and Schinckel, 2001).

$$m_t = m_m \times (1 - e^{-e^{d}t^{\omega}}) \quad (2.1)$$

where m_t is pig weight (kg) at age (t, days), m_m is the mature pig weight (kg), d is the exponential growth decay and ω is the kinetic order. For high-lean Belgian pigs, m_m, d and ω were selected as 134.4 kg, -11.844 and 2.39 respectively, assuming they had free access to feed and water (Leen et al., 2016).

The air temperature in the compartment was determined using the energy balance equation (Eq. 2.2) at a steady-state, and assuming the air in the compartment is perfectly mixed.

$$\rho C_p V_{comp} \frac{dT_i}{dt} = Q_s - \rho C_p VR(T_i - T_{out}) - U_{comp}A_{comp}(T_i - T_{sol-air}) \quad (2.2)$$

where ρ is air density (1.225 kg m^{-3}), C_p is the specific heat of air at constant pressure (1005.4 J kg^{-1} K^{-1}) and V_{comp} is the volume of the compartment (218.3 m^3). T_i and T_{out} (°C) are the compartment and outside air temperatures, respectively. U_{comp} (W m^{-2} K^{-1}) is the mean compartment heat transfer coefficient, A_{comp} (m^2) is the mean compartment surface area and VR (m^3 s^{-1}) is the ventilation rate.

The solar air temperature ($T_{sol-air}$, °C) was calculated using equations 2.3 – 2.7 (Albright, 1990; Roy et al., 2002) from the weather dataset (section 2.2.1).

$$T_{sol-air} = T_{out} + \frac{\alpha I}{h_c} \quad (2.3)$$

$$h_c = \frac{Nu \times k}{L} \quad (2.4)$$

$$Nu = 0.036 \times Re^{\frac{4}{5}} \times Pr^{\frac{1}{3}} \quad (2.5)$$

$$Re = \frac{u \times L \times \rho}{\mu} \quad (2.6)$$

$$Pr = \frac{C_p \times \mu}{k} \quad (2.7)$$

where α is surfaces solar radiation absorbance (dimensionless), I is local solar irradiance (W m^{-2}), h_c is convective heat transfer coefficient (W m^{-2} K^{-1}), Nu, Re and Pr are the Nusselt, Reynolds and Prandtl numbers. L is the characteristics length of the wall/roof (6.5 m), k is the thermal conductivity of air (W m^{-1} K^{-1}), μ is the dynamic viscosity of air (kg m^{-1} s^{-1}).

The sensible heat (Q_s, W) from the pigs was calculated from equations 2.8 – 2.10 (CIGR, 2002).

$$Q_s = k_s A_{act}(0.62 \times Q_{tot}^* + 1.15 \times 10^{-7} \times T_i^6) \quad (2.8)$$

$$Q_{tot}^* = Q_{tot} + 0.012 \times Q_{tot} \times (20 - T_i) \quad (2.9)$$

$$Q_{tot} = 5.09m^{0.75} + (1 - (0.47 + 0.003m))(n \times 5.09m^{0.75} - 5.09m^{0.75}) \quad (2.10)$$

where Q_{tot} (W) is the total heat production at 20 °C in the compartment, Q_{tot}^* (W) is the corrected total heat production at temperatures other than 20 °C, m is the pig weight (kg), n is the maintenance energy coefficient that was set at 3.1 for fattening pigs in the Netherlands. The house level water evaporation from wet surfaces was accounted for by the correction factor, k_s= 0.93 (CIGR, 2002).

Diurnal variation in pig heat production due to pig activity (A_{act}) was accounted for using the dromedary curve (CIGR, 2002).

$$A_{act} = 1 - a \times Sin\left(\frac{2\pi}{24} \times (h + 6 - h_{min})\right) \quad (2.11)$$

where A_{act} (dimensionless), a is the amplitude of the dromedary curve, h_{min} (hours) is the time of the day with minimum pig activity and h (hours) is the time of the day in a 24-hour clock. The a was set at 0.31 and h_{min} was set at 0.68 (Blanes and Pedersen, 2005).

The transmission heat transfer through the building walls were calculated using A_{comp} and U_{comp} from Table 2.1, which are 41.75 m^2 and 0.062 W m^{-2} K^{-1}, respectively, resulting in the equivalent U-value (U_{eq}) of 2.58 W K^{-1} (Eq. 2.12).

$$U_{eq} = A_{comp} \times U_{comp} \quad (2.12)$$

$$U_{comp} = \frac{(U_{endwall} \times U_{roof} \times U_{window})}{(U_{endwall} + U_{roof} + U_{window})} \quad (2.13)$$

The A_{comp} and U_{comp} were calculated using only the Roof$_{out}$ and Endwall$_{out}$ areas because the compartment's sidewalls, Roof$_{in}$ and Endwall$_{in}$ were assumed as adiabatic surfaces. This is because the adjacent compartments (Fig. 2.1a) were assumed to be occupied by pigs at the same weight with minimal heat transfer between the walls of the compartments. The overhead exhaust channel above Roof$_{in}$ and the low U value were assumed to reduce heat transfer through the roof. It was also assumed that there was minimal heat transfer from the central walk corridor to Endwall$_{in}$.

The relative humidity (RH) and CO_2 concentration in the compartment were calculated using the mass balance equations (Equations 2.14 – 2.16 and equations 2.20– 2.21, respectively).

$$V_{comp}\frac{dH_i}{dt} = VR(H_{out} - H_i) + \frac{Q_l}{h_{vap}} \quad (2.14)$$

$$Q_l = Q_{tot}^* - Q_s \quad (2.15)$$

$$h_{vap} = 2501 - 2.42T_i \quad (2.16)$$

Q_l (W) is the latent heat production and h_{vap} (J g^{-1}) is the heat of vaporization of water. H_{out} and H_i are outside and compartment absolute humidity (RH_{ab}, g m^{-3}). The RH_{ab} was calculated using equations 2.17 – 2.19 (Vaisala, 2013).

$$RH_{ab} = \frac{C \times p_w}{T} \qquad (2.17)$$

$$p_{ws} = A \times 10^{\left(\frac{m \times T_i}{T_i + T_n}\right)} \qquad (2.18)$$

$$p_w = \frac{p_{ws} \times RH}{100\%} \qquad (2.19)$$

where C (2.16679 g K J^{-1}), A (6.116441), m (7.591386) and T_n (240.7263) are constants. T_i is air temperature (°C) in the compartment, p_w and p_{ws} are the vapour and saturation vapour pressure (hPa), respectively. Note that the units for p_w and T in equation 2.19 are in Pa and K, respectively.

$$V_{comp} \frac{dC_i}{dt} = VR(C_{out} - C_i) + C_{comp} \qquad (2.20)$$

$$C_{comp} = Q_{tot} \times C_{prod} \times \rho_{CO_2} \qquad (2.21)$$

where C_i (mg m^{-3}) is the CO_2 concentration in the compartment, C_{out} is the outside CO_2 concentration, the total heat production (Q_{tot}), was converted from W to heat production units (hpu). i.e. 1000 W = 1 hpu (CIGR, 2020). C_{prod} is the pig CO_2 production (5.1389 × 10^{-5} m^3 s^{-1} hpu^{-1}, (CIGR (2002)), ρ_{CO_2} the density of CO_2 (1.98 × 10^{-6} mg m^{-3}), and C_{comp} (mg s^{-1}) is CO_2 production in the compartment. C_{out} was assumed as 719.2 mg m^{-3} (370 ppm) since experimental data was not available.

Ventilation systems in Flemish piggeries typically use proportional band temperature control systems (Van Gansbeke et al., 2009). Therefore, Eq. 2.22 was used as the ventilation control algorithm in the developed model.

$$V_R(T_i) = \left| \begin{array}{ccc} VR_{min} & for & T_i \leq T_{set} \\ VR_{min} + (T_i - T_{set})\frac{(VR_{max} - VR_{min})}{\Delta T_i} & for & T_{set} \leq T_i \leq T_{set} + \Delta T_i \\ VR_{max} & for & T_i \geq T_{set} + \Delta T_i \end{array} \right| \qquad (2.22)$$

where VR_{min} and VR_{max} (m^3 s^{-1}) are the minimum and the maximum ventilation settings. T_{set} is the set-point temperature. The bandwidth (ΔT_i) settings in the climate control computer was 5 °C.

2.2.4. Model validation

The developed model was validated using experimental data measured at Deerlijk (Belgium) in a fattening pig compartment (Fig. 2.2). The field measurements were taken from 14 – 20 August 2014. The experimental compartment was part of a fattening pig building built in 2005 that consisted of four separate compartments. During the measurements the average pig weight in the compartment was between 90 and 95 kg but during the model validation a constant pig weight of 90 kg was used. The pen floor in the compartment was divided into drainage, laying and dunging area.

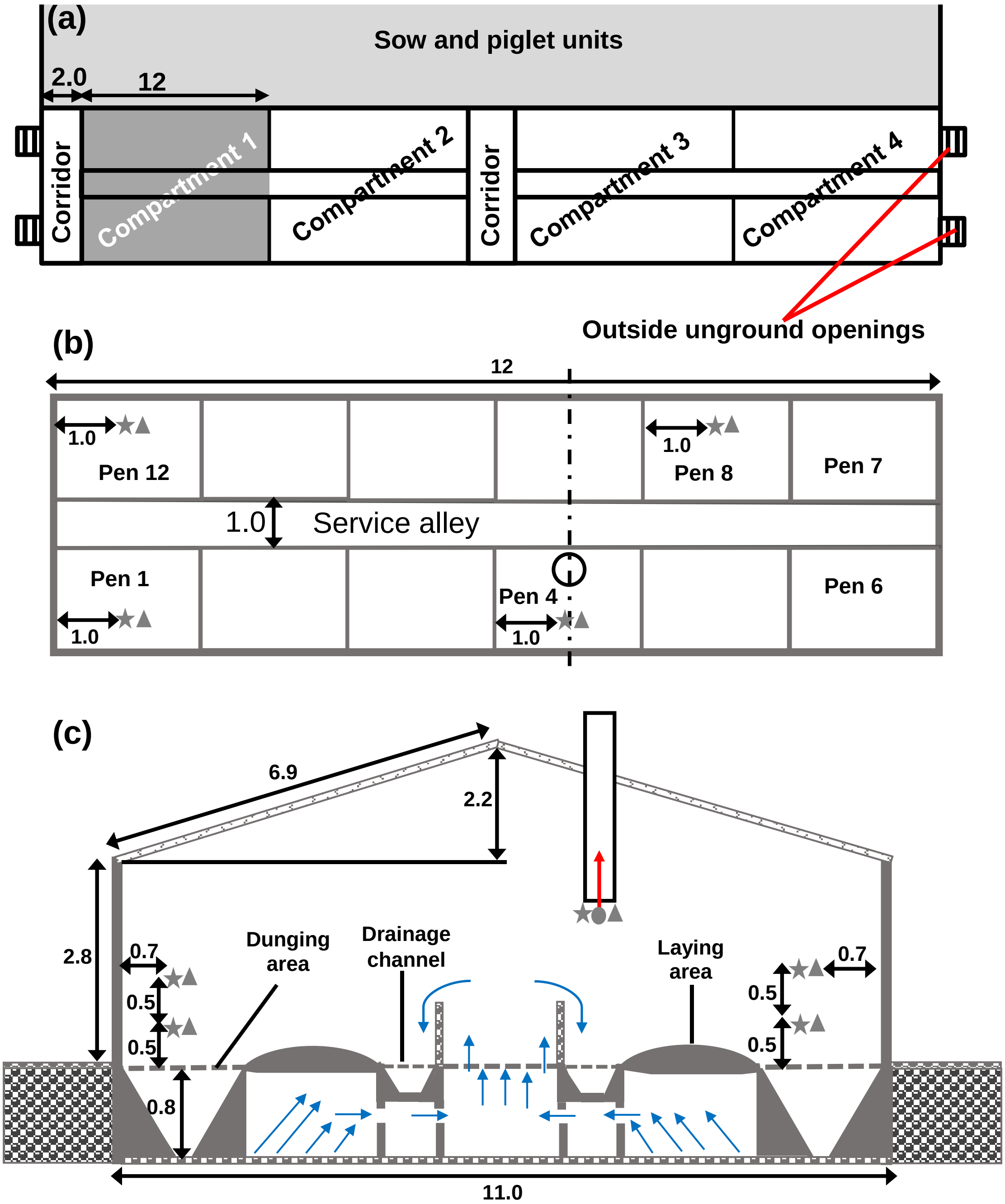

Fig. 2.2 —Deerlijk Pig farm in West Flanders (a) plane view of the pig farm (b) plane and (c) cross-sectional view of the experimental pig room (i.e. compartment 1). All dimensions are in meters and not to scale. Where star, circle and triangle represent the temperature, relative humidity and gas sampling locations.

The drainage and dunging section had slatted floors while the laying area had a convex solid floor, representing 20%, 40% and 40% of the total pen floor area, respectively. The compartment housed 156 pigs at the stocking density of 0.77 m^2 pig^{-1}. The pigs were dry fed, ad libitum and had unlimited access to water. In addition, the pig compartment was equipped with a UFAD system. The exhaust fan had a maximum fan capacity of 10,000 m^3 h^{-1}. Airflow in the compartment was controlled (Microfan BV, the Netherlands) by the thermometer located 1.6 m above the pen floor.

During the experiment, air temperature and CO_2 concentrations were measured at different sampling locations in the compartment, while the RH was measured only near the exhaust duct (Fig. 2.2). The exhaust temperature and RH were measured using EE08 humidity temperature sensors (E+E Elektronik, Engerwitzdorf, Austria) (accuracy ± 3% RH and ±0.5 °C) and logged to a Squirrel SQ2040 (Grant Instruments, Cambridge, UK) every 5 minutes. A Vantage Pro2 weather station (Davis Instruments Corp., Hayward, CA, USA) measured and logged the outdoor temperature, RH, solar radiation, wind speed and direction every 5 minutes. The outside and indoor CO_2 concentration were measured with a photoacoustic gas monitor (Innova 1314, Innova Air Tech Instruments, Santa Clara, CA, United States), which was calibrated by the Dutch Metrology Institute VSL per the ISO/IEC 17025 standards. A gas multipoint sampler (CBISS, A1-Envirosciences ltd., Wirral, United Kingdom) sequentially took the gas samples from the sampling locations via Teflon tubes to the gas analyser. Every 30 minutes, the gas analyser consecutively took 4 and 2 gas measurements at the outside and the indoor sampling locations in 2 and 4 minutes, respectively. At each location the last analysed gas sample was selected as the CO_2 concentration for the model validation.

2.2.5. Model application: case study simulations and evaluation criteria

The minimum and maximum ventilation requirements in a pig building differ depending on the country, as guidelines for maximum gaseous concentration levels (CO_2 and NH_3) in animal housing vary from country to country (CIGR, 1984, Table 1.2). In addition, the ventilation settings at the climate computer were shown in Table 1.3 to differ depending on the type of air inlet in the pig building. In Flanders, the ventilation settings for fattening pig buildings were adopted from the Dutch climate platform (Klimaatplatform varkenshouderij, 2008, Van Gansbeke et al., 2009). However, it was not clear how the ventilation settings were obtained. Vranken (1999) previously noted that the T_{set}, VR_{min} and VR_{max} were typically fixed at 20 °C, 10 m^3 h^{-1} pig^{-1} and 80 m^3 h^{-1} pig^{-1}, respectively throughout the fattening period in a fattening pig building in Flanders. Field survey at four fattening pig buildings equipped with UFAD systems during this PhD research revealed that the farmers applied different ventilation settings at the climate computer. The effect of different ventilation settings on indoor temperature, RH, CO_2 concentrations and ventilation rate in a pig building was thus evaluated using the validated indoor climate model. The simulations were performed during the winter and summer fattening periods for nine different ventilation settings (i.e., Treatments 1 – 9 (T1 – T9)) and a reference treatment (T_{ref}) (Table 2.2). The T_{ref} was the ventilation setting that was applied at the ILVO/UGent/HoGent fattening pig building.

Another aim of the case study simulation was to select three ventilation control settings with lower ventilation rates compared to T_{ref} to be tested during the field experiment in chapters 4 and 5. It was assumed that ventilation settings with lower ventilation rate will minimise NH_3 volatilisation from slurry in the pit and pig excretions on the pen floor. As indicated in section 2.1, this is because the air velocity that derives NH_3 volatilisation is closely linked to ventilation rate. However lower ventilation rates reduces indoor quality in animal buildings, therefore a CO_2 concentration limit of 3500 ppm was used as an additional selection criterion. This was checked by binning the simulated results in Microsoft Excel for the CO_2 concentrations and using the time-series plots.

Table 2.2. Ventilation settings in the case study simulations

Treatment	T_{set} (°C)	Weight (kg)	VR_{min} (m^3 h^{-1} pig^{-1})	VR_{max} (m^3 h^{-1} pig^{-1})
Ref	24	20 - 39	14.0	70.0
	23	40 - 59	14.0	70.0
	22	60 - 79	14.0	70.0
	21	80 - 120	14.0	70.0
T1	T_{Ref}	20 - 120	7.0	63.0
T2	T_{Ref}	20 - 120	10.5	66.5
T3	- 2 °C + T_{Ref}	20 - 120	14.0	70.0
T4	2 °C + T_{Ref}	20 - 120	14.0	70.0
T5	2 °C + T_{Ref}	20 - 120	10.5	63.0
T6	4 °C + T_{Ref}	20 - 120	7.0	63.0
T7	24	20 - 39	3.5	56.0
	23	40 - 59	7.0	59.5
	22	60 - 79	10.5	63.0
	21	80 - 120	14.0	70.0

Continue, Table 2.2.

Treatment	T_{set} (°C)	Weight (kg)	VR_{min} (m^3 h^{-1} pig^{-1})	VR_{max} (m^3 h^{-1} pig^{-1})
T8	24	20 - 39	3.5	56.0
	23	40 - 59	7.0	59.5
	22	60 - 79	10.5	63.0
	21	80 - 120	10.5	66.5
T9	25	20 - 39	3.5	56.0
	24	40 - 59	7.0	59.5
	23	60 - 79	10.5	63.0
	22	80 - 120	14.0	70.0

Bandwidth = 5 °C in all treatments; Ref = reference ventilation settings; T_{set} = set-point temperature; T_{Ref} = reference T_{set}.

2.3. Results and discussion

2.3.1. Model validation

The developed model predicted comparable indoor temperature and RH in the experimental compartment at the Deerlijk pig compartment. The adjust correlation coefficients (R^2_{adj}) for the indoor temperature at the nine different sampling locations ranged between 0.57 – 0.70 while the R^2_{adj} for the RH at the exhaust duct was 0.63 (Table 2.3). In addition, the average indoor temperature and RH during the 7-day measurement period were 24.6 ± 0.9 °C and 53.4 ± 4.5% compared to 23.9 ± 0.7 °C and 51.7 ± 3.7% in the steady-state model, respectively.

Table 2.3. Adjusted R^2 (R^2_{adj}), average, minimum (min) and maximum (max) temperature (T) and CO_2 concentration difference between the experimental and simulated results.

Location	R^2_{adj} T	R^2_{adj} CO_2	$\overline{\Delta T}$ (°C)	ΔT min (°C)	ΔT max (°C)	$\overline{\Delta CO_2}$ (ppm)	ΔCO_2 min (ppm)	ΔCO_2 max (ppm)
Pen4H1	0.63	0.03	0.29	-1.86	1.13	-343	-1316	386
Pen4H2	0.59	0.01	1.47	0.16	2.31	-375	-980	160
Pen8H1	0.66		0.67	-1.21	1.68			
Pen8H2	0.57	0.01	1.71	0.28	2.47	-188	-787	500
Pen1H1	0.70		0.05	-1.39	1.03			
Pen1H2	0.59	0.02	0.92	-0.47	1.70	-91	-749	685
Pen12H1	0.58	0.02	0.69	-0.57	1.47	-41	-670	719
Pen12H2	0.58	0.01	0.99	-0.42	1.79	-98	-803	864
Exhaust	0.57	0.03	-0.35	-1.91	0.52	-172	-833	561

Δ means difference between experimental and simulated results; $\overline{\Delta T}$ and $\overline{\Delta CO_2}$ means average temperature and CO_2 concentration difference.

Figures 2.3a and 2.3b show that the developed model captured similar diurnal indoor temperature and RH trends as in the experimental result. However, the steady-state model over-predicted the average CO_2 concentration during the 7-day measurement period by 179 ppm and did not capture the similar diurnal CO_2 concentration trends as the indoor temperature and RH results (Fig. 2.3, Table 2.3).

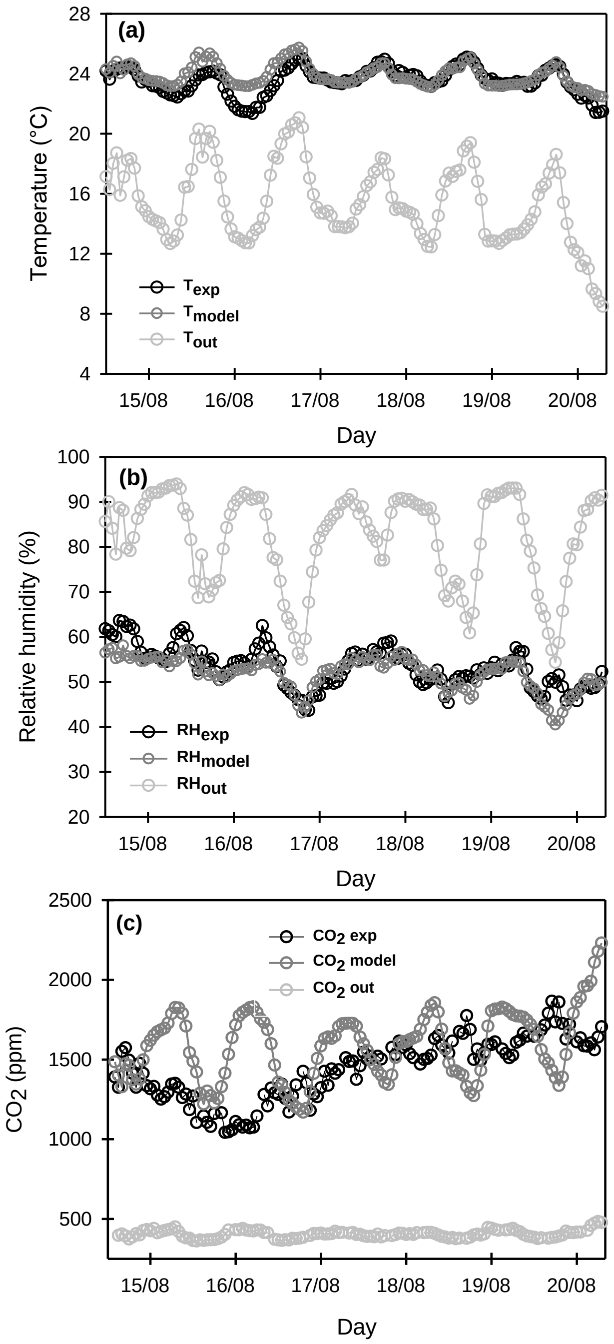

Fig. 2.3 — Diurnal variations in the outside (out), experimental (exp) and simulated (model) exhaust (a) temperature (T) (b) relative humidity (RH) and CO_2 concentration in the pig compartment.

This was probably because the developed model was unable to adequately capture the effect of pig activity on the CO_2 production. Apart from this, the model assumed perfect air mixing, which was not the case in the experimental compartment. The temperature and CO_2 concentration difference between the experimental and simulated results at different sampling locations show the lack of perfect air mixing in the experimental compartment (Figs. 2.4 and 2.5). For instance, air temperature at the higher heights above the pen floor was greater than the temperature measured near the pen floor. That is, the average temperature at H2 was greater than H1 in pen 4, pen 8, pen 1 and pen 12 by 1.4 °C, 1.0 °C, 0.9 °C and 0.3 °C during the measurement period.

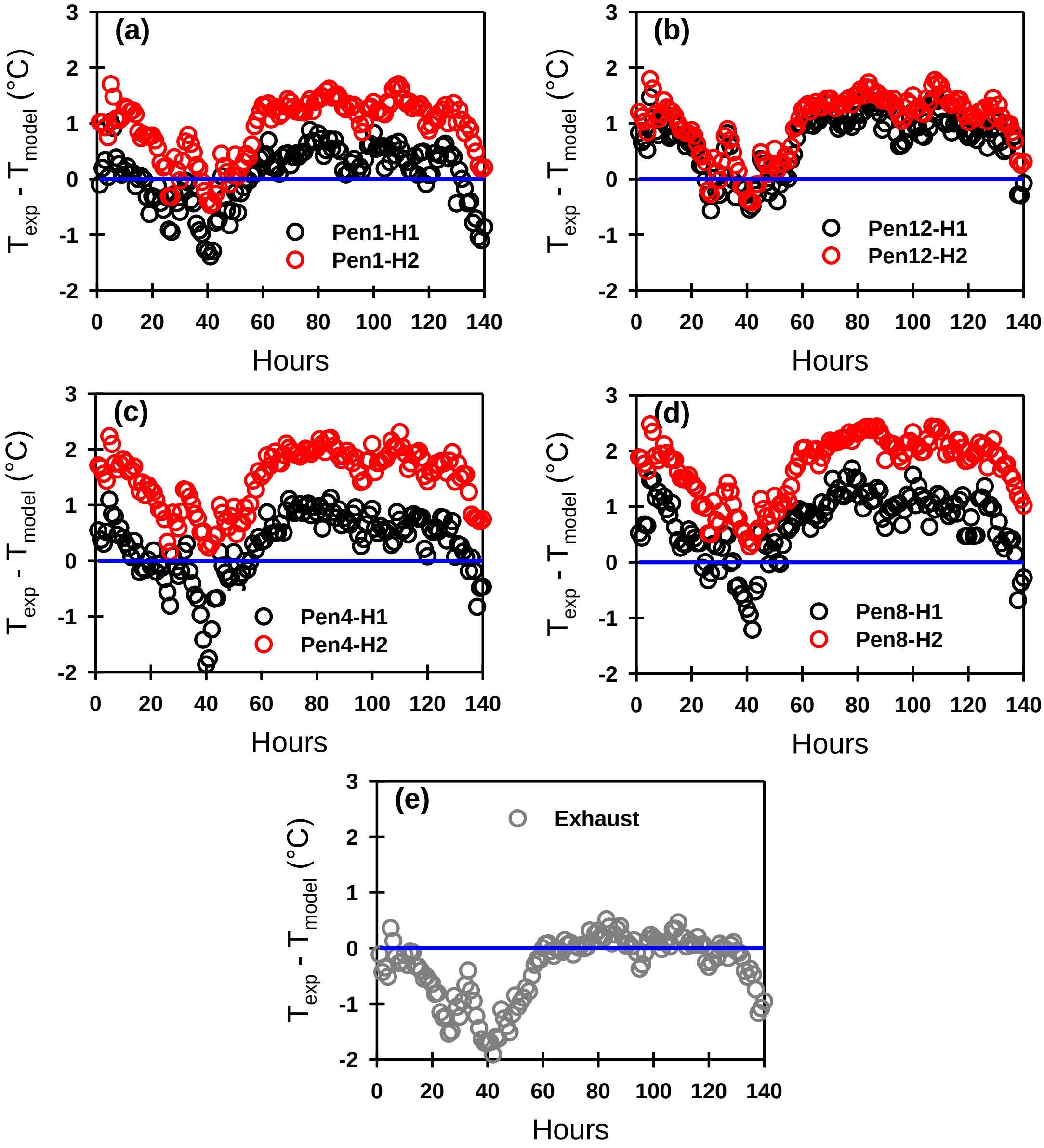

Fig. 2.4 — Temperature difference between the experimental (T_{exp}) and simulated (T_{model}) results at different sampling locations in the pig compartment. H1 and H2 represent sampling 0.5 m and 1.0 m above the slatted floor (Fig. 2.2 illustrates the sampling locations).

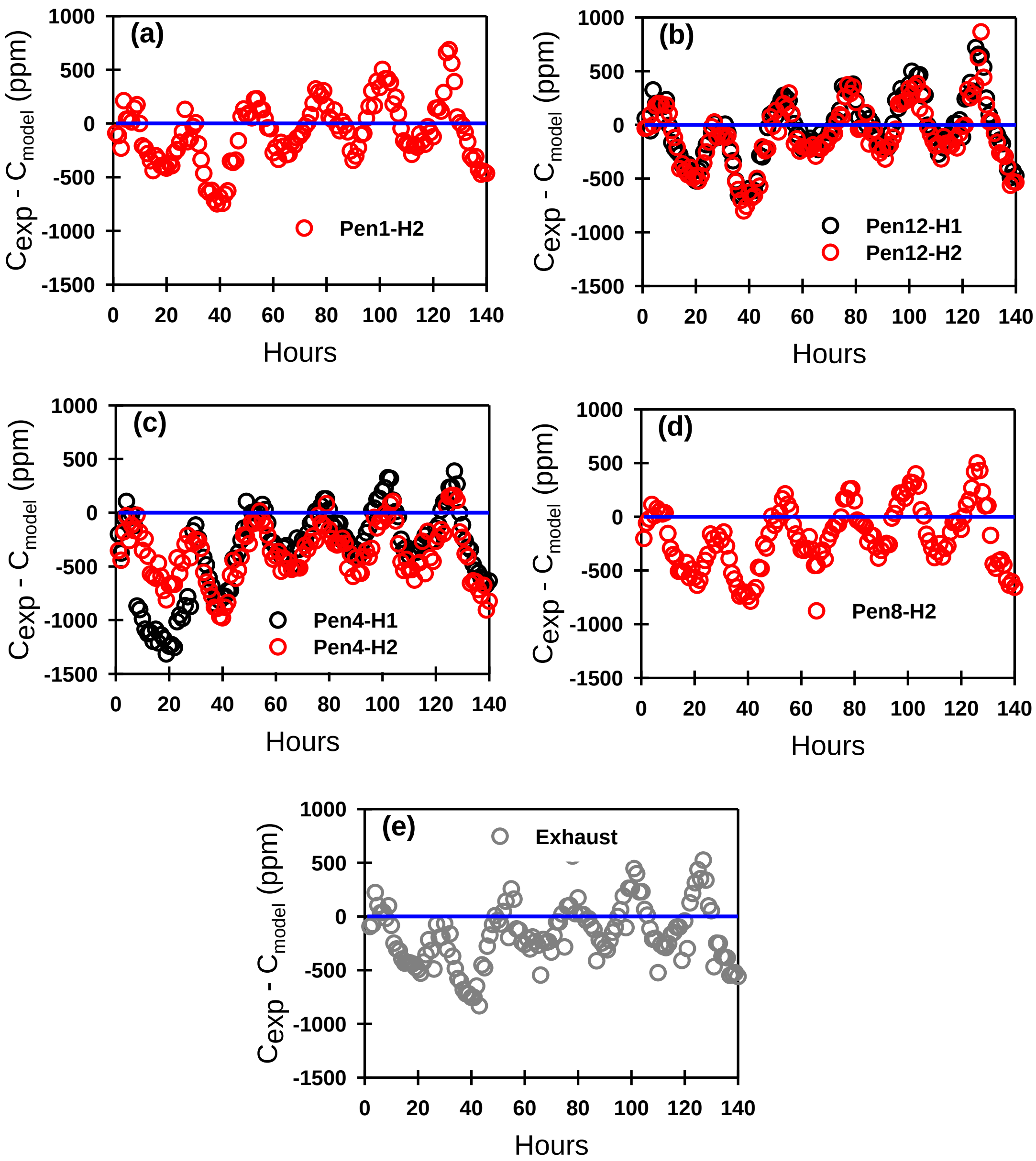

Fig. 2.5 — CO_2 concentration difference between the experimental (C_{exp}) and simulated (C_{model}) results at different sampling locations in the pig compartment. H1 and H2 represent sampling 0.5 m and 1.0 m above the slatted floor (Fig. 2.2 illustrates the sampling locations).

Similarly, the average CO_2 concentration at H2 was greater than H1 in pen 4 and pen 12 by 36 ppm and 59 ppm, respectively. These results agree with the displacement airflow principle in pig buildings equipped with UFAD systems (chapter 1). Apart from the lack of perfect mixing, the discrepancy in CO_2 concentrations was caused by air leakage between the test and neighbouring pig compartment. The manure stored in the slurry pit was only emptied at the end of the fattening period but the contribution of the stored slurry to CO_2 production (Pedersen et al., 2008) was not accounted for in the developed model. In addition, the steady-state model under-predicted the air temperature at the different sampling locations in the experimental compartment (Fig. 2.4). The reason was due to the lack of heat storage in the building walls in the model. Preconditioning of incoming air at the underfloor air channel was not also included in the model. Furthermore, pig urine and faeces deposited on the pen floor, and the slurry pit were additional heat sources which were not included in the model.

2.3.2. Promising ventilation control settings

Tables 2.4 and 2.5 show the average temperature and ventilation rate during the winter and summer simulations in the ILVO/UGent/HoGent pig compartment. Tables 2.4 and 2.5 also show the temperature, CO_2 concentration and ventilation ranges, as well as the percentage of time during the fattening periods that the CO_2 concentrations exceeded 3500 ppm. Figures 2.6 – 2.9 compare to the daily average indoor temperature, RH, CO_2 concentration and ventilation rate between the ten different ventilation settings. Indoor air temperatures in summer was higher than winter in all the ventilation settings due to warmer outside temperature in summer than in winter (Fig. 2.6). Indoor RH was more variable in summer than in winter in the different ventilation settings (Fig. 2.7). The indoor CO_2 concentrations were high in winter than in summer during the fattening period (Fig. 2.8). These results were influenced by the response of the ventilation settings during the two fattening periods.

Table 2.4. Winter simulation results.

Parameters	Reference	T1	T2	T3	T4	T5	T6	T7	T8	T9
Average T_i (°C)	17.8 (4.2)	21.7 (2.1)	19.8 (3.5)	17.2 (3.8)	18.3 (4.8)	20.6 (4.1)	24.3 (9.5)	21 (3.8)	21.7 (8.4)	22.3 (8.4)
T_i range (°C)	3.8 - 24.0	9.5 - 24.5	6.3 - 24.3	3.8 - 22.8	3.8 - 25.3	6.3 – 25.9	9.5 - 28.5	3.8 - 24.8	8.4 - 24.8	8.4 - 25.7
Average VR (m^3 h^{-1})	759 (190)	581 (270)	652 (234)	815 (260)	723 (134)	501 (177)	469 (184)	620 (294)	591 (288)	557 (263)
VR range (m^3 h^{-1})	672 - 2275	336 - 2148	504 - 2211	672 - 2738	672 - 1897	504 - 1818	336 - 1515	168 - 2275	168 - 2211	168 - 2018
CO_2 range (ppm)	904 - 3367	1394 - 4931	1073 - 4222	904 - 3371	904 - 3376	1073 - 4270	1414 - 5397	1338 - 3838	1366 - 4235	1458 - 4256
Time > 3500 ppm (%)	0	8	2	0	0	4	18	1	3	5

The values in the brackets are the standard deviations during the fattening period. The calculations were performed at the 15 minute sampling interval.

Table 2.5. Summer simulation results.

Parameters	Reference	T1	T2	T3	T4	T5	T6	T7	T8	T9
Average T_i (°C)	23.6 (3.1)	24.5 (2.4)	24.1 (2.8)	22.7 (3.2)	24.6 (3.2)	25.2 (2.7)	27.1 (2.1)	24.5 (2.3)	24.6 (2.3)	25.3 (2.1)
T_i range (°C)	6.6 - 38.0	11.2 - 38.4	8.2 - 38.2	6.6 - 38.0	6.6 - 38.0	8.2 - 38.4	11.2 - 38.4	18.7 - 38.0	18.7 - 38.2	18.7 - 38.2
Average VR (m^3 h^{-1})	1619 (903)	1463 (857)	1535 (884)	1893 (957)	1381 (820)	1276 (772)	1040 (708)	1521 (941)	1486 (899)	1367 (871)
VR range (m^3 h^{-1})	672 - 3360	336 - 3024	504 - 3192	672 - 3360	672 - 3360	504 - 3024	336 - 3024	168 - 3360	168 - 3182	168 - 3182
CO_2 range (ppm)	587 - 2492	606 - 2789	597 - 2535	563 - 2230	651 - 2774	674 - 2825	768 - 3178	626 - 3265	626 - 3265	660 - 3447
Time > 3500 ppm (%)	0	0	0	0	0	0	0	0	0	0

The values in the brackets are the standard deviations during the fattening period. The calculations were performed at the 15 minute sampling interval.

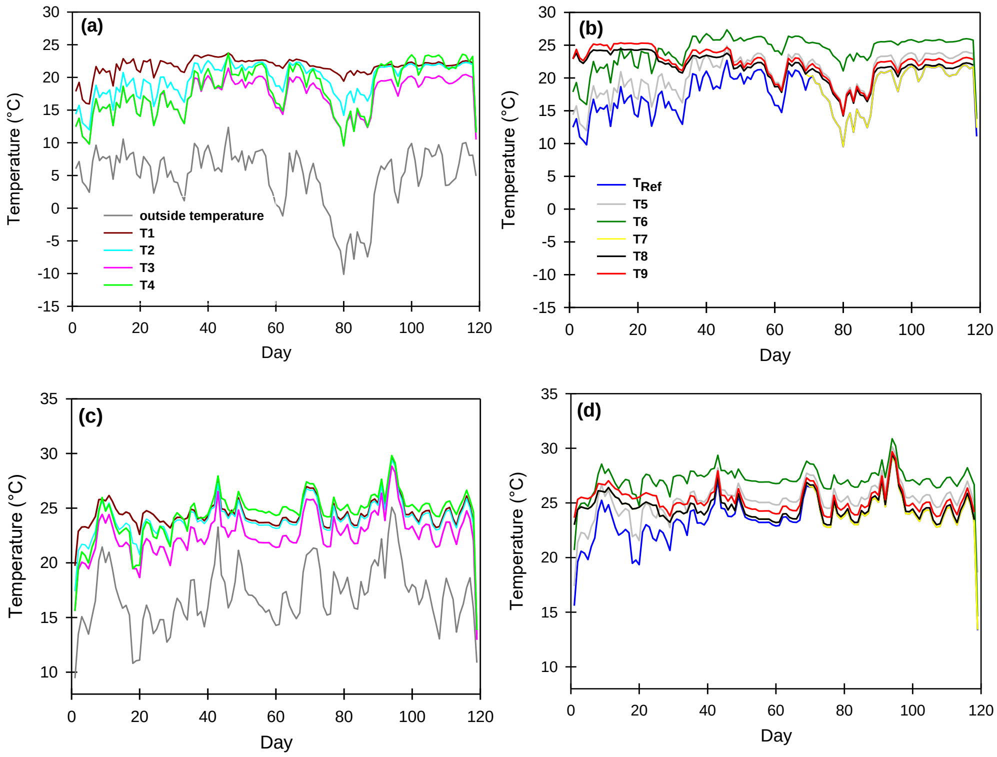

Figure 2.6 — Simulations of the daily average outside and indoor temperature in the reference (T_{ref}) versus ventilation settings in T1 – T9 during (a & b) winter and (c & d) summer.

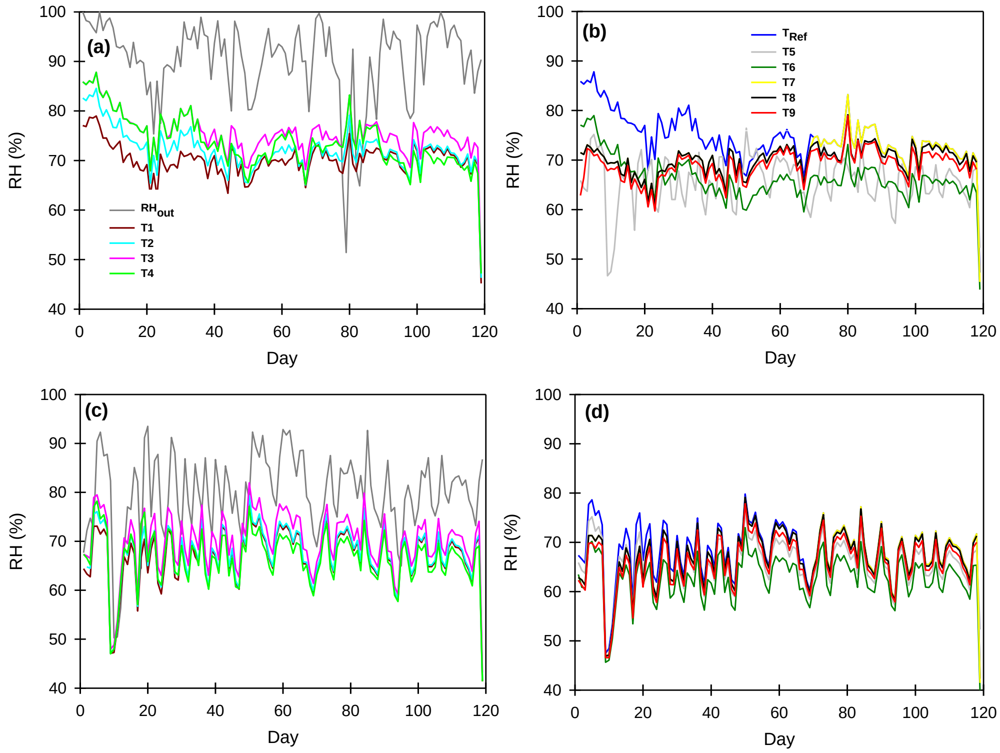

Figure 2.7 — Simulations of the daily average outdoor and indoor relative humidity (RH) in the reference (T_{ref}) versus ventilation settings in T1 – T9 during (a & b) winter and (c & d) summer.

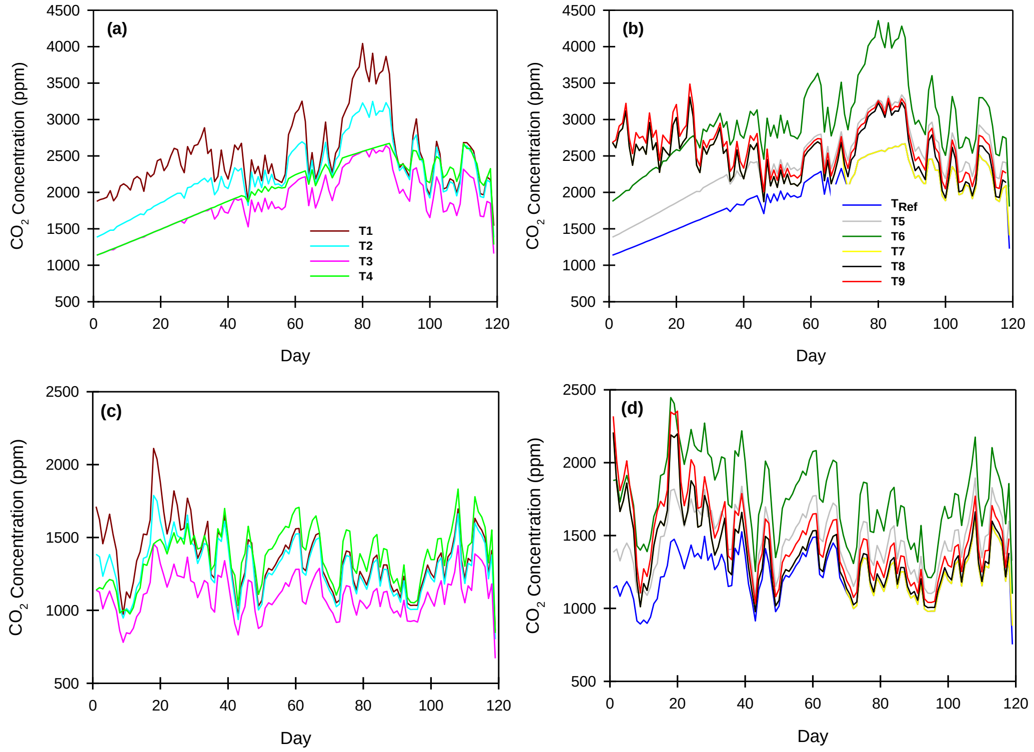

Figure 2.8 — Simulations of the daily average indoor CO_2 concentrations in the reference (T_{ref}) versus ventilation settings in T1 – T9 during (a & b) winter and (c & d) summer.

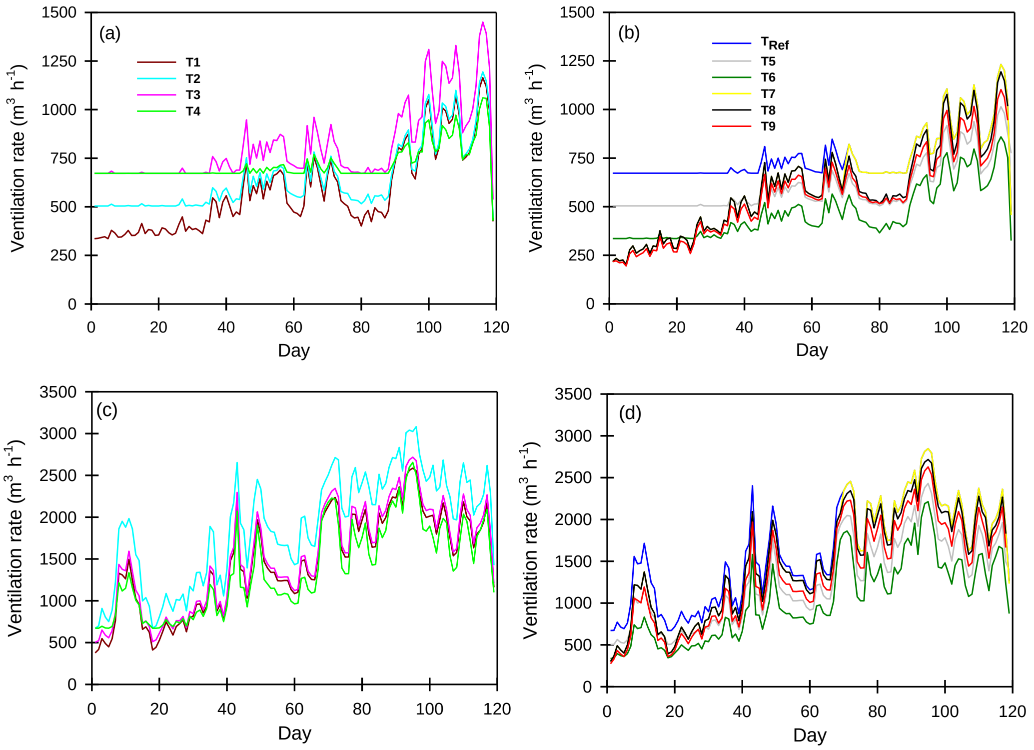

Figure 2.9 — Simulations of the daily ventilation rate in the reference (T_{ref}) versus ventilation settings in T1 – T9 during (a & b) winter and (c & d) summer.

Treatment 4 (T4) was selected as one of the ventilation settings that will be tested during the experiments in chapters 4 and 5. This was because of the lower CO_2 concentrations in winter than T_{ref} and the other eight ventilation settings (Fig 2.8, Table 2.4). In addition, the summer ventilation rate in T4 was lower than T_{ref}, T1, T2 and T3 (Fig. 2.9, Table 2.5). In winter, the average ventilation in T1 and T6 were 23% and 38% lower than T_{ref} (Table 2.4, Fig. 2.9). However, T1 and T6 were considered unsuitable because of the higher the CO_2 concentrations compared to the other ventilation settings during the winter simulation (Fig. 2.8). During 8% and 18% of the fattening period in winter the CO_2 concentrations in T1 and T6 were greater than 3500 ppm, respectively. Although the CO_2 concentration in T3 never exceeded the 3500 ppm concentration limit (Fig. 2.8), it was eliminated as potential ventilation setting because the average ventilation rates were during 7% and 17% of the fattening period greater than T_{ref} in winter and summer, respectively. Thus, the remaining ventilation settings are T2, T5, T7, T8 and T9.

Among the remaining control settings, T5 and T9 were selected as the ventilation settings that will be tested in the experiment in chapter 5 because they had higher reductions in ventilation rate compared to T2, T7 and T8 (Fig. 2.9, Tables 2.4 and 2.5). In T5, the average ventilation rates in winter and summer were reduced by 34% and 21%, respectively, compared to T_{ref}, while the average ventilation rates were reduced by 27% in winter and 16% in summer compared to T_{ref} in T9. The indoor CO_2 concentrations in T5 and T9 at 4% and 5% of the fattening period in winter were greater than the concentration limit of 3500 ppm compared to the 2%, 1% and 3% in the T2, T7 and T8, respectively. However, T5 and T9 were preferred over T2, T7 and T8 as a trade-off for reducing ventilation rate.

2.4. Conclusion

A validated steady-state balance model for predicting indoor temperature, RH and CO_2 concentrations was developed in this chapter. The model predicted comparable diurnal variations as the experimental data for indoor air temperature and RH. The model also predicted acceptable indoor CO_2 concentrations as the experimental results. After validating the model, simulations were performed at nine different ventilation settings compared to a reference setting to select three ventilation settings, which could potentially lower NH_3 emissions. Increasing the set-point temperature by 2 °C and maintaining the minimum (VR_{min}) and maximum (VR_{max}) ventilation settings (T4) as in the ventilation reference settings (T_{ref}) reduced the average ventilation rate by 5% in the winter and 15% in the summer. Increasing the T_{ref} set-point temperature by 2 °C and reducing the VR_{min} and VR_{max} by 5% and 10% (T5) compared to the T_{ref} reduced the average winter and summer ventilation rate by 34% and 21%, respectively. Increasing the set-point temperature by 1 °C and reducing the VR_{min} and VR_{max} as the pigs grow during the fattening period (T9), reduced the average winter and summer ventilation rate by 27% and 16%, respectively. The indoor air quality and NH_3 emission reduction performance of T4, T5 and T9 were tested in the experimental test platform in chapter 4. Field measurements were also performed in a pig rearing house (chapter 5) to validate the results in chapters 4, and to verify whether adjusting the VCS under practical conditions can fulfil the recommended indoor climatic requirements for pig production.

Chapter 3: Developing an experimental test platform (TP) equipped with artificial pigs and automatic urea spraying installation

This chapter was adapted from:

Tabase, R. K., Millet S., Brusselman, E., Vangeyte, J., Sonck, B., & Demeyer, P. (2018). Mimicking indoor climate dynamics and ammonia emission in a pig housing compartment using artificial pigs and an automatic urea spraying installation. *Agricultural Engineering International: CIGR Journal*, *21*(1), 40-50.

3.1. Introduction

The objective of this chapter is to develop two test platform (TP) compartments that can mimic indoor climate and NH_3 emissions from a real pig compartment. The TP compartments were equipped with artificial pigs and an automatic urea spraying installation to simulate pig urination on fully slatted pen floors. The performance of the TP was evaluated in two experiments. The first experiment evaluated the TP performance with respect to indoor climate and NH_3 emissions in one TP compartment and a compartment that was occupied by real pigs. The second experiment compared the performance between two TP compartments. The developed TP compartments were used (chapter 4) to investigate the relative performance and NH_3 transport behaviour using the ventilation control settings that were selected from the steady-state balance model (chapter 2). In addition, the developed TP was used to generate boundary conditions and to check the simulation accuracy of the developed CFD model (chapter 6).

3.2. Materials and methods

3.2.1. Test platform layout

The TP was developed in the fattening pig building at the ILVO/UGent/HoGent pig facility, Merelbeke, Belgium. Figure 3.1 presents the experimental facility. The pig building consists of 16 separate mechanically ventilated fattening pig compartments equipped with UFAD systems (Figs. 2.1 and 3.1). The TP compartments were developed in the two fully slatted pig compartments (13 and 14) which were each divided into eight pens and equipped with the mock-up pigs as heat source and an automatic spraying installation to mimic pig urination/NH_3 production by applying urea solution.

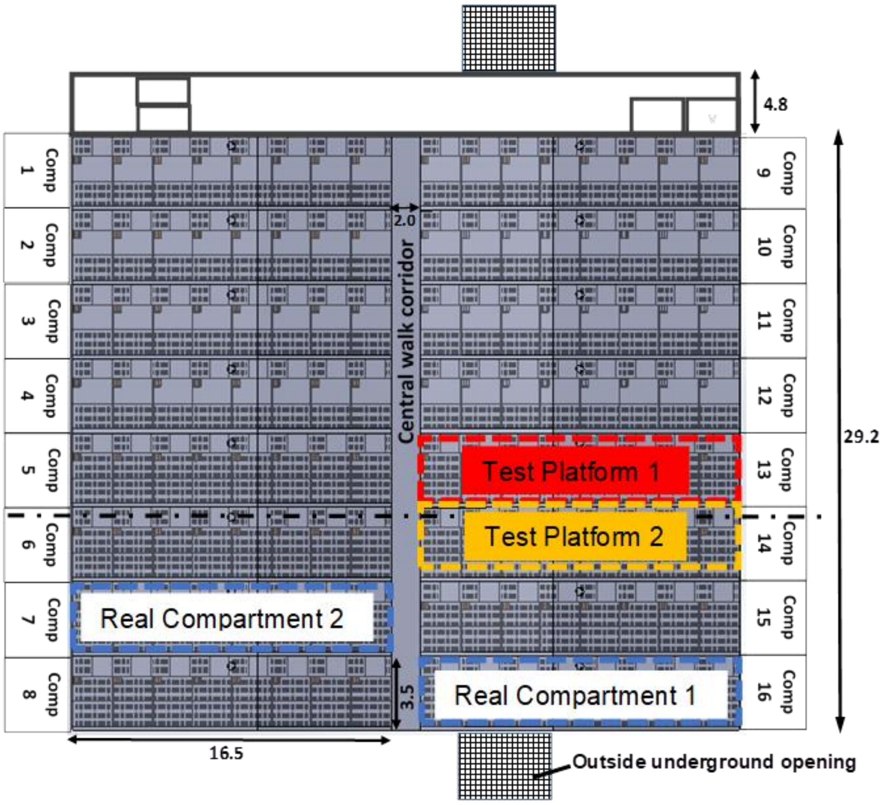

Fig. 3.1 — Plan view of the ILVO/UGent/HoGent fattening pig building (Comp is compartment and all dimensions are in meters).

3.2.2. Heat production system by mock-up pigs

The mock-up pigs were developed from 1.0 mm thick galvanized steel, shaped into semi-cylinders with a diameter of 0.3 m, length of 1.8 m and painted matte black (Fig. 3.2). Both ends of the mock-up pigs were enclosed with steel plates and 18 mm thick plywood insulated them against the floor. Each semi-cylinder represented two headless 50 kg real pigs in sternum lying position. The total exposed surface area of each mock-up pig (semi-cylinder) was approximately 1.0 m^2 as derived from Baxter (1984). Previously, Puma et al. (1999) used cylindrical tubes equipped with light bulb heaters to represent 13 – 35 kg nursery pigs, while Hoff et al. (2000) used semi-cylindrical tubes equipped with cone resistance heaters to simulate the sensible heat from 45 kg pigs in a laboratory scale pig house. In this study the mock-up pigs were heated with electrical heating cables (Danfoss B.V., Rotterdam, the Netherlands). To produce uniform surface temperature, the electrical heating cables were tightly fastened to the internal shell of the metal cases using plastic tie fasteners (Fig. 3.2). A 40 m long, ~300 W electrical heating cable heated two semi-cylinders. The average surface temperature of a mock-up pig was 33 °C (Fig. 3.2c). The surface temperature was measured with a VarioCAM thermographic camera (InfraTec GmbH, Dresden, Germany; range: -40 to

1200 °C; accuracy: ±2 °C). Figure 3.2d shows the mock-up pig arrangement in the pen. The mock-up pigs were located together in the pen powered by a 40 m long heating cable.

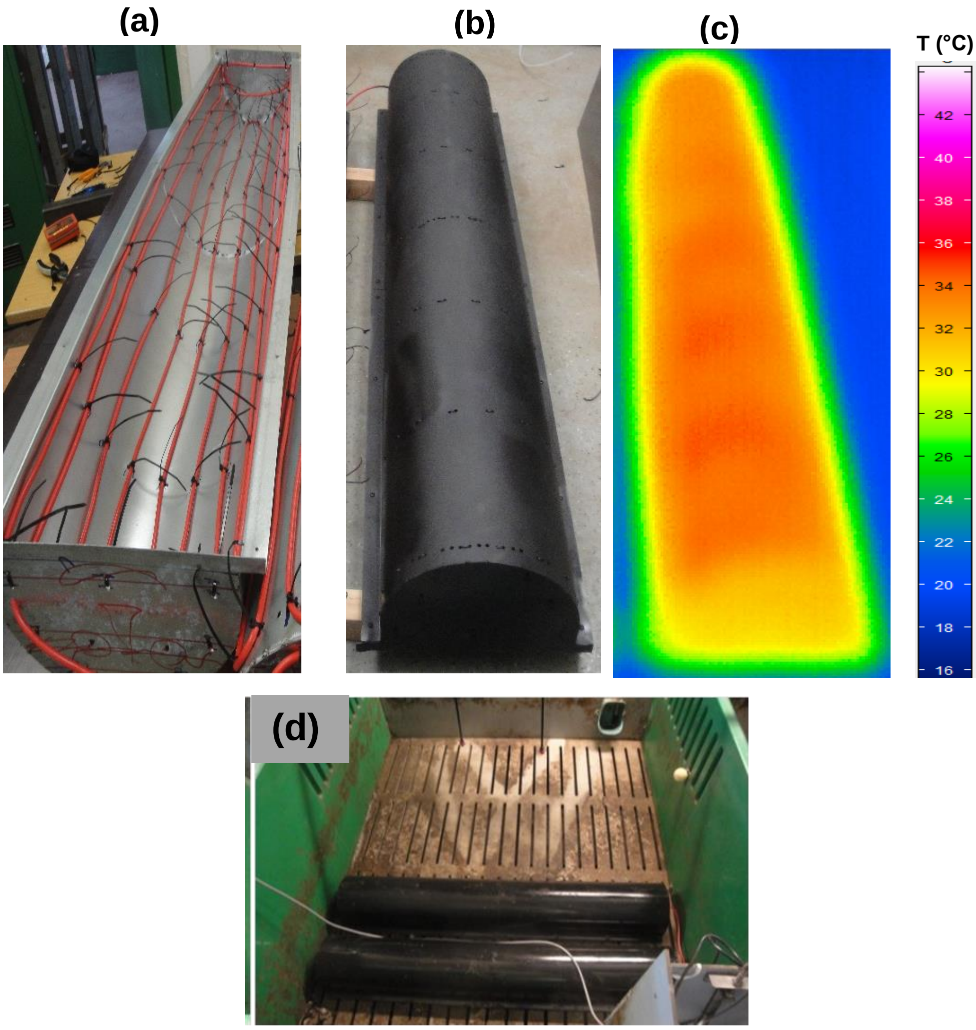

Fig. 3.2 — Mock-up pig development: (a) the internal wiring (b) painted (c) thermographic image of a heated mock-pig and (d) mock-up pig arrangement in the pen.

3.2.3. Urea application system by nozzle spray installation

The TP artificially mimicked pen fouling using an automatic nozzle spray installation developed at ILVO (Fig. 3.3). The study prepared 0.2 mol L^{-1} urea solution, which is within the range (0.1 - 0.6 mol L^{-1}) of real pig urine urea concentration (Canh et al., 1997). For simplicity, other chemical constituents present in real pig urine were not added to the urea solution. To prepare the urea solution of 0.2 mol L^{-1}, the required weight of 99% pure urea granules (Aveve N.V., Leuven, Belgium) were first manually weighed and poured into a 500 L mixing/storage tank after which the control box was programmed to automatically add the required volume of tap water to the tank. The mixture was mechanically stirred until all the urea granules were dissolved. A 1.1 kW centrifugal pump (Grundfos, Bjerringbro, Denmark) recirculated the solution from the mixing tank via a 2.4 kW, 200 L boiler to heat the solution to 37°C. When a three-way valve was switched on, the solution flowed via a 20-mm diameter pipe and was injected via flat jet spray nozzles (Tee jet technologies, Wheaton, IL, USA) in the TP compartment. The TP spray nozzles were arranged along the length of the pen area (Fig. 3.3). Two spray nozzles were arranged per pen at 0.5 m spacing and a height of 0.5 m from the spray nozzle orifice to the floor.

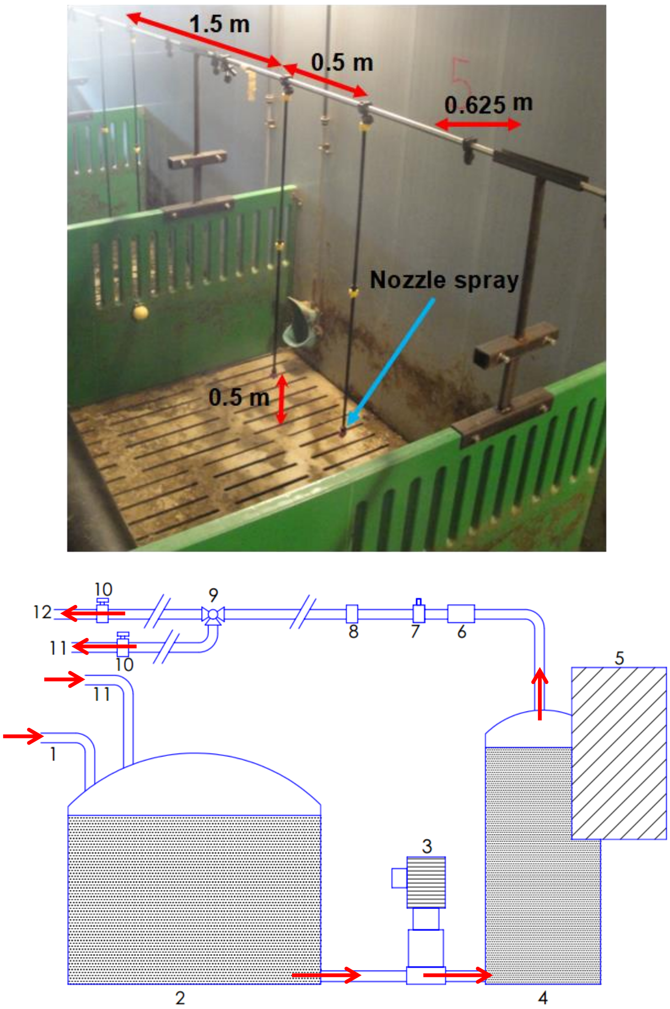

Fig. 3.3 — Nozzle spray installation (1) tap water (2) mixing tank (3) centrifugal pump (4) boiler (5) control box (6) pressure sensor (7) flow meter (8) temperature sensor (9) 3-way valve (10) valve (11) recirculation tube (12) to spray nozzle. The urea solution mixing tank, boiler, control box were located outside the pig building.

The wetted floor area in the TP compartment was estimated by measuring the width and length of the wetted floor in each pen floor after the first and last spray regimes in the experiment and taking the average of both measurements. The fouled pen floor area in the real pig compartment was not quantitatively measured during the experiment. The spray installation automatically applied 12 L urea solution in the TP compartment at 0.99 L min^{-1} in every three hours throughout the day and night at a pressure of 300 kPa and recirculation in the spray tank resumed after each spray regime. Approximately 96 L day^{-1} urea solution was sprayed in the TP. This is equivalent to 3 L pig urine per day, which is within the reported range of fattening pig (50 to 110 kg) urine excretion of 3 - 6 L day^{-1} (Canh et al., 1997). The pH of the prepared urea solution in the first experiment was measured using a compact pH 3310 meter (WTW, GmbH, Weilheim, Germany) each day. The second experiment urea solution pH was measured using a HACH pHC101 meter (HACH LANGE, GMBH, Düsseldorf, Germany).

3.2.4. Experiments to compare TP performance with a real pig compartment

The investigation conducted two separate experiments. In the first experiment, compartments 14 and 16 (Fig. 3.1) were used as the TP and real pig compartments, respectively from 7 – 11 July 2016. The experiment compared NH_3 emission rate, indoor temperature, relative humidity (RH), slurry and slurry pit headspace temperature between the TP and real pig compartments. To produce a similar ventilation pattern in both compartments, approximately 4.8 kW was continuously produced by 32 mock-up pigs (4 mock-ups per pen) in the TP compartment to simulate sensible heat production by the 32 pigs of 79 to 84 kg in the real compartment (CIGR, 2002). During the experiment, the calculated energy balance from ventilation and transmission heat loss (156 W pig^{-1}) in the compartment occupied by the real pigs was similar to the total heat input in the TP compartment (150 W pig^{-1}). On the contrary, the sensible heat production (134 W pig^{-1}) calculated from the CIGR (2002) equations for the pigs in the real compartment underestimated the ventilation and transmission heat loss. The investigation calculated the sensible heat Q_S (W) production from the real pigs using the CIGR (2002) heat and moisture production models (Eq. 2.8 - 2.10).

As indicated in chapter 2, Q_{tot} (W) is the total heat production at the thermoneutral temperature of 20°C. m is pig weight (at 82 and 25 kg in the first and second experiments, respectively), n is the maintenance energy coefficient (3.19 in the first experiment and 3.09 in the second experiment) at growth rate of 800 g day^{-1} in the Netherlands and K_S (0.95) is the correction factor for sensible heat production at the house level in a Northern European pig house. T_c is the measured average temperature in the compartment (at 25°C and 24°C in the first and second experiments, respectively). The total sensible heat production is the sum of Q_S and the pig activity heat production. The pig activity heat production is assumed as 8.6% of the metabolizable energy intake ($n \times 5.09m^{0.75}$) from Labussière et al. (2013). The ventilation heat and transmission heat loss in the real pig compartment of the first experiment was calculated using Table 2.1 and 3.1, and Equations 3.1 – 3.9 assuming a perfectly mixed room air, steady-state conditions and no significant contribution of solar and light heating.

$$Q_{VR} = VR \times \rho \times C_p \times (T_i - T_{GC}) \tag{3.1}$$

$$Q_{sidewall_{out}} = A_{sidewall_{out}} \times U_{sidewall_{out}} \times (T_{out} - T_i) \tag{3.2}$$

$$Q_{sidewall_{in}} = A_{sidewall_{in}} \times U_{sidewall_{in}} \times (T_{comp_{15}} - T_i) \tag{3.3}$$

$$Q_{endwall_{out}} = A_{endwall_{out}} \times U_{endwall_{out}} \times (T_{out} - T_i) \tag{3.4}$$

$$Q_{endwall_{in}} = A_{endwall_{in}} \times U_{endwall_{in}} \times (T_{out} - T_i) \tag{3.5}$$

$$Q_{roof_{out}} = A_{roof_{out}} \times U_{roof_{out}} \times (T_{out} - T_i) \tag{3.6}$$

$$Q_{window} = A_{window} \times U_{window} \times (T_{out} - T_i) \tag{3.7}$$

$$Q_{floor} = A_{floor} \times U_{floor} \times (T_{slurry} - T_{ground}) \tag{3.8}$$

$$Q_{shell} = Q_{sidewall_{out}} + Q_{sidewall_{in}} + Q_{endwall_{out}} + Q_{endwall_{in}} + Q_{roof_{out}} + Q_{floor} \tag{3.9}$$

Where, Q = heat loss (W); T_i, T_{GC}, T_{out}, $T_{comp_{15}}$, T_{slurry}, and T_{ground}= room, ground channel , outside, compartment 15 (Fig. 3.1), slurry and ground temperature (°C); A = area (m^2); U = U-value ($W\ m^{-2}\ K^{-1}$); VR = ventilation rate ($m^3\ s^{-1}$); C_p = specific heat capacity of air ($J\ kg^{-1}\ K^{-1}$); ρ = density of air ($kg\ m^{-3}$).

Table 3.1. Measured mean parameters used to calculate the ventilation and transmission heat loss from the real pig compartment in the first experiment.

Parameter	**Value**
Ventilation rate ($m^3\ s^{-1}$)	0.56
T_i (°C)	25
T_{GC} (°C)	19
T_{out} (°C)	20
T_{slurry} (°C)	20
T_{ground} (°C)	16
ρ_{in} ($kg\ m^{-3}$)	1.208
C_p ($J\ kg^{-1}\ K^{-1}$)	1006

The second experiment used compartments 13 and 14 simultaneously as the TP compartments and compartment 7 as the real pig compartment (Fig. 3.1) from 19 – 21 June 2017. The experiment compared NH_3 concentration and emission, indoor temperature and ventilation rate between the two TP compartments and the real compartment. In each TP, 16 mock-up pigs were placed (2 mock-ups per pen), continuously producing approximately 2.3 kW throughout the experiment, simulating sensible heat production by 32 growing pigs at approximately 50 kg (CIGR, 2002). The calculated total sensible heat production in the real pig compartment from 48 pigs at 25 kg according to the CIGR (2002) heat production equations was 2.6 kW.

3.2.5. Pit slurry and pen fouling

The TP compartment in the first investigation initially housed 25 to 60 kg pigs to foul the pen floors. The pigs were removed to an adjacent empty compartment before the experiment. The fouled floors were expected to contain enough urease enzyme to produce NH_3 during the urea spraying (Braam et al., 1997a). There was neither faecal deposition nor the use of artificial urease enzyme during the investigation. The TP compartment was left empty for 86 days before the start of the experiment and pigs occupied the real compartment from 20/04/2016 until 07/07/2016 when the experiment started. Both the real and TP compartment slurry pits contained ~ 0.14 m slurry depth after emptying and refilling them with slurry from a slurry storage tank before the experiment started.

The slurry storage tank contained a mixture of slurry from the fattening, farrowing, weaner and sow pig units. Slurry samples were randomly collected every day from five locations in the slurry pit from the top surface of the slurry to about 50 mm deep below the surface and stored at -18°C for total ammoniacal nitrogen (TAN) and pH analysis. A C3010 Multi-parameter analyzer (Consort bvba, Turnhout, Belgium) measured slurry pH and the slurry TAN concentration was analyzed with a Kjeltec 8400 analyzer (FOSS, Hilleroed, Denmark) using the BAM procedure (BAM/deel 3/05, 2015). The liquid slurry in the real compartment during the experiment had average TAN concentration of 1.76 ± 0.17 mg g^{-1} and pH of 7.10 ± 0.10 and the TP compartment had an average TAN concentration of 1.74 ± 0.14 mg g^{-1} and pH of 7.23 ± 0.07.

Real pigs in the second experiment occupied the compartment five days before the start of the experiment. Before occupying the real compartment, the pen floors were soaked with KENO™SAN (CID LINES N.V., Ieper, Belgium), cleaned with high-pressure hose and disinfected with VIROCID® (CID LINES N.V., Ieper, Belgium). The slurry pit was emptied before the pigs occupied the compartment. Slurry analyses were not performed in the real pig compartment because of a different ongoing experiment in this compartment. The TP compartments housed real pigs from ~25 kg until the slaughter weight to foul the pen floors. The TP compartments in the second experiment were emptied 5 and 18 days respectively before the start of the test. The slurry pits in the two TP compartments were emptied and refilled to slurry depth of 0.14 m, and randomly collected slurry samples from the top surface of the slurry to about 50 mm deep below the surface at the start and end of the test. The liquid slurry TAN concentration and pH were 2.46 mg g^{-1} and 7.28 at the start of the experiment and 2.06 mg g^{-1} and 7.70 at the end of the experiment in TP 1. The liquid slurry TAN concentration and pH were 2.09 mg g^{-1} and 7.66 at the start of the experiment and 1.90 mg g^{-1} and 7.90 at the end of the experiment in TP 2 (Fig. 3.1).

3.2.6. Indoor climate monitoring system

Indoor climatic conditions were continuously measured using EE08 RH & temperature sensors (E+E Elektronik, Engerwitzdorf, Austria) (Range: 0 to 100% RH, -10°C to 80°C temperature; accuracy ±3% RH and ±0.50°C) and U-type thermistors (Grant Instruments, Cambridge, UK), (range: -50°C to 150°C and accuracy < 0.2ºC). The EE08 sensor measured RH and temperature at the exhaust duct while the U-type thermistors measured slurry headspace and slurry temperature. Slurry headspace and liquid slurry temperatures were measured at 0.35 m above and 0.10 m below the slurry surface, respectively. All measured data were logged to a Squirrel SQ2040 (Grant Instruments, Cambridge, UK) data logger in 2 min interval. A Pt1000 (-50°C to +100°C) sensor of the “Hotraco System” (Hotraco Agri, Hegelsom, the Netherlands) measured the climate control temperature of the experimental compartments, 1.4 m above the floor in pen 3 (Figure 2.1c). The climate control temperature sensor was located at the same location in all other compartments at the experimental facility. Pt1000 sensors also measured the outside and the central underground air channel temperatures. In the central underground air channel the temperature sensor was located 2 m above the floor. The outside temperature sensor was located 1.4 m above the ground, under the eastern eave roof of the building.

The 'Hotraco System' controlled and measured ventilation rate. Ventilation rate was calculated from the measured exhaust duct damper opening size and the differential pressure between each compartment and the overhead central exhaust channel that was previously validated in a wind tunnel by 'Hotraco' (Hotraco Agri, Hegelsom, the Netherlands). An Orion-VS12 data logger (Hotraco Agri, Hegelsom, the Netherlands) logged ventilation rate, climate control temperature, outdoor and the central underground air channel temperatures in 1 min interval. A Fourier transform infrared spectrometer (FTIR) gas analyzer (Gasmet CX4000, Gasmet Technology Oy, Helsinki, Finland) monitored exhaust, slurry pit headspace and outside NH_3 concentrations during the study. The pit headspace gas sampling tubes were positioned 0.35 m above the slurry surface. After basic calibrations at Gasmet (Helsinki, Finland), the FTIR performed zero-point calibrations once every morning using N_2 gas during the investigation. The FTIR sequentially took three measurements per sample location every 30 minutes.

3.2.7. Ventilation system

A climate computer automatically controlled ventilation rate in both the TP and real compartments to maintain an indoor temperature of 22°C at minimum and maximum ventilation rates of 8 and 77 $m^3 h^{-1} pig^{-1}$ and a bandwidth of 5°C in the first experiment. The compartments in the second test had minimum and maximum ventilation settings at 14 and 70 $m^3 h^{-1} pig^{-1}$ to maintain an indoor temperature of 23°C at a bandwidth of 5°C. This represents the temperature set-point for 40 – 60 kg fattening pigs in the TP compartments. The set-point temperature in the real compartment was at 24°C for 20 – 40 kg pigs. The different set-point temperature in the TP compartments and the real compartment was because of another ongoing experiment in real pig compartment and could not be interfered with.

3.2.8. Data analysis

The study analysed all measured parameters using their hourly averages and calculated gaseous emission rates (ER) as the product of the ventilation rate and the gaseous concentrations. Six-data samples per hour per sample location from the FTIR were averaged for the gaseous concentrations. The hourly averages of ventilation rate and gaseous concentrations calculated the ER ($g h^{-1}$) as in equation 3.10:

$$ER = VR \times (C_{ex} - C_{out}) \tag{3.10}$$

Where VR ($m^3 h^{-1}$) is the ventilation rate, while C_{ex} and C_{out} ($g m^{-3}$) represent exhaust and incoming NH_3 concentrations respectively. SigmaPlot (Systat Software, San Jose, CA) was used to perform simple linear regression analysis and the graphical comparison of the hourly measured parameters between the TP and real compartments.

3.3. Results and discussion

Figure 3.4a compares the hourly ventilation rate and exhaust temperature between the TP and real compartments in the first experiment. During the measurement, the TP compartment recorded an average ventilation rate and exhaust temperature of 1916 ± 214 $m^3 h^{-1}$ and 25.0 ± 0.8°C compared to 2003 ± 236 $m^3 h^{-1}$ and 25.3 ± 1.1°C in the real compartment. The linear correlation (R^2) between the real and the TP compartments for the ventilation rate was 0.87. The R^2 for the exhaust temperature between the two compartments was also 0.87. The real compartment recorded slightly higher daily ventilation and exhaust temperature values than the TP compartment except between 03:00 - 10:00 a. m. in the second and third day of the experiment when the contrary was observed (Fig. 3.4a). Diurnal variations in pig activity/heat production seemed to explain this trend. That is active pig periods yielded higher indoor temperature/ventilation rate in the real compared to the TP compartment, and vice versa in less active periods. A larger linear relationship (R^2 = 0.97) was recorded between the TP and the real compartment for RH (Fig. 3.4b) although respiratory moisture production was not simulated in the TP compartment. Clearly, moisture evaporation from the larger wetted floor area in the TP compartment compensated for respiratory moisture production in the real compartment as similar ventilation/temperature were observed in both compartments.

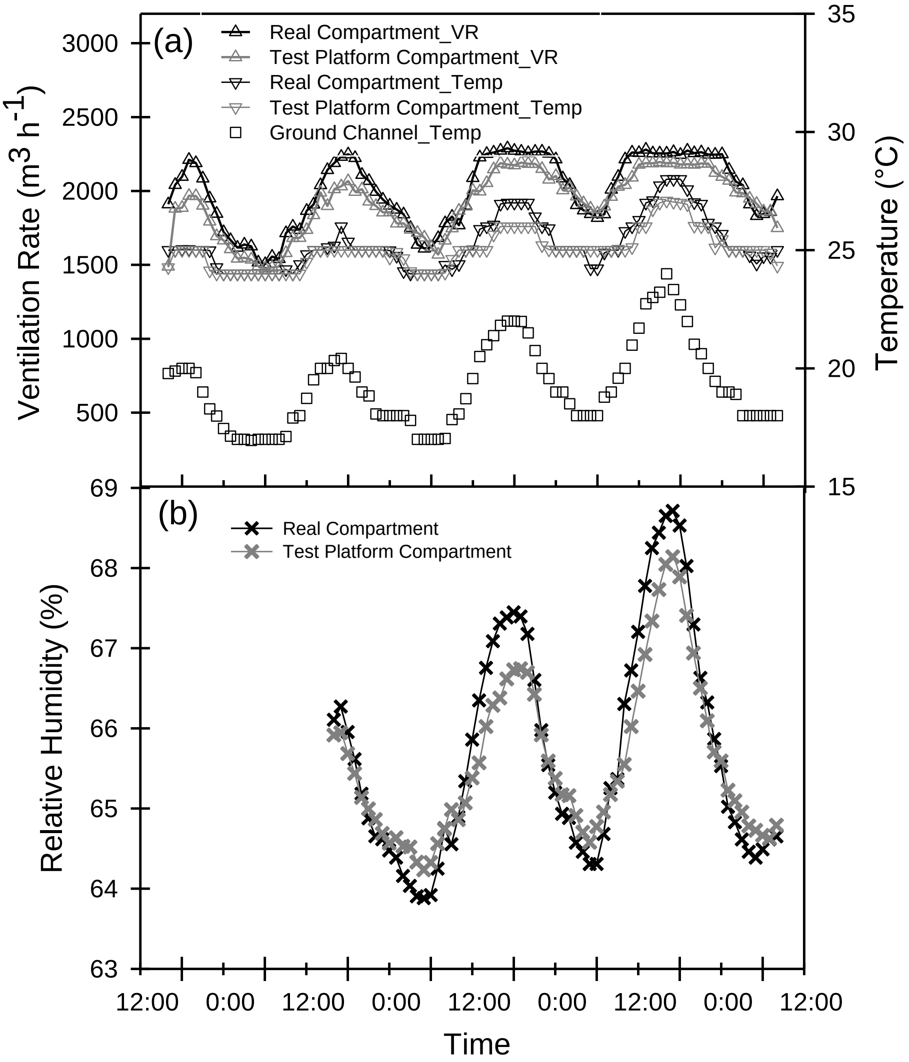

Fig. 3.4 — Diurnal temperature and RH for the first experiment (the missing data in RH was due to instrument failure) (a) ventilation rate, exhaust and outside temperature (b) RH in the real and TP compartment.

In the second experiment, the two TP compartments also produced similar diurnal trends in indoor temperature and ventilation rate as the real pig compartment, despite the different set-point temperatures, pig weight and number (Fig. 3.5). The differences in set-point temperatures, pig weight and number between the real and TP compartments is seen to result in relatively higher ventilation rates (31% – 46%) in the real pig compartments compared to the two TP compartments (Fig. 3.5b). Nonetheless, the indoor temperature in TP 1 and TP 2 linearly correlated with the real pig compartment at an R^2 of 0.96 and 0.97, respectively. Also, the ventilation rate in TP 1 and TP 2 linearly correlated with the real pig compartment at an R^2 of 0.95 and 0.97, respectively. The larger linear relationship in the indoor temperature (R^2 = 0.99) and ventilation rate (R^2 = 0.97) between TP 1 and TP 2 confirmed the similar diurnal variations in indoor temperature and ventilation rate between the two TP compartments (Fig. 3.5).

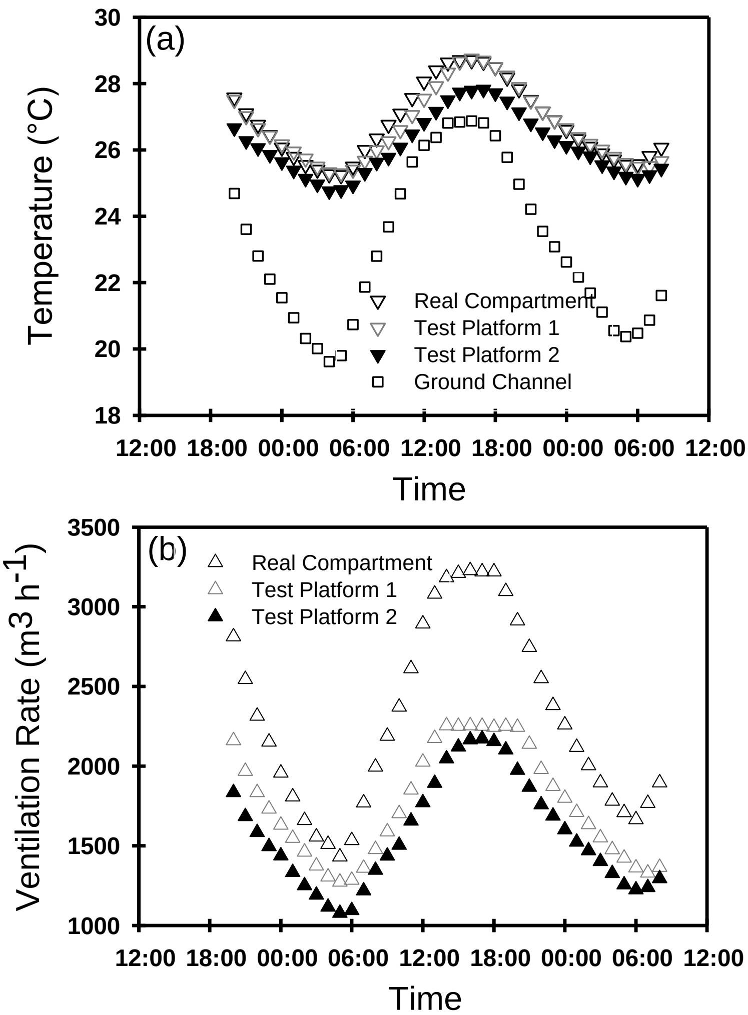

Fig. 3.5 — Diurnal temperature and ventilation rate in the real and TP compartments for the second experiment (a) exhaust and outside temperature (b) ventilation rate in the real and TP compartments for the second experiment.

Figure 3.6 compares the diurnal exhaust NH_3 concentration and emission rate between the real and the TP compartment in the first experiment. That are compartment 16 and 14, respectively (Fig. 3.1). An average NH_3 concentration of 7.7 ± 2.2 ppm was measured in the TP compartment compared to 5.8 ± 1.3 ppm in the real compartment (R^2 = 0.49). A lower linear correlation (R^2 = 0.27) was obtained for NH_3 emission between the TP and the real compartment as the TP produced higher NH_3 emissions (9.9 ± 2.6 g h^{-1} ~ 2.7 ± 0.7 kg pig^{-1}

year^{-1}) than the real compartment (7.6 ± 1.5 g h^{-1} ~ 2.1 ± 0.5 kg pig^{-1} year^{-1}). However, the scatter plot of the paired NH_3 emission differences between the real and test platform compartments, versus the paired mean NH_3 emission rates showed that 95% of the points fell within limit of agreement. This demonstrate good agreement between the data collected in the TP and real compartments (Fig. 3.7; Bland and Altman, 1986).The mean of the paired NH_3 emission differences in the real and test platform compartments was 2.7 g h^{-1}. In addition, the approximated emission factors were comparable to the 2.3 ± 2.0 to 3.5 ± 0.9 kg pig^{-1} year^{-1} for fully slatted pig buildings in Belgium (Philippe et al., 2007; Ransbeeck et al., 2013). The cited emission factors, however, were obtained from measured data spread over the whole year while calculated for only four days data in this study.

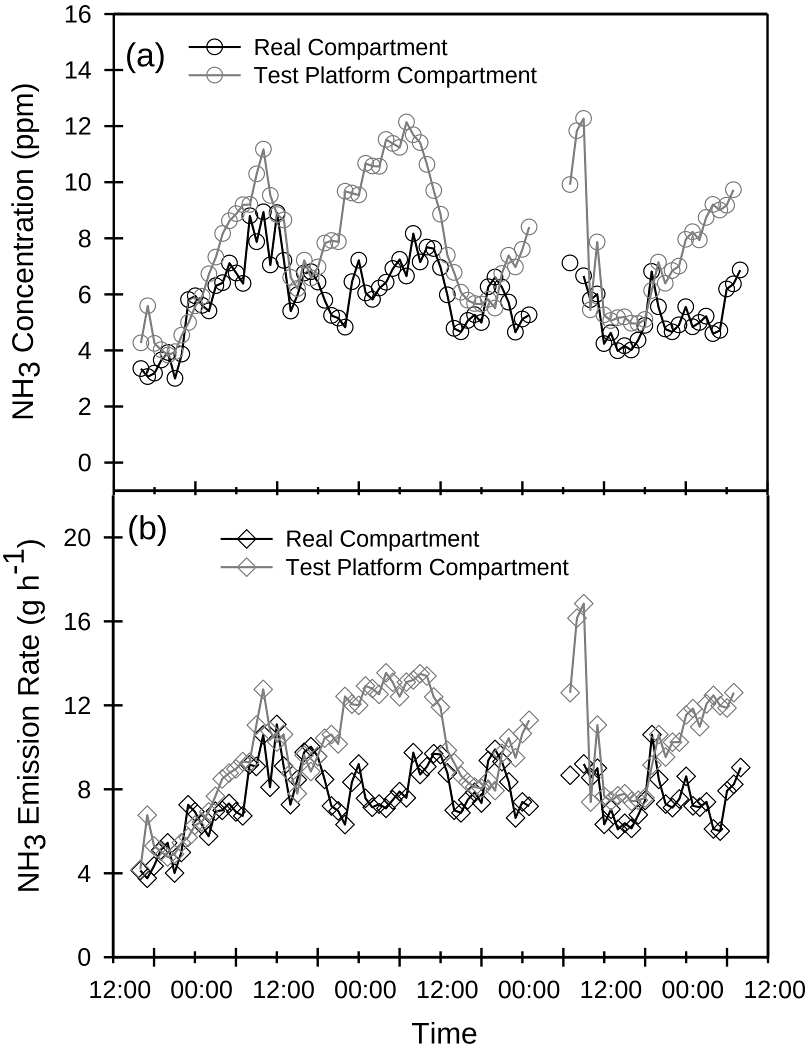

Fig. 3.6 — Diurnal exhaust NH_3 concentration and NH_3 emission rate in the real and TP compartment for the first experiment (missing data due to instrument failure) (a) exhaust NH_3 concentration (b) NH_3 emission rate

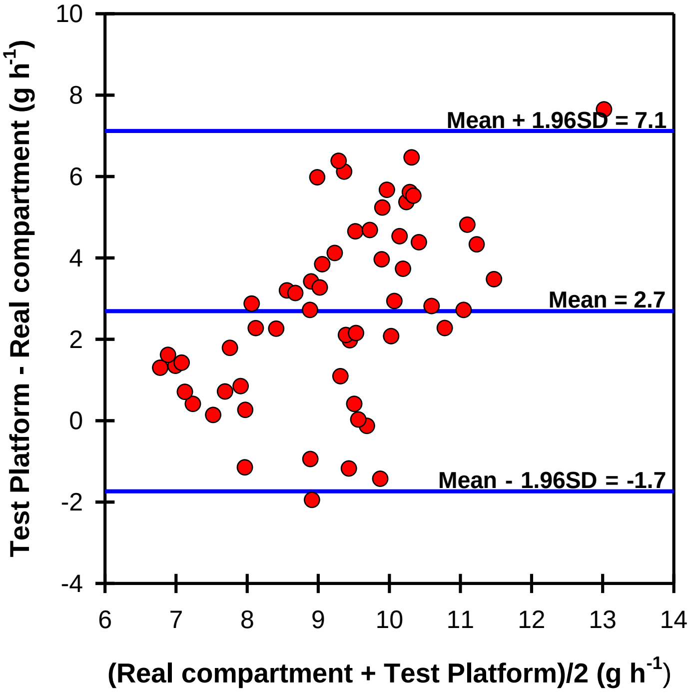

Fig. 3.7 — Plot of NH_3 emission differences between the real and test platform compartment relative to the mean NH_3 emission rates. 57 hourly measurements were taken in each compartment. SD is the standard deviation of the difference in of the NH_3 emission between the two compartments.

In the second experiment, the average hourly NH_3 concentration was 11.5 ± 4.1 ppm vs. 11.6 ± 2.8 ppm in TP 1 and TP 2, respectively (Fig. 3.8a). The average hourly NH_3 emission rate was 13.2 ± 3.0 g h^{-1} vs. 12.1 ± 2.9 g h^{-1} (R^2 = 0.63). Overall, the difference in NH_3 emission rate was 9% on average (Fig. 3.8b), which suggests a good repeatability for this kind of experiments. Of course, random errors occurred from the measurement equipment and in the ventilation rate (Fig. 3.5b) since there was about 10.5% difference in ventilation rate between the two TPs. Nevertheless, the scatter plot (Fig. 3.9a) of the paired NH_3 emission differences between TP1 and TP2 versus their paired mean NH_3 emission rates showed that 95% of the points fell within limit of agreement, demonstrating good agreement between the data collected in the two TP compartments (Bland and Altman, 1986). Indeed, the mean of the paired NH_3 emission differences between the two TP compartments was 1.2 g h^{-1}.

In contrast, limits of agreement of NH_3 production in TP1 and TP2 compared to the real compartment in the second experiment was wider than the first experiment (Figs. 3.7, 3.9b & 3.9c). However, 95% of the points in the scatter plot still fell within limits of agreement band. Furthermore, the test compartments in the second experiment captured a better diurnal trend in the NH_3 concentration and emission rate in the real pig compartment compared to the first experiment, although they both still overestimated the NH_3 emission (Fig. 3.8). The average hourly NH_3 concentration and emission rate were 5.4 ± 1.8 ppm and 7.5 ± 1.8 g h^{-1} in the real compartment compared 11.5 ± 3.9 ppm and 12.7 ± 3.0 g h^{-1} in the two TP compartments, respectively in the second experiment. TP 1 and TP 2 overestimated the average NH_3 emissions of the real compartment by 38% ($R^2 = 0.36$) and 44% ($R^2 = 0.37$), respectively.

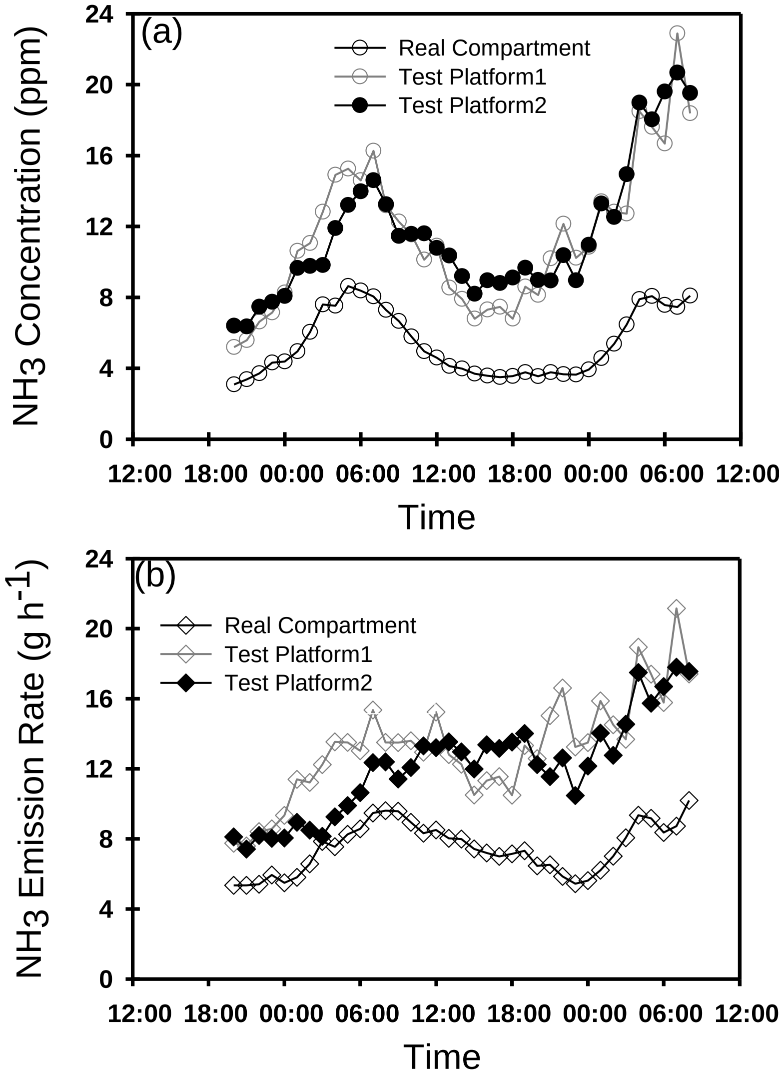

Fig. 3.8 — Diurnal exhaust NH_3 concentration and emission rate in the real and TP compartments during the second experiment (a) exhaust NH_3 concentration (b) NH_3 emission rate.

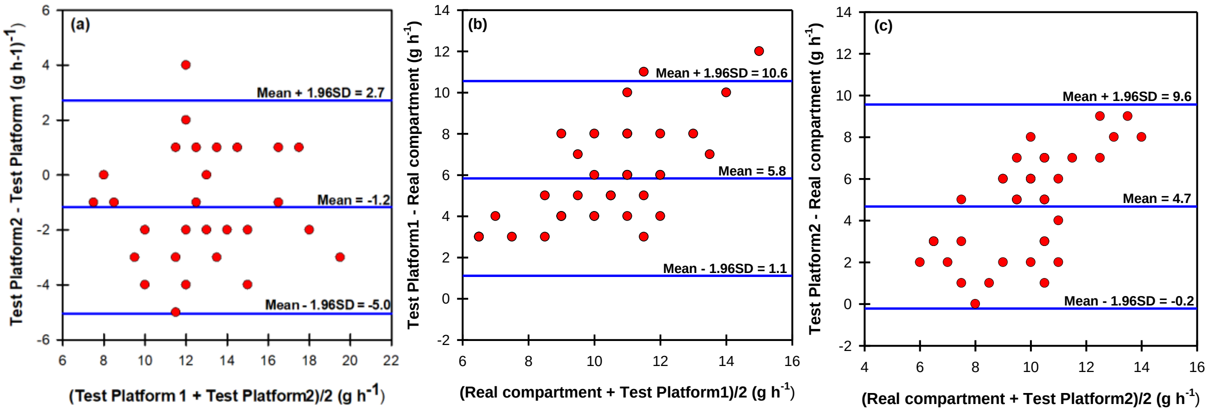

Fig. 3.9 — Bland–Altman plot of NH_3 emission differences between (a) real and test platform 1, (b) real and test platform 2 and (c) test platform 1 and test platform 2 compartments, relative to the average NH_3 emission rates. 37 hourly measurements were taken in each compartment. SD is the standard deviation difference in of the NH_3 emission between two of the compartments.

Figure 3.10 shows the diurnal slurry pit headspace NH_3 concentrations, temperature, and liquid slurry temperature in the first experiment. On average, the liquid and pit headspace temperature in the real compartment were 1.1°C ± 0.1°C and 2.3°C ± 0.5°C respectively, higher than the TP compartment. The lack of conductive heat transfer from mock-up pigs (insulated against the floor) positioned at the same location on the slatted floor throughout the experiment could explain the lower slurry pit temperatures in the TP compared to the real compartment. However, despite the higher slurry and headspace temperatures in the real compartment relatively lower headspace NH_3 concentrations were measured in the real than the TP compartment (Fig. 3.10a). The lack of faecal deposition in the TP compartment could have interfered with the results. Additionally, pig movement and heat production on the slatted floor by lying pigs, probably promoted higher airflow and interfered with the pit airflow pattern in the real compartment.

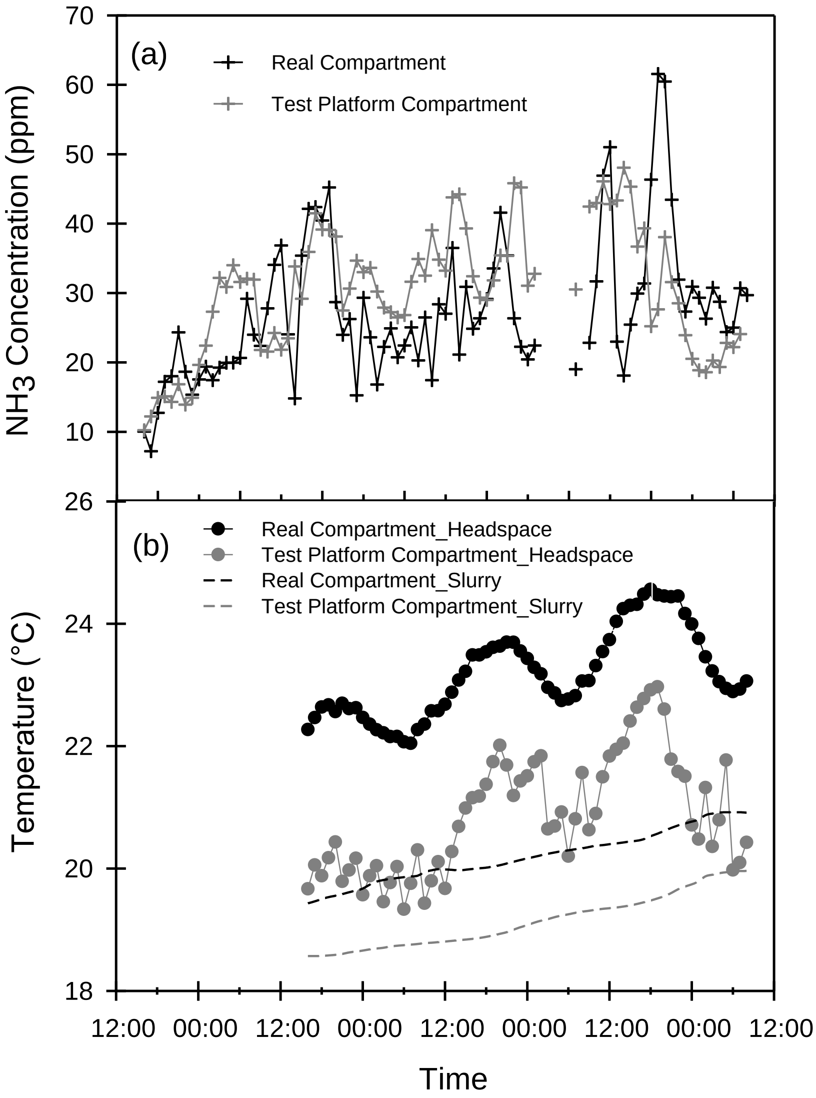

Fig. 3.10 — Diurnal slurry pit headspace NH_3 concentration and temperature and liquid slurry temperature in the real and TP compartments for the first experiment (missing data due to instrument failure) (a) slurry pit headspace NH_3 concentration (b) slurry pit headspace and liquid slurry temperature in the real and TP compartments for the first experiment (missing data due to instrument failure).

The higher NH_3 emissions in the TP compared to the real compartment was probably due to differences in pen floor fouling characteristics. The average wetted floor area in the TP was 0.8 ± 0.3 m^2 per pen (~ 0.2 m^2 pig^{-1} excluding slatted floor openings), while the visually inspected fouled pen floor area in the real pig compartment showed a less wetted floor area than in the TP compartments. Indeed, pen floors in the TP were wetted by pressurized urea solution droplets opposed to stream flow urination by pigs in the real compartment, consequently leading to a larger wetted floor area in the TP compared to the fouled pen area in the real compartment. Literature suggested that the fouled pen floor area in real pig housing is related to indoor temperature, floor type and pig weight and range between 0.07 – 0.11 m^2 pig^{-1} in a partly slatted fattening pig house with concrete slat width of 10 cm, slat gap size of 2.0 cm and opening area of 15% (Aarnink et al., 1996, Aarnink et al., 1997, Aarnink and Elzing, 1998).

The lack of faecal deposition in the TP, difference in chemical properties between pig urine and urea solution applied in the TP and slurry properties could also be contributory factors. Especially, as the TP compartment measured lower TAN concentration and higher slurry pH compared to the real compartment. Additionally, the average pH of the urea solution in the TP compartment (8.63 ± 0.14) was higher than the pH of fattening pig urine (7.48-7.87) reported in Canh et al. (1997) fed ~15.6% crude protein diet, as pigs in this study. Note that pig urine in the study of Canh et al. (1997) had the same urea concentration (0.2 mol L^{-1}) as the TP compartment. Furthermore, pig urine contains salts and organic acids with buffering effect that was absent in the prepared urea solution. Indeed, the experiment measured an average urea solution electrical conductivity (EC) of 6.2 µS cm^{-1} while in Willers et al. (2003) an average EC of 41200 µS cm^{-1} was measured in fresh pig urine.

The factors mentioned above (e.g. larger urea spray floor area and lack of pen floor faecal deposition in the TP compartment, and the difference in urea solution chemical properties compared to real pig urine etc.) are reported to strongly influence ammonia volatilization in livestock housing. Furthermore, diurnal variations in pig activity, urination and wallow behaviour also influenced NH_3 emission (Aarnink and Elzing, 1998). It could have been interesting to optimize the NH_3 emission performance in the TP compartments by modulating the heat production, urination frequency and the wetted floor area to simulate diurnal pig activity and urination behaviour throughout the day and/or add the various nitrogenous compounds and salts in real pig urine to the urea solution (Kool et al., 2006). However, the aim of this study was to generate similar climatic conditions/trends but not identical conditions, so that tests on the different emission reduction techniques could be tested in the TP compartment to acquire knowledge on pollutant transport behaviour focusing on relative rather than absolute emission reductions. Nonetheless, the similar NH_3 emission between the two TP compartments in the second experiment showed the facility could be used in such studies.

3.4. Conclusion

1. In the two experiments, the test platform captured comparable heat production and diurnal trends in indoor temperature, RH, ventilation rate and NH_3 concentrations as in a real pig compartment.
2. The second experiment showed 9% difference in the average NH_3 emission rate between the test platform 1 and test platform 2.
3. The test platform over-estimated the average hourly NH_3 emissions in the real pig compartment by 23% - 44% during the two experiments.
4. The over-estimation of NH_3 emission by the test platform compared to the real pig compartment was probably due to differences in pen fouling characteristics, liquid slurry and urea solution vs. pig urine chemical properties.
5. The similar NH_3 emission rates between the two test platform compartments in the second experiment indicates that the test platform could be used to perform relative performance testing of low-emission techniques.

Chapter 4: Effect of ventilation control settings on indoor climate and NH_3 emission in the experimental test platform (TP)

This chapter was adapted from:

Tabase, R. K., Millet, S., Brusselman, E., Ampe, B., Sonck, B., & Demeyer, P. (2018). Effect of ventilation settings on ammonia emission in an experimental pig house equipped with artificial pigs. *Biosystems Engineering*, 176, 125-139.

4.1. Introduction

The objectives of this chapter were to:

1. Test the effect of different ventilation set-point temperatures on indoor climate and NH_3 emissions.
2. Gain insight into factors affecting NH_3 emission in pig buildings equipped with UFAD systems.
3. Evaluate the effect of air displacement in the slurry pit headspace on NH_3 transport into the pig building.

These objectives tested the hypothesis that the process of air displacement in UFAD systems could influence NH_3 emission (section 1.7). Thereby the effect of 3 ventilation set-point temperatures fixed at 21, 23 and 25 °C (selected in Chapter 2) were tested using the full-scale test platform (TP) compartments in chapter 3. Using the TP compartments minimised disturbances from pigs and husbandry management. The current investigation served as a final check of the experimental setup for the field measurements with real pigs in chapter 5.

4.2. Materials and methods

4.2.1. Experimental facility and equipment

This investigation used the two test-platform compartments developed in chapter 3. Each fattening pig compartment was divided into 8 pens, equipped with mock-up pigs and automatic spraying installation at the ILVO/UGent/HoGent "Pig Campus", Merelbeke, Belgium (Fig. 4.1). The mock-up pigs artificially simulated heat production while the automatic spraying installation mimicked pig urination/NH_3 production by applying urea solution on the fully slatted floor of the test platform compartments (Fig. 2.1). As indicated in section 3.2.2, a 40 m long electrical heating cable heated two galvanised steel shaped into semi-cylinders to represent four pigs (Fig. 3.2). In each compartment, 16 mock-up pigs were placed (2 mock-ups per pen), continuously producing approximately 2.3 kW throughout the experiment, simulating the sensible heat production by 32 growing pigs of approximately 50 kg each (CIGR, 2002) to eliminate real pig disturbance during the measurements. Section 3.2.3 (Fig. 3.3) gives a detailed description of the urea spraying system. During this test, after the first and last spray regimes in the experiment, the averaged urinated floor area of 0.8 ± 0.3 m^2 per pen was determined by measuring the width and length of the wetted floor area (excluding gap openings) in each pen.

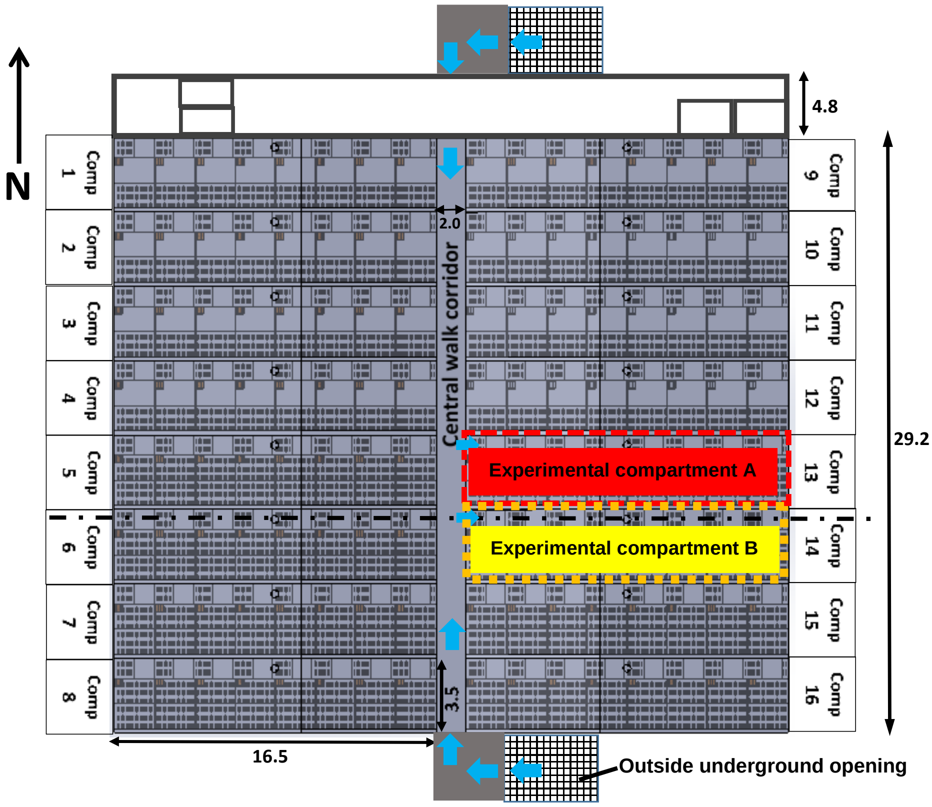

Fig. 4.1. — Plan view of the ILVO/UGent/HoGent fattening pig building (Comp = compartment; All dimensions are in meters).

4.2.2. Experimental design

The investigation compared the effect of 3 temperature settings (T_{set} = 21, 23 and 25 °C) on indoor climate and NH_3 emissions in 2 compartments (Fig. 4.1). Note that in the current investigation T_{set} = 21, 23 and 25 °C are identical to T3, CON and T4 (Table 2.2) in chapter 2. Ventilation rate was automatically controlled by setting the minimum ventilation rate to 14 m^3 h^{-1} pig^{-1} and the maximum ventilation rate to 70 m^3 h^{-1} pig^{-1} in the climate computer at a bandwidth of 5 °C for all treatments. T_{set} of 23 °C represented the reference treatment for 40 - 60 kg fattening pigs in Flanders. The experimental design simultaneously compared 2 set-point temperatures for each experimental run during 2 - 4 days, in a cross-replicate manner. Two such experimental series were set-up: one with and one without urea spraying.

The urea spraying experiment (USE) was conducted from the 19 June to 17 July 2017 (Table 4.1). Urea solution was sprayed in the 2 experimental compartments. The experimental compartments housed real pigs from ~25 kg until slaughter weight and were emptied before the start of the USE. The fouled pen floors were expected to contain enough urease enzymes to produce NH_3 during the USE (Braam et al., 1997a). There was neither faecal deposition nor the use of artificial urease enzyme in the investigation. During the USE, the study also verified the effect of urea spraying on NH_3 emission in a comparative ad hoc test using the 2 compartments on 11 July 2017 from 07:00 to 19:00.

Table 4.1. Experimental design the urea spraying experiment (USE).

Date	T_{set} in compartment 13 (°C)	T_{set} in compartment 14 (°C)
19 - 21 June	23	23
21 - 23 June	23	21
23 - 26 June	21	23
26 - 28 June	25	23
28 - 30 June	23	25
30 June - 03 July	21	25
03 - 05 July	25	21
05 - 07 July		23
07 - 10 July	23	
12 - 14 July		21
14 - 17 July		25

The compartments had the same set-point temperature (T_{set} = 23 °C) and similar slurry condition in the pit (pH of 7.66 vs. 7.55 and TAN concentration of 1.89 vs. 1.96, respectively). The test began with a period of no spraying from 07:00 to 09:00 in the 2 compartments. At 10:00 the automatic urea spraying began in one of the 2 compartments, while there was no urea spraying in the other compartment throughout the test. The non-urea spraying experiments (NUSE) were conducted from 27 July to 08 August 2016 (Table 4.2), comparing the 3 temperature settings without urea spraying. Similarly, the 2 experimental compartments in the investigation housed real pigs from ~25 kg until slaughter weight and then emptied before the start of the NUSE.

Table 4.2. Experimental design in the non-urea spraying experiments (NUSE)

Date	T_{set} in compartment 13 (°C)	T_{set} in compartment 14 (°C)
27 - 29 July	21	23
29 July - 01 August	23	21
01 - 04 August	21	25
04-08 August	25	21

The slurry pits in both the USE and the NUSE were emptied and refilled in the 2 experimental compartments before the start of each experimental run with new slurry from a slurry storage tank to 0.14 m slurry depth. Randomly collected slurry samples were taken at 5 locations at about 50 mm depth before the start and end of each experimental run. The slurry storage tank contained a mixture of slurry from the fattening, farrowing, weaner and sow pig units. The slurry samples were then stored at -18 °C until Total Ammoniacal Nitrogen (TAN) and pH analysis.

A C3010 Multi-parameter analyser (Consort bvba, Turnhout, Belgium) measured slurry pH. Slurry TAN concentration was analysed with a Kjeltec 8400 analyser (FOSS, Hilleroed, Denmark) using the BAM procedure (BAM/deel 3/05, 2015).

4.2.3. Indoor climate and emission measurements

Exhaust relative humidity (RH) and temperature were measured using Testo 175H1 humidity-temperature sensors/data loggers (Testo Inc, New Jersey, USA) (Range: 0 to 100% RH, -20 °C to +55 °C temperature; accuracy ±2% RH and ±0.40 °C). U-type thermistors (Grant Instruments, Cambridge, UK), (range: -50 to 150 °C and accuracy < 0.2 ºC) measured slurry pit headspace and slurry temperature. The slurry pit headspace temperature sensors were positioned 300 mm below the pen's slatted floor, while the slurry temperature sensor was located 50 mm below the liquid slurry surface. The high temperature sensor location was to allow tests at different slurry depths. The Testo sensor/data loggers measured and logged data at a sampling frequency of 1 min while slurry pit headspace air and liquid slurry temperatures were logged to a Squirrel SQ2040 (Grant Instruments, Cambridge, UK) every 2 min. Exhaust relative humidity (RH) and temperature were measured with EE08 humidity-temperature sensors (E+E Elektronik, Engerwitzdorf, Austria) (Range: 0 to 100% RH, -10 °C to 80 °C temperature; accuracy ±3% RH and ±0.50 °C) in the NUSE at a sampling frequency of 2 minutes. During the test, the slurry pit headspace temperature sensors were located 650 mm below the pen-slatted floor.

A Pt1000 (-50 °C to +100 °C) sensor of the "Hotraco System" (Hotraco Agri, Hegelsom, the Netherlands) measured the climate control (indoor) temperature in the 2 compartments, 1.4 m above the floor in pen 3 (Fig. 2.1c). Pt1000 sensors also measured the outside and ground channel temperatures. The outside temperature sensor was located 1.4 m above the ground under the eastern roof eave of the building. The underground channel temperature sensor was located 1.3 m above the floor of the central underground air channel (Fig. 2.1c).

The 'Hotraco System' controlled and measured the ventilation rate based on differential pressure measurements between the compartment and the overhead central exhaust channel. An Orion-VS12 data logger (Hotraco Agri, Hegelsom, the Netherlands) logged ventilation rate, climate control temperature, outdoor and ground channel temperatures at 1 min intervals. In addition to the indoor climatic parameter and ventilation rate measurements, the airflow pattern in the test compartments was also qualitatively determined by releasing smoke from a smoke generator (Mini Mist, Le Maitre Ltd, Surrey, UK) at the ground channel inlet.

A Fourier Transform Infrared Spectrometer (FTIR) gas analyser (Gasmet CX4000, Gasmet Technology Oy, Helsinki, Finland) monitored indoor (at the exhaust duct), slurry pit headspace and outside NH_3 and CO_2 concentrations during the investigation. After basic calibrations at Gasmet (Helsinki, Finland), the FTIR performed daily zero-point calibrations using N_2 gas during the investigation. The FTIR sequentially took 3 measurements per sample location in every 30 minutes.

The slurry pit headspace gas sampling tube was positioned 300 mm below the pen-slatted floor in the USE. The headspace gas sampling tube in the NUSE was located 450 mm below the pen-slatted floor. The higher headspace gas sampling tube in the USE was for convenience and to prevent slurry entering the gas sampling tube because the experiment also performed tests at higher slurry depths (results not presented in this study).

4.2.4. Data analysis

The study analysed all the measured parameters using their hourly averages and calculated gaseous emission rates (ER) as the product of ventilation rate and gaseous concentration. Six data samples per hour per sample location from the FTIR were averaged for the gaseous concentrations in the data analysis. The hourly averages of ventilation rate and gaseous concentrations calculated the ER (g h^{-1}) as in Eq. 3.10.

A Generalized Linear Mixed Modelling (GLIMMIX procedure, in SAS 9.4) approach was used to test treatment effect on indoor climate and gaseous emission by pooling all data from the USE and NUSE. Each investigated parameter had one linear mixed model. Terms in the models were T_{GC}, urea spraying (on or off), treatment (T_{set}), $T_{set} \times T_{GC}$ interaction and $T_{GC} \times$ urea spraying interaction as fixed effects. The interaction between T_{set} and urea spraying was not significant and therefore this interaction term was omitted from the final model. The response variables were NH_3 and CO_2 emission rate, exhaust and slurry pit headspace NH_3 and CO_2 concentration, indoor, slurry and slurry pit headspace temperature, exhaust relative humidity and ventilation rate. To explore the difference in the response variables between treatments, post-hoc tests were performed at 3 fixed T_{GC} (15, 18 and 22 °C) to illustrate the effect of the interaction term. T_{GC} was chosen at 25% (15 °C), 50% (18 °C) and 75% (22 °C) quantiles based on the range of data observed. The post hoc Tukey-Kramer method was used to test these differences at a total significance level of 0.05.

The statistical analysis added compartment and time as random effects to correct for common unknown environmental factors and the correlation between successive measurements modelled using a type 1-autoregressive structure. Dependent variables were considered normally distributed based on the graphical inspection of the residuals (histograms and QQ plots).

4.3. Results and discussion

4.3.1. Effect of urea spraying on NH_3 emission

During the USE ad hoc test, the effect of urea spraying on NH_3 emission was observed (Fig. 4.2). From 07:00 to 10:00, when there was no urea spraying in both test compartments, similar NH_3 emission and concentration trends were produced. Urea spraying started in one compartment at 10:00, resulting in NH_3 emission and concentration peaks at around 11:00. These peaks were absent in the other compartment without urea spraying (Fig. 4.2a & Fig. 4.2b). The compartment with urea spraying continued to produce the NH_3 peaks corresponding to the 3-hourly spray pattern of the spray installation. This trend was again absent in the compartment without spraying. This result proves that the sprayed urea acted as an extra source of NH_3 in the spraying compartment as every decomposed urea molecule produces 2 molecules of NH_3 and 1 molecule of CO_2 (Sommer et al., 2006). During the ad hoc test, the average NH_3 emission was 18% higher in the compartment with spraying compared to the compartment without spraying. Similarly, the exhaust NH_3 concentration was 18% higher in the former than the latter compartment. The renewal of decayed TAN concentration in the slurry pit from the regular spraying of the urea solution, the sprayed pen floors as extra emission sources and the heat contribution of the sprayed urea solution (37 °C) could explain the higher NH_3 concentration in the urea spraying compartment.

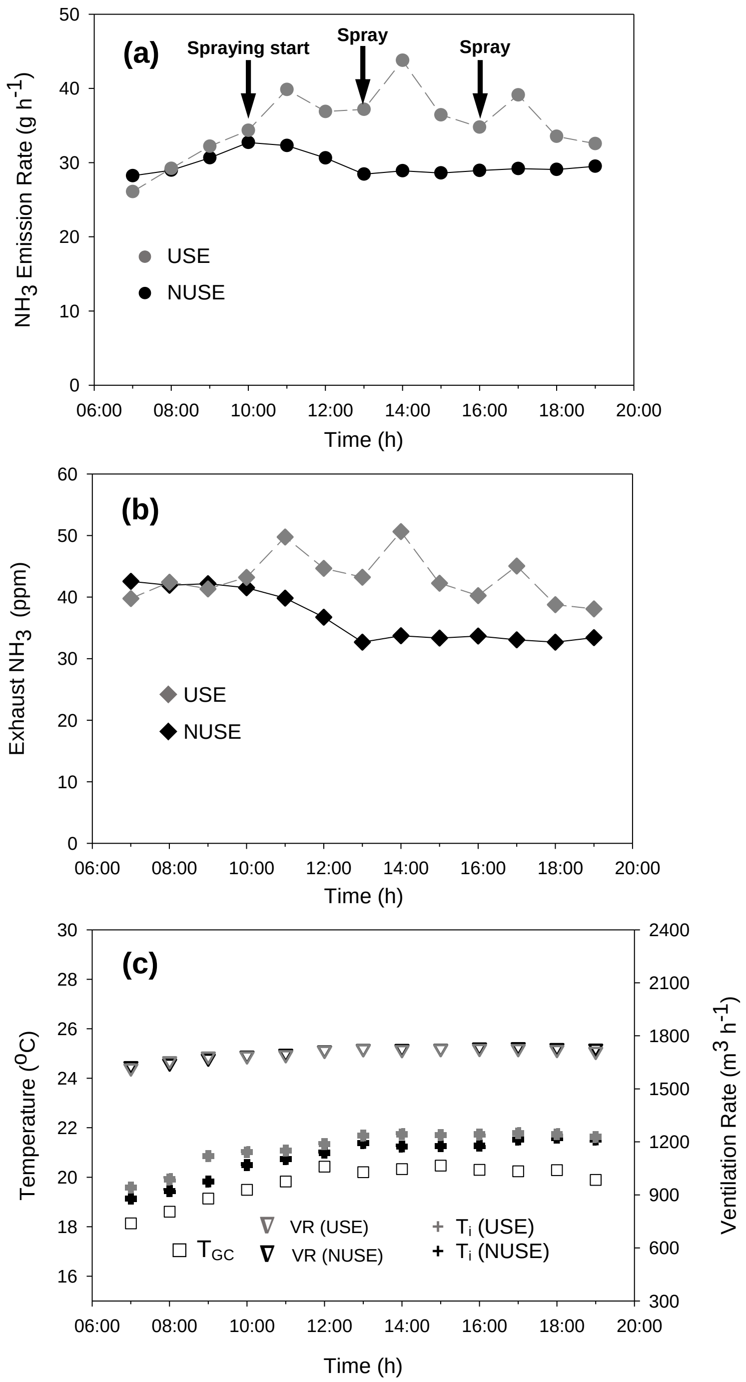

Fig. 4.2. — Diurnal variations in the hourly average (a) NH_3 emissions (b) exhaust NH_3 concentration and (c) T_i and VR at T_{set} (23 °C) between the compartment with urea spraying and the compartment without urea spraying during the ad hoc test.

To further assess the observed NH_3 emission and concentration peaks in the ad hoc test (Fig. 4.2), diurnal variations in the NH_3 and CO_2 concentrations between the USE and NUSE experiments were compared using data from a single experimental run comparing T_{set} (21 °C) and T_{set} (23 °C) (Fig. 4.3 & 4.4). The selected experimental run in the NUSE was from 30 July - 01 August 2016 and the USE from 21 – 23 June 2017. Similar to the peaks shown in Fig. 4.2, the NH_3 emission (Fig. 4.3a), exhaust and headspace NH_3 concentration (Fig. 4.4a) peaked correspondingly to the 3-hourly spray patterns in the USE, and these peaks were absent in the NUSE (Fig. 4.3c & 4.4c). These findings corroborates that extra NH_3 was produced by spraying the urea solution in the USE.

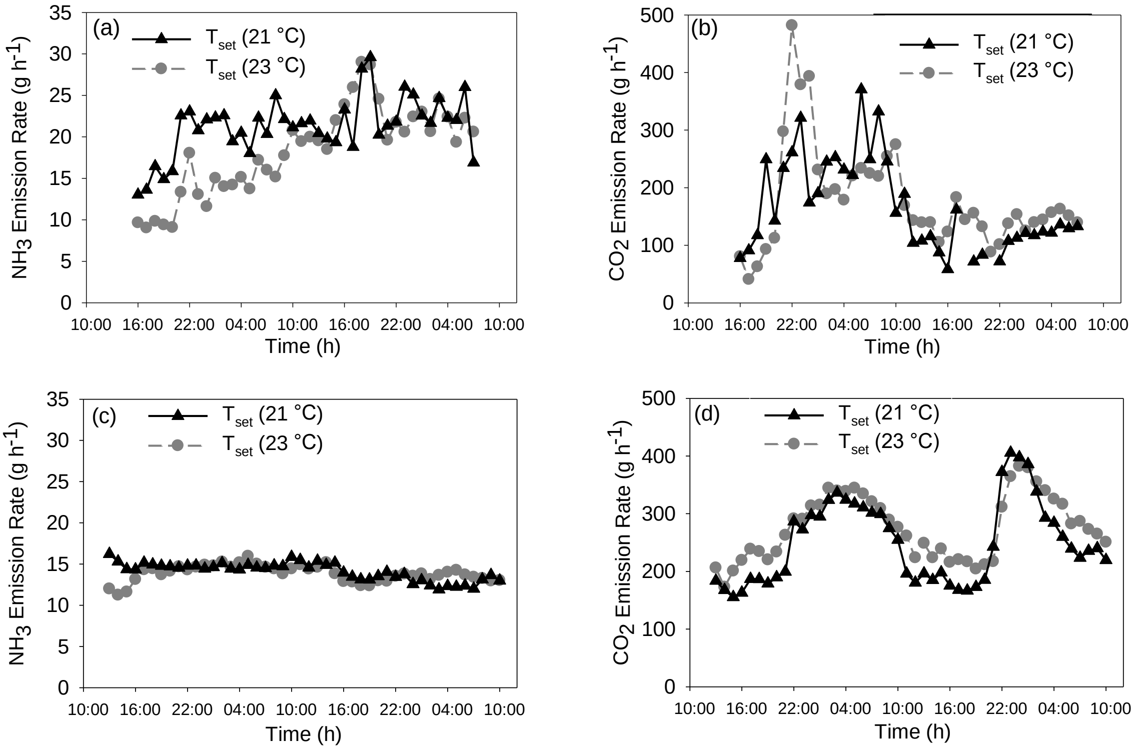

Fig. 4.3. — Diurnal variations in the hourly average NH_3 and CO_2 emissions between USE from 21 – 23 June 2017 (a & b) and NUSE from 30 July - 01 August 2016 (c & d) at T_{set} (21 °C) and T_{set} (23 °C). The figure only used data from one experimental run between T_{set} (21 °C) and T_{set} (23 °C) during the entire USE and NUSE experimental periods.

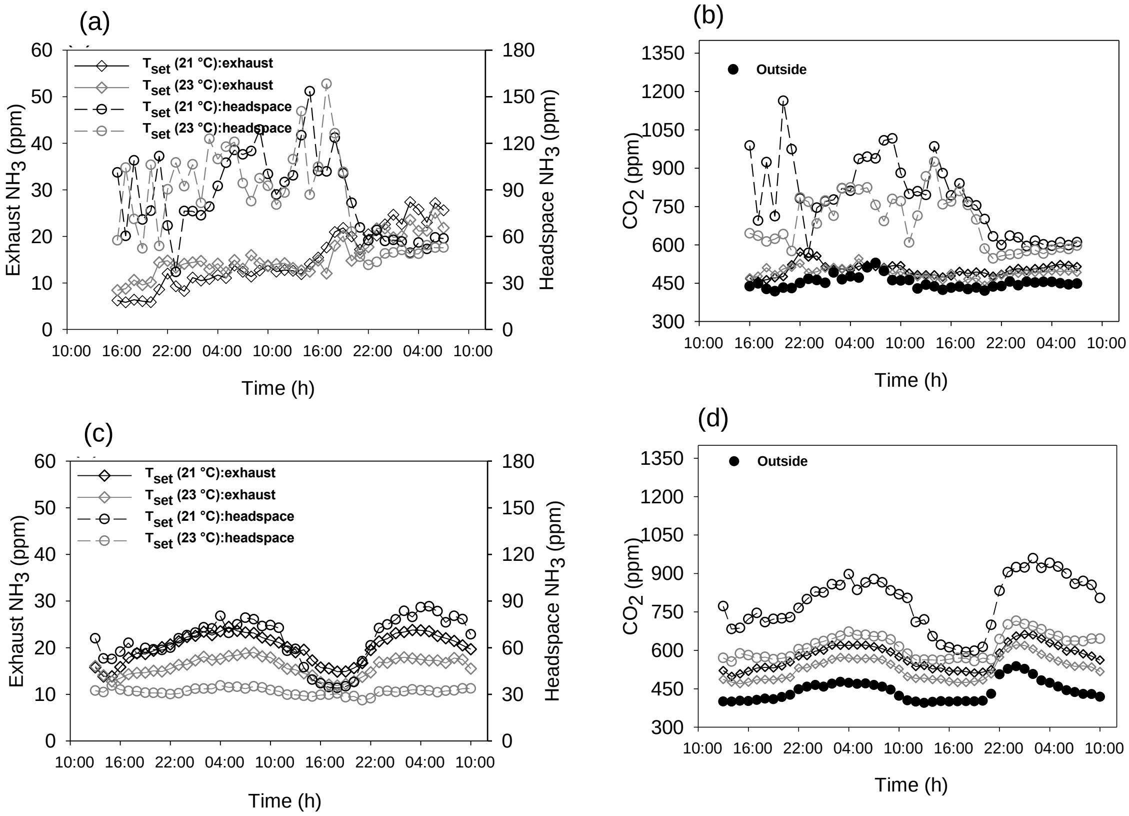

Fig. 4.4. — Diurnal variation in the hourly average exhaust headspace and outside NH_3 and CO_2 concentration between USE from 21 – 23 June 2017 (a & b) and NUSE from 30 July - 01 August 2016 (c & d) at T_{set} (21 °C) and T_{set} (23 °C). The figure only used data from one experimental run between T_{set} (21 °C) and T_{set} (23 °C) during the entire USE and NUSE experimental periods.

Furthermore, Fig. 4.3b and Fig. 4.4b also show CO_2 emission and headspace CO_2 concentration peaks in the USE, corresponding to the NH_3 emission and headspace NH_3 concentration peaks in Fig. 4.3a and Fig. 4.4a, respectively. Again, the CO_2 peaks corresponded to the 3-hourly spray patterns in the USE, and were absent in the NUSE (Fig. 4.3d & Fig. 4.4d), confirming the sprayed urea as an extra source of CO_2.

Comparing the USE and NUSE showed that the average NH_3 emission and exhaust concentration were 109% and 133% higher in the USE (Table 4.3). The greater NH_3 emission in the USE than the NUSE compared to the ad hoc test was because of the difference in slurry TAN concentration (P = 0.006) and pH (P = 0.002) between the USE and NUSE (Aarnink & Elzing, 1998), which were performed a year apart. This reason was that at the start of the experiment, the average slurry TAN concentration and pH in the USE were 2.24 ± 0.16 mg g^{-1} and 7.61 ± 0.21, while in the NUSE it was 1.86 ± 0.23 mg g^{-1} and 7.08 ± 0.16, respectively. The difference in slurry properties in the USE and NUSE was probably due to the difference in the proportion of slurry collected from the different pig units into the slurry storage tank (section 4.2.2) before the start of the experiments.

Table 4.3. Effect of urea spraying on indoor climate and NH_3 emission.

	Urea Spray (SEM)	No Urea Spray (SEM)
NH_3 ER (g h^{-1})	23.2^{b} (0.6)	11.1^{a} (0.6)
NH_3 (ppm)	35^{b} (1.0)	15^{a} (1.1)
VR (m^3 h^{-1})	1107 (18)	1113 (20)
T_i (°C)	24.8 (0.1)	24.5 (0.1)
RH (%)	61^{b} (1)	67^{a} (1)
CO_2 (ppm)	572 (5)	531 (6)
NH_3 HS (ppm)	114^{b} (6)	31^{a} (6)
T_{HS} (°C)	21.7^{b} (0.2)	22.2^{a} (0.2)
T_{slurry} (°C)	20.7^{b} (0.1)	20.5^{a} (0.1)
CO_2 ER (g h^{-1})	209.7 (8.9)	192.7 (10.0)
CO_2 HS (ppm)	890 (15)	735 (18)

Superscripts $^{a, b}$ within the same row indicates significant difference (P < 0.05) in the predicted least squares means between treatments. SEM = standard error of the mean.

At the end of the experiments, the average slurry TAN concentration and pH were 2.08 ± 0.20 mg g^{-1} and 7.72 ± 0.27 in the USE and 1.45 ± 0.16 mg g^{-1} and 7.21 ± 0.14 in the NUSE, respectively. Nonetheless, the difference in the state of slurry between the USE and NUSE are not expected to affect the main aim of this investigation, since statistical tests showed no difference in the initial slurry pH (P = 0.64) and TAN concentration (P = 0.67) between treatments (T_{set}) at the start of each USE and NUSE experimental run.

4.3.2. Effect of set-point temperature on indoor climate and ventilation rate

The conducted experiments showed that the ventilation system reacted to increasing T_{GC} by increasing the ventilation rate (Fig. 4.5) depending on the climate control set-point (T_{set}). This is explained by the fact that T_{GC} (P < 0.001), T_{set} (P = 0.04) and their interaction (P < 0.001) affect ventilation rate (Table 4.4). Similarly, with increasing T_{GC}, the indoor temperature (T_i) increased, and the magnitude of the T_i depended on the T_{set} (Fig. 4.5). Again, this was because the T_i depended on T_{GC} (P < 0.001), the T_{set} (P = 0.010), and their interaction (P < 0.001) (Table 4.4). Table 4.4 also shows T_{GC}, T_{set} and their interaction influence the exhaust RH although there was no clear difference between the different T_{set} as T_{GC} increased.

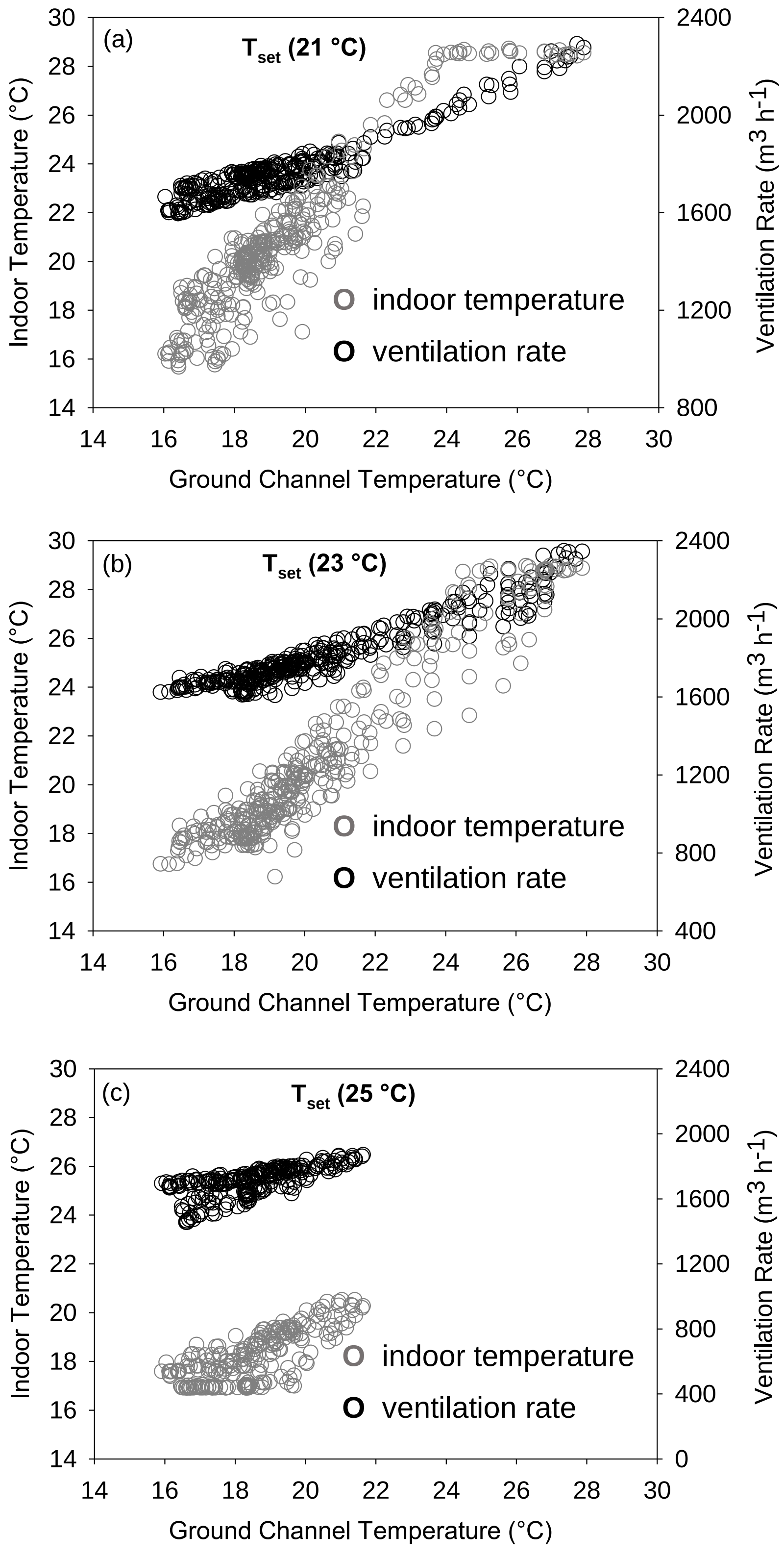

Fig. 4.5. — Relationship between the hourly average ground channel temperature, indoor temperature and ventilation rate in (a) T_{set} (21 °C), (b) T_{set} (23 °C) and (c) T_{set} (25 °C) during the entire experiment.

Table 4.4. Effect of T_{set} on indoor climate and NH_3 emission.

	T_{set} (21°C)	T_{set} (23 °C)	T_{set} (25°C)	SEM T_{set} (21 °C)	SEM T_{set} (23 °C)	SEM T_{set} (25 °C)	*P* T_{set}	*P* T_{GC}	*P* T_{set} ×T_{GC}	*P* Spray
NH_3 ER (g h^{-1})							0.066	<0.001	<0.001	0.024
T_{GC} = 15 °C	21.5^{a}	22.6^{a}	12.9^{b}	1.0	1.1	1.1				
T_{GC} = 18 °C	19.0^{a}	20.0^{a}	14.2^{b}	0.6	0.7	0.7				
T_{GC} = 22 °C	15.8	16.6	16.0	0.8	0.7	1.1				
CO_2 ER (g h^{-1})							0.175	<0.001	0.018	0.281
T_{GC} = 15 °C	295.2	293.5	197.2	16.2	17.9	19.6				
T_{GC} = 18 °C	230.9^{ab}	255.9^{a}	175.2^{b}	10.6	12.3	11.4				
T_{GC} = 22 °C	145.2	205.7	145.7	14.0	11.5	19.2				
NH_3 (ppm)							0.082	<0.001	0.004	0.022
T_{GC} = 15 °C	26^{b}	35^{ab}	46^{a}	1.6	1.7	1.9				
T_{GC} = 18 °C	21^{b}	27^{b}	37^{a}	1.2	1.3	1.2				
T_{GC} = 22 °C	15^{b}	16^{ab}	25^{a}	1.4	1.2	1.8				
CO_2 (ppm)							0.131	<0.001	0.060	0.06
T_{GC} = 15 °C	573^{b}	611^{ab}	667^{a}	8.5	9.3	10.1				
T_{GC} = 18 °C	535^{b}	573^{ab}	612^{a}	5.9	6.7	6.3				
T_{GC} = 22 °C	484	521	537	7.4	6.3	9.8				
VR (m^3 h^{-1})							0.040	<0.001	<0.001	0.713
T_{GC} = 15 °C	1047^{a}	672^{b}	447^{c}	28.2	30.6	32.6				
T_{GC} = 18 °C	1310^{a}	1028^{b}	617^{c}	20.6	22.7	21.7				
T_{GC} = 22 °C	1662^{a}	1502^{b}	843^{c}	24.9	21.8	31.7				
T_i (°C)							0.010	<0.001	<0.001	0.070
T_{GC} = 15 °C	22.3^{c}	23.1^{b}	24.7^{a}	0.10	0.10	0.11				
T_{GC} = 18 °C	23.4^{c}	24.2^{b}	25.2^{a}	0.08	0.09	0.08				
T_{GC} = 22 °C	24.8^{b}	25.7^{a}	25.8^{a}	0.09	0.08	0.11				
T_{ex} (°C)							0.051	<0.001	0.022	0.687
T_{GC} = 15 °C	22.7^{c}	23.6^{b}	24.4^{a}	0.13	0.14	0.13				
T_{GC} = 18 °C	23.5^{c}	24.4^{b}	25.1^{a}	0.11	0.12	0.12				
T_{GC} = 22 °C	24.6^{b}	25.5^{a}	26.0^{a}	0.12	0.12	0.13				
RH (%)							0.044	<0.001	<0.001	0.038
T_{GC} = 15 °C	68^{ab}	71^{a}	62^{b}	1.4	1.2	1.1				
T_{GC} = 18 °C	66	67	63	1.2	1.3	1.2				
T_{GC} = 22 °C	63	61	64	1.3	1.3	1.4				

Superscripts $^{a, b, c}$ within the same row indicates significant difference (P < 0.05) in the predicted least squares (LS) means between treatments. SEM = standard error of the LS-means.

T_{set} typically acts as a reference temperature based on which cooling by ventilation is staged in mechanically ventilated livestock buildings—above the set-point temperature ventilation increases aiming to cool the building (Harmon et al., 2012). In this investigation, with increasing T_{GC}, ventilation rate at T_{set} (21 °C) was higher than at T_{set} (23 °C) with opposite results between T_{set} 25 °C versus T_{set} (23 °C). Additionally, the T_i only rarely reached T_{set} for the different set-point temperatures. A probable reason is that the experiment was conducted during the summer (Fig. 4.6), characterised by the transport of warmer air into the building. Seedorf et al. (1998) and Smith et al. (2009) saw that at such conditions, T_i is often higher than the T_{set} and depends on the outdoor temperature. For example, at T_{GC} > 22 °C, T_{GC} limited the ability of the ventilation system to maintain the requested T_i especially in T_{set} (21 °C) and T_{set} (23 °C) (Fig. 4.5). At this situation, ventilation was already at the maximum and stayed constant as T_{GC} increased. This likely produced similar airflow patterns and could explain the similar indoor gaseous concentration and temperature between the 2 set point temperatures with increasing T_{GC}.

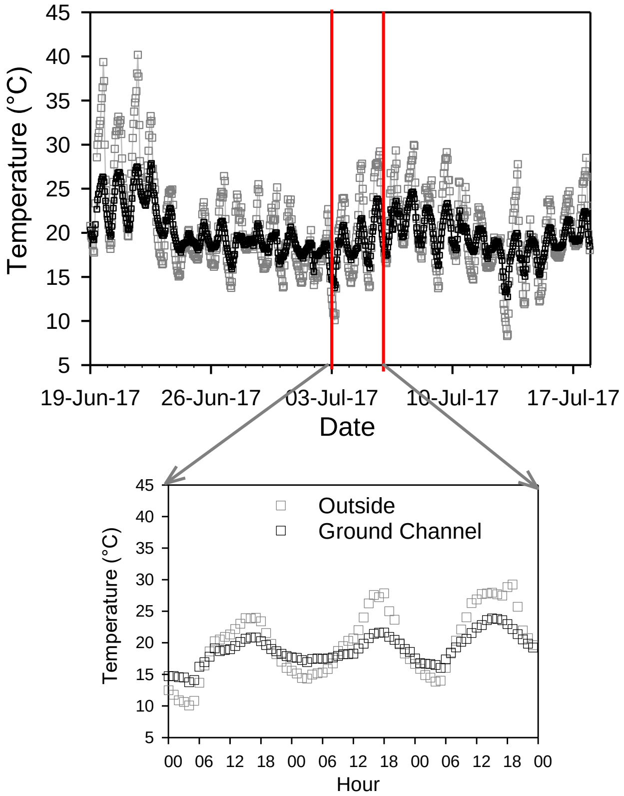

Fig. 4.6. — Hourly average outside and ground channel temperature during the entire USE.

Figure 4.5 further shows that a higher T_{set} in warmer seasons could reduce the effect of T_{GC} on T_i and ventilation rate, as T_{set} (25 °C) showed a less pronounced rise in T_i and ventilation rate compared to T_{set} (21 & 23 °C) with increasing T_{GC}. Meanwhile, the ventilation design at the pig facility minimised the influence of the high outdoor temperatures during the investigation (Fig. 4.6). Heat exchange between the underground air passage walls and incoming ambient air cooled the warmer outside air during the day and warmed the colder outside air during the night, producing more stable incoming air temperatures into the test compartments (Threm et al., 2012).

Concerning the USE, Figure 4.4a and 4.7b quantitatively illustrate the evolution of the pit headspace NH_3 concentrations and temperature, with respect to T_{GC} and ventilation rate (Fig. 4.7a) for T_{set} (21 °C) and T_{set} (23 °C) respectively. On the first day of the experiment, at T_{GC} > 22 °C, higher T_i, ventilation rate and T_{HS} values were observed for both T_{set} (21 °C) and T_{set} (23 °C). In this period, relatively low exhaust NH_3 concentrations were measured compared to the higher pit headspace NH_3 concentrations.

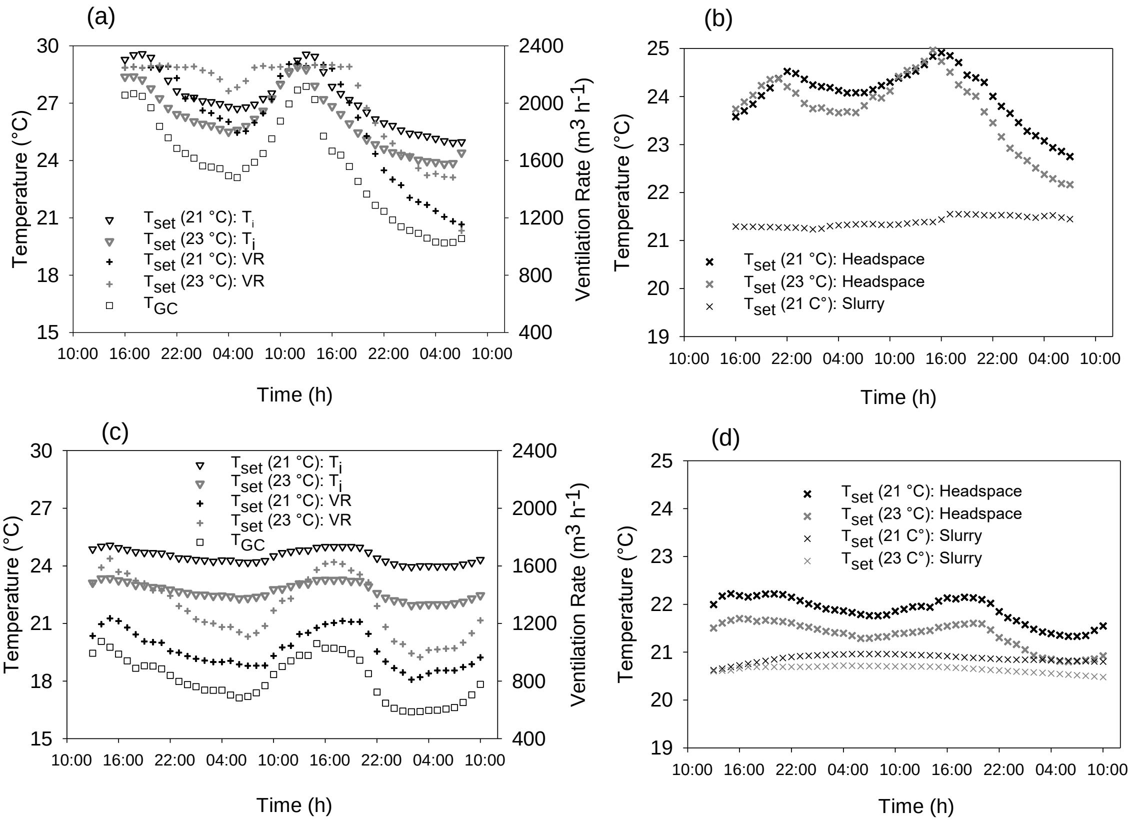

Fig. 4.7 — Diurnal variation in hourly average ground channel, room, headspace, slurry temperature and ventilation rate between USE from 21 – 23 June 2017 (a & b) and NUSE from 30 July - 01 August 2016 (c & d) at T_{set} (21 °C) and T_{set} (23 °C). The figure only used data from one experimental run between T_{set} (21 °C) and T_{set} (23 °C) during the entire USE and NUSE experimental periods.

However, after 18:00 of the second day of the experiment, a dip in T_{GC} by 4 °C reduced the headspace NH_3 concentration by 65 and 74 ppm and T_{HS} by 2.0 and 2.1 °C with a consequent increase in the exhaust NH_3 concentration 4.7 and 3.8 ppm in the two compartments. This suggests that when incoming air (T_{GC}) is colder than T_{HS}, a larger proportion of the incoming air could flow into the slurry pit displacing the ammonia rich pit headspace air into the compartment. This observed trend probably explains the influence of T_{GC} on the exhaust NH_3 and CO_2 concentrations (P < 0.001) and the interaction between T_{GC} and T_{set} on the exhaust

NH_3 concentrations (P = 0.004) (Table 4.4), slurry temperature (P = 0.002), T_{HS} (P < 0.001), and slurry pit headspace NH_3 concentration (P = 0.027) (Table 4.5).

Table 4.5. Effects of climate control T_{set} on slurry pit conditions.

				SEM			*P*			
	T_{set} (21°C)	T_{set} (23 °C)	T_{set} (25°C)	T_{set} (21°C)	T_{set} (23 °C)	T_{set} (25°C)	T_{set}	T_{GC}	$T_{set} \times T_{GC}$	Spraying
NH_3 HS (ppm)							0.110	0.217	0.027	0.024
T_{GC} = 15 °C	52^{b}	59^{b}	123^{a}	7.9	8.5	8.9				
T_{GC} = 18 °C	54^{b}	60^{b}	109^{a}	6.1	6.6	6.3				
T_{GC} = 22 °C	58	62	90	7.1	6.4	8.7				
CO_2 HS (ppm)							0.212	0.622	0.139	0.052
T_{GC} = 15 °C	690	689	969	32.4	35.9	39.4				
T_{GC} = 18 °C	690^{b}	726^{b}	951^{a}	21.2	24.5	22.8				
T_{GC} = 22 °C	689	775	928	27.9	22.9	38.5				
T_{HS} (°C)							0.049	<0.001	<0.001	0.040
T_{GC} = 15 °C	21.2^{b}	22.0^{a}	22.0^{a}	0.21	0.21	0.21				
T_{GC} = 18 °C	21.5^{b}	22.0^{a}	22.1^{a}	0.20	0.20	0.20				
T_{GC} = 22 °C	21.8^{b}	22.1^{ab}	22.4^{a}	0.20	0.20	0.21				
T_{Slurry} (°C)							0.391	0.021	0.002	0.045
T_{GC} = 15 °C	20.4	20.7	20.5	0.09	0.09	0.09				
T_{GC} = 18 °C	20.4^{c}	20.7^{a}	20.5^{b}	0.09	0.09	0.09				
T_{GC} = 22 °C	20.4^{b}	20.9^{a}	20.5^{b}	0.09	0.09	0.09				

Superscripts $^{a, b, c}$ within the same row indicates significant difference (P < 0.05) in the predicted least squares means between treatments. SEM = standard error of the LS-means.

As smoke tests in the compartments indicated a direct flow of some of the incoming air into the slurry pit (Fig. 4.8), it is assumed that the interaction between T_{GC} and T_{set} on the slurry pit headspace temperature and NH_3 concentration and consequently exhaust gaseous concentrations was caused by the displacement ventilation in the test compartments. Aarnink & Wagemans (1997) and van Wagenberg & Smolders (2002) saw a similar airflow pattern in a partly slatted UFAD pig building. Botermans & Jeppsson (2008) noted an increase in NH_3 emission in a similar pig building in winter due to the displacement of pit headspace NH_3 by incoming air into the animal occupied zone. Compared to the solid pen floor beside the underfloor air channel in the study of Aarnink & Wagemans (1997), the fully slatted pen floor in this study allowed more easy access of the incoming air from the slatted floor inlet into the slurry. This could potentially lead to a higher pollutant flux from the slurry pit into the room.

Exhaust NH_3 concentrations differed between T_{set} (21 °C) and T_{set} (25 °C) as T_{GC} increased. However, the respective difference in CO_2 concentrations decreased with increasing T_{GC}. There was no clear difference in NH_3 and CO_2 concentrations between the reference T_{set} and both T_{set} (21 °C) and T_{set} (25 °C) as T_{GC} increased (Table 4.4). Clearly, the decrease in exhaust NH_3 and CO_2 concentrations with increasing T_{GC} was caused by the increase in ventilation rate (Table. 4.4), which promoted the faster mass transport of fresh air into building to dilute the contaminant concentrations.

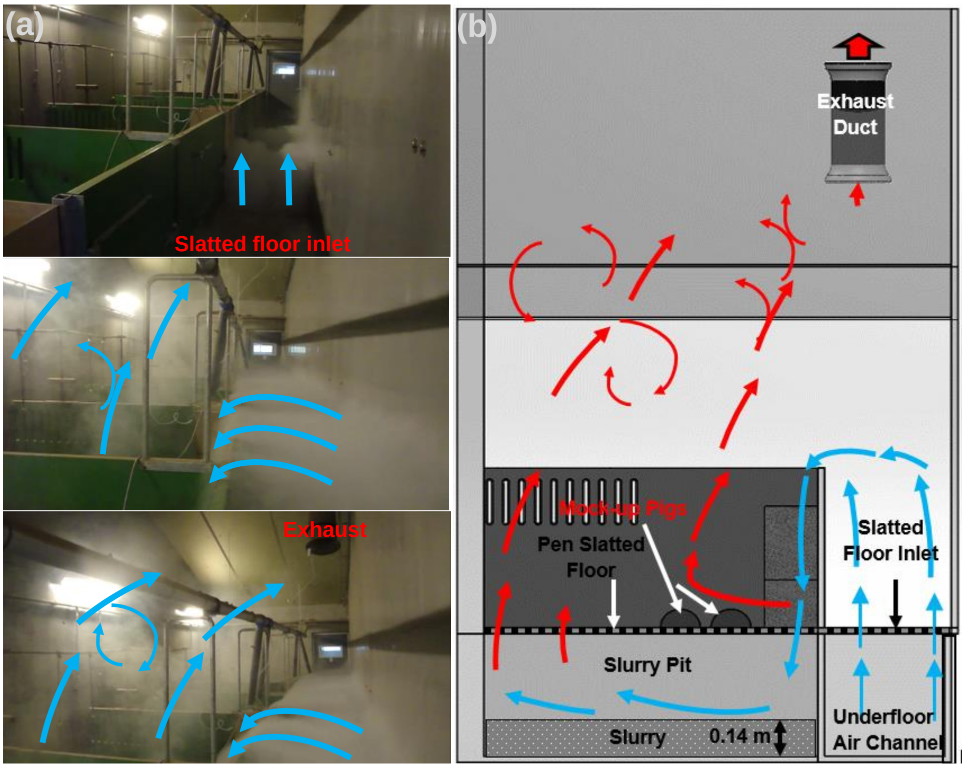

Fig. 4.8. — (a) Photographs of airflow pattern from the smoke test in the experimental compartment and (b) 2D sketch of the observed airflow pattern in the cross-sectional plane across the exhaust duct.

4.3.3. Effect of set-point temperature on ammonia emissions

The effect of different T_{set} (21, 23 and 25 °C) was tested to explore their potential of reducing NH_3 emission since the mass transport of NH_3 from the emitting sources in livestock buildings correlate with ventilation rate (Arogo et al., 1999; Blanes-Vidal et al., 2008; Ni et al., 1999b). Knowing that NH_3 emission also relates to temperature (Arogo et al., 1999; Cortus et al., 2008), the influence of the selected set-point temperatures on slurry (P = 0.391) and slurry pit headspace (P = 0.049) temperature was expected to be less significant compared to ventilation rate (P = 0.040). The reason for this is that increasing slurry temperature increases urea breakdown to NH_4 (Sommer et al., 2006). In addition, higher temperatures promote the volatilisation of NH_3 from pig slurry by decreasing the solubility of NH_3 gas and increasing the proportion of the TAN as NH_3 gas in slurry (Meisinger and Jokela, 2000; Arogo et al., 1999). In this investigation, T_{GC} interacted with T_{set} (P < 0.001) to influence NH_3 emission rate (Table

4.4). NH_3 emission rate decreased with increasing T_{GC} for T_{set} (21 °C) and T_{set} (23 °C). On the contrary, NH_3 emission increased with increasing T_{GC} for T_{set} (25 °C). However, it should be noted that no experimental data were obtained beyond T_{GC} of 22 °C for T_{set}` (25 °C) (Fig. 4.9).

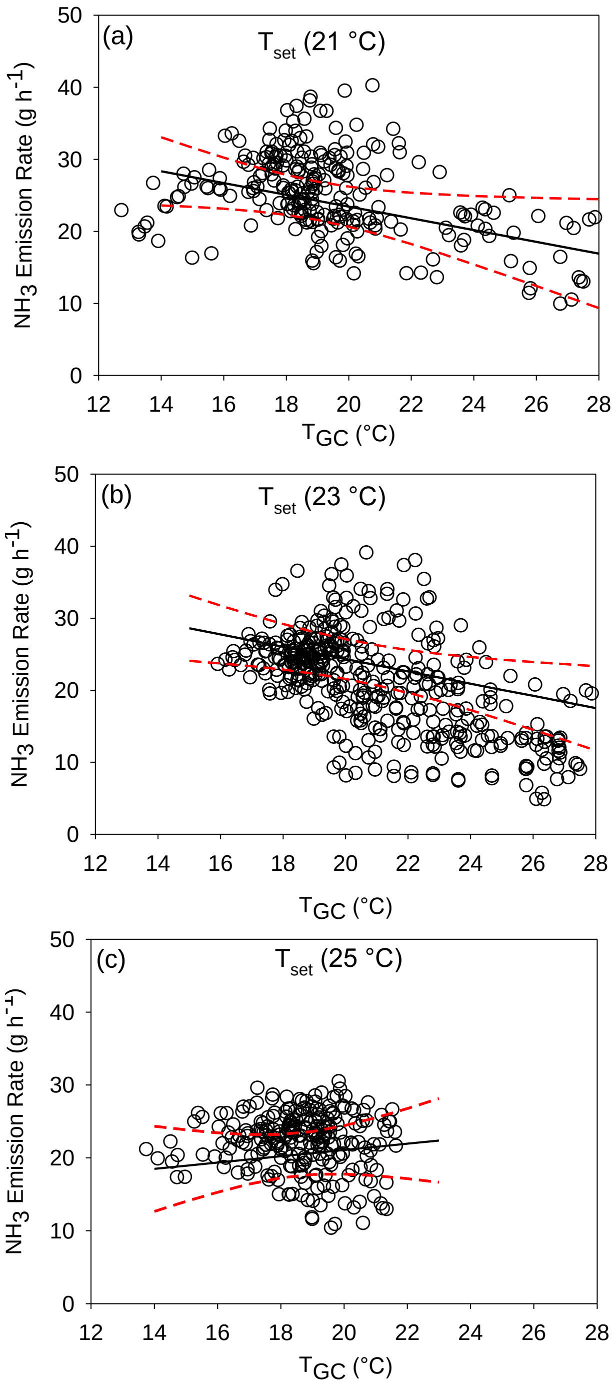

Fig. 4.9. — Comparison of generalised linear model (black: line), lower and upper least squared means (Red: dash lines) with hourly experimental data of NH_3 emission at different T_{GC} in only the USE at (a) T_{set} (21 °C), (b) T_{set} (23 °C) and (c) T_{set} (25 °C).

Ammonia emission rate did not differ between T_{set} (21 °C) and T_{set} (23 °C) as T_{GC} increased but differed between T_{set} (21 °C) and T_{set} (25 °C). Ammonia emission rate in T_{set} (25 °C) was (-75% & -67%) lower at T_{GC} of 15 °C and (-41% & -34%) lower at T_{GC} of 18 °C than T_{set} (21 °C) and T_{set} (23 °C), respectively. At T_{GC} of 22 °C, NH_3 emission between T_{set} (21 °C) and T_{set} (25 °C) were similar. The cumulative NH_3 emission in Fig. 4.10 shows that higher set-point temperatures could reduce NH_3 emission. In Table 4.4, the CO_2 emission in T_{set} (25 °C) was lower than T_{set} (23 °C). This was because the higher set-point temperatures in T_{set} (25 °C) decreased the ventilation rate, causing the build-up of CO_2 in the pit headspace (Tables 4.5). This result further confirms the hypothesis that higher set-point temperatures could reduce NH_3 emission. However, while this was the case in this investigation, extremely high set-point temperatures under conditions with real pigs may cause the pigs to adopt undesirable behaviour (e.g. wallowing in their excrements), reduce pig performance and welfare due to heat stress, which could potentially diminish the observed benefits in this investigation (Huynh et al., 2005a; Huynh et al., 2005b; Aarnink et al., 2006).

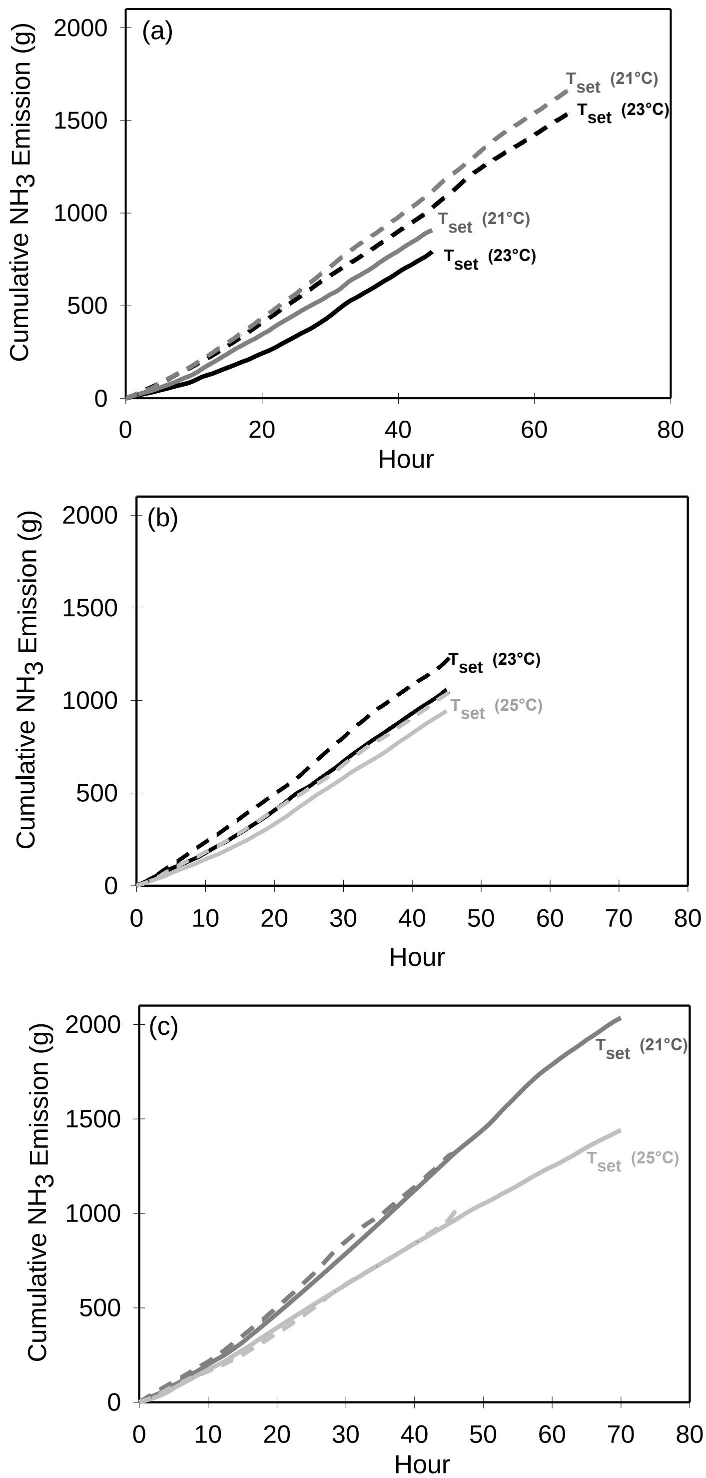

Fig. 4.10. — Cumulative NH_3 emission for the different set-point temperatures in the USE (a)T_{set} (21 °C) vs. T_{set} (23 °C) (b) T_{set} (23 °C) vs. T_{set} (25 °C) (c) T_{set} (21 °C) vs. T_{set} (25 °C). The solid and dash lines indicate different compartments.

As already discussed in section 4.3.2., smoke tests also showed that, apart from ventilation rate, airflow patterns equally affect NH_3 emission. The observed flow of some of the incoming air entering the slurry pit can explain the interaction between T_{GC} and T_{set} on the slurry pit headspace temperature, gaseous concentrations and NH_3 emission. In fact, earlier investigations show airflow patterns that enhance air exchange from slurry pits in livestock buildings could bring NH_3 from the slurry pit into the building and subsequently increase NH_3 emission (De Praetere & Van Der Biest 1990; Morsing et al., 2008; Ye et al., 2008b). In the investigated compartments, the displacement ventilation coupled with the fully slatted pen floors further promoted the air exchange between the slurry pit and the pig compartment by allowing the easy access of the incoming air into the slurry pit. Using only a partly slatted pen floor (Aarnink & Wagemans, 1997) or placing a low porosity slatted floor (Zong et al., 2014) at the front part of the pen close to the slatted floor inlet could reduce the direct flow of some of the incoming air into the slurry pit. However, there is a higher risk that the pigs would prefer to lay at the opposite and non-draughty section of the pen, thus leaving the solid floor or low porosity section as a dunging area, which is not preferable.

In order to avoid airflows entering the pit headspace, new underground air channel systems in pig buildings could consider delivering the incoming air from the underground air channel via alternative inlets, thereby aiming to reduce draught and displacement of emissions from the slurry pit into the room. Supplying incoming air through ceiling diffusers instead of UFAD could minimise draught on the pigs (van Wagenberg & Smolders, 2002; Hessel et al., 2010; Krommweh et al., 2014). This supply air system, however, can reduce the better air quality in pig buildings with UFAD systems at the animal occupied zone (Aarnink & Wagemans, 1997; van Wagenberg & Smolders, 2002).

About 60% of the total NH_3 emissions come from the slurry pit in pig buildings (Hoeksma et al., 1992; Aarnink et al., 1996; Kai et al., 2005). This investigation therefore aims to estimate the influence of headspace air displacement in the pit on NH_3 transport to pig buildings equipped with UFAD systems. The Archimedes number (Ar) and the Contaminant Pit Removal (CPR) parameter may be used in these investigations. The Ar number is often used to characterise airflow patterns in displacement ventilation systems as the dimensionless ratio of the buoyant to the inertial force in the supply air jets going through the slatted floor into the Animal Occupied Zone (AOZ), (Faulkner et al., 1995; Nielsen, 2000; Park & Holland, 2001).

$$Ar = \frac{Buoyancy\ Force}{Inertia\ Force} = \frac{g\Delta Td}{T_i v^2} \tag{4.1}$$

Where, g is gravitational acceleration (g s^{-2}), T_i is room temperature measured 1.4 m above the floor in pen 3 (K), $\Delta\mathrm{T}$ is the $T_i - T_{GC}$ (K), v is the air velocity at the face of the slatted floor inlet (m s^{-1}) and d is characteristic length, taken as the width of the service alley in the compartment (1.0 m). This investigation calculated v as the ventilation rate divided by the total slot opening area of the slatted floor inlet (1.34 m^2). Typically, the higher the Ar the more the incoming air gravity current is deflected by the thermal plume from the mock-up pigs at the AOZ.

The CPR in this investigation is derived from the contaminant removal effectiveness parameter applied by van Wagenberg and Smolders (2002) to calculate pollutant removal effectiveness at AOZ in a pig house. In this investigation, the interest was the negative effect of bringing NH_3 from the slurry pit headspace into the compartment. Therefore,

$$CPR_{x,p,t} = \frac{C_{x,ex,t} - C_{x,in,t}}{C_{x,p,t} - C_{x,in,t}} \tag{4.2}$$

Where, $CPR_{x,p,t}$ is CPR at point p at time t for contaminant x, considered as NH_3 in this investigation, $C_{x,ex,t}$ is the NH_3 concentration in the exhaust air at time t (ppm), $C_{x,in,t}$ is NH_3 concentration of the incoming air at time t (ppm) and$C_{x,p,t}$ is NH_3 concentration at point p chosen as the pit headspace in this study at time t (ppm).

Generally, $CPR = 1$ implies uniform air mixing, $CPR < 1$ means short-circuiting of the incoming air (and therefore no effective air exchange) and $CPR > 1$ stands for effective contaminant removal at the AOZ. According to van Wagenberg & Smolders (2002), CPR is typically greater than 1 at the AOZ in displacement ventilation systems. In the case of this investigation, the calculated CPR was always less than 1 which corresponds to an ineffective air exchange in the pit headspace (Fig. 4.11). Nonetheless, the CPR increased with increasing Ar at T_{set} = 21, 23 and 25 °C (Fig. 4.11). Implying more NH_3 was brought out, from the pit headspace to the room as the contribution of the buoyancy force to the airflow at the AOZ increased, compared to the momentum force of the outgoing air jets from the slatted floor inlet. This phenomenon occurred especially at higher $T_i – T_{GC}$ and lower ventilation rate (Fig. 4.12 & 4.13). On the contrary, lower $T_i – T_{GC}$ and higher ventilation rates suggest a greater contribution of the momentum force of the outgoing air jets at the slatted floor inlet to the airflow at the AOZ, compared to the buoyancy force. This may imply that under these conditions most of the incoming air flowed over the pen floor without entering the slurry pit. In fact, short-circuiting of incoming air in pig buildings was reported for UFAD systems in summer at high ventilation rate and high incoming air temperature. This especially occurs in buildings that position the exhaust duct above the slatted floor inlet at the height of less than 3 m (Klimaatplatform varkenshouderij, 2006; Adrion et al., 2013).

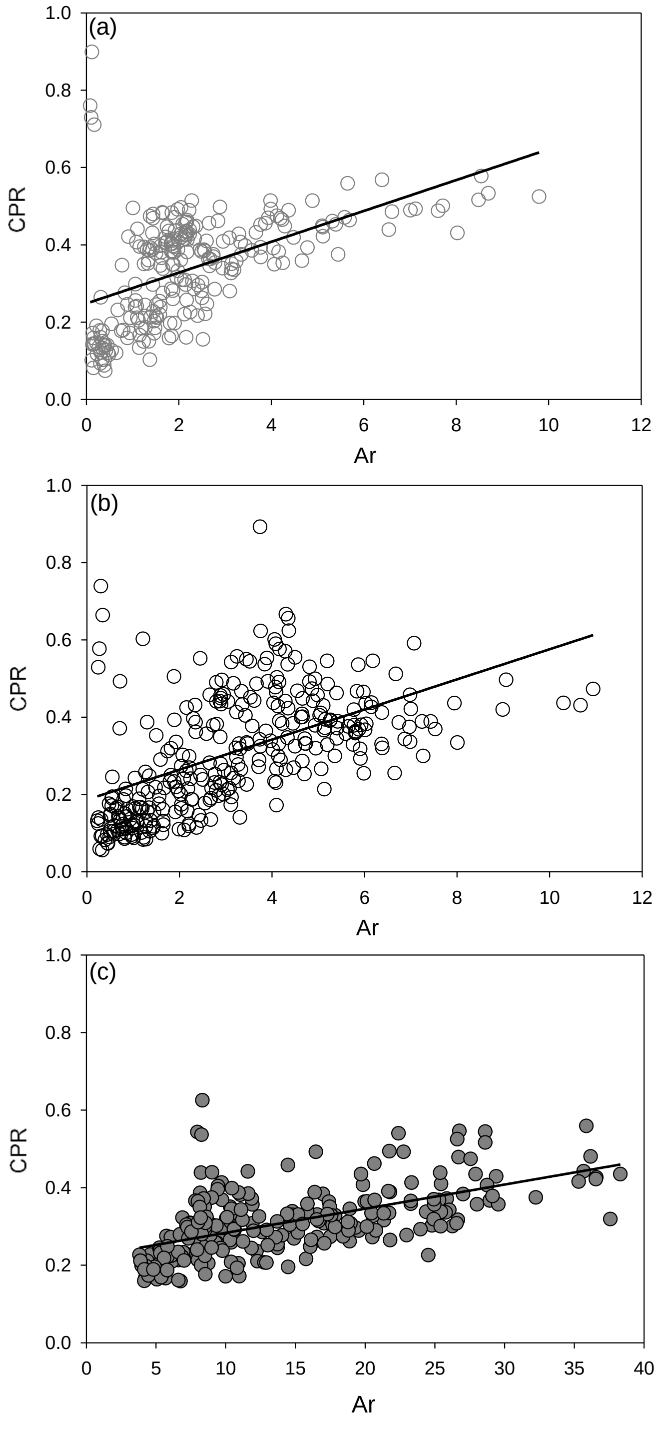

Fig. 4.11. — Relationship between slurry pit headspace NH_3 removal and Archimedes number at (a) T_{set} (21 °C) (b) T_{set} (23 °C) and T_{set} (25 °C) during the urea spraying experiment. Adjusted R^2 = 0.27, 0.22 and 0.33 in T_{set} (21 °C), T_{set} (23 °C) and T_{set} (25 °C), respectively.

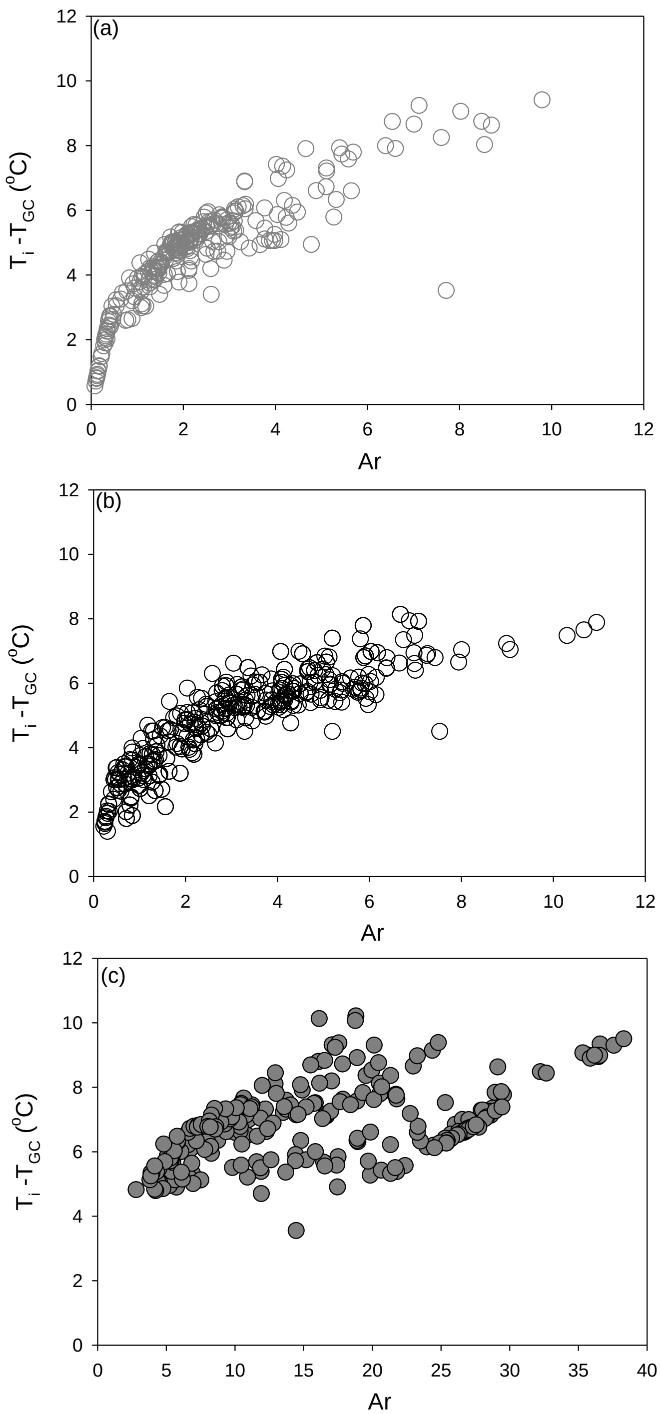

Fig. 4.12. — Relationship between $T_i - T_{GC}$ and Archimedes number at (a) T_{set} (21 °C) (b) T_{set} (23 °C) and T_{set} (25 °C) during the USE period.

Finally, although Fig. 4.11 shows the potential of low NH_3 removal from the slurry pit at low Ar, the influence of the Ar at this level on the thermal comfort of real pigs has not been verified. Therefore, it would be interesting that future studies use modelling tools such as Computational Fluid Dynamic (CFD) to characterise the air velocity and temperature distribution in the compartment. CFD allows simulating different building configurations at different climatic scenarios while obtaining high-resolution air velocity and temperature fields. This could stimulate research in the direction of optimising UFAD systems on reduction of draught on pigs and contaminants removal from the slurry pit to the room using for example the Ar as a control parameter (Kwon et al., 2015). UFAD systems in pig buildings are noted to provide better indoor air quality, more efficient cooling at the AOZ and lower heating and ventilation requirements compared to mixing ventilation systems (Threm et al., 2012).

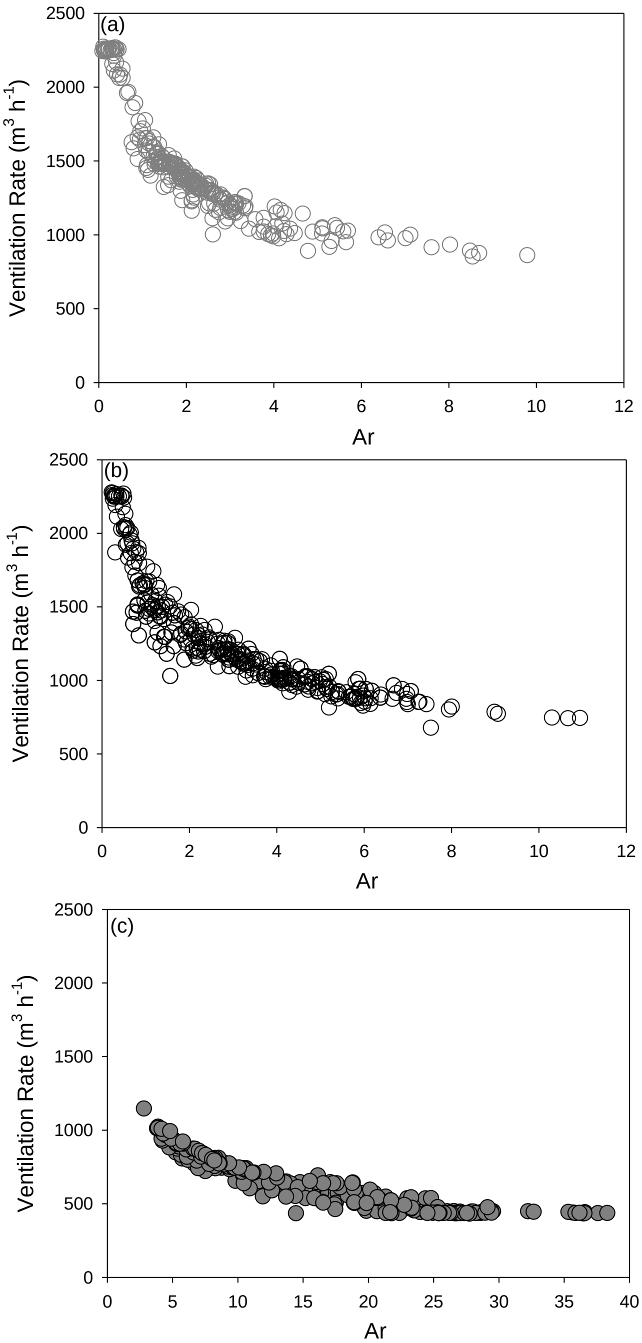

Fig. 4.13. — Relationship between ventilation rate and Archimedes number at (a) T_{set} (21 °C) (b) T_{set} (23 °C) and T_{set} (25 °C) during the USE period.

4.4. Conclusions

1 This experimental study found ground channel temperature to be a key factor affecting NH_3 emissions from a UFAD pig house (P < 0.001). It interacted with the ventilation set-point temperature (T_{set}) (P < 0.001) to influence NH_3 emission. Reducing the reference T_{set} from 23 to 21°C had no clear effect of on NH_3 emission, although the strategy affected ventilation rate and indoor temperature. Increasing the reference T_{set} from 23 to 25 °C reduced hourly NH_3 emission rate by 43% at T_{GC} 15 °C and 29% at ground channel temperature 18 °C. Ammonia emission between the 3 set-point temperatures did not differ at ground channel temperature of 22 °C.

2 An important explanatory phenomenon is the occurrence of displacement airflows entering the slurry pit, thereby transporting headspace NH_3 into the compartment. This phenomenon is promoted by higher differences between the room and ground channel air temperature, and therefore occurs especially at lower ventilation rates.

3 NH_3 displacement from the slurry pit headspace into the room positively correlated with the Archimedes number of the incoming air from the slatted floor inlet to the animal occupied zone.

Chapter 5: Effect of ventilation control settings on ammonia and odour emissions from a pig rearing building

This chapter was adapted from:
Tabase, R. K., Millet, S., Brusselman, E., Ampe, B., De Cuyper, C., Sonck, B., & Demeyer, P. (2020). Effect of ventilation control settings on ammonia and odour emissions from a pig rearing building. *Biosystems Engineering*, *192*, 215-231.

5.1. Introduction

Ventilation in modern pig buildings is mostly controlled by the settings of a computerised climate controller. However, field surveys show that farmers who are less familiar with these control systems can often poorly tune the control settings, resulting in higher VRs which can increase NH_3 and odour emissions (Vranken, 1999; Smith et al., 2009; Harmon et al., 2012). Using computer simulations, Vranken (1999) and Zhang et al. (2009) showed that optimally tuning the ventilation control settings (VCS) at the climate computer can reduce NH_3 and odour emissions by decreasing the VR. Thus, adapted ventilation control settings in pig housing can complement other high-performance BATs and further reduce the emissions from pig rearing buildings.

The effect of 9 different ventilation scenarios on the indoor climate and VR were assessed in chapter 2, via computer simulations, in a pig house by adjusting the set-point temperature (T_{set}), and the minimum (VR_{min}) and maximum (VR_{max}) ventilation settings. The results showed for 3 scenarios, 5 to 34% and 15 to 21% reductions in the winter and summer VRs, respectively, during two different fattening periods compared to the reference VCS. Subsequently, a preliminary test on the effect of T_{set} on NH_3 emissions in an experimental pig house equipped with artificial pigs revealed that increasing the T_{set} from 23 °C to 25 °C reduced the NH_3 emissions by 29 – 43% due to the relative reduction in the VR (chapter 4). The artificial pigs were made from galvanized steel, shaped into semi-cylinders with electrical heating cables to simulate sensible heat production from 50 kg pigs. However, validating these results in an actual pig production barn was still deemed necessary before developing practical recommendations. Therefore, an experiment was designed to:

1. Verify whether adjusting the VCS under practical conditions can fulfil the recommended indoor climatic requirements for pig production.
2. Verify under practical conditions whether NH_3 and odour emissions can be reduced by adjusting the VCS.
3. Understand the interaction between airflow and the NH_3 release from the emitting sources in the pig house with underfloor air distribution system.
4. Develop NH_3 and odour emission factors for the different VCS in the fattening house based on the case-control approach of the VERA test protocol (VERA, 2018).

These objectives were achieved by conducting a full-scale experiment using 8 compartments in 3 fattening rounds during 2016 – 2017, comparing the effect on NH_3 and odour emissions and on pig performance of the 3 promising VCS identified in chapter 2 with the reference ventilation setting at the ILVO/UGent/HoGent fattening pig building.

5.2. Materials and methods

5.2.1. Experimental facility and ventilation system

Experiments were performed at the ILVO/UGent/HoGent fattening pig building, Merelbeke, Belgium (Fig. 2.1). The pig house consisted of 16 separate (i.e. slurry pit and exhaust) underfloor air inlets in mechanically ventilated fattening pig compartments (8 partly and 8 fully slatted). This investigation used the 8 fully slatted compartments, which were each divided into 8 pens. The underfloor air inlet system in each of the compartments had slatted floor openings at the service alley.

The ventilation system operated as follows: negative pressure at the exhaust duct of diameter 0.45 m induced fresh air into the central underground air channel from outside the experimental facility (Fig. 2.1). The incoming air then passed through the underfloor air channel beneath the service alley and through the slatted floor inlet into the compartment. The ventilated air then exited the compartment via an exhaust duct to the central overhead exhaust channel. Each of the central overhead exhaust channels was equipped with two 0.9 m diameter fans (Rotor BV, Eibergen, the Netherlands) with a maximum ventilation capacity of 55,000 m^3 h^{-1} fan^{-1}, ventilating all compartments in the row served by the central exhaust system. The exhaust ducts in each compartment had a maximum airflow capacity of 3,700 m^3 h^{-1} and were equipped with an adjustable damper and a differential pressure transmitter (Type 699, Huba Control, Würenlos, Switzerland) (range 0 to 100 Pa; accuracy < 0.5% f.s.). Additionally, a central underground air channel had four 24m-long water tube heaters that generate 200 W m^{-1} $tube^{-1}$ when the incoming air dropped below 10 °C (Fig. 2.1c). Each compartment had a separate slurry pit that was filled to the maximum slurry depth of 0.14 m via the overflow tube from the slurry pit to the outside storage tank. Moreover, the slurry in each compartment was emptied at least once every fortnight during the investigation.

5.2.2. Experimental design and the tested ventilation control settings

The present study compared the effect of three VCS (i.e. T1, T2 and T3 in Table 5.1) and the reference strategy (CON) on the indoor climate, NH_3, CO_2 and odour emissions during the 3 fattening periods. The experiment began in August 2016, using the VERA protocol case-control design until November 2017 (VERA, 2018). During the experiment, the effect of the investigated treatments on the pig performance was also monitored. The T_{set} at the beginning of fattening period was 24 °C for the CON but this decreased to 21 °C at the end of the fattening period. However, VR_{min} and VR_{max} in the CON were fixed at 14 m^3 h^{-1} pig^{-1} and 70 m^3 h^{-1} pig^{-1} respectively, throughout the fattening period.

Table 5.1. Ventilation Control Settings (VCS) for the control (CON) and the 3 treatments (T).

Treatment	T_{set} (°C)	V_{phase} (Day)	VR_{min} (m^3 h^{-1} pig^{-1})	VR_{max} (m^3 h^{-1} pig^{-1})
CON	24	0 - 28	14.0	70.0
	23	29 - 48	14.0	70.0
	22	49 - 77	14.0	70.0
	21	78 - 120	14.0	70.0
T1	*26*	0 - 28	14.0	70.0
	25	29 - 48	14.0	70.0
	24	49 - 77	14.0	70.0
	23	78 - 120	14.0	70.0
T2	*26*	0 - 28	**10.5**	**63.0**
	25	29 - 48	**10.5**	**63.0**
	24	49 - 77	**10.5**	**63.0**
	23	78 - 120	**10.5**	**63.0**
T3	*25*	0 - 28	***3.5***	***56.0***
	24	29 - 48	***7.0***	***59.5***
	23	49 - 77	***10.5***	***63.0***
	22	78 - 120	***14.0***	***70.0***

For T1, the T_{set} was set at +2 °C higher than the CON, while the VR_{min} and VR_{max} were fixed at the same level as the CON throughout the fattening periods. In T2, the T_{set} was set at +2 °C higher than the CON, while the VR_{min} and VR_{max} settings were fixed at 75% and 90% of the CON, respectively, throughout the fattening periods. The T_{set} in T3 was set at +1 °C higher than the CON while the VR_{min} and VR_{max} settings were initially fixed at 25% and 80% of the CON ventilation requirement, respectively at the start of the fattening period, and progressively increased by 25% and 5% of the CON ventilation requirements, respectively, as the pigs grew during the fattening period (Table 5.1). Furthermore, the climate control computer automatically controlled the VR according to the selected VCSs at (day 0 – 28), (day 29 – 48), (day 49 – 77) and (day 78 – 120) ventilation phases (V_{phase}), in the climate control computer at a bandwidth of 5 °C for all the VCSs (Table 5.1). Equation 2.22 shows the algorithm used during the investigation, in the climate control computer.

The experimental design included a duplicate of each VCS in each fattening period. The ILVO/UGent/HoGent pig barn applied the 3-week management system. Therefore, in each fattening round, a VCS was randomly assigned to 2 of the 8 compartments in 3 batches (Tables 5.2 – 5.4). Each compartment housed 48 pigs with 6 pigs per pen at a stocking density of 0.83 m^2 pig^{-1}, fed *ad libitum* in 3 feeding phases (Table 5.5) with free access to water. Half of the pigs were a cross between a Piétrain boar and a RA-SE hybrid sow, the other half were a cross between a Piétrain boar and a TOPIGS hybrid sow, evenly assigned to an equal number of pens per compartment by sex and genetics at the average pig age of 10 weeks.

Table 5.2. The experimental design in fattening round 1.

	Round 1			Start	Finish
Batch 1	Compartment 6 **CON (1)**	Compartment 13 **T1 (1)**	Compartment 15 **T2 (1)**	11-Aug-16	16-Nov-16
Batch 2	Compartment 5 **T3 (1)**	Compartment 14 **CON (1)**	Compartment 7 **T1 (2)**	01-Sep-16	12-Dec-16
Batch 3	Compartment 8 **T2 (2)**	Compartment 16 **T3 (2)**		22-Sep-16	27-Dec-16

Table 5.3. The experimental design in fattening round 2.

	Round 2			Start	Finish
Batch 1	Compartment 7 **T2 (1)**	Compartment 6 **T3 (1)**		19-Jan-17	08-May-17
Batch 2	Compartment 14 **T2 (2)**	Compartment 5 **T1 (1)**	Compartment 15 **CON (1)**	08-Feb-17	15-May-17
Batch 3	Compartment 8 **T3 (2)**	Compartment 16 **T1 (2)**	Compartment 13 **CON (2)**	01-Mar-17	12-Jun-17

Table 5.4. The experimental design in fattening round 3.

	Round 3			Start	Finish
Batch 1	Compartment 5 **T2 (1)**	Compartment 6 **T1 (1)**	Compartment 7 **CON (1)**	14-Jun-17	04-Oct-17
Batch 2	Compartment 8 **CON (2)**	Compartment 16 **T2 (2)**	Compartment 15 **T3 (1)**	08-Jul-17	11-Oct-17
Batch 3	Compartment 14 **T1 (2)**	Compartment 13 **T3 (2)**		26-Jul-17	15-Nov-17

Table 5.5. Pig feed ingredients and nutritional compositions.

Ingredient composition, %	20 - 45 kg	45 - 70 kg	70 - 115 kg
Wheat	34.68	40.00	40.00
Barley	15.00	-	-
Soybean meal	11.94	3.51	3.50
Corn	9.19	4.56	7.06
Wheat gluten feed	-	6.71	10.87
Rapeseed meal	5.38	7.16	0.51
Sunflower meal	-	4.15	7.00
Barley meal	5.00	13.00	13.00
Wheat bran	5.00	7.00	7.00
Palm kernel flakes	3.00	4.00	5.00
Beat pulp	2.00	2.00	-
Beet molasses	1.50	1.50	1.50
Animal fat	1.50	0.88	0.03
Limestone	1.25	1.10	1.10
L-Tryptophan	1.23	1.27	0.26
L-Threonine	0.94	1.04	1.03
L-Lysine	0.72	0.66	0.69
DL-Methionine	0.13	0.07	0.06
Premix piglets	0.75	-	-
Salt	0.38	0.28	0.27
Monocalciumphosphate	0.11	-	-
Choline	0.06	0.06	0.06
Vitamins & minerals	0.25	0.75	0.75
Biolys 70 (LYS 54.6%)	-	0.30	0.30
Nutrient composition (%)			
Moisture	12.55	12.11	12.19
Crude protein	16.50	15.63	14.50
Crude fat	3.90	4.12	3.48
Crude ash	4.95	4.72	4.59
Ca	0.73	0.65	0.60
P	0.43	0.45	0.45
Digestible P	2.60	2.10	1.80
AID-Lysine	1.05	0.97	0.87
AID-Methionine	0.35	0.31	0.28
AID-Methionine + Cysteine	0.64	0.61	0.55
AID-Tryptophan	0.22	0.20	0.17
AID-Threonine	0.72	0.67	0.60
Net energy (MJ/kg)	9.60	9.50	9.40

AID = apparent ileal digestible

Pigs were weighed individually at the start of the fattening period and before the change of feeding phase. The supplied feed was weighed on pen basis. Pens shifted to the second and third feeding phase at an average pen body mass of 45 and 70 kg, respectively. On the day before slaughter, the pigs were weighed in groups (i.e. per pen) and individually on the day of slaughter. The pigs were slap-marked individually on the day of slaughter, and the carcass data was requested from the slaughterhouse. Note that in this investigation, the pigs were slaughtered at similar live weight (LW), but not at similar age, and two batches of pigs went to slaughter per compartment at the slaughter weight ~ ≥ 115 kg. The average daily feed intake (DFI), daily gain (DG) and the gain/feed ratio (G:F) were calculated per feeding phase and over the entire experiment.

5.2.3. Indoor climate and emission measurements

A Pt1000 (-50° C to +100° C) sensor of the "Hotraco System" (Hotraco Agri, Hegelsom, the Netherlands) measured the climate control temperature (indoor temperature (T_i)) in the compartments, at 1.4 m above the floor in pen 3 (Fig. 2.1d). The T_i sensor was located at this same location in all compartments at the experimental facility. Two Pt1000 sensors also measured the outside temperature (T_{out}) and the central underground air channel temperature (T_{GC}). The T_{out} sensor was located 1.4 m above the ground under the eastern eave roof of the building. The T_{GC} sensor was located 1.3 m above the floor of the air channel. The 'Hotraco System' controlled and measured the VR. The VR was calculated from the measured exhaust duct damper opening size and the differential pressure between each compartment and the overhead central exhaust channel that was previously validated in a wind tunnel by 'Hotraco' (Hotraco Agri, Hegelsom, the Netherlands). An Orion-VS12 data logger (Hotraco Agri, Hegelsom, the Netherlands) logged the VR, T_i, T_{out} and T_{GC} at 1 min intervals. The relative humidity (RH) and temperature (T_{ex}) at the exhaust duct were only measured during the third fattening round (Table 5.4) using the Testo 175H1 humidity-temperature sensors/data loggers (Testo Inc, New Jersey, USA) (RH range: 0 to 100%, temperature range:-20 °C to +55 °C; accuracy ±2% for RH and ±0.40 °C for temperature). The Testo sensor/data loggers measured and logged the data at a sampling frequency of 1 min. In addition to the indoor climatic parameters and VR measurements, airflow pattern in the test compartments were qualitatively determined by releasing smoke from a smoke generator (Mini Mist, Le Maitre Ltd, Surrey, UK) at the underfloor air channel of the compartment.

A Fourier Transform Infrared Spectrometer (FTIR) gas analyser (Gasmet CX4000, Gasmet Technology Oy, Helsinki, Finland) continuously measured the exhaust (in the exhaust duct) and outside gaseous concentrations (NH_3, CO_2, CH_4, N_2O) during this study. After the factory calibrations at Gasmet (Helsinki, Finland), the FTIR performed zero-point calibrations once every morning using N_2 gas. The FTIR sequentially took a minimum of 3 measurements per sampling location every 1 h.

Odour samples were collected in six sampling days per VCS in each fattening round (i.e. three sampling days per duplicate treatment), evenly distributed over the fattening period. On each sampling day, 3 consecutive 30 min samples were collected per compartment. Hence for each VCS the total number of samples taken amounted to 6 sampling days per fattening round × 3 samples per day × 3 fattening rounds = 54 samples during the entire study. The odour samples were collected at the exhaust duct (Fig. 2.1d) between 10 a.m. and 1 p.m. using PTFE tubes. The lung principle was used to collect the samples into the 40 L Nalophan (Foodpack Benelux, Harderwijk, the Netherlands) bags, as described in detail by Hove (2018). The collected odour samples were then transported and analysed at the ILVO odour lab within 2 h after the collection. In the laboratory, odour concentrations were determined by forced choice olfactometry using a TO9 Olfactometer (Olfasense GmbH, Kiel, Germany) in compliance with the EN 13725 standards (CEN, 2003). Each sample was analysed twice by 4 qualified panellists, resulting in 8 individual threshold estimates (ITEs). The odour concentration of each sample in OU_E m^{-3} was calculated as the geometric mean of the ITEs. Before the odour analysis, the panellists were individually screened using n-butanol and their measuring history was evaluated to ensure they still complied with both panel selection criteria of CEN (2003).

5.2.4. Data analysis

All data for temperature, relative humidity, VR and the gaseous (i.e. NH_3 and CO_2) concentrations were firstly processed as hourly averages. The hourly (j) gaseous emission rates (ER_{ij}, g h^{-1}) per treatment (i) were then calculated from these data as in Eq. 5.1:

$$ER_{ij} = VR_{ij} \times \left(C_{ex_{ij}} - C_{in_{ij}}\right) \quad (5.1)$$

Where VR (m^3 h^{-1}) is the ventilation rate while C_{ex} and C_{in} (g m^{-3}) represent exhaust and incoming gas concentrations, respectively. The daily (k) gaseous emission rates (ER_{ik} , g d^{-1}) per treatment (i) were calculated as the cumulative emission over the 24 h in one day.

$$ER_{ik} = \sum ER_{ij} \quad (5.2)$$

The odour ER on each sampling day was determined based on the 3 odour samples. Since odour is log-normal distributed (Bilsen, Moonen, Aerts, Baeyens, Van Laer, 2016), the average odour concentration was calculated as:

$$logC_{av} = \frac{\sum_{i=1}^{n} logC_l}{n} \quad (5.3)$$

where: C_{av} = the average odour concentration (OU_E m^{-3}); C_l = measured odour concentration of sample l (OU_E m^{-3}) and n = the number of odour samples. The odour ER per VCS (i) on each sampling day (k) was calculated by multiplying the log transformed average odour concentration by the average VR (m^3 s^{-1}) during the measurement period as in Eq. 5.4 divided by the number of pigs in the compartment (OU_E s^{-1} pig^{-1}).

$$ER_{jk} = \frac{VR_{ik} \times \left(C_{av_l}\right)}{a} \tag{5.4}$$

The current investigation used the hourly average exhaust NH_3 and CO_2 concentrations in the different VCSs to assess the air quality in the pig barn. This was because the gaseous concentrations were measured only in the exhaust duct during the experiment. In addition, this investigation used the recommended 20 ppm and 3,000 ppm maximum CO_2 and NH_3 concentration limits from the CIGR (1984) to assess the influence of the VCS on the indoor air quality. This was because the guidelines for the maximum gaseous concentration limits in livestock housing vary between different countries. For example, the maximum NH_3 concentration limit in the different EU countries ranges from 10 ppm to 50 ppm, whereas the maximum CO_2 concentration limit ranges from 2,000 ppm to 5,000 ppm (CIGR, 1984).

5.2.4.1. Calculations according to the VERA protocol

The NH_3, CO_2 and odour emission factors were calculated per treatment based on the case-control approach of the VERA test protocol (VERA, 2018) using a minimum of six different, 24-h measurements distributed over the fattening period according to additional requirements. Therefore, since this study provided continuous measurements over entire fattening periods, the daily NH_3 and CO_2 emissions in each treatment and their duplicates were averaged over the first (i.e. 0 – 50%) and second half (i.e. 50 – 100%) of the fattening period, evenly distributed into the six 2-months period in the year. In doing so, we ensured that the daily averaged gaseous emissions in the second half of the fattening period were evenly distributed within the year to improve the accuracy of the computed gaseous emissions, since most emissions occur during the second half of the fattening period. Similarly, this procedure was used to compute the odour emission factors using the data of six measurement days per treatment and their duplicates, which were evenly distributed over the fattening period/year. The NH_3 and CO_2 emissions were subsequently converted from g pig^{-1} d^{-1} into kg pig^{-1} yr^{-1} and corrected for 36 days in the year that the pig building was empty. The unit of the odour emissions factor remained at OU_E s^{-1} pig^{-1}.

5.2.4.2. Statistical analysis

A generalised linear mixed modelling (GLIMMIX procedure, in SAS 9.4) approach was used to test the treatment effect on indoor climate and gaseous emissions, with one linear mixed model per investigated parameter. The terms in the gaseous models were treatment, T_{GC}, ΔT (T_i - T_{GC}), V_{phase}, Treatment × T_{GC}, Treatment × ΔT and Treatment × V_{phase}. The response variables were C_{ex}, ER, T_i and VR. The statistical analyses of the gaseous ERs were performed on g d^{-1} kg-LW^{-1} basis, where d and LW, represent the day and live weight, respectively. Compartment and time were added to the model as random effects to correct for common unknown environmental factors at compartment level and the correlation between successive measurements was modelled using a type 1-autoregressive structure. To explore the difference in the response variables between the treatments, *post hoc* tests on the least squares means were performed at two fixed T_{GC} (i.e. 10 and 17 °C) combined with two fixed ΔT (i.e. 5 and 10 °C) to illustrate the effect of the interaction terms. A *post hoc* test with a Tukey-Kramer correction for multiple comparisons was used to test these differences at a total significance level of 0.05. Furthermore, the overall difference between T1, T2, T3 and the CON VCS for the NH_3 and odour emissions and the other measured variables were statistically tested using Dunnett's test, which was corrected for the measurement period and the fattening round at the significance level of 0.05. The dependent variables were considered normally distributed based on the graphical inspection of the residuals (histograms and QQ plots).

A general linear mixed-effect modelling approach was used to test the effect of the VCS on pig performance (bodyweight, DFI, DG and gain:feed ratio) and lean meat percentage using the R Statistical Software Package (R Core Team, 2017). Performance parameters were analysed for the entire growing-finishing period with VCS, sow line, sex and body mass at start as fixed effects and compartment and round as random effects, and per feeding phase using a longitudinal model that included VCS × phase, sow line × phase, sex and bodyweight at start as fixed effects, and compartment and round as random effects. Lean meat percentage was analysed with VCS, sow line and cold carcass weight as fixed effects, and slaughter date, compartment and round as random effects. The pen was considered as the experimental unit for the analysis of performance, the animal was considered as the experimental unit for the analysis of lean meat percentage. Differences were considered significant if $P < 0.05$. When the P-value for interaction terms was above 0.1, the interaction was excluded from the final statistical model. A post hoc test with a Tukey-Kramer correction for multiple comparisons was used to compare treatment means.

5.3. Results and discussion

5.3.1. Effect of the VCS on indoor air quality and pig performance

Figure 5.1 shows the boxplot (with the outliers) of the hourly average NH_3 and CO_2 concentrations measured in the exhaust duct during the experiment between T1, T2, T3 and the CON. Overall, the average NH_3 and CO_2 concentrations in all the VCSs were below the maximum limits in the CIGR (1984) guideline (20 ppm and 3,000 ppm, respectively). In some cases, the hourly average NH_3 and CO_2 concentrations in all the VCSs exceeded the maximum concentration limits. Nonetheless, the air quality in the CON was higher than T1, T2 and T3. For example, during the entire experiment the hourly average NH_3 concentration in the CON exceeded the maximum concentration limit in 5.5% of the total measuring hours (12,681). Moreover, in 11.6%, 31.4% and 16.5% of the total measuring hours, the NH_3 concentrations in T1, T2 and T3 were higher than maximum NH_3 limit. The CO_2 concentration in the CON exceeded the maximum CO_2 limit for the total measuring hours by 0.8% compared to 0.3%, 5.0% and 5.3% respectively in T1, T2 and T3.

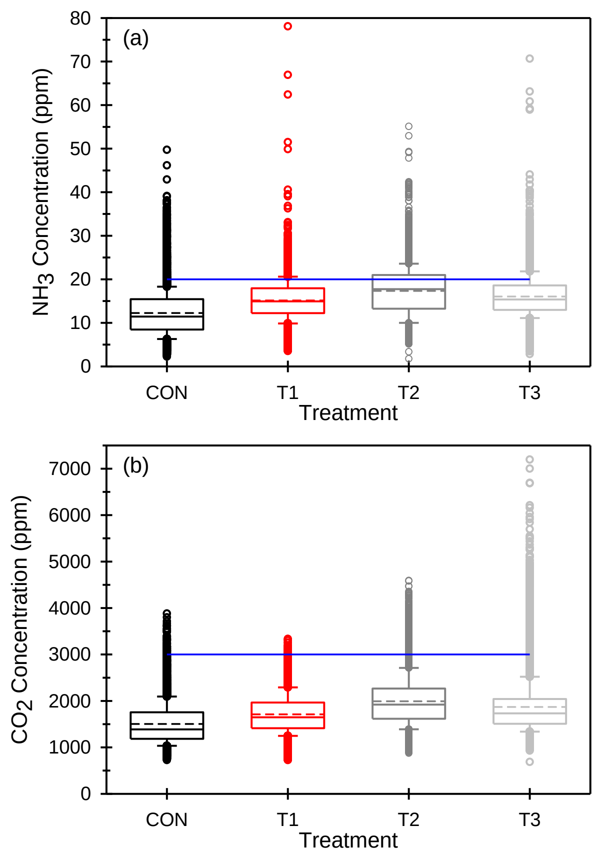

Fig. 5.1 — Boxplot (with outliers) of the exhaust NH_3 and CO_2 concentration between CON—Black; T1—Red; T2— Dark grey and T3—Light grey during the entire experiment. The dash and solid lines in the boxplots are the mean and median NH_3 and CO_2 concentrations, and the blue lines are the maximum NH_3 and CO_2 concentration limits in the CIGR (1984).

The higher gaseous concentrations in the VCSs occurred mostly in winter when the temperature of the inlet air was low and when the pig weight was low (Fig. 5.2). As a result, at the beginning of the fattening round, the ventilation system operated at the VR_{min} in all the VCSs (Fig. 5.2c). Nevertheless, the gaseous concentrations were higher than the CON by reducing the VR_{min} in T2 and T3 (Figs. 5.2a & 5.2b), which can negatively affect the animal health, welfare, performance and the farmer's working environment (Donham et al., 2002; Wathes et al., 2003).

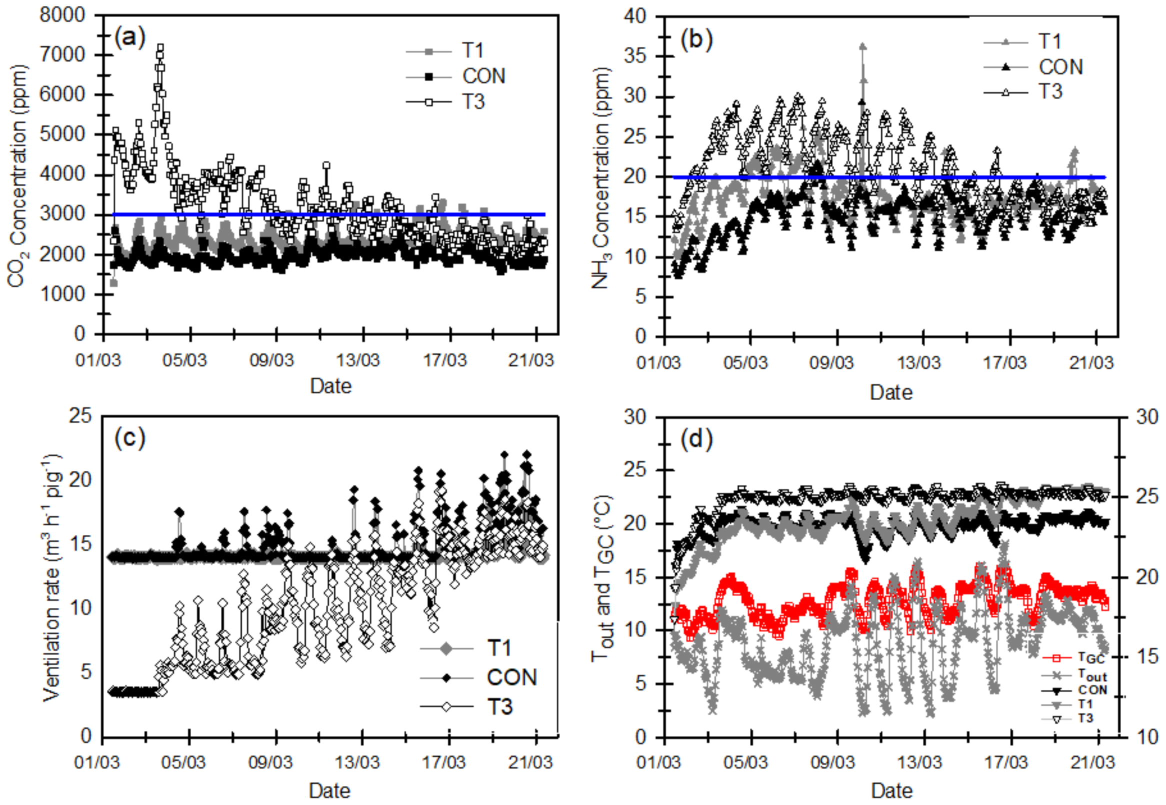

Fig. 5.2 — Hourly average (a) CO_2 (b) NH_3 (c) ventilation rate and (d) air temperatures at the start of the fattening period in winter between CON; T1 and T3, under simultaneous measurement in summer; where the blue lines are the maximum NH_3 and CO_2 concentration limits in the CIGR (1984).

It is therefore not recommended to apply T2 and T3 in winter in order to achieve an acceptable indoor air quality. It is possible to improve the indoor air quality in T2 and T3 as seen in T1 by increasing the VR_{min} to the CON, (Figs. 5.2a & 5.2b). However, the higher room temperature in T3 than the CON (Fig. 5.2d) implies that in this occasion increasing the VR_{min} is a trade-off to provide the young pigs with the optimum room temperature and the need to improve indoor air quality in the absence of supplementary heating. This is often a dilemma for the farmer (Smith et al., 2009). Apart from the higher NH_3 and CO_2 concentrations in the winter when the pig weight was low (Fig. 5.2), higher NH_3 and CO_2 concentrations were also observed in autumn towards the end fattening period. This occurred when the inlet air temperature decreased and the body weight of the pigs was high because the pigs excreted more urine and faeces (Figs. 5.3c & 5.3f). Also, the outlier in NH_3 concentrations was from of the emission peaks after emptying the slurry pit, which occurred in all the VCSs (Fig. 5.1a).

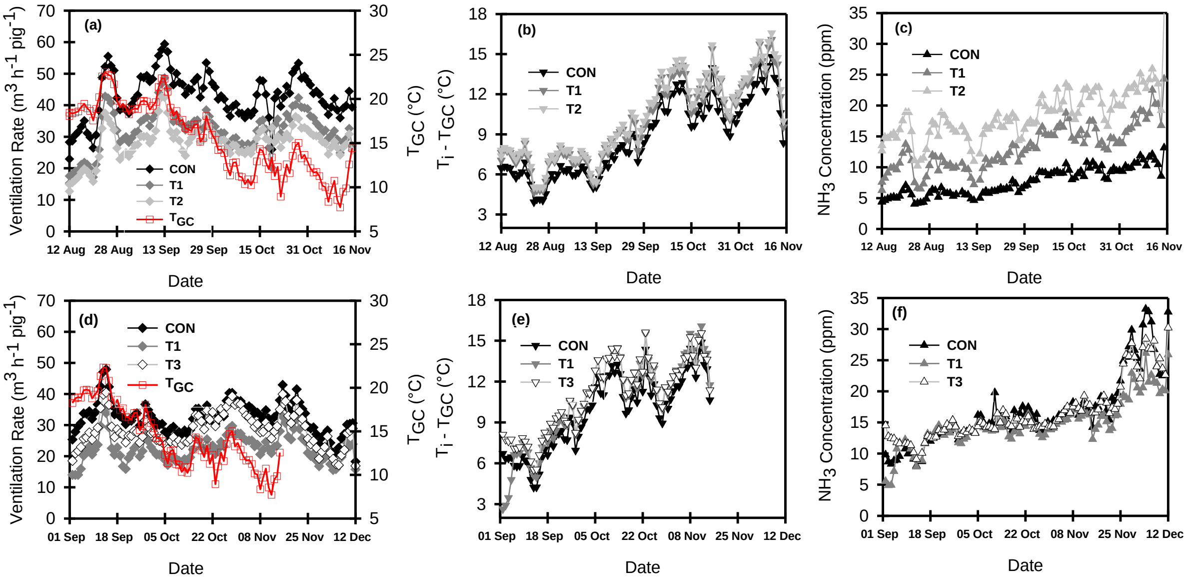

Fig. 5.3 — Daily average ventilation rate, ΔT and exhaust NH_3 concentration from 11 August – 16 November 2016 (a – c) and 01 September – 12 December 2016 (e – f) during the fattening period between CON—Black; T1—Dark grey, T2—Light grey and T3—White, under simultaneous measurement.

In the present investigation, only the relative humidity of the exhaust air was measured during the third fattening period from June to November 2017. Therefore, due to the shorter measuring period compared to the gaseous concentration measurements, detailed analysis was not performed on the effect of the VCS on the exhaust relative humidity. However, the calculated average relative humidity showed similar exhaust RH between the three new VCSs and the CON during the measuring period. The hourly average exhaust relative humidity in T1, T2 and T3 are 61.8 ± 5.1%, 61.8 ± 5.1% and 62.2 ± 5.4%, respectively, compared to 61.6 ± 5.4%. According to CIGR (1984), the average exhaust relative humidity in all the treatments were between the recommended minimum (40%) and maximum values (80%) for livestock housing.

The overall average DG, DFI, gain/feed ratio and the lean meat percentage in all the treatments (Table 5.6) agree with the pig performance results reported in Flemish pig production (AHDB, 2017). Furthermore, the pig performance results did not reveal significant differences with respect to the DG, DFI, gain/feed ratio or lean meat percentage between the three new VCSs and the CON, except for the DFI during the first feeding phase, which demonstrated lower DFI in T3 than the CON (Table 5.6). Although, little research has been performed on the effect of CO_2 and NH_3 on the pig performance, the lower VR_{min} in T3 during the first feeding phase probably lead to the accumulation of other noxious pollutants, which lowered DFI in T3 than the CON (Donham et al., 2002; Wathes et al., 2003).

Table 5.6. Effect of the VCS on the pig performance (means ± SE).

	Treatment				*P*-value		
	CON	T1	T2	T3	Phase	Treatment	Treatment × Phase
Body weight (kg)					<0.001	0.274	NS
End phase 1	48.7 ± 0.5	47.6 ± 0.6	48.4 ± 0.4	46.3 ± 0.6			
End phase 2	73.0 ± 0.7	71.7 ± 0.9	72.9 ± 0.6	71.8 ± 0.7			
End phase 3	118.5 ± 0.9	116.8 ± 0.8	119.1 ± 0.5	116.6 ± 0.7			
DFI (kg)					-	-	0.045
End phase 1	1.53^{a} ± 0.02	1.46^{ab} ± 0.02	1.43^{ab} ± 0.03	1.37^{b} ± 0.03			
End phase 2	2.05 ± 0.03	1.98 ± 0.04	2.07 ± 0.04	1.99 ± 0.03			
End phase 3	2.62 ± 0.04	2.55 ± 0.03	2.56 ± 0.04	2.55 ± 0.03			
DG (g)					<0.001	0.320	NS
End phase 1	801 ± 13	767 ± 16	770 ± 10	736 ± 12			
End phase 2	874 ± 19	854 ± 17	875 ± 19	856 ± 14			
End phase 3	901 ± 12	887 ± 13	904 ± 12	875 ± 12			
G:F (kg kg^{-1})					<0.001	0.723	NS
End phase 1	0.53 ± 0.01	0.52 ± 0.01	0.55 ± 0.01	0.54 ± 0.01			
End phase 2	0.43 ± 0.01	0.43 ± 0.00	0.42 ± 0.01	0.43 ± 0.00			
End phase 3	0.35 ± 0.00	0.35 ± 0.00	0.36 ± 0.01	0.34 ± 0.00			
Overall performance							
DFI (kg)	2.19 ± 0.03	2.12 ± 0.02	2.14 ± 0.03	2.10 ± 0.02	-	0.195	-
DG (g)	866 ± 10	847 ± 9	860 ± 9	835 ± 8	-	0.396	-
G:F (kg kg^{-1})	0.40 ± 0.003	0.40 ± 0.002	0.40 ± 0.004	0.40 ± 0.003	-	0.263	-

NS, not significant; Different letters indicate significant differences between treatments.

5.3.2. Effect of the VCS on ventilation rate

Table 5.7 uses two different data sets to compare the hourly average ventilation rate between the three new treatments and the CON. The first data set is the hourly average ventilation rate collected during the continuous measurement of the NH_3 and CO_2 concentrations. The second data set is the overall average ventilation rate collected during the odour sampling. The gaseous concentration dataset showed that T1, T2 and T3 significantly lowered the ventilation rate by 17 – 28% compared to the CON (36.1 m^{-1} h^{-1} pig^{-1}). Similarly, the odour data set confirmed that the overall average ventilation rate in T1, T2 and T3 were significantly reduced by 14 – 27% compared to the CON (36.3 m^{-1} h^{-1} pig^{-1}). The average daily ventilation rates between the three new treatments and the CON (Figs. 5.3 & 5.4) verified the results in Table 5.7. Also, the comparable reductions in the average ventilation rate between the gaseous and the odour datasets were expected, because the sampling strategy applied during odour measurement strictly adhered to the VERA protocol (section 5.2.4.1).

Table 5.7. Effect of ventilation control settings on the hourly average indoor temperature, ventilation rate, CO_2, NH_3, odour concentrations and emission rate.

Variable	**T1**	**T2**	**T3**	**CON**
^{x} T_i (°C)	25.0 (1.1) ***	25.4 (1.4) ***	24.9 (0.9) ***	24.0
^{y} T_i (°C)	25.0 (1.4) *	24.9 (1.2) *	25.0 (1.3) *	23.7
^{x}VR (m^3 h^{-1} pig^{-1})	27.0 (-25%) ***	25.9 (-28%) ***	29.9 (-17%) **	36.1
^{y}VR (m^3 h^{-1} pig^{-1})	27.2 (-25%) **	26.7 (-27%) ***	31.1 (-14%) *	36.3
CO_2 concentration (ppm)	1774 (13%) †	1999 (28%) **	1824 (17%) *	1564
NH_3 concentration (ppm)	15.4 (21%)	17.5 (38%) *	15.8 (25%)	12.7
Odour concentration (OU_E m^{-3})	1413 (-3%)	1708 (17%)	1774 (22%)	1457
CO_2 emission rate (g h^{-1} pig^{-1})	59 (-9%)	67 (3%)	64(-2%)	65
NH_3 emission rate (g h^{-1} pig^{-1})	0.28 (-3%)	0.29 (1%)	0.3 (3%)	0.29
Odour emission rate (OU_E s^{-1} pig^{-1})	10 (-34%) *	12 (-22%)	15 (-5%)	16

† 0.1 > p > 0.05; * 0.05 > p > 0.01; ** 0.01 > p > 0.001; *** p < 0.001, in brackets is the difference

^{x} T_i and ^{x} VR for the NH_3 and CO_2, and ^{y} T_i and ^{y} VR for odour data

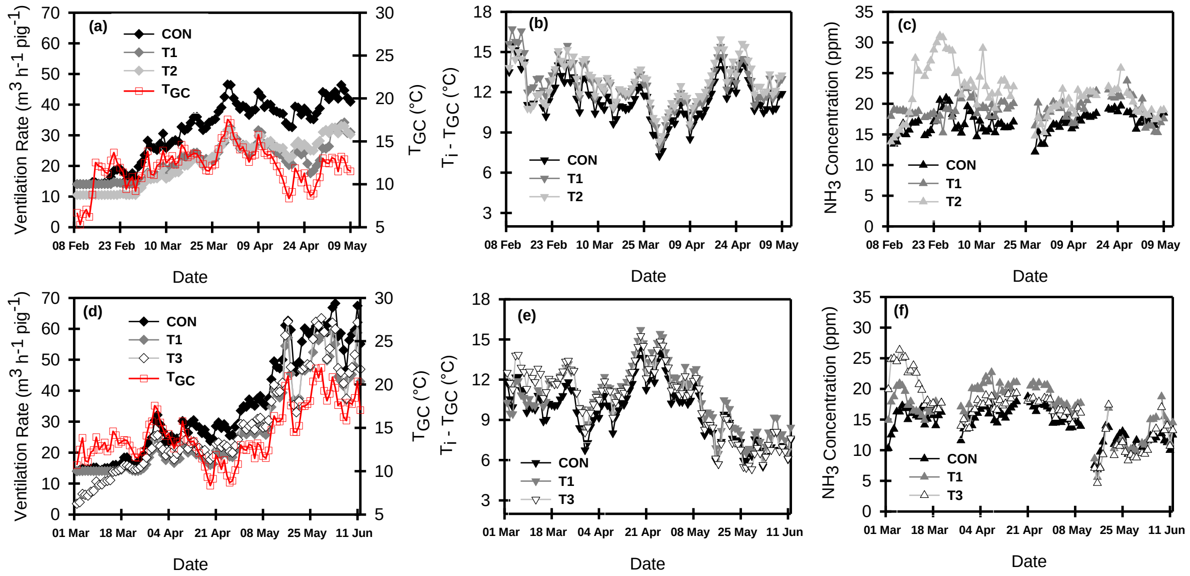

Fig. 5.4 — Daily average ventilation rate, ΔT and exhaust NH_3 concentration from 8 February – 10 May 2017 (a – c) and from 01 March – 12 June 2017 (e – f) during the fattening period between CON—Black; T1—Dark grey, T2—Light grey and T3—White, under simultaneous measurement.

In Table 5.7, it was clear that adjusting the T_{set} alone in T1 lowered the average hourly ventilation rate to a level similar to T2 and had a greater effect on lowering the hourly average ventilation rate than in T3. This was because the effect of simultaneous adjustment of the T_{set}, VR_{min} and VR_{max} in T2 and T3 on reducing the ventilation rate was seen only during the beginning of the fattening period in winter compared to T1 (Figs. 5.4a & 5.4d). Furthermore, the minor effect of the requested VR_{min} and VR_{max} in reducing the hourly average ventilation rate in T2 and T3 was because the ventilation system mainly operated within the ventilation bandwidth (Fig. 5.5). The fact that the T_{GC} did not drop below 0 °C in winter and did not increase above 28 °C in summer (Fig. 5.6) explain why the VCSs operated within the ventilation bandwidth and less at the extreme VR_{min} and VR_{max}. Another reason was that the higher T_{set} in T1, T2 and T3 compared to the CON (Table 5.1) lowered the effect of T_{GC} and T_{out} on the T_i, particularly on hotter days. This minimised the climate computer operation at the VR_{max} in the three new treatments compared to the CON. This assumption was previously verified in the experimental pig house equipped with the mock-up pigs (chapter 4), where the T_{set} was adjusted by either -2 °C or +2 °C compared to the reference strategy. Furthermore, the central underground air channel affected the T_{GC} as follows: supplementary heating in the air channel was turned on at $T_{GC} < 10$ °C (Fig. 2.1c) and the underground air channel served as a heat sink in summer, thus cooling the incoming air, and a heat source in winter, thereby heating the incoming air (Deglin et al., 1999; Threm et al., 2012). Together these effects explain the relatively stability T_{GC} compared to the more variable T_{out} (Fig. 5.6).

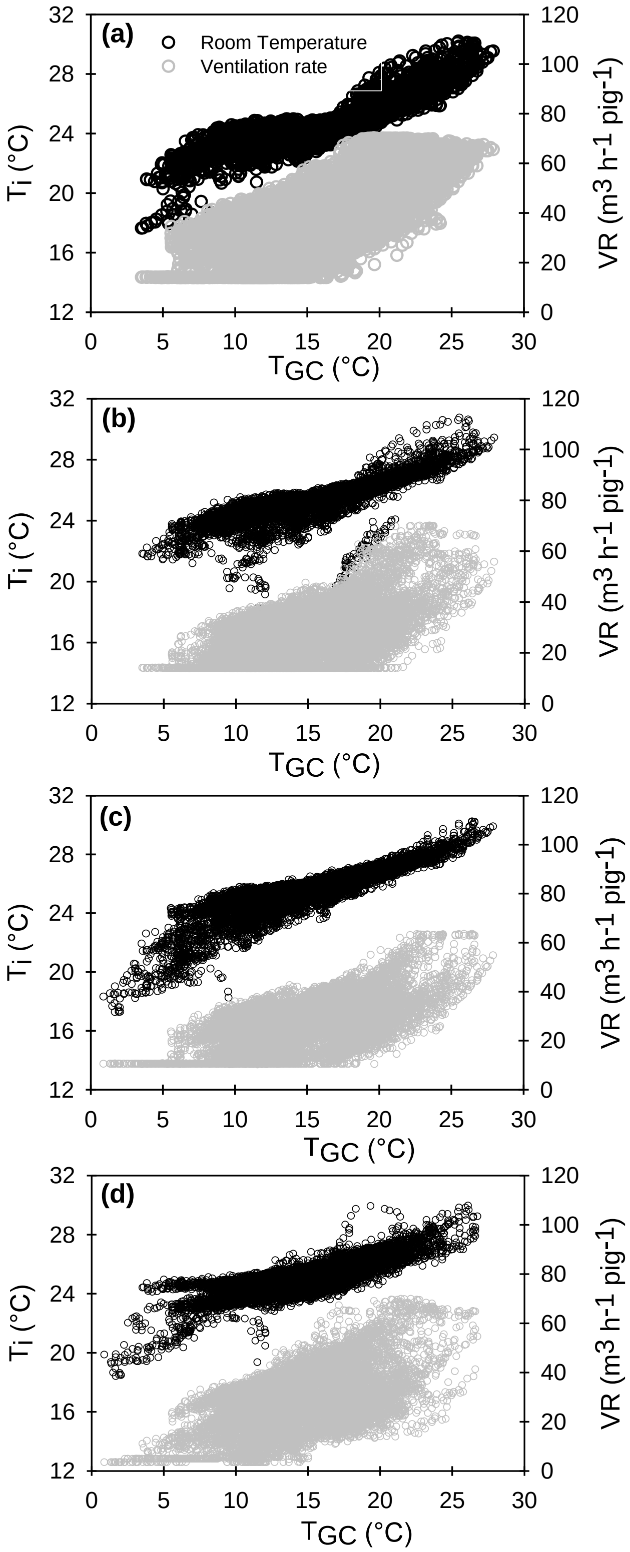

Fig. 5.5 — Effect of T_{GC} on the hourly average T_i and VR in the (a) CON, (b) T1, (c) T2 and (d) T3.

Nonetheless, in this experiment, the hourly average ventilation rate increased with increasing T_{GC} and depended on the VCS (Fig. 5.5), which is consistent with the experiment in pig house equipped with the mock-up pigs (chapter 4). It is not surprising, given the above outcome, that the effect of the VCS alone on the daily average ventilation rate was noted as a trend, while the daily average ventilation rate depended on the T_{GC} and V_{phase} and their interaction with the VCS (Table 5.8).

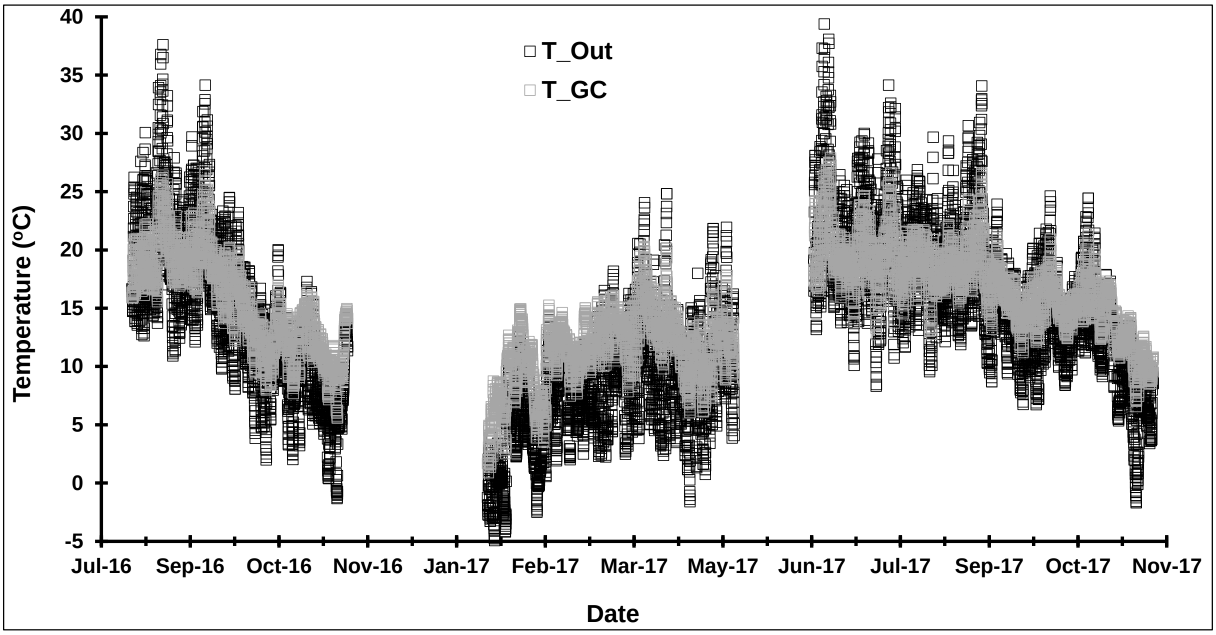

Fig. 5.6 — Hourly average outside and ground channel temperature during the experiment.

Table. 5.8. *P* values of the VCS, T_{GC}, ΔT and V_{phase} on daily average indoor temperature, ventilation rate, CO_2, NH_3 concentration and emission rate.

	P values						
Response variable	Treatment	T_{GC}	Treatment × T_{GC}	ΔT	Treatment × ΔT	V_{phase}	Treatment × V_{phase}
T_i (°C)	***	***	***			***	***
VR (m^3 h^{-1})	†	***	***			***	***
CO_2 (ppm)	***	***	***	*	***	***	***
NH_3 (ppm)	*		**	***	**	***	
CO_2 ER (g d^{-1} kg-LW^{-1})	***	***	***	***	***	***	***
NH_3 ER (g d^{-1} kg-LW^{-1})	***	***	***	***	***	***	***

† $0.1 > p > 0.05$; * $0.05 > p > 0.01$; ** $0.01 > p > 0.001$; *** $p < 0.001$

5.3.3. Effect of the VCS on air temperature, odour and gaseous concentrations

The hourly average room temperature monitored during this experiment (i.e. the gaseous concentration measurement) show that T1, T2 and T3 significantly increased the room temperature by 0.9 – 1.4 °C compared to the CON (24.0 °C), (Table 5.7). The reason for this is, the new VCS represents a significant reduction in ventilation rate and thus retains more of the pig generated heat in the compartments compared to the CON. Contrary to our results, Kim et al. (2007) did not demonstrate significant differences in room temperature between the three ventilation regimes after adjusting the ventilation rate by 20%, 40% and 60%. This may have been because their experiment was performed only in spring and autumn and was restricted to pigs that were more than 50 kg heavier than in our experiment. Furthermore, in the present experiment the hourly average room temperature in the treatments increased with increasing T_{GC} and the room temperature depended on the specified VCS (Fig. 5.5). The above findings are confirmed by the effects of VCS, T_{GC}, V_{phase} and their interaction with T_i (Table 5.8).

Adjusting the VCS in T1, T2 and T3 increased the hourly average exhaust NH_3 concentrations by 21 – 38% compared to the CON (12.7 ppm) (Table 5.7). However, only the exhaust NH_3 concentration in T2 significantly differed from the CON. The adjusted VCSs in T1, T2 and T3 significantly increased the hourly average exhaust CO_2 concentrations as compared to the CON (1,564 ppm) by 13 – 28% (Table 5.7). A marginal decrease in the average odour concentration was seen in T1 (-3%), but the odour concentration in T2 and T3 increased by 17% and 22% compared to the CON (1457 OU_E m^{-3}), respectively. However, despite the odour increments in T2 and T3, no significant differences are seen in the odour concentrations between T2, T3 and CON (Table 5.7). The main reason for the higher NH_3, CO_2 and odour concentrations in the new VCS was because reducing the VR lowered the gas dilution rate in the compartment compared to the CON. Indeed, comparing the daily average ventilation rate with the exhaust NH_3 concentrations suggests a declining trend in the exhaust NH_3 concentrations with increasing daily average ventilation rate, T_{GC} and vice versa (Fig. 5.4).

In addition, the results show that the exhaust NH_3 concentrations were affected by seasonal variations in T_{GC} and ventilation rate, as well as pig weight . For instance, at the beginning of the fattening round in summer when the daily average T_{GC} was higher than 18 °C, the daily average exhaust NH_3 concentrations in all the treatments were relatively low (Fig. 5.3). However, the daily average exhaust NH_3 concentrations gradually increased with decreasing T_{GC} in the same fattening round during autumn. On the contrary, when the fattening round started in winter at the daily average T_{GC} below 15 °C (Fig. 5.4), the exhaust NH_3

concentrations were comparatively high in all the treatments. This is because the compartments operated at VR_{min}. However, the exhaust NH_3 concentrations gradually decreased with increasing ventilation rate during the fattening round in spring (Figs. 5.4). Apart from the effect of the T_{GC} on the exhaust NH_3 concentration, Fig. 5.4 shows that the VCSs in T1, T2 and T3 influenced the exhaust NH_3 concentrations. That is, reducing the VR_{min} to 3.5 m^3 h^{-1} pig^{-1} in T3 at the beginning of the fattening period increased the exhaust NH_3 concentration compared to the CON. However, toward the end of the fattening period when T3 and CON operated at the same VR_{min} and VR_{max} (Table 5.1), their exhaust NH_3 concentrations were similar. The above result is in line with the effect of the V_{phase} on the exhaust NH_3 and CO_2 concentrations in Table 5.8.

Furthermore, comparing the ΔT (T_i – T_{GC}) with the exhaust NH_3 concentration shows higher exhaust NH_3 concentrations in the three new VCSs than CON (Figs. 5.3c & 5.4c), but only when concurrently the ΔT (Figs. 5.3b & 5.4b) in the 3 VCS was higher than CON and their ventilation rate (Figs. 5.3a & 5.4a) was markedly less than CON. However, the effect of the ΔT and VR on the exhaust NH_3 concentration difference between T1, T3 and CON was not so clear, despite the comparatively low ventilation rate in T1 and T3 compared to CON (Figs. 5.3d – 5.3f). These results demonstrate that, despite the contribution of the ventilation rate to the gas dilution level in the pig building, T_{GC}, ΔT and their interaction with the VCS (Table 5.8) influence the airflow pattern and slurry pit air exchange rate in the compartment (De Praetere and Van Der Biest, 1990; Aarnink et al., 1995; Zong et al., 2015). Indeed, the results of the experiment in chapter 4 and the observed airflow pattern during the smoke test (Fig. 5.7) agree with this assumption.

Fig. 5.7 — Airflow pattern in the compartment during the smoke test.

It is therefore hypothesised that some of the incoming air entered the slurry pit and transported the NH_3 to the compartment due to the higher ΔT and the cooler T_{GC} than the T_i (Figs. 5.3d –

5.3f). Another hypothesis is that less incoming air entered the slurry pit at warmer T_{GC} and reduced ΔT due to short-circuiting of the inlet air to the exhaust duct (Figs. 5.4d – 5.4f). The latter hypothesis, higher in CON compared to T1, T2 and T3 was due to its comparatively high ventilation rate. Indeed, experiments in pig buildings (with underfloor air inlets) noted this phenomenon as a drawback (Aarnink and Wagemans, 1997; Botermans and Jeppsson, 2008; Klimaatplatform varkenshouderij, 2006).

In the present investigation, the effect of the T_{GC}, ΔT and their interaction with the VCS (Table 5.8) on the slurry pit air exchange and the exhaust NH_3 concentration were evaluated using the Archimedes number (Ar). The Ar is often used in displacement ventilation systems to characterise airflow patterns. The Ar represents the ratio of the buoyancy forces to the inertia forces acting on a fluid (Etheridge and Sandberg, 1996).

$$Ar = \frac{Buoyancy\ Force}{Inertia\ Force} = \frac{g\Delta Td}{T_i v^2} \tag{5.5}$$

where, g is gravitational acceleration (m s^{-2}), T_i is room temperature (K) measured 1.4 m above the floor in pen 3 in all the compartments, ΔT is the $T_i - T_{GC}$ (K), v is the air velocity at the face of the slatted floor inlet (m s^{-1}) and d is characteristic length, chosen as the width of the underfloor inlet (1.0 m). In this investigation, the v was calculated as the VR divided by the total slot opening area of the slatted floor inlet (1.34 m^2). Typically, the higher the Ar the greater the buoyancy force of incoming air and the airflow to the animal occupied area, while a lower Ar implies an increase in short-circuiting of the incoming air to the exhaust duct due to the stronger inlet air momentum.

In Fig. 5.8, the hourly average exhaust NH_3 concentrations increased with increasing Ar because the ΔT increased from the lower T_{GC} and ventilation rate. The lower exhaust NH_3 concentrations in the CON than T1 and T2 are partly caused by the short-circuiting of the supply air to the exhaust duct due to the lower Ar in the CON. Thus, apart from the higher gas dilution in CON that resulted in the lower exhaust NH_3 concentrations compared to T1 and T2, the short-circuiting of the supply air to the exhaust was a contributory factor. Conversely, the comparatively high CON NH_3 concentration in winter (Fig. 5.8a) than in summer (Fig. 5.8c) was partly due to the incoming air entering the slurry pit and transporting the NH_3 into the compartment from the higher Ar in winter. This assumption concurs with the results in the experiment with the mock-up pig (chapter 4), which demonstrated the relationship between the Ar and the NH_3 removal from slurry pit, and explains why the T_{GC} and ΔT interacts with the VCS to affect the exhaust NH_3 concentration (Table 5.8).

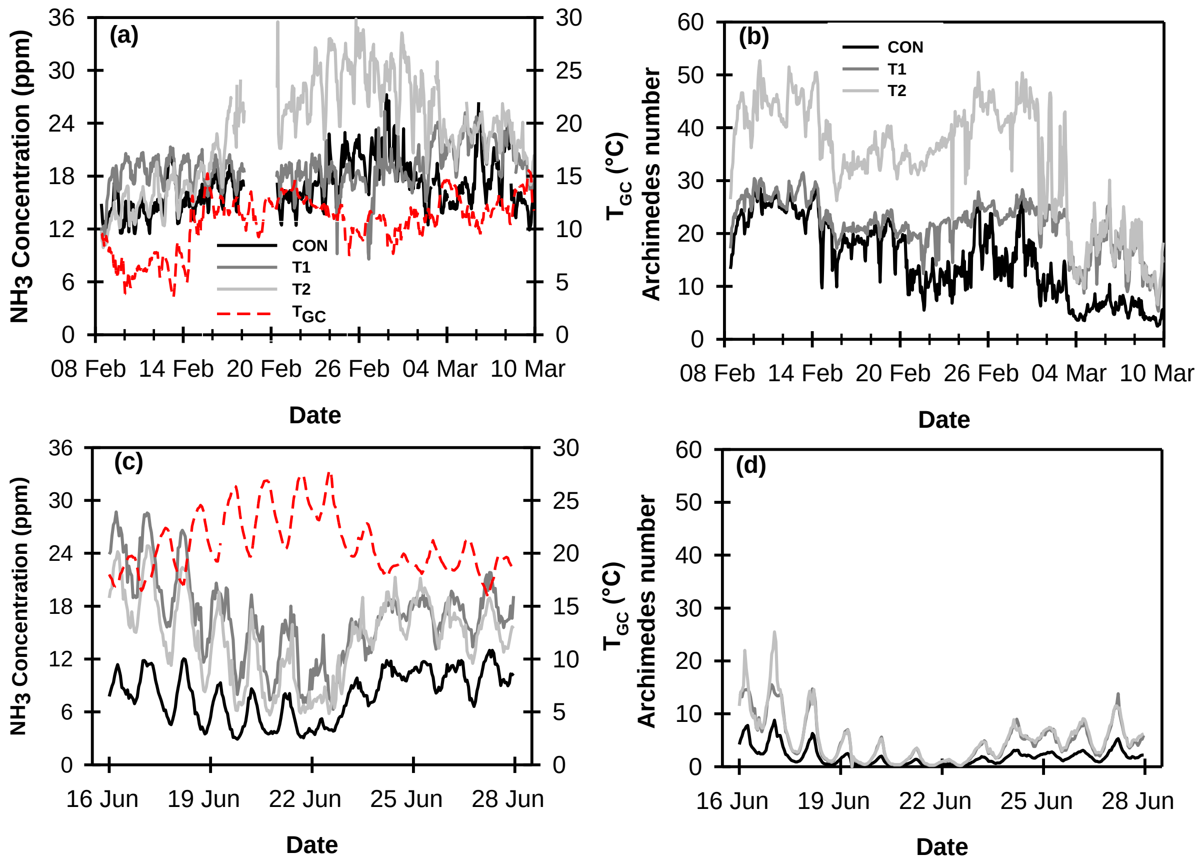

Fig. 5.8 — Hourly average NH_3 concentration and Archimedes number in (a & b) winter and in (c & d) summer during the fattening period between CON—Black; T1—Dark grey and T2—Light grey, under simultaneous measurement.

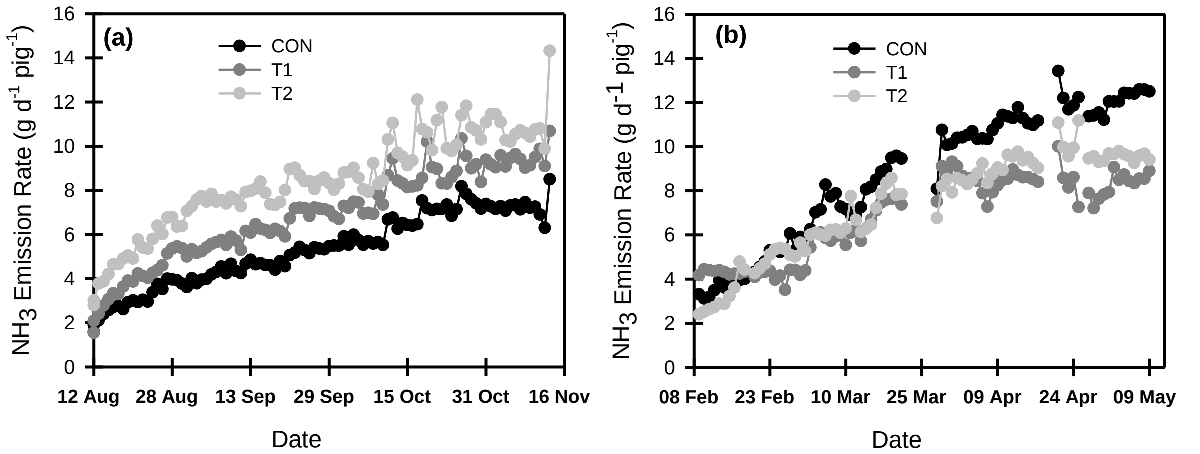

Fig. 5.9 — Daily average NH_3 emission from (a) 11 August – 16 November 2016 and (b) 8 February – 10 May 2017 during the fattening period between CON—Black; T1—Dark grey and T2—Light grey, under simultaneous measurement.

5.3.4. Effect of the VCS on the gaseous and odour emissions

In the present investigation there was no significant difference in the hourly average NH_3 emissions between the three new VCS and CON (Table 5.7). Similarly, no significant difference was found in the hourly average CO_2 emissions between the three VCSs and CON (Table 5.7). The emission results are contrary to the expected result, given that T1, T2 and T3 significantly reduced the hourly average ventilation rate compared to CON (Table 5.7). In addition, it was demonstrated in chapter 4 that adjusting the T_{set} by +2 °C can reduce NH_3 emissions by 29 – 43% due to the 33 – 40% reduction in the ventilation rate compared to the CON. Of course, the experiment in the pig house with the mock-up pigs was limited to only summer. In addition, the mock-up pigs simulated the sensible heat production from only 50 kg pigs, in comparison to the current investigation which was carried out throughout the year. Nonetheless, T1 significantly reduced the odour emission by 34% compared to the CON (16 OU_E s^{-1} pig^{-1}, Table 5.7). Despite numerical differences, the observed less odour emissions in T2 and T3 did not significantly differ from CON (Table 5.7).

The reason for the lack of differences in hourly average NH_3 and CO_2 emission rates between T1, T2, T3 and the CON was partly due to seasonal variations in the airflow patterns in pig building, in particular the air exchange rate in the slurry pit due to the season-dependent T_{GC} and ΔT. This is because despite the effect of the ventilation level on emissions, the gaseous release and transport from the slurry pit depended on airflow pattern and slurry pit air exchange rate in the compartment (De Praetere and Van Der Biest, 1990; Aarnink et al,, 1995; Kim et al., 2007; Zong et al., 2015). Indeed, the exhaust NH_3 and CO_2 concentrations and their emission rate are influenced by the T_{GC}, ΔT, V_{phase} and the interactions with the VCS (Table 5.8). It is important to note, however, that apart from the above factors, differences in other minor factors such as pig activity, extraction and lying behaviour in the different ventilation regimes also affect the NH_3 and odour emission rate (Aarnink et al, 1995).

Table 5.9 illustrates the effect of T_{GC}, ΔT, V_{phase} and their interactions with the VCSs on the daily indoor climate, NH_3 and CO_2 emission rate. It is apparent that assessing the effect of T1, T2 and T3 on reducing the daily NH_3 emissions on the basis of the V_{phase} at different T_{GC} and ΔT that, reductions in NH_3 emissions only occur at T_{GC} = 10 °C & ΔT = 10 °C, and T_{GC} = 17 °C & ΔT = 5 °C. However, at T_{GC} = 17 °C & ΔT = 10 °C there was an opposite effect of the three new VCS on the daily NH_3 emissions compared to the CON, particularly in T3. Apparently, during the warmer days of the year, when the daily average T_{GC} and VR exceeded 17 °C and 42 m^3 h^{-1} pig^{-1} (Fig. 5.3a), respectively, the exhaust NH_3 concentration in CON was lower than the three new VCSs (Fig. 5.3c).

Table 5.9. Effect of VCS on daily average indoor temperature, ventilation rate, NH_3, CO_2 concentration and emission rate

	[Day 0-28]				[Day 29-48]				[Day 49-77]				[Day 78-120]			
	CON	**T1**	**T2**	**T3**	**CON**	**T1**	**T2**	**T3**	**CON**	**T1**	**T2**	**T3**	**CON**	**T1**	**T2**	**T3**
T_i (^oC)																
T_GC = 10	22.6^{b}	23.3 (0.7)^{a}	23.8 (1.2)^{a}	23.7 (1.1)^{a}	22.7^{b}	23.9 (1.2)^{a}	24.1 (1.4)^{a}	23.8 (1.1)^{a}	22.8^{c}	24.4 (1.6)^{a}	24.3 (1.5)^{a}	23.8 (1.0)^{b}	22.8^{c}	24.3 (1.5)^{ab}	24.6 (1.8)^{a}	24.0 (1.2)^{b}
T_GC = 17	24.5^{c}	25.0 (0.4)^{bc}	25.0 (1.0)^{a}	25.4 (0.8)^{ab}	24.7^{c}	25.6 (0.9)^{ab}	26.0 (1.3)^{a}	25.4 (0.7)^{b}	24.8^{c}	26.0 (1.2)^{a}	26.2 (1.4)^{a}	25.5 (0.6)^{b}	25.8^{c}	26.0 (1.2)^{b}	26.4 (1.7)^{a}	25.6 (0.9)^{b}
VR ($m^3\ h^{-1}\ pig^{-1}$)																
T_GC = 10 ^oC	16.8^{a}	11.2 (-34%)^{b}	13.4 (-20%)^{ab}	11.0 (-35%)^{b}	24.6^{a}	17.4 (-29%)^{b}	17.9 (-27%)^{b}	18.8 (-24%)^{b}	32.5^{a}	24.1 (-26%)^{c}	22.9 (-30%)^{c}	28.1 (-14%)^{b}	35.8^{a}	25.6 (-28%)^{b}	25.5 (-29%)^{b}	33.2 (-7%)^{b}
T_GC = 17 ^oC	31.6^{a}	23.4 (-26%)^{b}	23.7 (-25%)^{b}	22.1 (-30%)^{b}	39.3^{a}	29.6 (-25%)^{b}	28.2 (-28%)^{b}	29.9 (-24%)^{b}	47.3^{a}	36.3 (-23%)^{bc}	33.2 (-30%)^{c}	39.2 (-17%)^{b}	50.6^{a}	37.8 (-25%)^{c}	35.8 (-29%)^{c}	44.3 (-12%)^{b}
CO_2 (ppm)																
T_GC = 10 & ΔT = 10 ^oC	1880^{c}	1973 (5%)^{c}	2425 (29%)^{b}	2942 (56%)^{a}	1763^{c}	1914 (9%)^{bc}	2268 (29%)^{b}	2693 (53%)^{a}	1697^{c}	1871 (10%)^{bc}	2104 (24%)^{ba}	2413 (42%)^{a}	1658^{c}	1803 (9%)^{bc}	2088 (26%)^{ba}	2227 (34%)^{a}
T_GC = 17 & ΔT = 5 ^oC	1518^{c}	1573 (4%)^{c}	1942 (28%)^{b}	2362 (56%)^{a}	1400^{c}	1515 (8%)^{bc}	1786 (28%)^{ab}	2114 (51%)^{a}	1334^{b}	1471 (10%)^{b}	1621 (22%)^{ab}	1833 (37%)^{a}	1296^{b}	1404 (8%)^{ab}	1605 (24%)^{ab}	1647 (27%)^{a}
T_GC = 17 & ΔT = 10 ^oC	1505^{b}	1731 (15%)^{ab}	2002 (33%)^{a}	1734 (15%)^{ba}	1388^{b}	1673 (21%)^{ab}	1845 (33%)^{a}	1486 (7%)^{b}	1322^{b}	1629 (23%)^{a}	1681 (27%)^{a}	1205 (-9%)^{b}	1283^{bc}	1562 (22%)^{ab}	1665 (30%)^{a}	1019 (-21%)^{c}
NH_3 (ppm)																
T_GC = 10 & ΔT = 10 ^oC	13.4	14.4 (8%)	15.3 (14%)	13.5 (1%)	14.6	14.9 (2%)	15.7 (7%)	13.2 (-9%)	15.0	15.6 (4%)	16.0 (6%)	12.8 (-15%)	16.0	16.7 (4%)	17.7 (11%)	14.4 (-10%)
T_GC = 17 & ΔT = 5 ^oC	10.0	10.8 (8%)	11.5 (14%)	11.0 (10%)	11.2	11.2 (0%)	11.8 (5%)	10.7 (-4%)	11.6	12.0 (3%)	12.1 (4%)	10.3 (-12%)	12.6	13.0 (4%)	13.8 (10%)	11.9 (-6%)
T_GC = 17 & ΔT = 10 ^oC	9.6^{b}	14.0 (45%)^{a}	15.9 (65%)^{a}	15.7 (63%)^{a}	10.8^{b}	14.4 (33%)^{ab}	16.2 (50%)^{a}	15.4 (43%)^{a}	11.2^{b}	15.1 (35%)^{a}	16.5 (47%)^{a}	14.9 (33%)^{ab}	12.2^{b}	16.2 (33%)^{a}	18.2 (49%)^{a}	16.5 (36%)^{a}
CO_2 ER $\times 10^3$ ($g\ d^{-1}\ kg\text{-}LW^{-1}$)																
T_GC = 10 & ΔT = 10 ^oC	661^{a}	605 (-8%)^{a}	753 (14%)^{a}	409 (-38%)^{b}	518^{a}	492 (-5%)^{a}	618 (19%)^{a}	324 (-37%)^{b}	437^{a}	413 (-5%)^{a}	515 (18%)^{a}	252 (-42%)^{b}	357^{a}	228 (-19%)^{ab}	425(19%)^{a}	169 (-53%)^{b}
T_GC = 17 & ΔT = 5 ^oC	668^{a}	618 (-7%)^{ab}	761(14%)^{a}	525 (-29%)^{b}	525^{ab}	505 (-4%)^{ab}	625 (19%)^{a}	392 (-25%)^{b}	443^{ab}	426 (-4%)^{ab}	521 (17%)^{a}	320 (-28%)^{b}	364^{ab}	301 (-17%)^{ab}	433 (19%)^{a}	237 (-35%)^{b}
T_GC = 17 & ΔT = 10 ^oC	705	653 (-7%)	682 (-3%)	704(0%)	562	539 (-4%)	547 (-3%)	619 (10%)	481	461 (-4%)	442 (-8%)	547 (14%)	401	336 (-16%)	354 (-12%)	463 (16%)
NH_3 ER $\times 10^4$ ($g\ d^{-1}\ kg\text{-}LW^{-1}$)																
T_GC = 10 & ΔT = 10 ^oC	21.7^{a}	18.7 (-14%)^{a}	20.0 (-8%)^{a}	7.8 (-64%)^{b}	20.8 ^{a}	14.9 (-28%)^{b}	16.9 (-19%)^{ab}	5.8 (-72%)^{c}	19.6^{a}	12.8 (-35%)^{b}	14.5 (-26%)^{ab}	4.3 (-78%)^{c}	18.4^{a}	8.4 (-54%)^{bc}	12.5 (-32%)^{ab}	2.9 (-84%)^{c}
T_GC = 17 & ΔT = 5 ^oC	23.7^{a}	22.8(-4%) ^{a}	23.1 (-2%)^{a}	14.8 (-37%)^{b}	22.8^{a}	19.1 (-16%)^{a}	20.0 (-12%)^{a}	12.8 (-44%)^{b}	21.6^{a}	17.0 (-22%)^{ab}	17.7 (-18)^{ab}	11.3 (-48%)^{b}	20.4^{a}	12.6 (-38%)^{b}	15.6 (-23%)^{ab}	9.9 (-52%)^{b}
T_GC = 17 & ΔT = 10 ^oC	25.6^{c}	30.8 (20%)^{ab}	28.8 (12%)^{bc}	33.7 (31%)^{a}	24.8^{b}	27.0 (9%)^{b}	25.7 (4%)^{b}	31.6 (28%)^{a}	23.6^{b}	24.9 (6%)^{b}	23.4 (-1%)^{b}	30.2 (28%)^{a}	22.4^{b}	20.5 (-8%)^{b}	21.3 (-5%)^{b}	28.7 (28%)^{a}

This reduced the NH_3 emissions in the CON (Fig. 5.9a) compared to the three new VCSs, despite the higher VR in the CON. In contrast, when the daily average T_{GC} and VR was lower than 14 °C and 32 m^3 h^{-1} pig^{-1} (Fig. 5.4a), respectively, the difference in the exhaust NH_3 concentrations between the three new VCSs and CON was rather small (Fig. 5.4c). This increased the NH_3 emission in the CON compared to the three new VCS (Fig. 5.9b). These findings show that for the new VCSs to decrease the NH_3 emissions they need the same or less exhaust NH_3 concentration as the CON (Eq. 5.1). Therefore, the contradictory NH_3 emission trends in the CON compared to the three new VCSs were likely due to the fact that the T_{GC}, ΔT and their interaction with the VCS (i.e. ventilation rate) affected the airflow pattern in the pig barn as the ventilation principle in the pig barn is by air displacement.

5.3.5. Ammonia and odour emissions according to the VERA protocol

From the VERA protocol, the yearly average NH_3 emission rate in the three new VCSs ranged between 2.26 – 2.46 kg pig^{-1} $year^{-1}$ compared to 2.38 – 2.53 kg pig^{-1} $year^{-1}$ in CON (Table 5.10). The yearly average CO_2 emissions from the three new VCSs ranged between 476 to 527 kg pig^{-1} $year^{-1}$ compared to 511 – 552 kg pig^{-1} $year^{-1}$ in CON. The yearly average odour emissions of the three new VCS ranged between 11.3 – 13.6 OU_E s^{-1} pig^{-1} compared to 14.7 OU_E s^{-1} pig^{-1} in the CON. The yearly average NH_3 emission from the CON in the present study (Table 5.10) was within the reported emissions of 2.2 ± 1.4 kg pig^{-1} $year^{-1}$ in Van Ransbeeck et al. (2013) and 2.3 kg pig^{-1} $year^{-1}$ from Philippe et al. (2007) in Belgium. Moreover, it was encouraging that the NH_3 emission factors in T1 and T2 were lower than the NH_3 emission limit of 2.6 kg pig^{-1} $year^{-1}$ for the BAT in intensive fattening pig housing (EC, 2017). The yearly average odour emissions from all treatments were within the reported odour emission range in literature. For example, the odour emissions in Belgium range between 5.4 OU_E s^{-1} pig^{-1} and 34.1 OU_E s^{-1} pig^{-1} (Van Langenhove and De Bruyn, 2001; Romain et al., 2013), and in Ireland, from 10 and 16 OU_E s^{-1} pig^{-1} (Heyes et al., 2006). The reported yearly average odour emissions from the Netherlands (22 – 24 OU_E s^{-1} pig^{-1}) are higher than the emissions in the present study (Ogink and Groot Koerkamp, 2001; Mol and Ogink, 2003). The yearly average CO_2 emissions (Table 5.10) in the present study fell within the reported emission range, such as 420 ± 312 kg pig^{-1} $year^{-1}$ in Van Ransbeeck et al. (2013) and 572 kg pig^{-1} $year^{-1}$ in the study of Philippe et al. (2007). In Table 5.10, the yearly average gaseous and odour emissions calculated using the VERA protocol (VERA, 2018) indicate relatively different emission reductions when compared to the result in Table 5.7.

Table 5.10. Yearly average ± standard deviations of the air temperature, ventilation rate, CO_2, NH_3, odour concentrations and emission rate using all the measurement days (n) according to the case-control approach.

Variable	T1	n	CON	n	T2	n	CON	n	T3	n	CON	n
$^x T_{out}$ (°C)	13.3 ± 5.7	504	13.3 ± 5.7	504	15.0 ± 5.3	396	15.0 ± 5.3	396	13.6 ± 5.5	302	13.6 ± 5.5	302
$^x T_{GC}$ (°C)	15.1 ± 3.8	447	15.1 ± 3.8	447	16.0 ± 3.7	396	16.0 ± 3.7	396	15.5 ± 3.4	275	15.5 ± 3.4	275
$^x T_i$ (°C)	25.1 ± 1.1 (1.1)	504	24.0 ± 1.2	504	25.7 ± 1.1 (1.2)	396	24.5 ± 1.1	396	25.0 ± 1.2 (0.8)	302	24.2 ± 1.2	302
$^y T_i$ (°C)	25.1 ± 1.1 (1.0)	17	24.1 ± 2.0	18	25.4 ± 2.3 (1.3)	18	24.1 ± 2.0	18	24.9 ± 0.9 (0.8)	18	24.1 ± 2.0	18
^{x} VR ($m^3\ h^{-1}\ pig^{-1}$)	26.5 ± 10.3 (-26%)	504	35.8 ± 11.9	504	28.8 ± 8.5 (-29%)	396	40.3 ± 10.0	396	31.7 ± 11.9 (-13%)	302	36.6 ± 11.7	302
^{y} VR ($m^3\ h^{-1}\ pig^{-1}$)	25.1 ± 10.3 (-26%)	17	34.1 ± 12.0	18	27.0 ± 8.9 (-21%)	18	34.1 ± 12.0	18	29.5 ± 11.1 (-13%)	18	34.1 ± 12.0	18
CO_2 Conc. (ppm)	1818 ± 400 (10%)	462	1659 ± 442	462	1675 ± 481 (22%)	357	1369 ± 402	358	1786 ± 553 (16%)	268	1546 ± 390	270
NH_3 Conc. (ppm)	16.6 ± 4.1 (19%)	462	13.9 ± 5.0	462	15.7 ± 5.3 (39%)	357	11.3 ± 4.0	358	15.7 ± 4.6 (18%)	268	13.3 ± 5.2	270
Odour Conc. ($OU_E\ m^{-3}$)	1640 ± 481 (12%)	17	1470 ± 633	18	1631 ± 785 (11%)	18	1470 ± 633	18	1700 ± 666 (16%)	18	1470 ± 633	18
CO_2 ER ($kg\ pig^{-1}\ yr^{-1}$)	476 ± 115 (-14%)	462	552 ± 149	462	492 ± 117 (-4%)	357	511 ± 135	359	527 ± 118 (-1%)	268	532 ± 143	270
NH_3 ER ($kg\ pig^{-1}\ yr^{-1}$)	2.26 ± 0.70 (-11%)	462	2.53 ± 0.87	462	2.39 ± 0.64 (0%)	357	2.38 ± 0.77	358	2.46 ± 0.72 (2%)	268	2.42 ± 0.85	270
Odour ER ($OU_E\ s^{-1}\ pig^{-1}$)	11.3 ± 4.5 (-23%)	17	14.7 ± 8.8	18	11.5 ± 4.9 (-22%)	18	14.7 ± 8.8	18	13 ± 6.1 (12%)	18	14.7 ± 8.8	18

$^x T_i$ and ^{x} VR for the NH_3 and CO_2, and $^y T_i$ and ^{y} VR for odour data; in brackets is the difference

In particular, the yearly average NH_3 emission reduction in T1 was 11% less than the CON while the overall hourly average emission reduction was 3% in the Table 5.7. However, the 23% lower odour emissions in T1 from the VERA protocol (Table 5.10) was 34% less than CON (Table 5.7). A possible explanation for the difference in the emission reductions in Table 5.7 and Table 5.10 is that the Dunnett's test polled all the data together in each treatment for the statistical analysis, while the VERA protocol approach compares each VCS with the CON on the case-control basis, i.e. by using only the datasets when simultaneous measurements were taken between the VCS and the CON. Furthermore, the computed yearly average emissions from the VERA protocol adhere to the sampling strategy requirements with respect to the measurement period and the distribution of the measurement days over the year and the production cycle. In doing so, the VERA protocol places more emphasis on the second (50 – 100% days) than the first half (0 – 50% days) of the fattening cycle, given that more emissions occurred in second rather than the first half fattening cycle (Tables 5.11 – 5.13), in addition to the higher random/systemic variations due the heavier pigs and the higher VR (Dekock et al., 2009).

Therefore, a calculation of the yearly average NH_3 emission reductions between the new VCSs and the CON by strictly applying the recommended minimum of the six, 24-h measurement days of the VERA protocol showed higher variations in yearly average NH_3 emission reduction in the new VCSs from the 20 different randomly selected, six measurement days (Fig. 5.10). Hence, the yearly average NH_3 emission difference between T1, T2, T3 and the CON strategy ranged between 8% to -23%, 23% to -6% and 14% to -6% compared to overall average emission difference of -11%, 0% and +2%, respectively, which used all the available measurement days. In fact, others have shown similar variations in the yearly average NH_3 emissions after applying different sampling protocols (Kafle et al., 2018; Mosquera and Ogink, 2011). Thus, the results in Fig. 5.10 indicate that strict application of the VERA protocol of the minimum six measurement days is an unreliable method for estimating emissions, especially the type of emission reduction strategy studied in the present investigation. This is because of the effect of T_{GC}, ΔT, V_{phase} and their interactions with the VCSs on the indoor climate and NH_3 emission rate (Table 5.8).

Nonetheless, Tables 5.11 – 5.13 show that maximum emission reduction (i.e. 19 – 21% in T1, 12 – 18% in T2 and 16% in T3) was obtained during the second half (50 – 100% days) than in the first half of the fattening round (0 – 50% days) but only from January – August. This is because from September to December, T2 and T3 rather emitted 29% and 11% more than CON, compared to the 7% less NH_3 emission in T1 than CON.

Table 5.11. The ventilation rate, NH_3 concentration and emission difference grouped into the first and second half fattening periods, and evenly distributed within the year from all the available measurement days in VERA Protocol between T1 and CON. In brackets are the differences.

		T1			CON		
Fattening cycle (%)	**Day**	NH_3 ER (g pig^{-1} day^{-1})	NH_3 Conc. (ppm)	VR (m^3 h^{-1} pig^{-1})	NH_3 ER (g pig^{-1} day^{-1})	NH_3 Conc. (ppm)	VR (m^3 h^{-1} pig^{-1})
0 – 50	0 – 365	5.4 (-1%)	16.0 (3.2)	22.1 (-26%)	5.5	12.8	29.7
50 – 100	0 – 120	8.5 (-21%)	19.1 (2.8)	27.1 (-32%)	10.7	16.3	39.9
	121 – 240	8.5 (-19%)	16.7 (1.8)	34.1 (-23%)	10.6	14.9	44.4
	241 – 365	7.9 (-7%)	15.7 (2.2)	31.5 (-23%)	8.5	13.5	41.1

Table 5.12. The ventilation rate, NH_3 concentration and emission difference grouped into the first and second half fattening periods, and evenly distributed within the year from all the available measurement days in VERA Protocol between T2 and CON. In brackets are the differences.

		T2			CON		
Fattening cycle (%)	**Day**	NH_3 ER (g pig^{-1} day^{-1})	NH_3 Conc. (ppm)	VR (m^3 h^{-1} pig^{-1})	NH_3 ER (g pig^{-1} day^{-1})	NH_3 Conc. (ppm)	VR (m^3 h^{-1} pig^{-1})
0 – 50	0 – 365	5.9 (9%)	20.7 (7.7)	18.9 (-37%)	5.4	13	29.8
50 – 100	0 – 120	8.8 (-18%)	19.6 (3.3)	27.3 (-32%)	10.7	16.3	39.9
	121 – 240	7.8 (-12%)	16.5 (3.0)	28.8 (-27%)	8.8	13.5	39.3
	241 – 365	9.2 (29%)	17.9 (7.7)	32.8 (-26%)	7.1	10.1	44.3

Table 5.13. The ventilation rate, NH_3 concentration and emission difference grouped into the first and second half fattening periods, and evenly distributed within the year from all the available measurement days in VERA Protocol between T3 and CON. In brackets are the differences.

		T3			CON		
Fattening cycle (%)	**Day**	NH_3 ER (g pig^{-1} day^{-1})	NH_3 Conc. (ppm)	VR (m^3 h^{-1} pig^{-1})	NH_3 ER (g pig^{-1} day^{-1})	NH_3 Conc. (ppm)	VR (m^3 h^{-1} pig^{-1})
0-50	0-365	6.3 (10%)	16.6 (4.1)	25.1 (-17%)	5.8	12.5	30.4
50-100	0-120						
	121-240	8.3 (-16%)	13.3 (0.4)	39.6 (-16%)	9.8	13.7	46.9
	241-365	9.0 (11%)	14.9 (1.0)	37.0 (-4%)	8.2	15.9	38.6

This result explains why the yearly average NH_3 emissions in T2 and T3 from the VERA protocol were 0% and 2% more than CON respectively (Table 5.10). Therefore, although Table 5.7 indicated no significant difference in the hourly average NH_3 emissions between the new VCS and the CON, Tables 5.11 – 5.13 highlight the seasonal and pig weight effects on the NH_3 emission reduction performance in the tested VCSs and signify the potential to reduce the NH_3 emissions in T1.

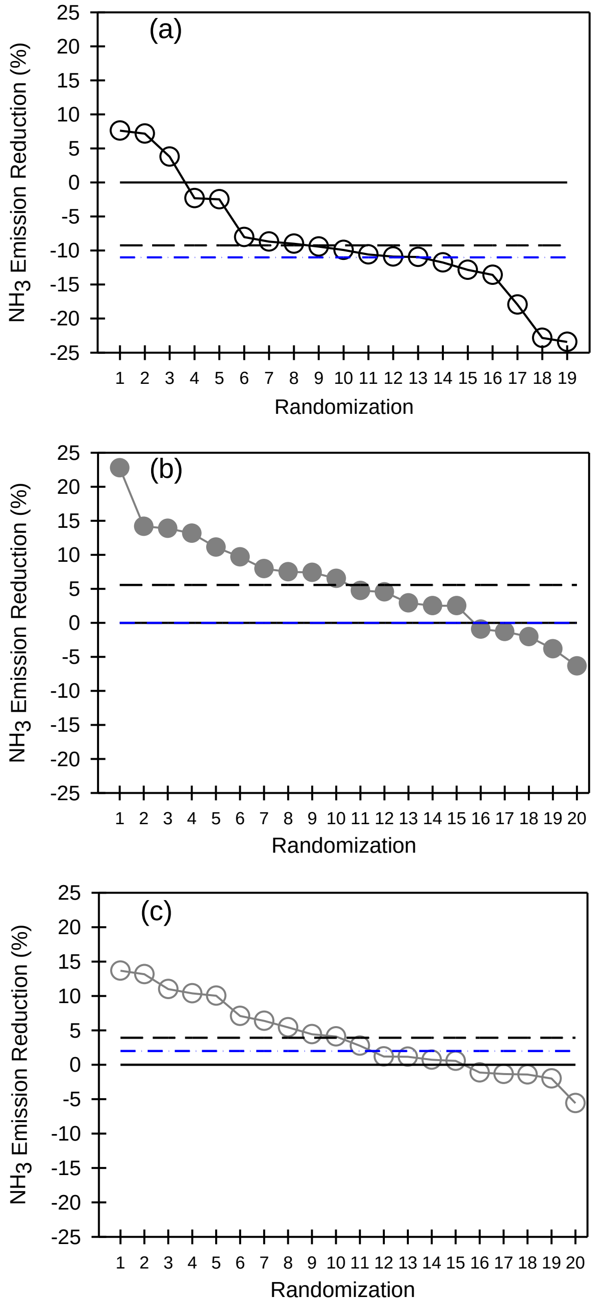

Fig. 5.10 — The percentage reduction in the NH_3 emission in (a) O —T1, (b) ● —T2 and (c) O —T3 from the randomly selected 20 different six measurement days of the VERA protocol, ordered from lowest to highest reduction. (——) is line of no difference; **(– – –)** is the average of all 20 different randomisation and (**– • –**) is from all days.

5.4. Implications for future research

The results of the present study confirm seasonal changes in the room airflow pattern affecting the slurry pit air exchange rate and the overall NH_3 emissions. Changing the inlet location from the slatted floor to a higher level in the pig house under winter conditions might promote better mixing and warming of the incoming air before it reaches the animal occupied area. Doing so might reduce the amount of incoming air directly entering the slurry pit and bringing NH_3 into the compartment. During colder seasons, baffles/flaps can also be installed at the top of the solid pen partition besides the slatted floor inlet to direct the incoming air away from the slurry pit and promote more mixing and warming up of the incoming air before reaching the animal occupied area. Indeed, this strategy was applied in Sweden to reduce draught on pigs due to the colder climate (Jeppsson and Botermans, 2014). An example of this strategy was implemented at the partly slatted section of the ILVO/UGent/HoGent pig facility using porous curtains above the solid pen partitions. It would be interesting to assess the effect of the above strategies in reducing the slurry pit air exchange using Computational Fluid Dynamics (CFD), as CFD allows different building configurations to be simulated at different climatic scenarios while obtaining high-resolution air velocity and temperature fields at the emitting source.

5.5. Conclusion

No significant differences in pig rearing performance was shown for the different ventilation control settings, except for daily feed intake, which was reduced in the first feeding phase of T3 compared to the control setting (CON). The results demonstrated that the ventilation setting T1, with an increased T_{set} by +2 °C compared to CON, significantly reduced the odour emission by 34% compared to the CON setting. Despite the significant decrease in ventilation rate, the three new ventilation control settings did not substantially reduce the hourly average NH_3 emissions compared to CON. However, calculating annual NH_3 emission factors based on the VERA protocol showed the potential of T1 to reduce the annual NH_3 emissions by 11% compared to CON. The lack of the significant difference in the hourly average NH_3 emissions between the tested ventilation control settings and CON was due in part to the seasonal variation in pig housing airflow patterns. This was caused by the air exchange rate in the slurry pit from the diurnal and seasonal variations in the ground channel air temperature (T_{GC}) and the temperature difference between the room and T_{GC}. The results indicate that, despite the importance of the ventilation rate on emissions, the influence of airflow patterns on pollutant transport from the slurry pit is similarly essential on emissions in pig housing.

This chapter evaluated the VERA test protocol's, case-control sampling strategy for calculating the average of NH_3 emission reduction over 1 year from T1, T2 and T3 compared to CON.

Thereby 20 different VERA compliant sampling sequences of six, 24-hour measurement days were selected. The results showed large variations in the calculated respective yearly average NH_3 emission reductions (T1: -23 to 8%; T2: -6 to 23%; T3: -6 to 14%).

Chapter 6: CFD simulation of airflows and ammonia emission in a pig compartment with underfloor air distribution system: Model validation at different ventilation rates

This chapter was adapted from:

Tabase, R. K., Bagci, O., De Paepe, M., Aarnink, A. J., & Demeyer, P. (2020). CFD simulation of airflows and ammonia emissions in a pig compartment with underfloor air distribution system: Model validation at different ventilation rates. *Computers and Electronics in Agriculture*, *171*, 105297.

6.1. Introduction

It was reported in chapters 4 & 5 that the Archimedes number was positively correlated with the NH_3 transport from the slurry pit into the compartment due to the air displacement principle in pig buildings equipped with the UFAD systems. In order to minimise the NH_3 generation/transport from the slurry pit into the pig compartment, the key factors supporting the undesirable airflow pattern need to be identified. Identifying the important factors that support the undesirable airflow and NH_3 emissions can be achieved by using cost-effective modelling tools instead of the field experiments, to understand the NH_3 generation and transport processes from the emitting slurry pit depending on the ventilation rate (VR) and the airflow patterns within the pig building. Moreover, the use of cost-effective modelling tools can lead to the development of NH_3 emission mitigating techniques, improving the indoor air quality and the animal thermal comfort (Bjerg and Andersen, 2010; Bjerg and Zhang, 2013). It was indicated in chapter 1 (section 1.5) that mathematical modelling tools have advantages over detailed NH_3 emission studies in field experiments, as field studies require long term and multi-sensor/location measurements. Furthermore, field experiments are time-consuming and impractical to conduct due to low air speeds in the slurry pit and animal disturbance. In such investigations, CFD offers a valuable alternative as it provides detailed spatial air velocity and temperature distributions in the AOZ and at the NH_3 emitting sources (Sapounas et al., 2009; Bjerg and Andersen, 2010; Bjerg and Zhang, 2013).

However, modelling NH_3 release from the emitting source in animal buildings can be a challenge, because of the complex chemical and physical processes involved in NH_3 volatilisation. This often makes it difficult to determine realistic boundary conditions for NH_3 release at the emitting source in order to close the governing equations in CFD simulations of full-scale livestock building (Bjerg et al., 2013). In the absence of experimental data on the slurry properties and air conditions at the emitting surface, most of the NH_3 release boundary conditions in CFD simulations of full-scale animal buildings were defined as a constant concentration at the emitting surface (Sapounas et al., 2009). For example, in the CFD simulations of Bjerg and Andersen (2010), and Bjerg and Zhang (2013), the NH_3 release boundary condition was specified as a constant concentration from the slatted floor and the slurry surface in the pit. In addition, the NH_3 concentration at the emitting surfaces during the CFD simulations were estimated by calibrating the annual NH_3 emissions from a Danish animal building, resulting in a certain percentage of the total emission from the slatted floor and the slurry pit. The limitation of this approach, however, is that the NH_3 emission becomes independent of the air conditions just above the emitting surface (Bjerg et al., 2013) and thus, contrary to the chemical and physical processes involved in the NH_3 generation that was described above. (Fig. 1.2)

More realistic NH_3 release boundary conditions can be determined based on the dissociation and Henry's law constant equations and experimentally derived data of pH, total ammoniacal nitrogen (TAN) and temperature at the slurry/urine surface. Until now, this approach was only implemented in the CFD simulations of wind tunnel and reduced-scale models where the slurry pH, TAN and temperature were measured under controlled conditions (Rong et al., 2010; Rong et al., 2015). However, it was recently reported in Rong and Aarnink (2019) that NH_3 emissions derived from wind tunnel and reduced-scale experiments were significantly lower compared to full-scale experiments. Because the NH_3 mass transfer coefficient depends on airflow patterns due to the geometry of the building, internal partitions, animal presence, inlets and exhaust locations etc. Thus far, only Drewry et al. (2018) attempted to simulate NH_3 emission in a full-scale livestock building using realistic NH_3 release boundary conditions. The NH_3 concentration boundary condition at the slurry surface of the cattle barn in the CFD model of Drewry et al. (2018) was computed by a user defined function (UDF) based on the measured slurry pH and TAN concentration during the field experiment. Hence, from the acid dissociation and the Henry's law constant equations, the UDF spatially calculated the NH_3 generation at the emitting surface using the simulated results of the air temperature from the defined cells above the slurry surface.

The computational approach for modelling NH_3 release by Drewry et al. (2018) is not yet implemented in a commercial pig barn which is equipped with a UFAD system. To the best of our knowledge, only Adrion et al. (2013) and Rong and Aarnink (2019) have attempted to develop a CFD model of a pig building with an UFAD system. However, in the study of Adrion et al. (2013) they excluded the slurry pit and did not validate the model. The CFD simulations of Rong and Aarnink (2019) were carried out under isothermal conditions without pigs, and the model was not validated either. Moreover, the NH_3 emission boundary condition was only specified at the pen floor and did not include the slurry pit. Therefore, the objectives of the present study were to:

1. Develop a validated CFD model of a pig compartment with an UFAD system capable of predicting the indoor air temperature, velocity, CO_2 and NH_3 emissions.
2. Evaluate the air velocity, temperature and gaseous concentration distributions in the compartment at different ventilation rates.
3. Evaluate the slurry pit air exchange rate for different ventilation rates in the compartment.

This model was validated using experimental data consisting of indoor temperature, air velocity, CO_2 and NH_3 concentrations. The NH_3 release boundary condition implemented in this investigation was similar to the Drewry et al. (2018) approach.

6.2. Materials and methods

6.2.1. Experimental pig housing

Experiments were carried out at the ILVO/UGent/HoGent fattening building (Fig. 6.1) to collect the experimental data, used as the boundary conditions and for validating the CFD model. The experiments were conducted in the compartments with fully slatted floors. A description of the pig building and the ventilation system were given in sections 2.2.1, 4.2.1 and 5.2.1. Table 2.1 gives the material descriptions and the overall heat transfer coefficients (U) of the pig compartments.

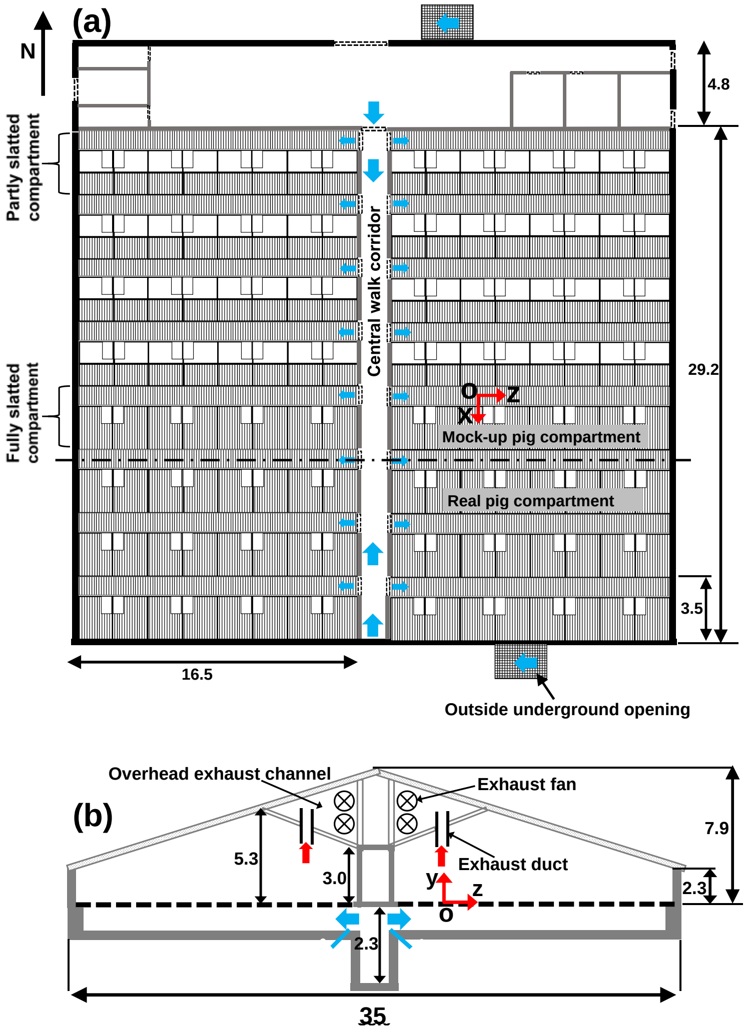

Fig. 6.1. ILVO/UGent/HoGent pig building (a) plan view and (b) sectional view. The origin (O) of the pig barn is at (0, 0, 0) with all dimensions in meters.

6.2.2. Experimental setup for the CFD model validation

6.2.2.1. Experiment with mock-up pigs

The purpose of the mock-up pig experiment was to provide representative boundary condition settings and to check the simulation accuracy of the CFD model with the experimental results of air velocity and temperature. The experiment was conducted between 26 May and 3 June 2016. The compartment was equipped with 16 mock-up pigs (Figs. 3.2, 6.2 & 6.3) as heat sources instead of real pigs. This was to eliminate disturbances to the pigs during the measurements. The density of the mock-up pigs was 1.25 m^2 pig^{-1} in the compartment which was greater than minimum space allowance of 1.0 m^2 pig^{-1} for finishing pigs according to the Council Directive 2008/120/EC (Directive C., 2008). Chapter 3 (section 3.2.2) gives a detailed description of the mock-up pigs that were used in the present investigation.

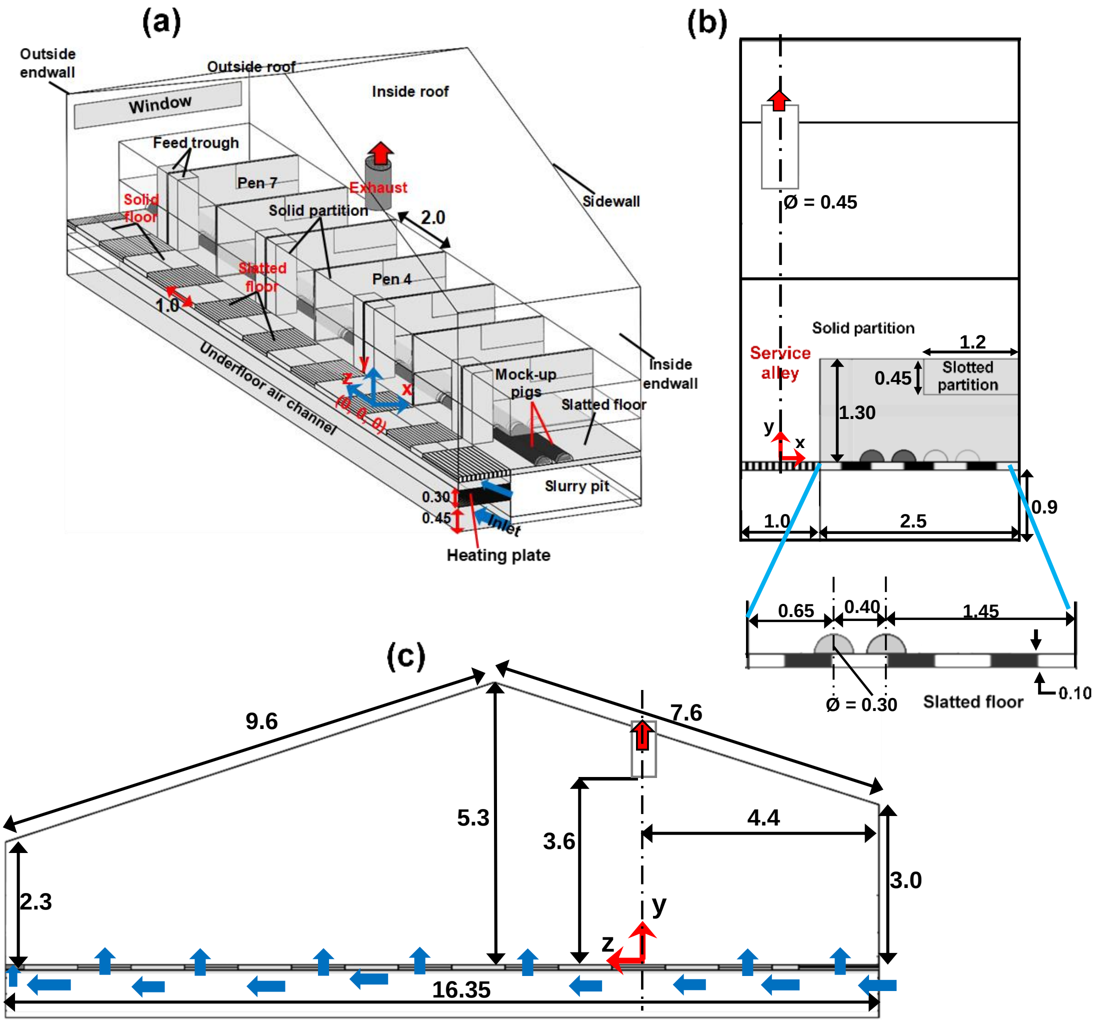

Fig. 6.2. Geometry of the pig room (a) isometric view (b) side view and (c) cross-sectional view. The origin (O) of the pig barn is at (0, 0, 0) with all dimensions in meters.

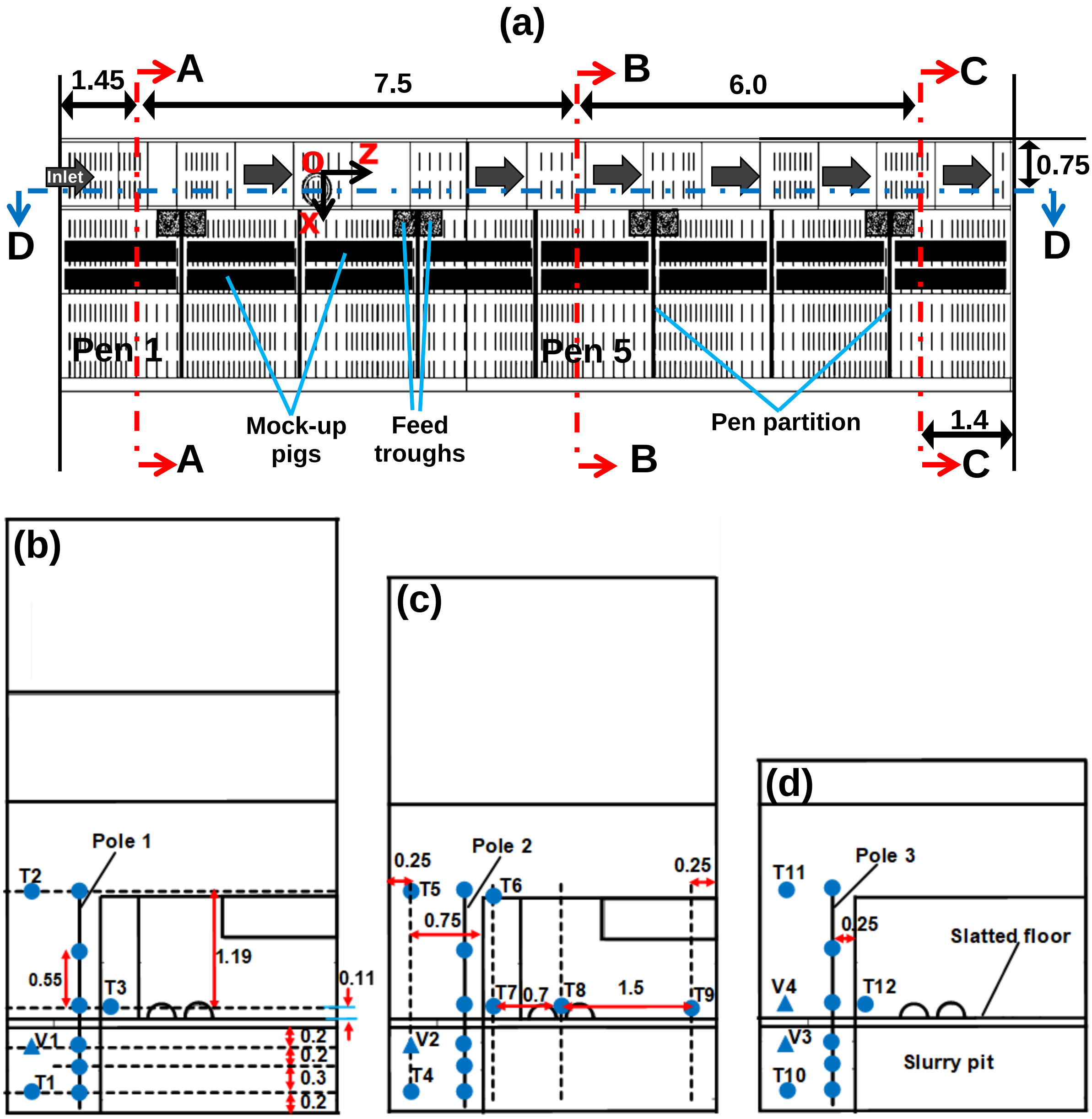

Fig. 6.3. Sampling points in the compartment occupied by the mock-up pigs (a) plan view, (b) cross-section A-A (z = -3.0 m), (c) cross-section B-B (z = 4.5 m), (d) cross-section C-C (z = 10.5 m) and D-D is the sectional view along the underfloor air channel in the CFD model. Circles indicate temperature (T) sensors and triangles indicate the ultrasonic anemometers (V) (All dimensions are in meters).

The experiment was run at ventilation levels of 11 m^3 h^{-1} pig^{-1} (level 1), 34 m^3 h^{-1} pig^{-1} (level 2), 62 m^3 h^{-1} pig^{-1} (level 3) and 92 m^3 h^{-1} pig^{-1} (level 4). These ventilation rates are within the compartment's minimum (336 m^3 h^{-1}) and maximum (3360 m^3 h^{-1}) ventilation capacity and are also within the minimum and maximum ventilation requirements for 50 kg pigs in barns with UFAD systems in Flanders (Belgium), ranging from 11 to 70 m^3 h^{-1} pig^{-1} (Van Gansbeke et al., 2009). The ventilation levels were selected to allow for the detailed assessment of the influence of VR on the airflow characteristics at the UFAC and its effects on the air distribution in the AOZ, and to provide an indication of the range of applicability of the CFD model during the validation study. Consequently, the air velocity and temperature sampling points were more focused on the UFAC and in pen 5 of the compartment (Fig. 6.3). In addition, the sampling strategy was regarded helpful in this experiment as it was excluded from the CUAC in the CFD model up to the UFAC inlet (Figs. 6.2). Fig. 6.3 illustrates the sampling locations of the air temperature and velocity during the experiment. During the experiment, each ventilation level was set up from 16:00 until 09:00 the next day. This was because the outside and CUAC temperatures were more stable during this period compared to the measurements from 17:00 – 10:00 (Fig. 6.4).

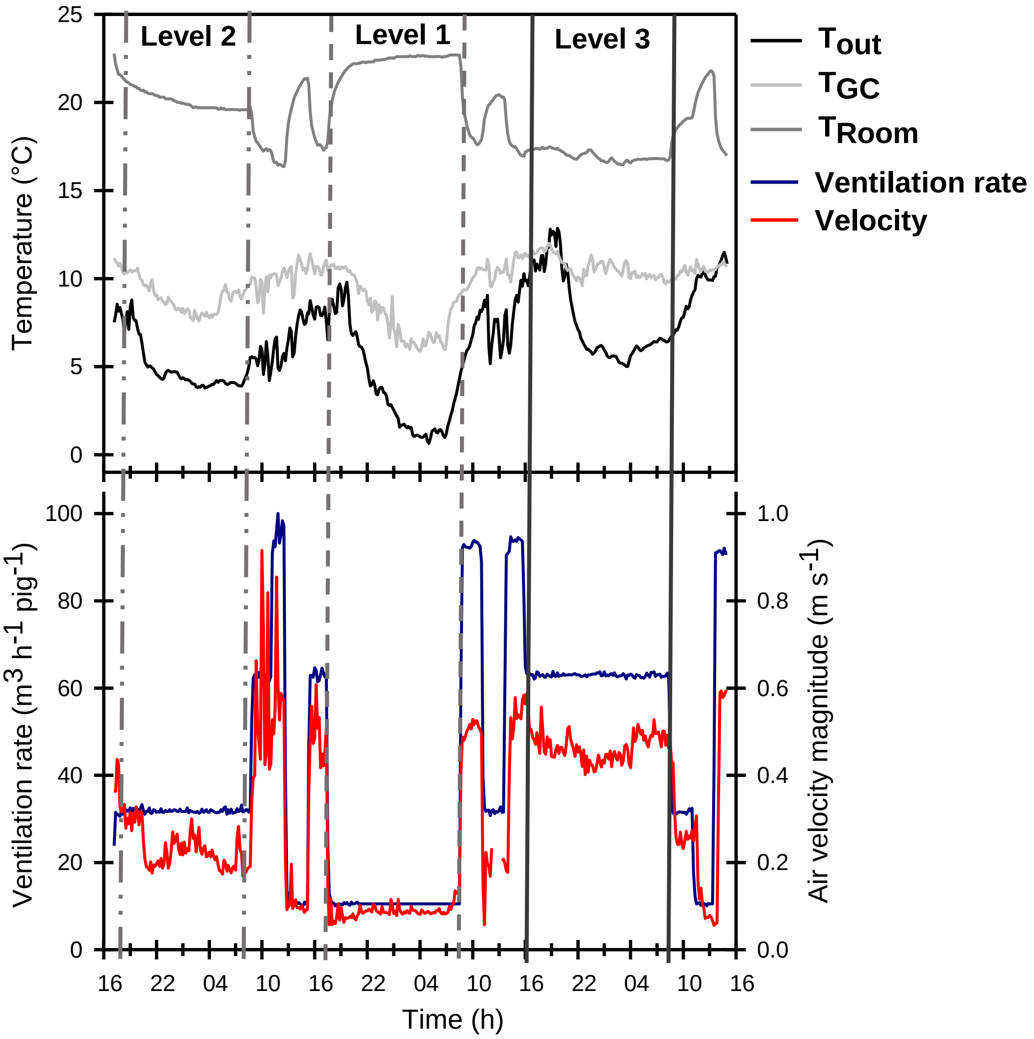

Fig. 6.4. Time-series plot of 10 min averages of the outside, CUAC, room temperature, ventilation rate and the air velocity magnitude at V1 during the mock-up pig experiment. The ventilation rate at level 1, level 2 and level 3 are 11, 34 and 62 $m^3\ h^{-1}\ pig^{-1}$, respectively.

Furthermore, as the compartment wall temperatures were measured between 07:00 and 09:00, the study extracted the average VR, air temperatures and velocity readings in each of the ventilation levels between 07:00 and 09:00 every 10 minutes. These data were used as the boundary conditions and for validating the CFD model. An Orion-VS12 data logger (Hotraco Agri, Hegelsom, Netherlands) then logged VR and the outside, CUAC and ventilation control temperatures every minute.

Pt1000 (-50 °C to +100 °C) sensors of the "Hotraco System" (Hotraco Agri, Hegelsom, Netherlands) monitored the outside, CUAC and the compartment temperatures, respectively. The outside temperature sensor was placed 1.4 m above the ground under the eastern roof eaves of the building, the CUAC temperature sensor was positioned 1.3 m above the floor of the CUAC (Fig. 6.1) and the ventilation control temperature sensor was located 1.4 m above the floor in pen 3 (Fig. 6.2a). The VR was calculated from the linear relationship between the differential pressure (Type 699, Huba Control, Würenlos, Switzerland) (Range 0 to 100 Pa; accuracy < 0.5% f.s.) between the compartment and the overhead exhaust channel, and the damper opening size at the exhaust duct in the compartment. 'Hotraco' previously validated this relationship in a wind tunnel test (Hotraco Agri, Hegelsom, Netherlands).

Four 3D ultrasonic anemometers (Thies, Göttingen, Germany; range: 0.01 to 75 m s^{-1} and accuracy: ±0.1 m s^{-1}) measured the air velocity at the UFAC (Fig. 6.3). Deutsche WindGuard Wind Tunnel Services (GmbH) previously calibrated the 3D anemometers. A Delphin 200 logger (Delphin Technology AG, Bergisch Gladbach, Germany) continuously logged the air velocity from the ultrasonic anemometers at a sampling frequency of 1 Hz. An EE06 Relative Humidity (RH) and temperature sensor (E+E Elektronik, Engerwitzdorf, Austria) measured the exhaust temperature and RH, range: 0 to 100% RH and -40 °C to 60 °C temperature and accuracy: ±2.5% RH and ±0.3 °C temperature. Thirty U-type thermistors (Grant Instruments, Cambridge, UK), range: -50 to 150 °C and accuracy < 0.2 ºC measured the UFAC and compartment temperatures (Fig. 6.3). The measured RH and temperature were continuously logged to a Squirrel SQ2040 (Grant Instruments, Cambridge UK) logger every 2 minutes. A handheld Fluke 568 infrared thermometer (Fluke Corporation, Everett, WA, USA), range: -40 to 800 °C and accuracy: ±1.0 °C measured the compartment wall surface temperature. The wall temperatures were derived as the average temperature from multiple measurement spots on each wall of the compartment.

6.2.2.2. Experiment with real pigs

The purpose of the experiment with the real pigs was to provide the CFD model with appropriate boundary conditions and validation data of the air temperature, CO_2 and NH_3

concentrations in the UFAC, in the slurry pit headspace and at the exhaust duct. Fig. 6.5 shows the air temperature and the NH_3 concentration sampling locations during the experiment. Measurement was taken on 9 November 2016 between 10:30 to 11:00 in the compartment that was occupied by 48 pigs (8 pens with 6 pigs per pen) at an average weight of 90 kg.

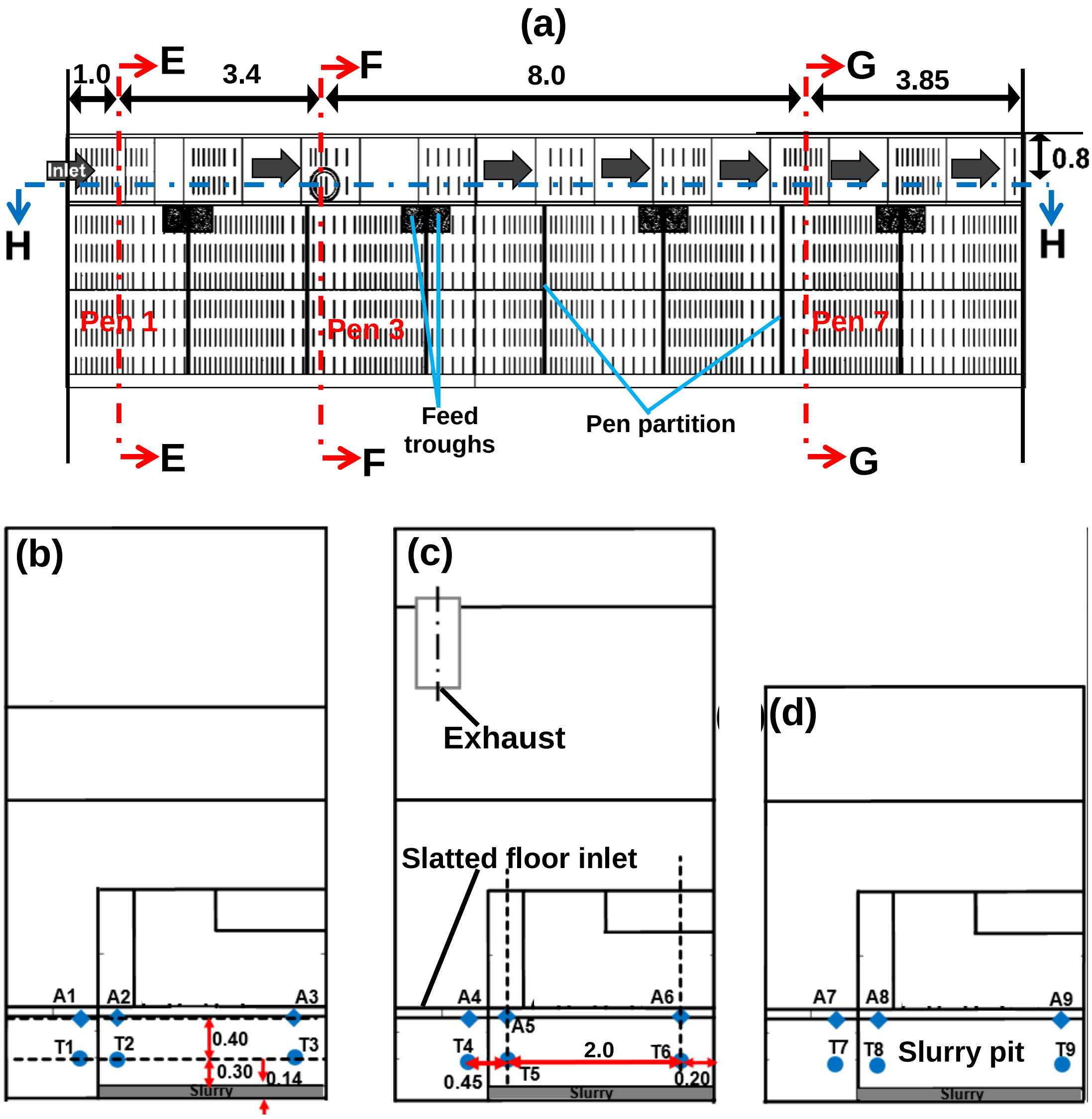

Fig. 6.5. Sampling location in the compartment occupied by real pigs (a) plan view, (b) cross-section E-E (z = -3.4 m), (c) cross-section F-F (z = 0.5 m), (d) cross-section G-G (z = 8.0 m) and H-H is the sectional view along the underfloor air channel in the CFD model. Circles indicate temperature sensors (T) and diamonds indicate GASTEC NH_3 diffusion tube (A) locations (All dimensions are in meters).

A Fourier Transform Infrared Spectrometer (FTIR) gas analyser (Gasmet CX4000, Gasmet Technology Oy, Helsinki, Finland) measured the exhaust NH_3 and CO_2 concentrations. The FTIR was zero-point calibrated using N_2 gas one hour before the experiment. Every 30 minutes, the FTIR took 3 continuous air samples per minute and per sampling location at the exhaust duct of the compartment and outside the pig barn. Consequently, all 3 air samples measured per sampling location were averaged as the supply and exhaust gaseous concentrations for the validation test. In the UFAC and slurry pit headspace, a single temperature measurement was performed using a Testo 175T3 thermometer (Range: -50 °C to +1000 °C; accuracy ±0.5 °C, Testo Inc., New Jersey, USA) at each sampling point, one at a time from T1 – T9 (Fig. 6.4) over approximately 1 minute per sampling location. Concurrently, a single UFAC and slurry pit headspace NH_3 concentration was also taken, one at a time from A1 – A9 (Fig. 6.4) using a GASTEC diffusion tube (Gastec Corp., Ayase, Japan, Range: 0.5 to 78 ppm) during the temperature measurements.

The Pt1000 sensors, like in the experiment with the mock-up pigs (section 6.2.2.1), monitored the outside, CUAC and ventilation control (compartment) temperatures. The outside, CUAC and compartment temperature sensors were all kept at the same sampling locations as in section 6.2.2.1. The coordinates of the ventilation control temperature sensor (T10) in the pig compartment was x = 1.75 m, y = 2.4 m and z = 0.5 m (Fig. 6.2). The measurement principle of the VR in the pig compartment was previously described in section 6.2.2.1. The same Orion-VS12 data logger recorded the VR and the outside, CUAC and compartment temperatures at 1 min intervals.

In addition, the airflow pattern in the compartment was determined by releasing smoke from a smoke generator (Mini Mist, Le Maitre Ltd, Surrey, UK) at the UFAC. Slurry samples were taken at a depth of 50 mm from the slurry surface and stored at -18 °C until Total Ammoniacal Nitrogen (TAN) and pH analyses. A C3010 Multi-parameter analyser (Consort bvba, Turnhout, Belgium) measured the slurry pH whereas the slurry TAN concentration was analysed with a Kjeltec 8400 analyser (FOSS, Hilleroed, Denmark) using the BAM procedure (BAM/deel 3/05, 2015).

6.2.3. CFD model development

6.2.3.1. Computational geometry and grid

The CFD model was developed by first building a 3D geometry of the compartment using SolidWorks. The geometry was then imported into ANSYS ICEM CFD 15 to generate a hexahedral structured mesh. Four mock-up pigs per pen were included in the CFD model (Fig. 6.6), so that depending on the number of pigs in a particular simulation case, the wall boundary type of the extra pigs could be to change to an interior boundary type and vice versa.

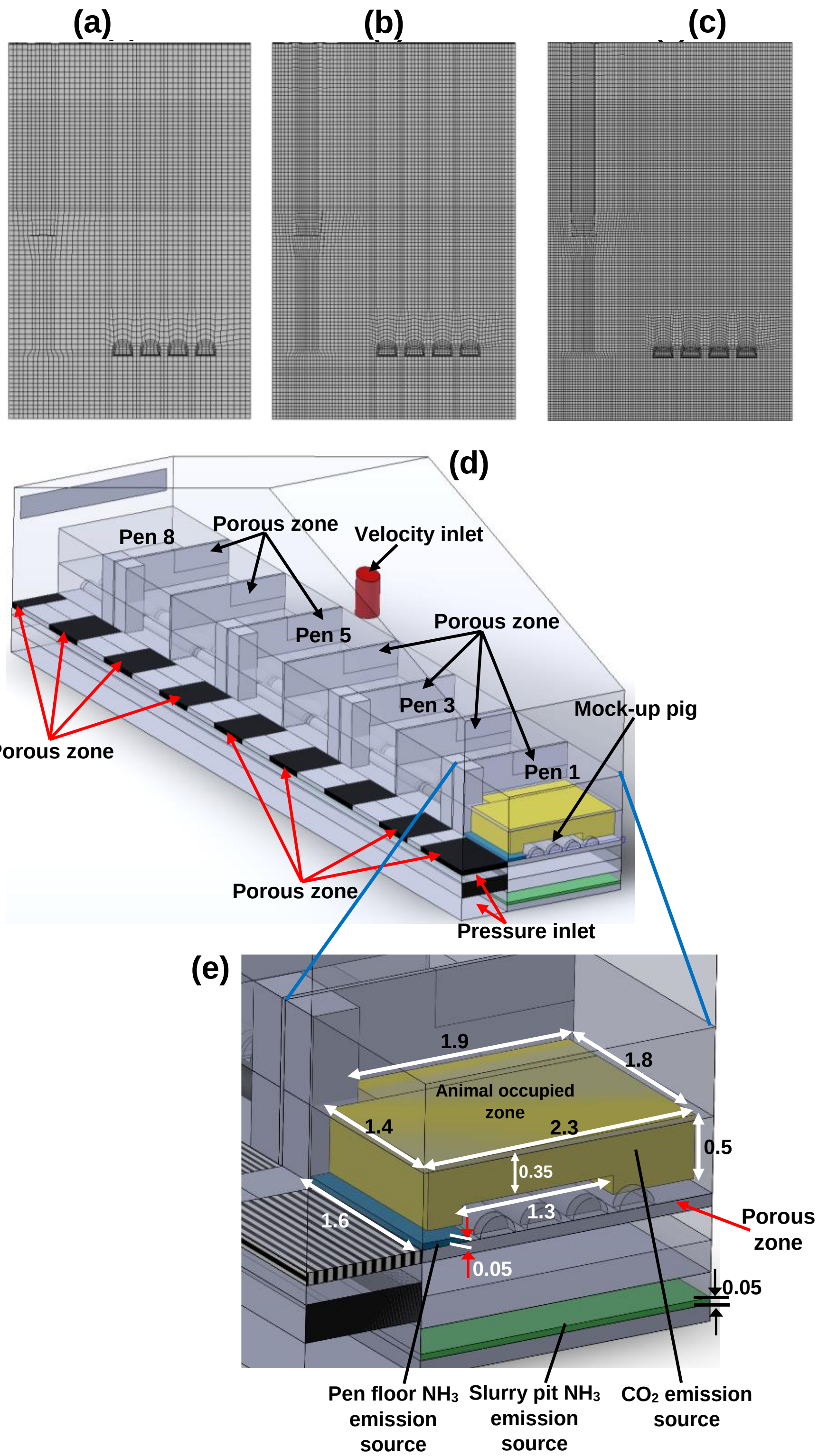

Fig. 6.6. Surface grids across the centre of pen 3: (a) coarse (b) medium (c) fine grids, and (d) the boundary conditions in the CFD domain and (e) an illustration of the NH_3 and CO_2 emission sources in pen 1 (All dimensions are meters).

To ensure that the grid resolution did not affect the simulated results, grid independence tests were performed at 3 different grid resolutions totalling 1046918 cells (coarse, Δ_3), 2817689 cells (medium, Δ_2) and 6086088 cells (fine, Δ_1). The grids were non-uniformly distributed within the compartment domain (Fig. 6.6) and the volume size of the grids ranged from 3.45 × 10^{-6} m^3 to 6.54 × 10^{-4} m^3 in Δ_3, from 1.14 × 10^{-6} m^3 to 2.25 × 10^{-4} m^3 in Δ_2 and from 1.04 × 10^{-6} m^3 to 1.26 × 10^{-4} m^3 in Δ_1. In areas expected to generate steep flow gradients such as above the simulated pigs (Fig. 6.6), the cell density was higher. The Grid Convergence Index (GCI) method, which is based on Richardson Extrapolation (Roache, 1994), was used to quantitatively estimate the discretisation error. The goal of the GCI is to evaluate the error band (%) for a given simulation result (i.e. temperature in the present study) such that the exact solution is within the confidence of 95% (Eça and Hoekstra, 2006). The GCI is calculated as follows:

$$GCI_{i+1,i} = F_S \frac{|\varepsilon_{i+1,i}|}{r^p_{i+1,i} - 1} \tag{6.1}$$

$$\varepsilon_{i+1,i} = \frac{\phi_{i+1} - \phi_i}{\phi_i} \tag{6.2}$$

$$p = \frac{In\left|\frac{\varepsilon_{32}}{\varepsilon_{21}}\right|}{In(r)} \tag{6.3}$$

where i is the grid size, F_S is the “safety factor”, ε is the relative error, r is the grid refinement ratio ($\frac{\Delta_1}{\Delta_2}$ and $\frac{\Delta_2}{\Delta_3}$), p is the order of convergence and ϕ is the solution variable. $F_S = 1.25$ was selected in this study, which was within the suggested range of 1.25 – 3.0 according to Roache (1994). The grid refinement ratios in the present study were $\frac{\Delta_2}{\Delta_3} = 1.39$ and $\frac{\Delta_1}{\Delta_2} = 1.29$.

The grid sensitivity tests were performed at ventilation rate of 62 m^3 h^{-1} pig^{-1} (level 3) of the field experiment with the mock-up pigs using the air temperature at the 31 sampling points (Fig. 6.3). Table 6.1 presents the boundary conditions used in the grid independence test. During the grid sensitivity test, all simulation parameters and boundary conditions remained unchanged, except size of the grids in each simulated case. In this analysis, $p = 2.2$ was taken as the average value over the 31 monitored temperature points. Figure 6.7 compares the effect of the grid resolution on the monitored temperature points in the compartment with the mock-up pigs and Fig. 6.8 displays the corresponding quantitative grid verification at GCI_{21}. The temperature profiles in Fig. 6.7 showed close calculations between the medium (Δ_2) and the fine (Δ_1) grids, which was confirmed by the average GCI_{21} of 2.3% compared to the average value of 5.0% in GCI_{32}. Therefore, given the small GCI_{21}, the medium grid was considered for further analysis, since further refining the grid was not expected to significantly improve the computed results.

Table 6.1. CFD boundary conditions for validating the compartment with the mock-up pigs at ventilation level 1 (11 m^3 h^{-1} pig^{-1}), level 2 (34 m^3 h^{-1} pig^{-1}), level 3 (62 m^3 h^{-1} pig^{-1}) and level 4 (92 m^3 h^{-1} pig^{-1}).

Boundary	Type	Heat transfer	Level 1	Level 2	Level 3	Level 4
Exhaust	Velocity inlet (m s^{-1})	-	-0.6	-1.9	-3.5	-5.2
Inlet	Pressure inlet (0 Pa)	$T_{opening}$ (°C)	T_{Prof}[a]	T_{Prof}[a]	T_{Prof}[a]	T_{Prof}[a]
Mock-up pigs	Wall (no-slip)	Heat flux (W m^{-2})	56	56	56	56
Sidewalls	Wall (no-slip)	T_{wall} (°C)	20	19	17	17
Endwall 1	Wall (no-slip)	T_{wall} (°C)	21	20	18	18
Endwall 2	Wall (no-slip)	T_{wall} (°C)	17	17	16	17
Window	Wall (no-slip)	T_{wall} (°C)	19	17	15	16
Roof	Wall (no-slip)	T_{wall} (°C)	21	19	17	17
Slatted floor	Porous media	-	-	-	-	-
Slotted pen partition	Porous media	-	-	-	-	-
Solid floor (service alley)	Wall (no-slip)	T_{wall} (°C)	17	15	14	13
Pen wall	Wall (no-slip)	T_{wall} (°C)	21	17	15	14
Pen partition	Wall (no-slip)	T_{wall} (°C)	23	19	18	17
Slurry pit wall	Wall (no-slip)	T_{wall} (°C)	17	17	16	16
UFAC wall	Wall (no-slip)	T_{wall} (°C)	15	14	13	12

[a] T_{Prof} refers to the interpolated temperature profile at the UFAC inlet using the constant interpolation method in ANSYS Fluent from the coordinates and their corresponding temperature in Table 6.2.

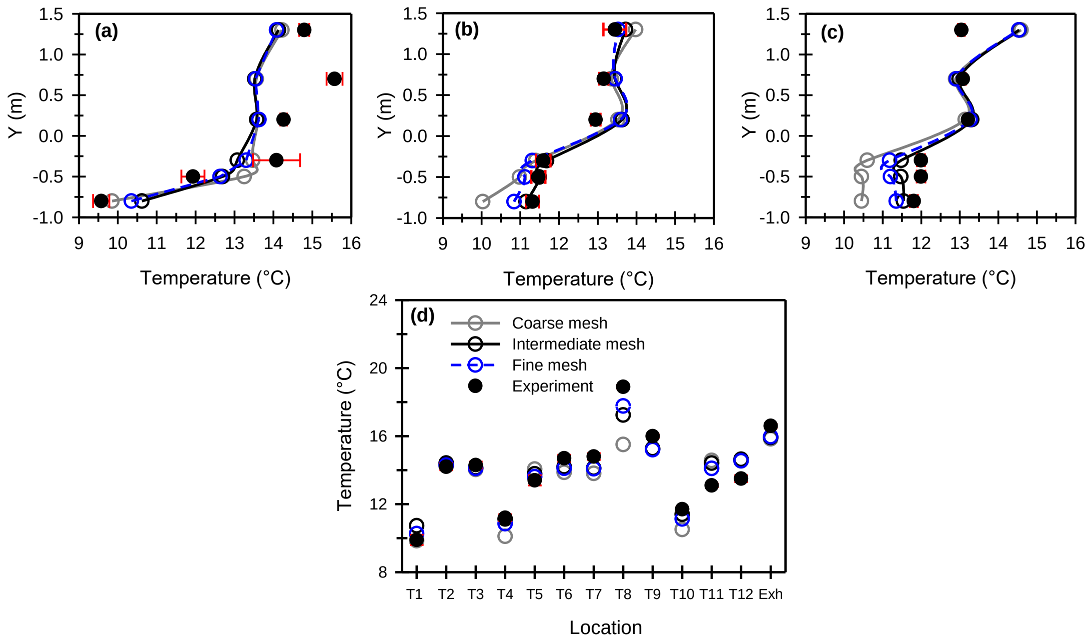

Fig. 6.7. Effect of grid resolution on air temperature in (a) pole 1 (b) pole 2 (c) pole 3 and (d) at point T1 – T12 and the exhaust (Exh) with experiment; coarse grid;: medium grid and fine grid. The sampling locations are shown in Fig. 6.3 and the error bars are the standard deviations.

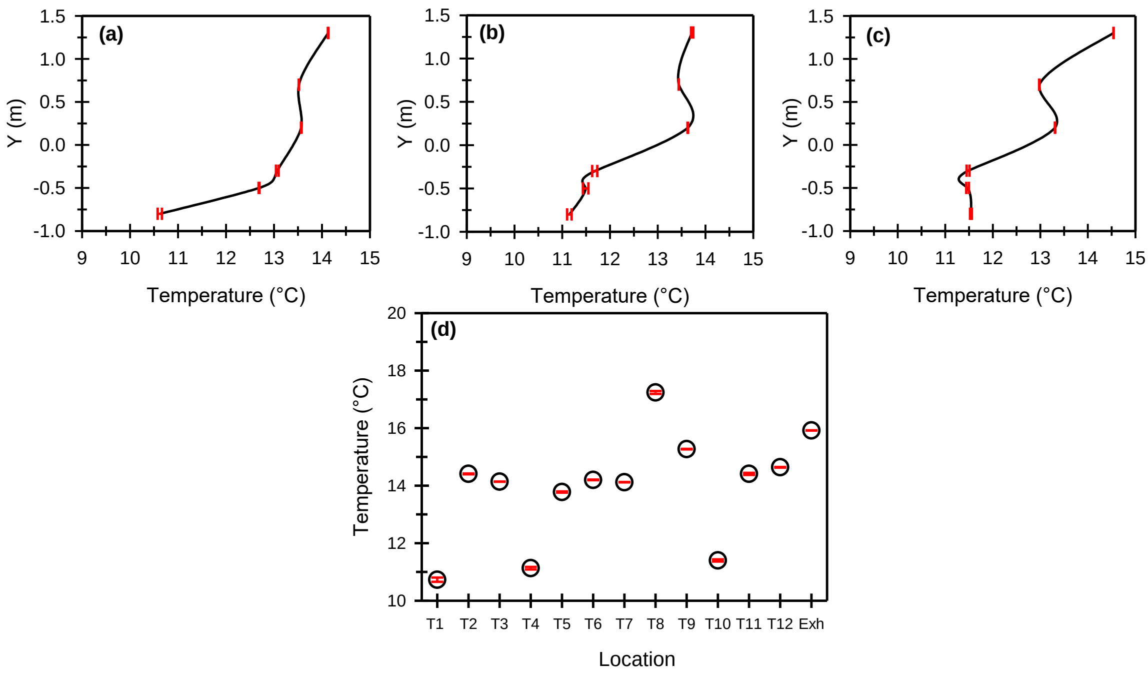

Fig. 6.8. Medium grid solutions of the air temperature in (a) pole 1 (b) pole 2 (c) pole 3 and (d) at points T1 – T12 and the exhaust (Exh) with the discretization error bar (red) (GCI_{21}) calculated using equation 1. The sampling locations are shown in Fig. 6.3.

6.2.3.2. Porous media modelling

The slatted floor (Fig. 6.9b) and the slotted pen partitioning (Fig. 6.9c) were treated as porous media. The porous media assumption was chosen in order to achieve computational efficiency by reducing the grid densities at the boundary-layer of slatted floor and the slotted pen partitioning in the CFD model (Wu et al., 2012; Yin et al., 2016). Before applying the porous media approach, the resistance coefficients (i.e. D and F) in Eq. 6.4 were derived via a virtual CFD wind tunnel of the slatted floor and slotted pen partitioning (Fig. 6.9a). After assigning the boundary conditions (see Fig. 6.9a), simulations were performed at inlet air velocities of 0.05, 0.15, 0.30 and 0.5 m s^{-1} in the slatted floor, and 0.05 0.10, 0.15 and 0.2 m s^{-1} in the pen partitioning virtual wind tunnels, perpendicular to the simulated surfaces. The air velocities in the virtual wind tunnel models were chosen to match the air velocity ranges measured in the compartment during the mock-up pig experiment. The inertial resistance coefficients (F, m^{-1}) and viscous resistance coefficients (D, m^{-2}) were then derived by fitting the pressure drop across the virtual wind tunnels and their corresponding inlet velocities in Eq. 6.4.

$$\frac{\Delta P}{l} = F\frac{1}{2}\rho|u|u + D\mu u \qquad (6.4)$$

where ΔP is the pressure drop through the porous material (Pa), l is the porous material thickness (m), μ is air viscosity (N s m^{-2}), ρ is air density (kg m^{-3}) and u is air velocity (m s^{-1}).

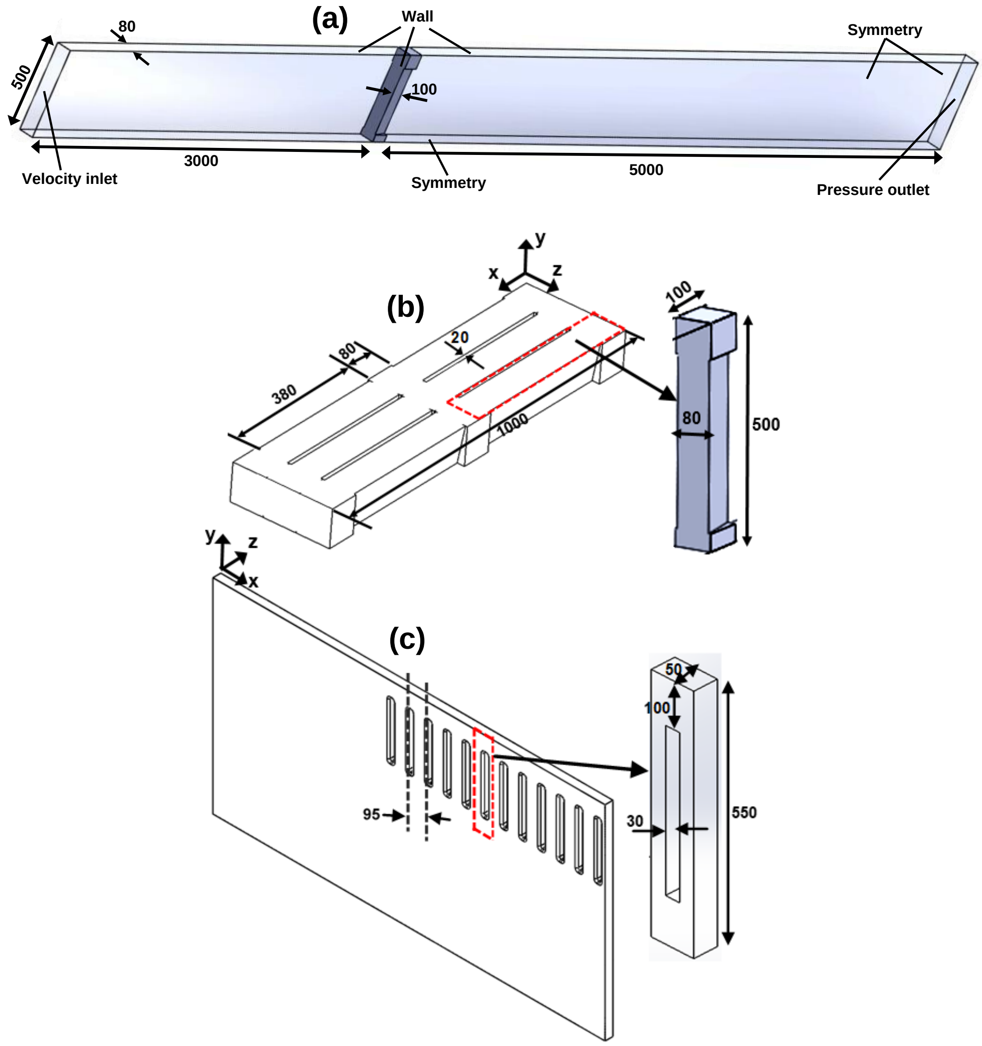

Fig. 6.9. The virtual CFD wind tunnel model used to derive resistance coefficients of the porous media (a) geometry and boundary types (b) section of the simulated slatted floor and (c) pen partition (All dimensions are in mm).

The derived F was 640 m^{-1} and 569 m^{-1} and D was 29060 m^{-2} and 95000 m^{-2} for the slatted floor and the slotted pen partitioning, respectively. The F and D values were only set in the y-direction of the slatted floor and in the z-direction of the slotted pen partitioning (Figs. 6.9b & 6.9c) at the porosity of 15.4% and 19.5%, respectively. In addition, the F and D in the x and z directions of the slatted floor, and in the x and y directions of the slotted pen partitioning were set at higher values (i.e. $F \times 10^2$ and $D \times 10^2$) compared to the derived F and D values in order to represent obstruction to airflow in these directions (Figs. 6.9b & 6.9c).

6.2.3.3. Modelling approach for the NH_3 and CO_2 emissions

It was assumed that the slurry pit and urine puddles on the pen floor were the main NH_3 emission sources in the pig compartment (Hoeksma et al., 1992; Aarnink et al., 1997; Kai et al., 2006, Ni et al., 2000). The urine puddle area was assumed as 0.10 m^2 pig^{-1} per pen, which was within the reported range of 0.07 – 0.11 m^2 per fattening pig in literature (Aarnink et al., 1996; Aarnink et al., 1997). The NH_3 production from both the slurry surface in the pit and the pen slatted floor were computed based on the slurry properties and environmental conditions at the air-slurry boundary layer. Therefore, a user-defined function (UDF) was developed treating the first cells of the respective meshes (with a height of 0.05 m) as an NH_3 volume source. That is, the UDF spatially calculated NH_3 production (Eq. 6.5) using the numerical results of the air velocity and the air temperature from the defined cell volume, assuming equilibrium between NH_4^+ and NH_{3_l} in the slurry/urine puddle (Eq. 1.3) and the equilibrium between $NH_{3_l}$and NH_{3_g}at the slurry/urine liquid film and the gas boundary layer (Eq. 1.2) (Aarnink and Elzing, 1998).

$$ER_{NH_3} = \frac{k \times f \times [TAN]}{H \times 0.05} \tag{6.5}$$

where, ER_{NH_3} (kg m^{-3} s^{-1}) is the NH_3 emission from the volume source, k (m s^{-1}) is the mass transfer coefficient, f (dimensionless) is the un-ionised fraction of the TAN concentration in urine puddle/slurry and H is the dimensionless Henry's law constant. The f, H and k were calculated using Eq. 6.6 – 6.8 (Zhang et al., 1994; Aarnink and Elzing, 1998).

$$f = \frac{10^{pH}}{10^{pH} + 5 \times 10^{(0.00897 + \frac{2727}{T})}} \tag{6.6}$$

$$H = 1431 \times 1.053^{(293-T)} \tag{6.7}$$

$$k = 50.1 \times u^{0.8} \times T^{-1.4} \tag{6.8}$$

where u (m s^{-1}) and T (K) are the air temperature and air velocity at the emitting source derived for each cell from CFD the model.

6.2.3.4. Numerical method

The study assumed airflow in the CFD model as turbulent, steady, incompressible, Newtonian and three-dimensional. The flow, turbulence, energy and species variables were numerically solved using ANSYS Fluent 15, which in this case used the steady Reynolds-Averaged Navier–Stokes (RANS) equations (Versteeg and Malalasekera, 2007) and employs the finite volume method. The steady RANS model was closed using the shear stress transport k-ω turbulence model, given that earlier studies have demonstrated that the shear stress transport (SST) k-ω model provides superior indoor airflow predictions in enclosed environments with natural convection and buoyancy flows compared to the k-ε turbulence models (Stamou and Katsiris, 2006; Zhang et al., 2007; Gilani et al., 2016). Additionally, Rong et al. (2010) showed that the SST k-ω model was more suitable for simulating NH_3 mass transport from surfaces compared to the k-ε turbulence model in a mechanically ventilated pig house, because of its superiority in solving boundary layer flows.

The pressure-based solver was selected to calculate the airflow in the compartment in a segregated manner using the SIMPLE algorithm, which couples the pressure and velocity. For the discretisation of the advection terms of the governing equations, the second order upwind scheme was used for momentum, turbulent kinetic energy, dissipation rate and the energy conservation and the species transport equations. The multispecies model was enabled to simulate the NH_3 and CO_2 transport within the computational domain. The incompressible ideal gas law was used to define the material properties of the gas mixture and to calculate the air density and buoyancy effect on the airflow. Based on the information in He et al. (2010), the NH_3 and CO_2 mass diffusivities in air were described as a function of the air temperature. The body-force-weighted scheme was applied for the pressure.

Based on previous CFD simulations (Van Wagenberg et al., 2004; Srebric et al., 2008), the present model included only the convective but not the radiation part of the sensible heat loss from the pigs (section 6.2.2.1) in the CFD model of the compartment occupied by the mock-up pigs. This was because the convective heat loss was considered much more significant and the difference in temperature between facing surfaces was not sufficiently high in order to make the radiation heat loss pronounced. Thus, it was assumed that the radiative heat part of the sensible heat production was indirectly included by specification of the compartment wall temperature. It was assumed that the solutions were converged when the absolute residuals for the energy and species declined to less than 10^{-7}, and the continuity, velocity, turbulence became less than 10^{-3}. In addition, the mass and energy imbalances of the computational domain at less than 0.2% were also checked as additional criteria for the iteration convergence. After the convergence of the flow, turbulence and energy variables, the species transport equation was activated to calculate mass transport of the NH_3 and CO_2. The CFD simulations were performed by Dell PowerEdge R620 with two Intel Xeon E5-2680v2 (2.8GHz, 10 cores; CPUs, 12 x 8 GB; DDR3 1600 ECC memory).

6.2.4. Boundary conditions for validating the CFD model

6.2.4.1. Inlet and outlet boundary conditions

Table 6.1 shows the boundary conditions used to validate the model in the compartment with the mock-up pigs (section 6.2.2.1). During the validation, the inlet thermal condition was assigned as a temperature profile by interpolating the 4 temperature readings from the field experiment located 1.45 m away from the UFAC inlet (Figs. 6.3a & 6.3b). Air temperature in the UFAC inlet was not measured in the experiment due to the lack of sensors. Table 6.2

shows the interpolated temperature readings at the four ventilation levels. At the UFAC inlet opening, a uniform turbulence boundary condition was used in the CFD model.

Table 6.2. The interpolated underfloor air channel inlet temperature profiles at the four ventilation rates in the CFD model obtained from the field experiment in the compartment occupied by the mock-up pigs.

Coordinates[a]			Ventilation rate			
x (m)	y (m)	z (m)	11 m^3 h^{-1} pig^{-1}	34 m^3 h^{-1} pig^{-1}	62 m^3 h^{-1} pig^{-1}	92 m^3 h^{-1} pig^{-1}
0.20	-0.8	-4.5	10.3 °C	8.8 °C	9.6 °C	11.0 °C
-0.25	-0.8	-4.5	9.5 °C	8.3 °C	9.9 °C	11.0 °C
0.20	-0.5	-4.5	13.3 °C	10.0 °C	11.9 °C	11.2 °C
0.20	-0.3	-4.5	16.1 °C	12.1 °C	14.1 °C	11.6 °C

[a] These coordinates are with respect to Fig. 6.2.

This study initially applied turbulence intensity of 5% and a viscosity ratio of 10 for the inlet velocities from 0.1 to 1.0 m s^{-1} corresponding to inlet Reynolds numbers of 6.0×10^3 to 6.0×10^4, which are in the range of low to medium turbulence level according to the ANSYS Fluent users' guide. A preliminary comparison of the simulated results with experimental data at this inlet turbulent condition showed the model could not accurately predict the UFAC temperature farther away from the UFAC inlet. This was because of the lack of air mixing at the UFAC inlet due to the exclusion of the underground air channel upstream of the UFAC inlet (Figs. 6.1 & 6.2). Furthermore, the 0.30 m high heating plate at the top of the UFAC inlet covering 30% of the opening area (Figs. 6.1c & 6.2a) affected the airflow characteristics at the UFAC inlet. Subsequently, a hydraulic diameter and turbulence intensity boundary condition was applied, and the turbulence level adjusted from 5 to 20% at a fixed inlet hydraulic diameter of 0.95 m.

Since the temperature profile in the UFAC inlet was not measured in the compartment that was occupied by the real pigs (section 6.2.2.2), a uniform inlet temperature boundary condition was assumed during the CFD model validation. Preliminary tests in the CFD model using a uniform and a temperature profile boundary condition at the UFAC inlet from the experimental data in the compartment occupied by the mock-up pigs showed similar temperature distributions inside the compartment (appendix, Fig. A). Therefore, the UFAC inlet was the average CUAC temperature (12 ° C) obtained by the field measurements in the compartment with the real pigs (section 6.2.2.2). The other inlet boundary conditions during the validation of the CFD model with the real pigs included the UFAC inlet hydraulic diameter of 0.95 m and turbulence intensity of 20% derived from the model tuning in section 6.2.2.1 (Fig. B, appendix), while the exhaust opening velocity (3.0 m s^{-1}) was derived from the average VR of 35 m^3 h^{-1} pig^{-1} during the field measurement.

6.2.4.2. Wall and pig thermal boundary conditions

Animal heat loss in CFD models is often represented either as a constant surface temperature or as a surface heat flux or as the volume heat source of the convective portion of the sensible heat loss (Van Wagenberg et al., 2004, Seo et al., 2012; Bjerg and Zhang, 2012). The surface heat flux boundary condition was used in the current study. However, since the partition between the convective and radiative (C-R ratio) heat loss around the simulated pigs is hard to determine (Norton et al., 2010), and an incorrectly defined convective heat loss could affect the indoor airflow (Srebric et al., 2008), sensitivity tests were first performed at different C-R ratios. The current CFD model evaluated the appropriate thermal boundary condition for the simulated pigs at the convective heat loss of 100%, 50% and 30% of the total heat production during the mock-up pig experiment. The convective heat fluxes of 187, 93 and 56 W m^{-2} were specified for the total heat production of 169 W per mock-up pig and the exposed surface area of ~1.0 m^2 for the C-R ratios of 100:0, 50:50 and 30:70 with the same boundary conditions of the simulated compartment during the sensitivity test (Table 6.1). At ventilation level 3, the convective heat loss sensitivity test was performed so that the simulated air temperature agreed best with the experimental result at the 31 temperature sampling locations (Fig. 6.3). The C-R ratio of 30:70 was selected as the suitable pig thermal boundary condition, since both the 100:0 and 50:50 C-R ratios over-predicted the experimental temperature at the 31 sampling locations compared to the 30:70 C-R ratio.

For the validation of the model with the real pigs in the compartment, the wall temperature boundary condition was 22 °C, the solid floor at the service alley, UFAC and slurry pit wall temperatures were set at 12 °C. The wall temperatures were checked by the handheld infrared thermometer (section 6.2.2.1). In addition, the porous media boundary condition was applied at the pen partitioning and the slatted floor, while all the other boundary types remained the same as in the mock-up pig validation test (Table 6.1). The pigs (6 per pen) in the compartment were also modelled as semi-cylinders of the same dimension as the mock-up pigs (section 6.2.2.1). It was assumed each semi-cylinder represented 2 headless pigs in sternum lying position (Fig. 3.2), i.e. 3 semi-cylinders per pen (Fig. 6.6). The real pig geometry was simplified in the CFD model to achieve computational efficiency by reducing the grid densities at the boundary-layer of the pig body surface. In addition, Seo et al. (2012) confirmed that there was no effect on the overall accuracy of the CFD model by simplifying the pig geometry as a semi-cylinder in the pig barn. The heat production was set as a surface flux of 240 W m^{-2} per semi-cylinder, derived from the total exposed surface area of ~1.0 m^2 and the sensible heat production of 110 W pig^{-1} from CIGR (2002) heat and moisture production equations. Latent heat was of course produced by the real pigs but this was not directly simulated in the CFD model. To account for the latent part of the heat production in the CFD model, the sensible heat (radiation + convection) that was calculated from the CIGR (2002) equations was adjusted so that exhaust temperature in the CFD model agreed with the experimental result. In this case the exhaust temperature in CFD model agreed best with the experiment result a C:R ratio of 100:0.

6.2.4.3. NH_3 and CO_2 boundary conditions

Using the experimental data in Aarnink et al. (2018), it was initially specified that the urine puddle pH and TAN concentration were 8.5 and 3.3 kg m^{-3} respectively. However, after the model tuning during the validation test, the urine puddle pH and the TAN concentration were subsequently increased to 8.8 and 3.5 kg m^{-3} in the CFD model, respectively. It was assumed that the pH and TAN concentration at the urine puddle remained constant during the experiment. This was in accordance with earlier work by Aarnink and Elzing (1998), which recognized that the pH of pig urine increased quickly from 7 after the conversion of urea began to 8.5 when 11% of urea was converted to NH_3 in urine and 9.1 when 95% of urea was transformed to NH_3.

The TAN concentration of the slurry in the pit was set as the bulk slurry TAN concentration (3.14 kg m^{-3}) measured during the field experiment (section 6.2.2.2). The slurry surface pH was set as 8.5 after the model tuning from the measured bulk slurry pH of 7.5 (section 6.2.2.2) during the model validation test. Again, the assumed slurry pH was in accordance with literature, which suggests that the pH at the top segment of slurry (< 5 mm depth) is up to 1 unit greater than the bulk slurry pH due to the settling of solid matter and physiochemical interactions involving NH_3 and CO_2 gas loss from the slurry surface (Aarnink and Elzing, 1998; Hafner et al. 2012; Aarnink et al., 2018).

CO_2 production in the compartment was modelled using the measured CO_2 emission (i.e. 107.9 g h^{-1} pig^{-1}) from the field experiment. The CO_2 emission rate was calculated as the product of the hourly average VR and the difference between the exhaust and supply air CO_2 concentrations (Eq. 5.1). The CO_2 production of 6.42×10^{-5} kg m^{-3} s^{-1} per pen was then applied to the AOZ of the volume ~1.645 m^3 per pen (Fig. 6.6d). No CO_2 production was applied to the slurry. This was because it was assumed that only a small fraction of the CO_2 was produced in the slurry pit, since the slurry pit was emptied 10 days before the start of the field experiment (Pedersen et al., 2008). Note that the volume source of the CO_2 in the pen, i.e. the AOZ, was defined as 0.1 m away from all wall surfaces. Adding the pen walls into the CO_2 production zone resulted in very high CO_2 concentrations near the wall surfaces in the pen. Indeed, due to the lower air velocities at the walls, the CO_2 at the boundary layer of the wall was mainly transported by the diffusion portion of the species transport equation. This resulted in unrealistic high concentration gradients between the wall and the air near the wall. The inlet CO_2 was set as 460 ppm from the field experiment. The relatively high inlet CO_2 was due to the location of the background gas sampling tube (close to the outlet of the air scrubber at the pig facility) and a nearby uncovered solid manure storage area. The surface below the NH_3 volume source in the slurry pit was assumed as adiabatic with a non-slip wall boundary condition. It was assumed that the thermal condition at the slurry surface was adiabatic, because the slurry temperature was not measured during the field experiment. The slurry surface temperature in the pit will also be difficult to measure, as the temperature will be heterogeneous due to pig movement, excretion, lying behaviour and heat transfer from the pigs and slatted floor to the slurry surface.

6.2.5. Post-processing of the simulated data

The current study used the parameter of throw height (T_H, m) to evaluate the effect of supply air characteristics at the slatted floor inlet on the airflow pattern and temperature distribution in the compartment. According to Lin and Tsai (2014), the T_H is the maximum vertical height the supply air can reach at the slatted floor inlet. The T_H is the function of momentum to the buoyancy flux ratio of the supply air (Eq. 6.10), referred to as the thermal length (l_m, m) scale (Etheridge and Sandberg, 1996). The T_H was calculated using Eq. 6.9 – 6.12.

$$T_H = K_t l_m \tag{6.9}$$

$$l_m = \frac{{M_0}^{3/4}}{{B_0}^{1/2}} \tag{6.10}$$

$$M_0 = Q_{room} u_{in} \tag{6.11}$$

$$B_0 = \frac{g Q_{room}\ \Delta T}{T_{AOZ}} \tag{6.12}$$

where g (m s^{-2}) is gravitational acceleration, T_{AOZ} (°C) is average temperature at AOZ (i.e. volumetrically averaged over the 8 pens), $\Delta\mathrm{T}$ (°C) is the $T_{AOZ} - T_{in}$. The T_{in} and u_{in} (m s^{-1}) are the average supply air temperature and air velocity at the face of the porous media in the service alley, respectively. K_t is the proportional constant of T_H taken as 1.85 in Lin and Tsai (2014), Q_{room} is the supply air volume flow rate (m^3 s^{-1}) at the face of the porous media in the service alley. M_0 is the initial specific jet momentum flux (m^4 s^{-2}) and B_0 is the initial specific jet buoyancy flux in m^4 s^{-3} (Etheridge and Sandberg, 1996; Lin and Tsai, 2014).

Additionally, the simulated temperature distribution of the compartment was characterised using the dimensionless θ_{UFAC} and θ_{AOZ}, and the $T_{1.3} - T_{-0.8}$ (°C).

$$\theta_{UFAC} = \frac{T_{1.3} - T_{in}}{T_{exh} - T_{in}} \quad (6.13)$$

$$\theta_{AOZ} = \frac{T_{AOZ} - T_{in}}{T_{exh} - T_{in}} \quad (6.14)$$

where T_{exh} (°C) is the exhaust air temperature, $T_{1.3}$ (°C) represents the average temperature in the vertical profile form the 6 sampling points at y = 1.3 m at the service alley, while $T_{-0.8}$ (°C) represents the average temperature from the other 6 sampling locations at y = -0.8 in the UFAC.

In the pig compartment, the slatted floor in the pen functions as both air inlets and outlets for the slurry pit headspace. Assuming continuity, the air exchange rate, AER_{pit} (h^{-1}) in the slurry pit was calculated from;

$$AER_{pit} = \frac{\frac{1}{2}\int |v_y| dA}{V_{pit}} \quad (6.15)$$

where, $|v_y|$ (m s^{-2}) is the absolute y-velocity component at slatted floor inlet and A is the area of the porous media at the service alley and V_{pit} is the volume of the slurry pit. The present study defined the human breathing zone (HBZ) as the volume of air at; x = -0.4 to 0.4 m, y = 1.3 to 2.0 m and z = -4.3 to 11.85 m (Fig. 6.2) in the service alley. Fig. 6.6d illustrates the volume of the AOZ in each pen. The air exchange rate in the compartment was calculated as;

$$AER_{comp} = \frac{VR}{V_{comp}} \quad (6.16)$$

where VR (m^3 h^{-1}) is the ventilation rate and V_{comp} is the volume of the compartment.

6.3. Results and discussion

6.3.1. Model validation

6.3.1.1. Air temperature

Figures 6.10 & 6.11 compare the simulated and measured air temperatures at the 31 sampling locations in the compartment occupied by the mock-up pigs. Figure 6.11 shows that both the simulated and measured vertical temperature gradients at the UFAC dropped as the VR increased in the compartment. In the CFD model, the average vertical temperature gradients at y = -0.8 m in the UFAC and y = 1.3 m above the UFAC were 7.7 ± 1.2 °C, 6.6 ± 0.5 °C, 3.0 ± 0.4 °C and 2.1 ± 0.3 °C at the ventilation rates of 11, 34, 62 and 92 m^3 h^{-1} pig^{-1}, respectively. In contrast, the average vertical temperature gradients during the field experiment were 10.0 ± 1.8 °C, 7.2 ± 2.6 °C, 2.9 ± 1.6 °C and 1.9 ± 1.5 °C at ventilation rates 11, 34, 62 and 92 m^3 h^{-1} pig^{-1}, respectively. The outcome above was encouraging, considering that this sort of phenomenon is characteristic of airflow in UFAD systems (Wan and Chao, 2005; Lin and Tsai, 2014).

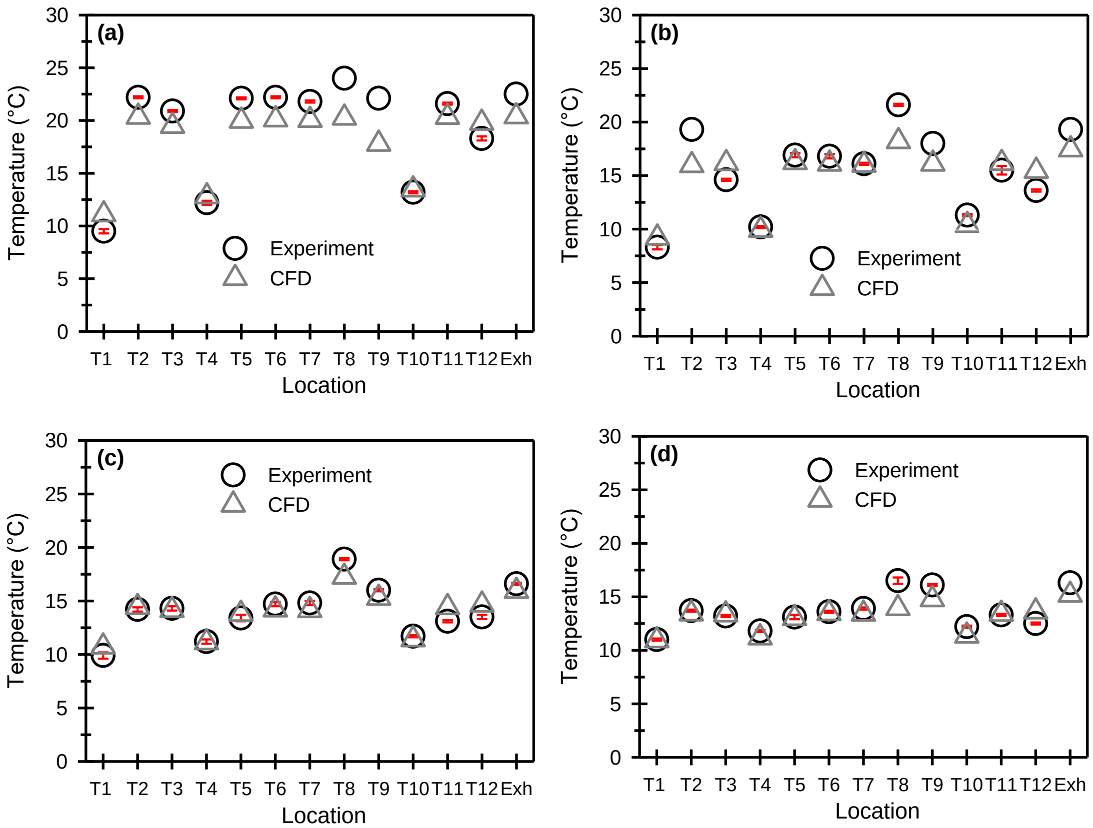

Fig. 6.10. Comparison of CFD with the experimental air temperature at sampling locations T1 – T12 and the exhaust (Exh) in the compartment with the mock-up pigs at ventilation rate of 11 (a), 34 (b), 62 (c) and 92 m^3 h^{-1} pig^{-1} (d). The sampling locations are shown in Fig. 6.3 and the error bars are the standard deviations.

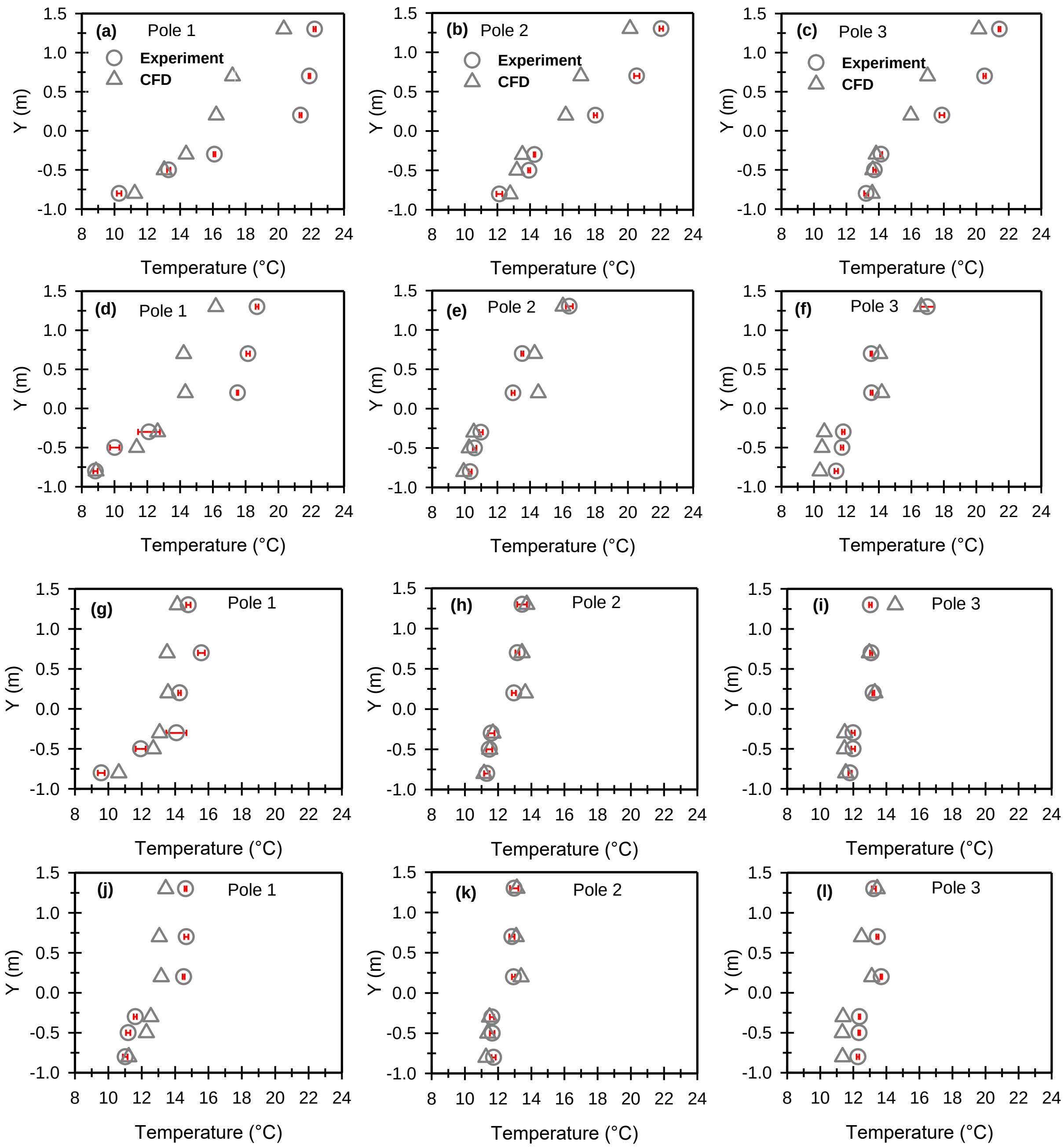

Fig. 6.11. Comparison of (Δ) CFD with the (O) experimental air temperature at poles 1 – 3 in the compartment with the mock-up pigs at ventilation rate of 11 (a – c), 34 (d – f), 62 (g – h) and 92 m^3 h^{-1} pig^{-1} (j – l). The sampling locations are shown in Fig. 6.3 and the error bars are the standard deviations.

Figure 6.12 compares the deviations in air temperature between the simulated and measured results at the 31 sampling locations in the compartment (Fig. 6.3). For the lower ventilation rates (11 & 34 m^3 h^{-1} pig^{-1}) the deviations between the simulated and measured air temperatures were less than 10% (Figs. 6.12a & 6.12b) at 20 sampling locations. At the higher ventilation rates (62 & 92 m^3 h^{-1} pig^{-1}), the majority (29 sampling locations) of the temperature deviations between the simulated and measured results were less than 10% (Figs. 6.12c & 6.12d). The deviations were larger than 20% only at two and one sampling locations at ventilation levels 1 & 2, respectively (Figs. 6.12a & 6.12b).

Moreover, at ventilation level 1 in the compartment with the mock-up pigs, the CFD model underestimated some of the air temperatures measured above the slatted floor inlet (at y = 0.0 – 1.3 m) in poles 1 – 3 (Fig. 6.11a – 6.11c). The simulated air temperature in the service alley at ventilation level 1 underestimated the measured values by 1.9 – 5.1 °C at pole 1, 1.8 – 3.4 °C at pole 2 and 1.3 – 3.5 °C at pole 3. It is also observed in the AOZ (i.e. T3, T6 – T9 and T12) and at points T2, T5 and T11 (Fig. 6.10a) that the measured air temperatures are under-predicted by the CFD model. The underestimating temperature trends were mainly restricted to pole 1 at the higher VR, which decreased with increasing VR (Fig. 6.12).

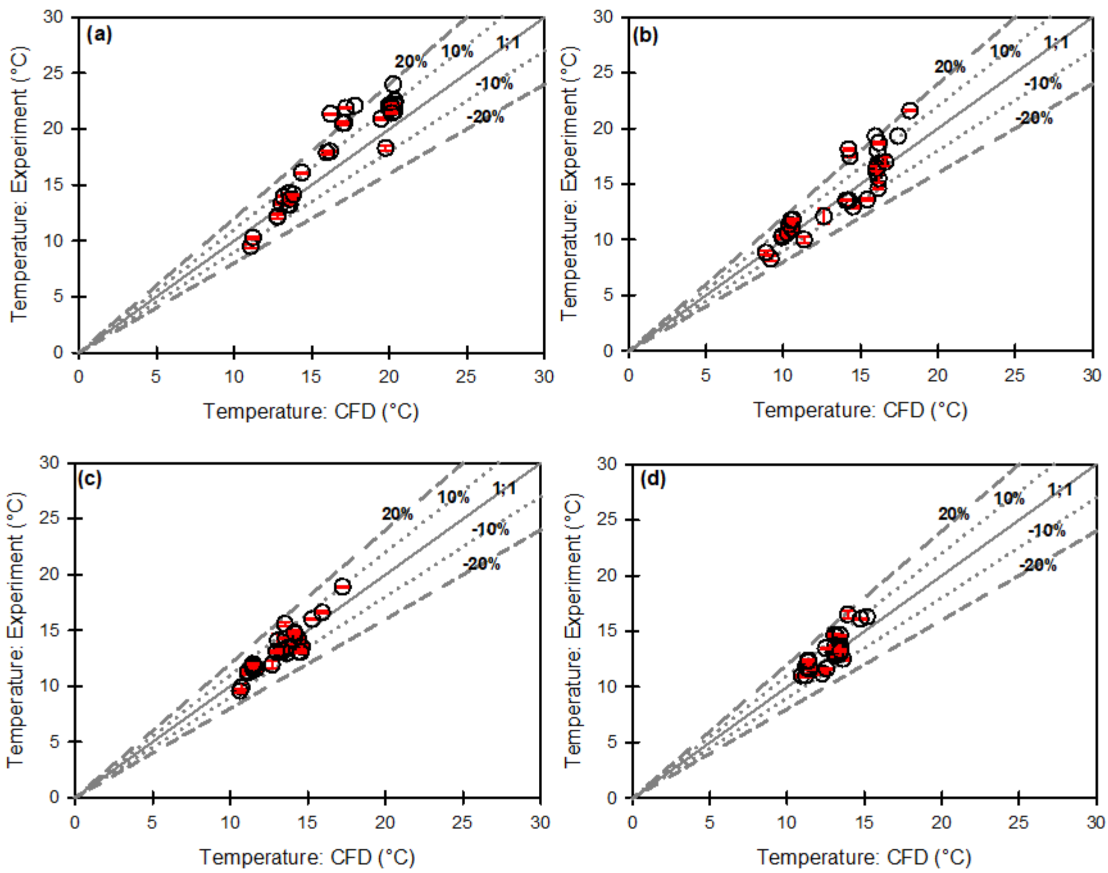

Fig. 6.12. Deviations between CFD and experimental air temperatures in the compartment with the mock-up pigs at ventilation rate of (a) 11, (b) 34, (c) 62 and (d) 92 m^3 h^{-1} pig^{-1}. The error bars are the standard deviations.

The following factors in the CFD model altered the actual airflow pattern in the experimental compartment's UFAC, resulting in lower temperatures than the measured values at the service alley. First, simplifying the UFAC inlet in the CFD model (Fig. 2.1 vs Fig. 6.1) reduced the potential for air mixing and heat transport from the heating plate to the UFAC inlet in the simulated compartment. The reason is that the incoming air from the CUAC entered UFAC at an acute angle and not perpendicular as specified in the CFD model. Indeed, there was a better agreement between the simulated and measured temperature at the service alley in poles 2 – 3 than pole 1 due to the enhanced air mixing at the back compared to the front end of the UFAC inlet (Figs.6.13 & 6.14). Second, imposing the temperature profile of the inlet rather than the heat flux on the 0.30 m high heating plate at the CFD model's UFAC inlet (Figs. 2.1c) underestimated the heat input of the supply air compared to the experimental situation. This assumption was confirmed from a detailed temperature measurement in the inlet of the UFAC using 12 temperature sensors (Fig. C, appendix) after the experiment.

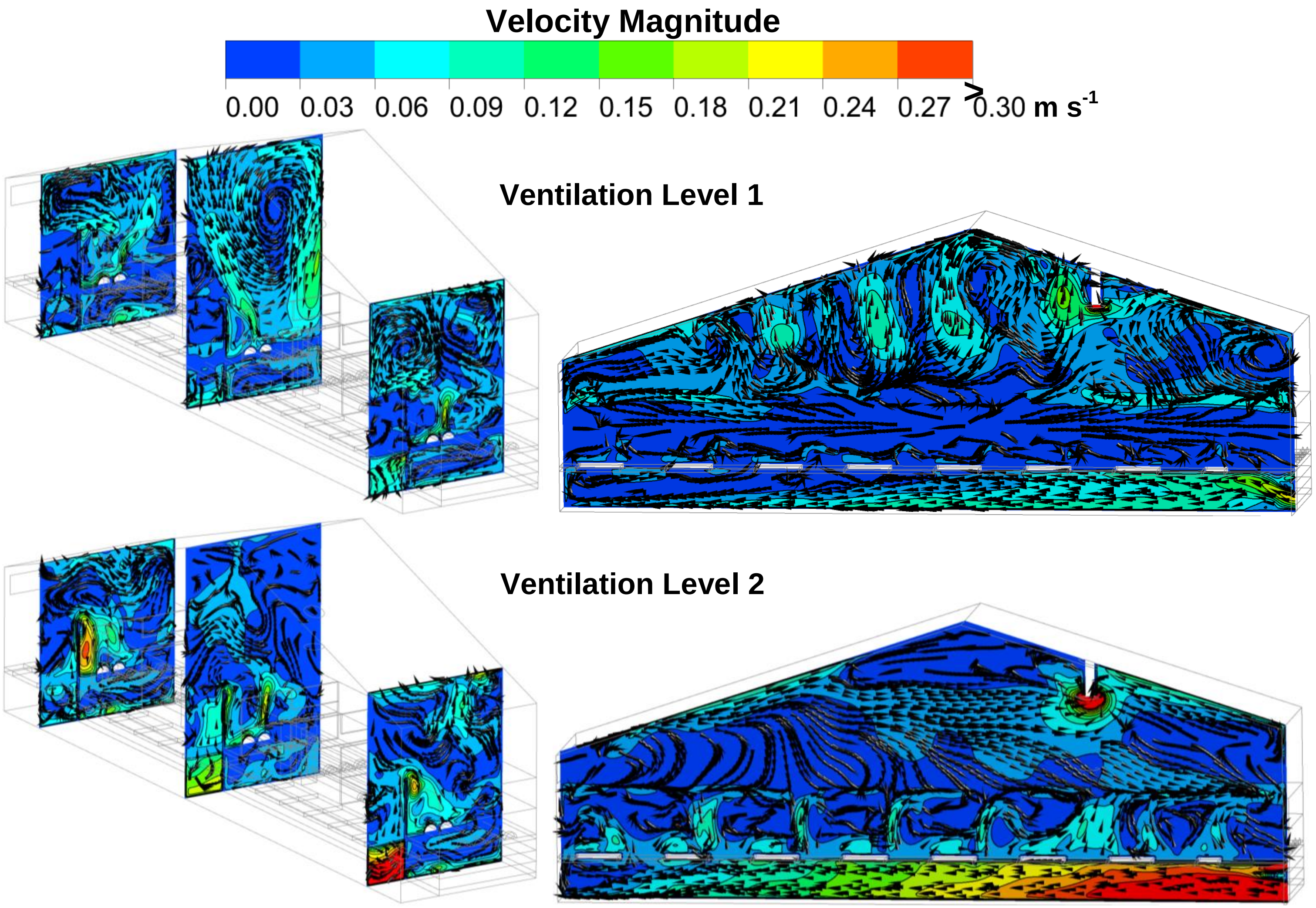

Velocity Magnitude
0.00 0.03 0.06 0.09 0.12 0.15 0.18 0.21 0.24 0.27 > 0.30 m s-1
Ventilation Level 1
Ventilation Level 2

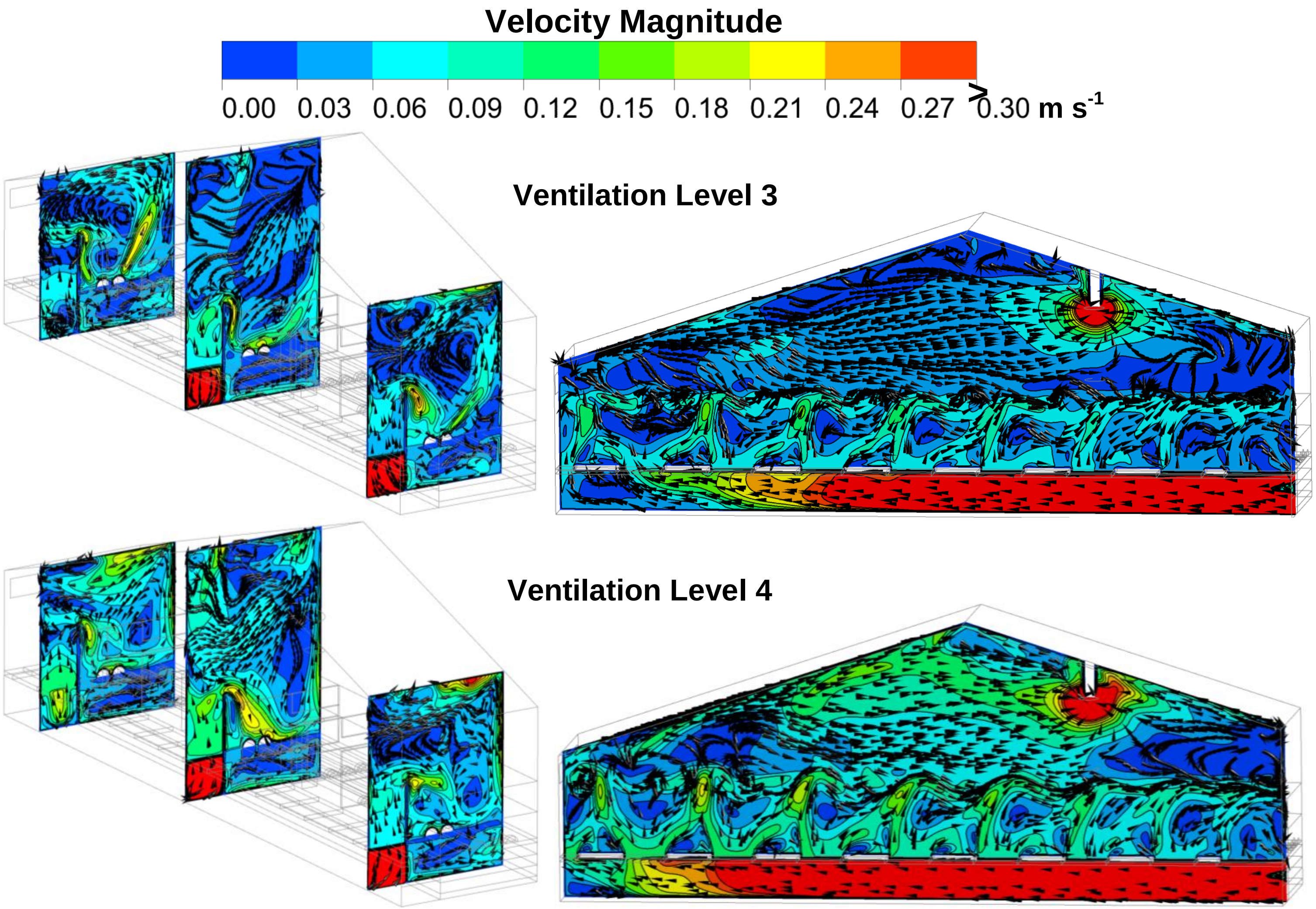

Fig. 6.13. The predicted air velocity magnitude contours and airflow streamlines in sections A-A, B-B, C-C and D-D in the compartment with the mock-up pigs at ventilation level 1 (11 m^3 h^{-1} pig^{-1}), level 2 (34 m^3 h^{-1} pig^{-1}), level 3 (62 m^3 h^{-1} pig^{-1}) and level 4 (92 m^3 h^{-1} pig^{-1}).

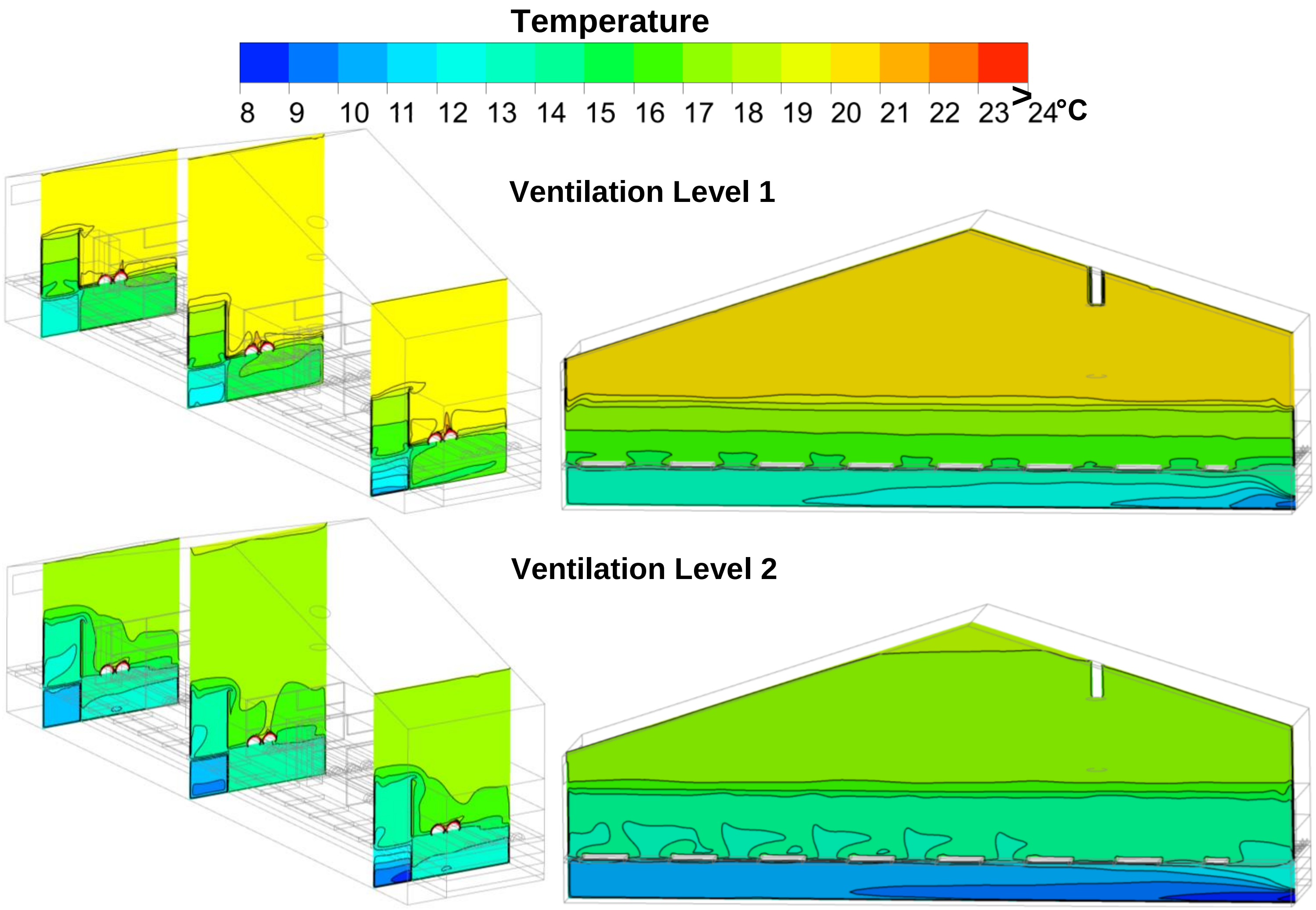
Temperature
8
9
10
11
12
13
14
15
16
17
18
19
20
21
22
23
>24°C
Ventilation Level 1
Ventilation Level 2

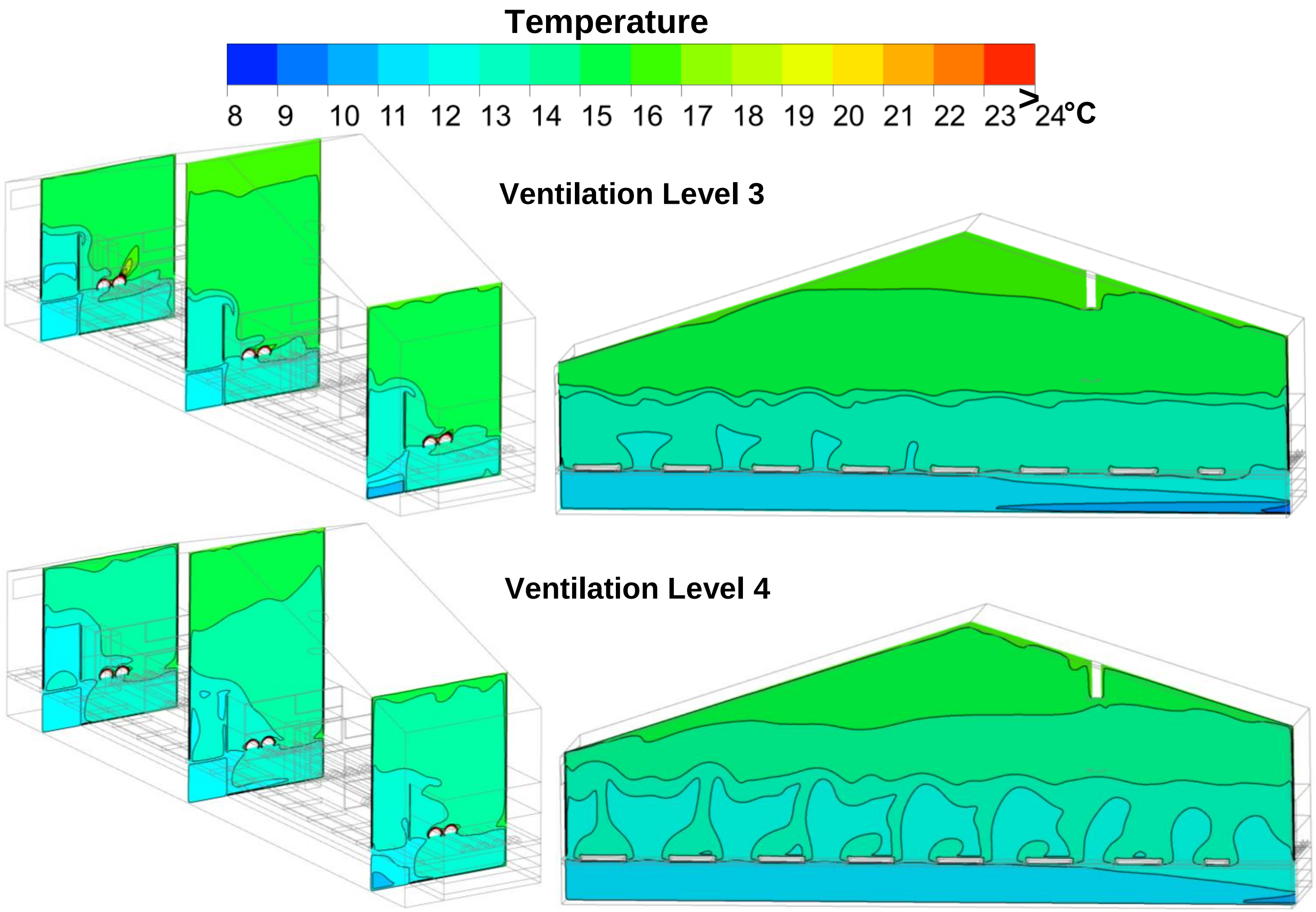

Fig. 6.14. The predicted air temperature contour in sections A-A, B-B, C-C and D-D in the compartment with the mock-up pigs at ventilation level 1 (11 m^3 h^{-1} pig^{-1}), level 2 (34 m^3 h^{-1} pig^{-1}), level 3 (62 m^3 h^{-1} pig^{-1}) and level 4 (92 m^3 h^{-1} pig^{-1}).

Third, the porous media assumption at the slatted floor inlet in the CFD model underestimated the air speed exiting the slatted floor, the heat transport in slats, and the air mixing above the slatted floor at the UFAC compared to the experiment. The CFD model predicted lower air velocity at sampling location V4 compared to the measured value (Fig. 6.15). This confirms that the porous media assumption of the slatted floor inlet underestimates the air speed exiting the slatted floor. Indeed, ANSYS FLUENT calculates the air speed exiting the porous medium based on the volumetric flow rate without the solid slat blockages in them. This assumption can produce relatively low air speeds above the porous media, and generate low turbulence compared to the actual situation due to the absence of solid slats in porous media (Zong et al., 2014; Rong et al., 2015). Nonetheless, Fig 16a confirms that the CFD model adequately predicted the air temperatures measured during the field experiment as majority of deviations between the simulated and measured air temperatures were less than 5% (Fig. 17a).

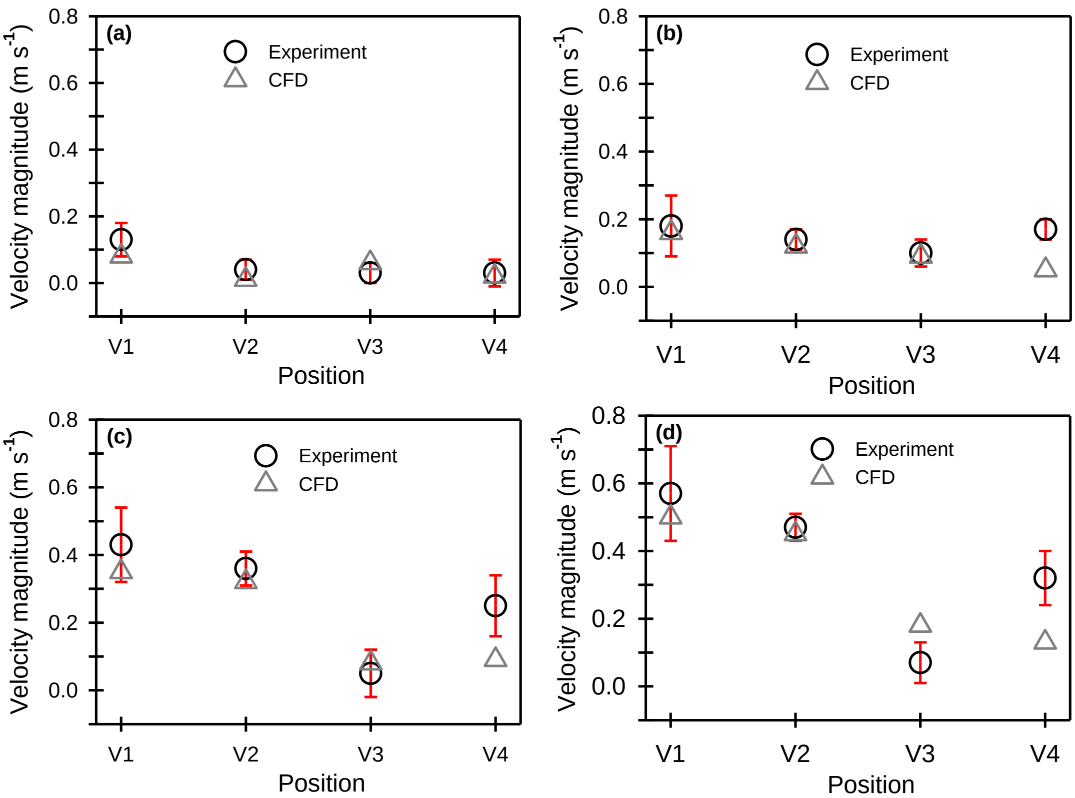

Fig. 6.15. Comparison of CFD with the experimental air velocity magnitude at sampling locations V1 – V4 in the compartment with the mock-up pigs at ventilation rate of 11 (a), 34 (b), 62 (c) and 92 m^3 h^{-1} pig^{-1} (d). The sampling locations are shown in Fig. 6.3 and the error bars are the standard deviations.

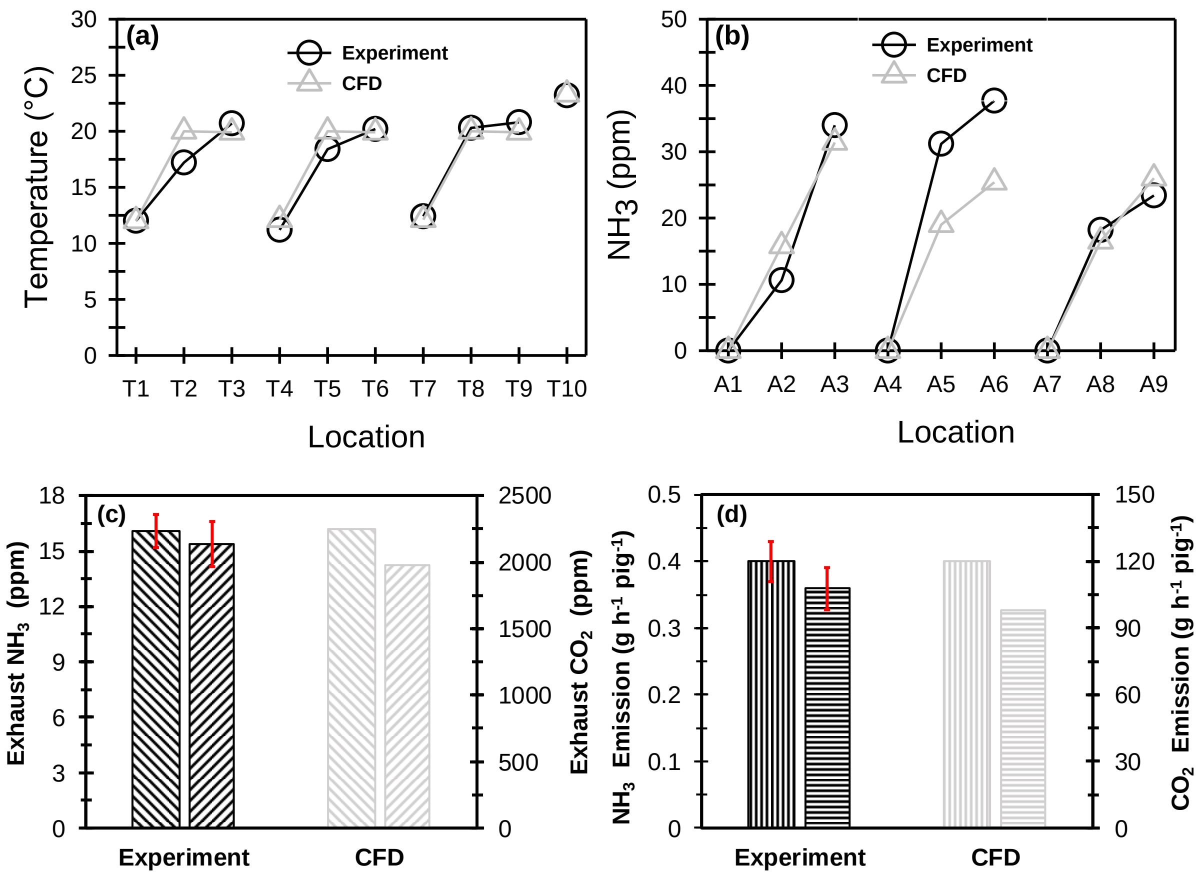

Fig. 6.16. Comparison of CFD with the experimental (a) air temperature at sampling locations T1 – T10 (b) NH_3 concentration at sampling locations A1 – A9, (c) exhaust NH_3 and CO_2 concentrations, and (d) NH_3 and CO_2 emission rate in the compartment with the real pigs. The sampling locations are shown in Fig. 6.5 and the error bars are the standard deviations.

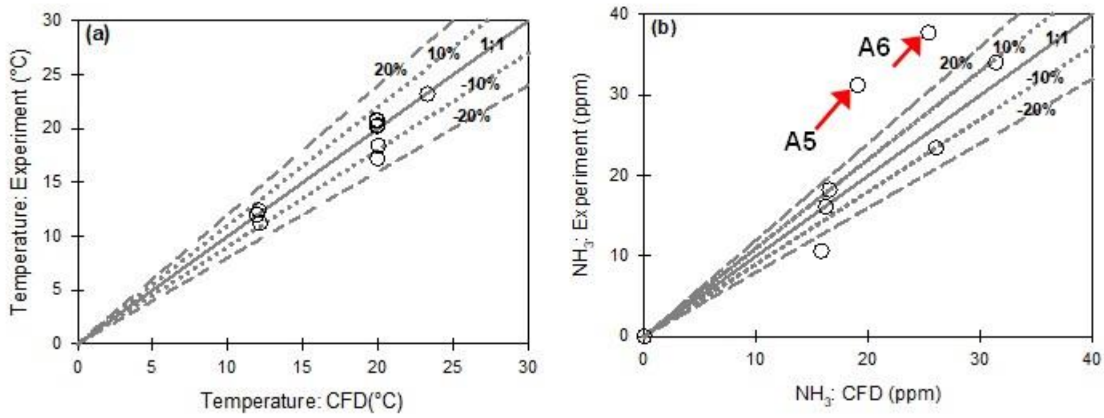

Fig. 6.17. Deviations between CFD and experimental (a) air temperature and (b) NH_3 concentration in the compartment occupied by the 48 real pigs at ventilation rate of 35 m^3 h^{-1} pig^{-1}. The error bars are the standard deviations.

6.3.1.2. Airflow pattern and velocity

The CFD model predicted a similar airflow pattern as was seen in the compartment occupied by the real pigs during the smoke test (Fig. 6.18). Both studies show the gradual rise of the incoming air from the slatted floor inlet until the height of the solid pen partitioning towards the service alley. Fig. 6.19a indicates the incoming air warming up during its rise in the service alley and then it descends into the AOZ. A fraction of the incoming air flows into the slurry pit at the section of the pen floor near the service alley and then exits at the other section of the pen towards the sidewall (Fig. 6.18). The remaining part of the incoming air flows over the heated mock-up pigs with recirculation and air mixing above the AOZ. The air then exits the compartment at the exhaust duct. In Fig. 6.18, both the simulated and measured airflows show the large recirculation vortex in the anticlockwise direction that spanned from the AOZ to the service alley. This qualitative result gives confidence in the reliability of the CFD model, given that a similar airflow pattern was observed in chapters 4 and 5. After the qualitative validation of the airflow pattern, quantitative comparisons can now be made between the simulated and measured air velocities in the compartment that was occupied by the mock-up pigs.

Fig. 6.15 compares the simulated and measured air velocities in the compartment occupied by the mock-up pigs. There was a good agreement between the simulated and measured values. Most of simulated air velocities deviated less 20% of the experimental data and were within the standard deviations of the experimental results, except at sampling location V4 which underestimated experimental results above 20% (Fig.20). The outliers at V4 were previously attributed to the porous media assumption for the slatted floor inlet in the CFD model.

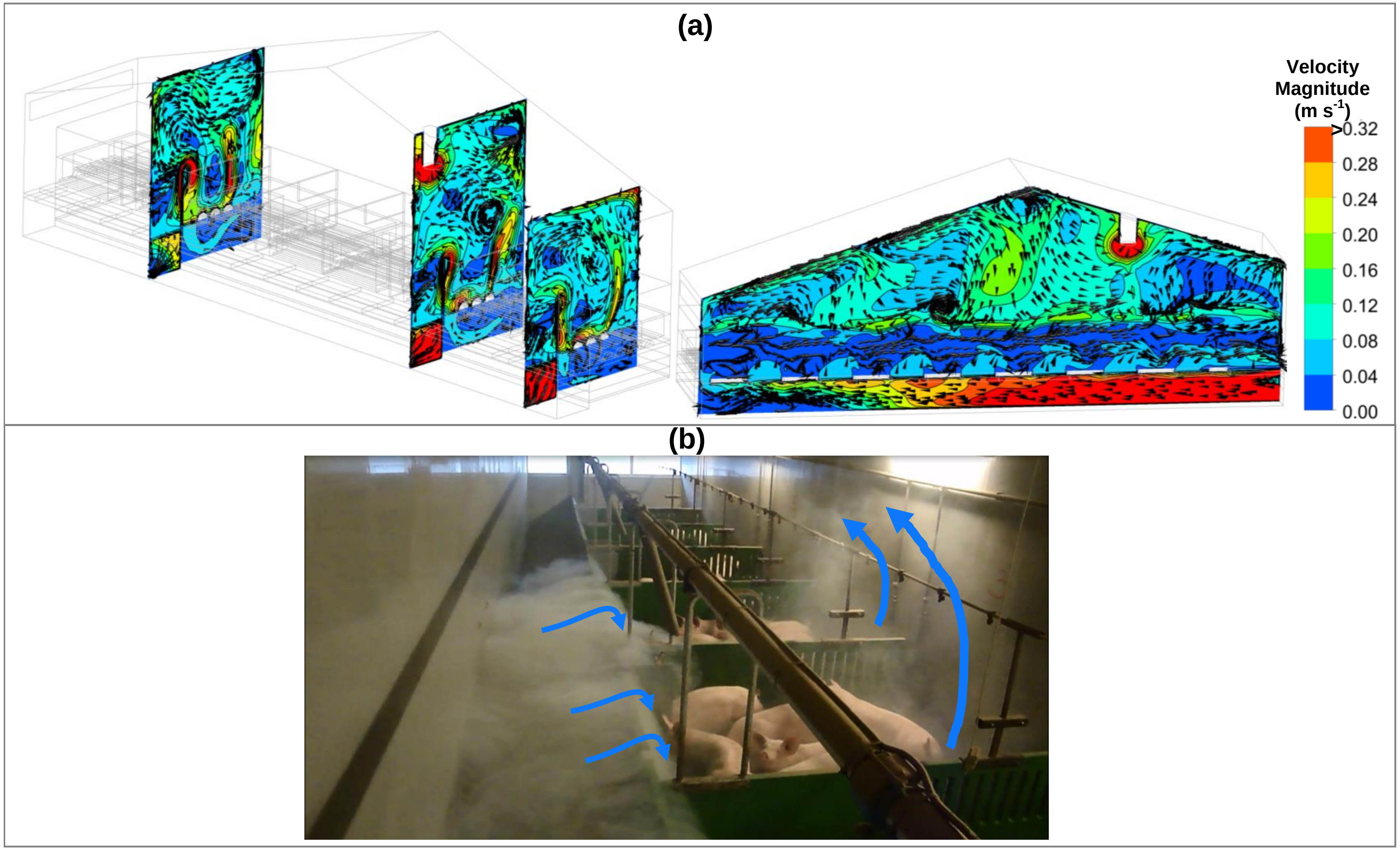

Fig. 6.18. (a) The predicted air velocity magnitude contours and airflow streamlines in sections E-E, F-F, G-G and H-H and (b) the observed airflow pattern during the smoke test in the compartment with the real pigs.

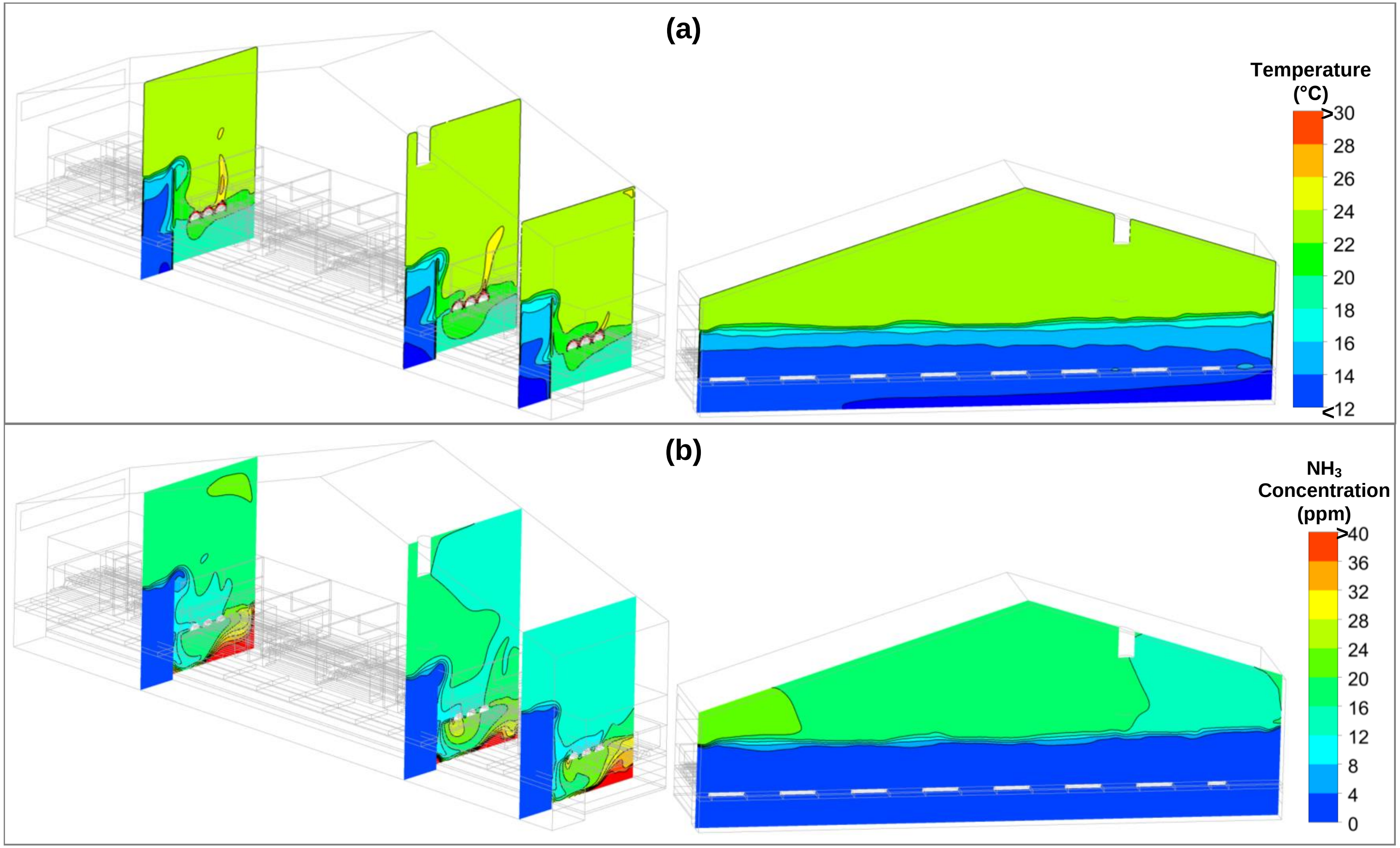
(a)
Temperature (°C)
>30
28
26
24
22
20
18
16
14
<12
(b)
NH_3 Concentration (ppm)
>40
36
32
28
24
20
16
12
8
4
0

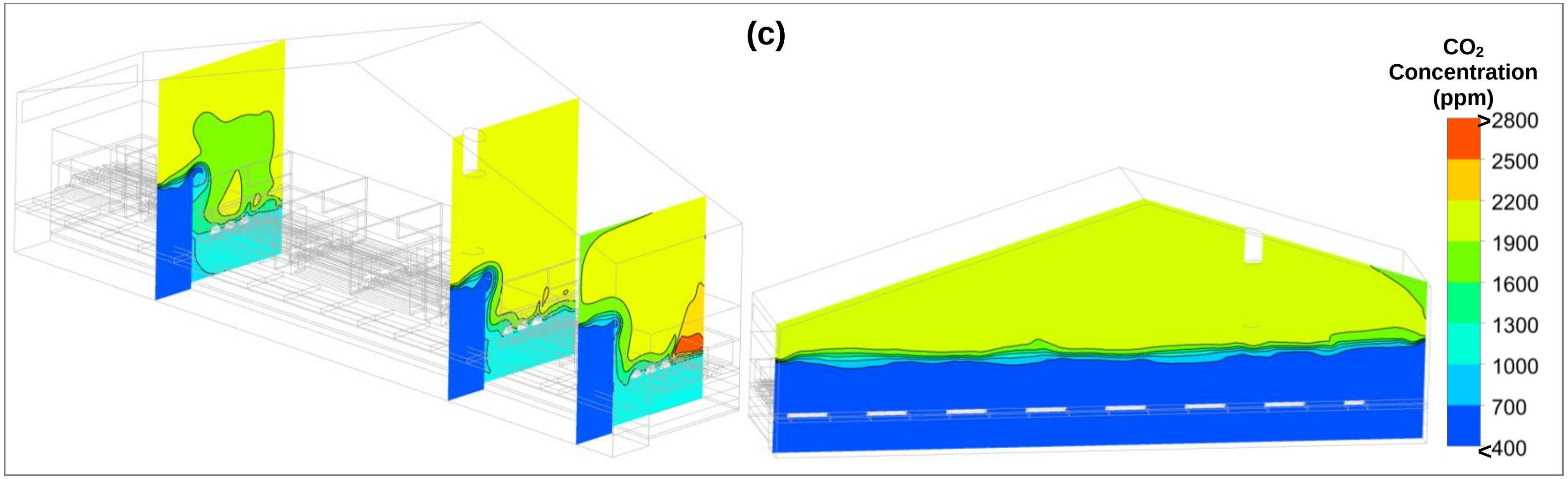

Fig. 6.19. The predicted (a) air temperature (b) NH_3 and (c) CO_2 concentration contours in sections E-E, F-F, G-G and H-H of the compartment with the real pigs.

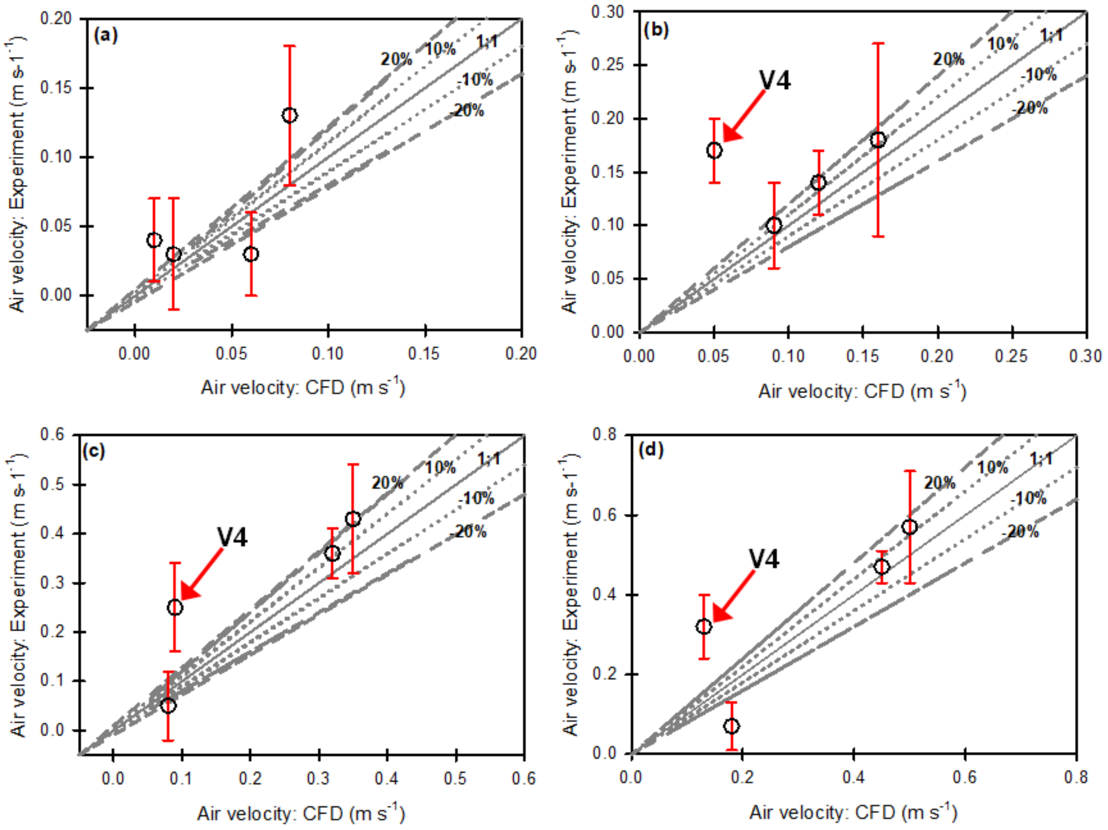

Fig. 6.20.Deviation between CFD and experimental air velocity in the compartment with the mock-up pigs at ventilation rate of (a) 11, (b) 34, (c) 62 and (d) 92 m^3 h^{-1} pig^{-1}. The error bars are the standard deviations.

6.3.1.3. Gaseous concentrations and emission rates

Figure 6.16b compares the simulated NH_3 concentrations with the measured values in the compartment with the real pigs at the UFAC and in the slurry pit headspace. Figs. 6.16c & 6.16d also compare the simulated and measured exhaust NH_3 and CO_2 concentrations and their calculated emission rates. Compared to the experimental results, the CFD model adequately simulated the exhaust NH_3 and CO_2 concentrations and their emission rates. The simulated exhaust NH_3 and CO_2 concentrations were 16.2 ppm and 1981 ppm compared to measured concentrations of 16.1 ± 0.9 ppm and 2138 ± 169 ppm, respectively. In contrast to the measured values of 0.379 ± 0.025 and 107.9 ± 9.5 g h^{-1} pig^{-1}, the simulated NH_3 and CO_2 emission rates were 0.398 and 98.0 g h^{-1} pig^{-1}, respectively. It was obvious that the predicted CO_2 emission in the CFD model was similar to the measured value, since the CO_2 release boundary condition was based on a fixed input, thus generated a fixed output value in the CFD model.

In Fig. 6.16b, both the simulated and measured results show that the highest NH_3 concentrations in the slurry pit were at A3, A6 and A9, next to the sidewall, far from the slatted floor inlet, while the levels of NH_3 at A2, A5 and A8 nearer to the slatted ground inlet were lower than A3, A6 and A9. Figs. 6.18a and 6.19b show that A2, A5 and A8 are in the flow path of the incoming air entering the slurry pit. Thus, the lowest NH_3 concentrations were in the UFAC at A1, A4 and A7, where fresh air is delivered to the compartment. The average NH_3 concentration simulated and measured at A1, A4 and A7 is < 0.5 ppm, and simulated and measured concentrations at A2, A5 and A8 were 17.1 ± 1.7 and 20.0 ± 10.4 ppm, respectively. In contrast, at A3, A6 and A9 the average NH_3 concentrations simulated and measured were 27.6 ± 3.3 and 31.7 ± 7.4 ppm, respectively. Clearly, the NH_3 distribution in the slurry pit followed the displacement airflow pattern that was previously noted in chapters 4 and 5. Also, Botermans and Jeppsson (2008) observed that due to the displacement airflow, the incoming air entered into the slurry pit, promoting NH_3 release into the compartment and causing the pigs to drop their manure at the draughty portion of the pen next to the slatted floor inlet, further promoting the NH_3 emission.

Fig. 17b shows that the CFD model adequately simulated the NH_3 concentrations during the field measurements as majority of deviations between the simulated and measured results were less than 10%. Even so, in the slurry pit headspace at sampling locations A5 and A6, the CFD model under-predicted the measured NH_3 concentrations by 12.2 and 12.3 ppm (Fig. 6.16b), respectively. The relatively low NH_3 concentrations in the CFD model at A5 and A6 (Fig. 6.5c) compared to the measured values were partly due to the different airflow patterns in the CFD and field experiment, caused by pig movement and human presence during gas and temperature sampling (Fig. 6.18b). Also, the fact that the NH_3 concentrations were measured at one location at a time instead of simultaneously could have caused this discrepancy. With this happening during the entire measurement period, it was likely that the airflow pattern in the compartment changed due to the air turbulence and buoyancy effect.

Furthermore, in the CFD model it was assumed that all pigs laid down fixed in a sternum position and in a regular pattern, which was not the case during the field measurements (Fig. 6.18b). Park and Holland (2001) showed that the vertical location of the convective heat source in the room could affect the airflow distribution in displacement ventilation systems. In addition, the CFD model assumed the same floor fouling area for all pens, including the one located close to the service alley. However, by visual inspection during the experimental trials, the fouling area in pen 3 of the compartment (with locations A5 and A6) was relatively larger than the other pens. Nonetheless, in combination with the validation results of the compartments occupied by the mock-up pigs and the real pigs, respectively, the developed UFAD compartment CFD model was considered to be satisfactory and adequate to be used in future studies.

6.3.2. Model application

6.3.2.1. Indoor airflow pattern and velocities

In Fig. 6.13, the velocity of the supply air leaving the slatted floor at the UFAC increased with increasing VR. Ventilation levels 1 and 2 showed two distinct airflow patterns at the service alley, while the airflow patterns at ventilation level 3 and level 4 were similar. The lower VR at ventilation level 1 caused the momentum of the incoming air to instantly diminish above the slatted floor inlet, creating many eddies at floor level. At ventilation level 2 (34 m^3 h^{-1} pig^{-1}), the supply air travelled at a higher vertical distance from the slatted floor inlet compared to ventilation level 1 (11 m^3 h^{-1} pig^{-1}) due to the higher VR than ventilation level 1. However, the air velocity distributions in sections A-A, B-B and C-C across the service alley in ventilation level 2 were not uniform, because the supply air momentum is still not strong enough. Thus the incoming air tended to flow towards the solid pen partitioning instead of towards the sidewall in the service alley. This was because the temperatures were higher at the AOZ than at the service alley (Figs. 6.13 & 6.14). Another factor is because of the greater buoyancy force coming from the AOZ compared to the momentum force of the supply air from the slatted floor inlet. In contrast, the greater momentum of supply air from the slatted floor inlet and the reduced temperature difference between the service alley and the AOZ at ventilation levels 3 and 4 generated comparatively uniform air velocity distributions across the service alley in sections A-A, B-B and C-C below the maximum height of solid pen partitioning (Figs. 6.13 & 6.14).

Fig. 6.13 shows that the distribution of supply air at the service alley affects the airflow pattern at the AOZ. Therefore, the airflow pattern at the AOZ and the slurry pit air exchange rate were characterised using the concept of the supply air throw height (T_H). The contours of temperature in section D-D of Fig. 6.14 also show that the temperature contour of the supply air from the slatted floor inlet above a certain height is roughly comparable to that of the free air in the service alley. According to Lin and Tsai (2014), this height could also indicate T_H of the supply air.

Table 6.3 displays the calculated T_H in the CFD model at the various ventilation levels. The results in Table 6.3 and Fig. 6.13 suggest that the T_H affects the airflow patterns at the AOZ. For instance, the T_H of 0.09 m at ventilation level 1 produced two vortices in the pen and two other vortices at the higher level of the pig compartment in section A-A. In sections B-B and C-C, farther away from the inlet of the UFAC, the multiple vortices seen in section A-A coalesced into a single large vortex at opposite airflow directions. The airflow pattern in sections A-A, B-B and C-C at ventilation level 2 were relatively similar; however, the lateral airflow over the mock-up pig was not strong enough to reach the sidewall of the AOZ. At ventilation levels 3 and 4 there was one large primary vortex in the anticlockwise direction in sections A-A, B-B and C-C. However, the lower T_H at ventilation level 3 in comparison to level 4 caused the air entering the pen to attach to the solid pen partitioning towards the service alley. In contrast, at ventilation level 4 the greater T_H rather created a stagnant region beside the solid wall partition in the AOZ and the incoming air hit the sidewall of the pens.

Table 6.3. Simulated l_m and T_H at the UFAC in the compartment at different ventilation rate.

VR (m^3 h^{-1} pig^{-1})	AER_{pit} (h^{-1})	AER_{pit}/AER_{comp}	M (m^4 s^{-2})	B (m^4 s^{-3})	l_m (m)	T_H
11[a]	10.4	7.0	0.0010	0.0128	0.0486	0.09
34[a]	19.8	4.0	0.0103	0.0272	0.1963	0.36
62[a]	24.1	2.6	0.0363	0.0364	0.4362	0.81
92[a]	26.1	1.9	0.0822	0.0420	0.7488	1.39
35[b]	16.5	2.2	0.0250	0.1339	0.1717	0.32

[a] There are 32 pigs at average weight of 50 kg in the compartment and [b] there are 48 pigs at average weight of 90 kg in the compartment.

Figure 6.21a illustrates the simulated average and standard deviations, and Table 6.4 lists the corresponding minimum and maximum of the air velocities at the AOZ in each pen in the compartment with 48 pigs at the average weight of 90 kg and VR of 35 m^3 h^{-1} pig^{-1}. The air velocities were lower at the human breathing zone (HBZ) than the AOZ. This was because the porous media model (slatted floor) at the walking alley diffuses the momentum of the incoming air, while the pigs increased the air velocity at the AOZ due to the buoyancy effect. As expected, the average air velocity at the AOZ was below 0.25 m s^{-1}, which agreed with the reported average air velocity in the literature for barns with UFAD systems (Botermans and Jeppsson, 2008 and Adrion et al., 2013). However, in the present study, there was a large variation in the air velocity at the AOZ compared to the HBZ (Figs. 6.18a, 6.21a and Table 6.4). The maximum air velocity in the AOZ falls in the range of 0.44 – 0.53 m s^{-1} compared to 0.25 m s^{-1} at the HBZ. The higher air velocities which exceeded 0.3 m s^{-1} could be a source of draught on the pigs (ASAE, 2012) at the AOZ, especially in the areas with air temperatures less than 20 °C (Fig. 6.19a, Table 6.4).

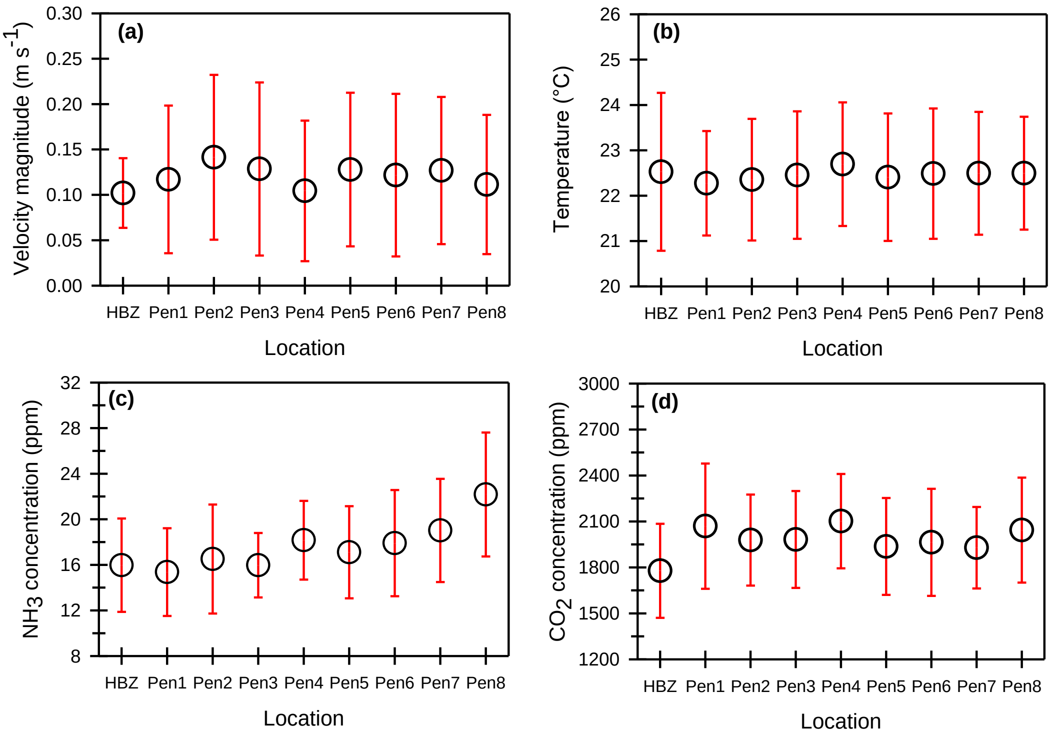

Fig. 6.21. Simulated average (circle) and standard deviation (error bars) of the (a) air velocity magnitude (b) temperature (c) NH_3 and (d) CO_2 concentrations at the AOZ in pen 1 – 8 and at the HBZ in the compartment with 48 pigs at the average weight of 90 kg and VR of 35 $m^3\ h^{-1}\ pig^{-1}$.

Table 6.4. Simulated minimum and maximum (min, max) air velocity magnitude, temperature, NH_3 and CO_2 concentrations at the farmer's breathing zone (FBZ) and the animal occupied zone in the pens of the compartment occupied by 48 pigs at the average weight of 90 kg and ventilation rate of 35 $m^3\ h^{-1}\ pig^{-1}$.

Pen	Velocity (m s^{-1})	Temperature (°C)	NH_3 concentration (ppm)	CO_2 concentration (ppm)
FBZ	(0.00, 0.25)	(14.6, 23.7)	(0.0, 22.5)	(457, 1990)
Pen 1	(0.00, 0.49)	(17.8, 39.9)	(3.9, 31.4)	(803, 3063)
Pen 2	(0.00, 0.46)	(18.6, 38.6)	(5.3, 42.8)	(992, 2782)
Pen 3	(0.00, 0.52)	(19.3, 39.0)	(6.3, 26.5)	(1058, 2717)
Pen 4	(0.00, 0.46)	(19.4, 37.7)	(8.1, 32.1)	(1163, 3022)
Pen 5	(0.00, 0.46)	(18.8, 41.7)	(5.8, 37.0)	(950, 2798)
Pen 6	(0.00, 0.53)	(18.9, 41.5)	(7.2, 45.2)	(1044, 2947)
Pen 7	(0.00, 0.44)	(19.2, 37.0)	(7.8, 38.1)	(1062, 2688)
Pen 8	(0.00, 0.46)	(19.7, 34.9)	(11.3, 53.3)	(1268, 3106)

6.3.2.2. Indoor temperature distribution

The simulated air temperature contours in Fig. 6.14 confirmed that increasing the VR from level 1 – 4 created a more uniform temperature distribution from the slatted floor inlet to the maximum height of the solid pen partitioning (Fig. 6.2) at the service alley. However, the thermal stratification in the compartment was limited more to the service alley at the lower VR, with no noticeable difference in the AOZ temperature and the free space above the pens. This was because of the weak momentum at the slatted floor inlet from the very low supply air velocity (Figs. 6.13 & 6.14) compared to the buoyancy flux from the heated pigs, which allowed the incoming air to warm up during its rise at the service alley before falling into the AOZ. Indeed, the supply air T_H calculated in Table 6.3 appears to explain the temperature stratification characteristics in the compartment with the mock-up pigs at the lower VR. Thus, at ventilation levels 1 and 2, the supply air momentum flux (M) was lower than the pigs' buoyancy flux, resulting in the T_H of 0.09 m and 0.36 m, respectively (Table 6.3).

Owing to the reduced T_H at ventilation level 1, it was obvious that in the service alley the temperature stratification was more substantial than in ventilation level 2 (Figs. 6.11 & 6.14). Of course, Fig. 6.22a shows that the $T_{1.3} - T_{-0.8}$ decreased from 7.7 ± 1.2 °C to 2.0 ± 0.3 °C at the UFAC as the T_H increased from 0.09 to 1.39 m. Also, Fig. 6.22b confirms that at lower T_H the θ_{UFAC} is very close to the θ_{AOZ} but the difference between θ_{UFAC} and θ_{AOZ} widens with increasing T_H. It was also apparent that the greater VR (35 m^3 h^{-1} pig^{-1}) in the compartment with 48 pigs than ventilation level 1 (i.e. 11 m^3 h^{-1} pig^{-1}) with 32 pigs still produced $\theta_{UFAC} \cong \theta_{AOZ}$.

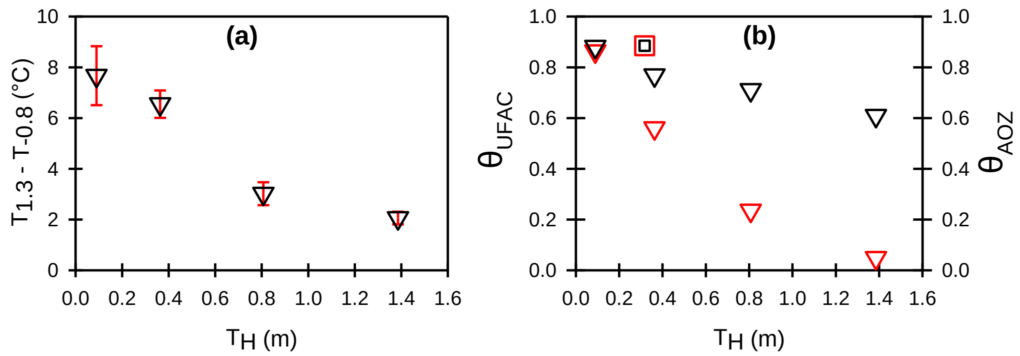

Fig. 6.22. Relationship between (a) T_H and $T_{1.3} - T_{-0.8}$ (with $T_{1.3} - T_{-0.8}$ as the vertical temperature gradient at the UFAC and the service alley). (b) T_H and θ_{UFAC} (red), T_H and θ_{AOZ} (black) are in the compartment with the 32 pigs at VR of 11, 34, 62 and 92 m^3 h^{-1} pig^{-1}, respectively (triangles) and (squares) is in the compartment with 48 pigs at the VR of 35 m^3 h^{-1} pig^{-1}. The error bars are the standard deviations.

This result indicates the effect of the heat load and spread area of the pigs in the pen on the air temperature distribution in the room. The reason is that the pig heat load in the compartment occupied by the 48 pigs was 6.4 times greater than the compartment with 32 pigs, owing to the greater number of pigs and pig weight.

At ventilation levels 3 and 4 when the T_H was 0.81 m and 1.39 m, respectively, it can be seen that relatively uniform vertical temperature profiles were maintained above the slatted floor inlet at the UFAC from y = 0 – 1.3 m (Figs.6.11 & 6.14). The results also show that at T_H > 0.8 m, there was a slight decrease in the vertical temperature profiles at the UFAC compared to T_H < 0.8 m (Fig. 6.22a). At T_H > 0.8 m, the temperature distribution at the UFAC was momentum-dominated from the higher supply air speed than from the buoyance flux from the pigs (Table 6.3). However, the widening difference between θ_{UFAC} and θ_{AOZ} as the T_H increased in Fig 6.22b confirmed the short-circuiting of the incoming air at the higher VRs and explains why the temperature distribution between the AOZ and the free area above the pens was less uniform compared to the lower VR.

Indeed, at ventilation levels 3 & 4 (Fig. 6.14), there was a noticeable difference in the temperature contours of the different pens in the AOZ and the free space temperature above the AOZ. As previously noted, this temperature distribution was attributed to the increased supply air momentum from the very high air velocity at the slatted floor inlet (Fig. 6.13), which encouraged the incoming air to mix with the compartment's surrounding air at the higher level above the slatted floor inlet in the service alley before falling into the AOZ. It was also noted in Fig. 6.14 (section D-D) that the relatively warmer region near the roof is expanding. This is due to the short–circuiting of the supply air to the exhaust opening. Thus, the temperature difference at y = 1.3 m in the service alley and the exhaust air was 0.2 °C, 1.2 °C, 1.8 °C and 1.9 °C at the ventilation levels 1 – 4, respectively.

In Fig. 6.21b, there was no noticeable difference in the average air temperatures at the HBZ and the AOZ in the different pens, as the very low supply air speed from the slatted floor inlet (Fig. 6.18a) allowed the incoming air to warm up during its rise at the service alley before falling into the AOZ. A similar result was previously reported in the compartment with the mock-up pigs at ventilation level 1 (Fig. 6.14). Nonetheless, the simulated minimum and maximum temperatures at the AOZ of the compartment with the real pigs was approximately 4 °C and 15 °C higher than HBZ (Table 6.4), respectively, due to the heat generated by the pigs. Fig. 6.21b showed that the average temperature at the HBZ was more variable than the AOZ, as the HBZ was near to the supply air inlet (Figure 6.19b).

6.3.2.3. Indoor NH_3 and CO_2 concentration distributions

Figure 6.21c illustrates the average NH_3 concentration while Table 6.4 lists the corresponding minimum and maximum concentrations at the AOZ in each pen and the HBZ at the service alley in the pig compartment. The NH_3 concentrations were lower at the HBZ than the AOZ in the pens. There was no noticeable difference in the NH_3 concentration at the HBZ and the AOZ in the pens close to the inlet of the UFAC (i.e. pen 1 – 3). However, the average NH_3 concentration increased in the pens farther away from the inlet of UFAC (i.e. AOZ 4 – AOZ 8), which indicates potential air quality problems. The average NH_3 concentration difference between the HBZ and the AOZ in pens 1 – 3 was < 0.5 ppm, while the average NH_3 concentrations were 2.2, 1.14, 1.9, 3.0 and 6.2 ppm greater in the AOZ 4 – 8 than the HBZ, respectively. Indeed, the NH_3 concentration contours in section H-H (Fig. 6.19b) confirmed that there was an increase of the NH_3 concentrations from the inlet of UFAC to the rear end of the UFAC inlet near pen 8 in the service alley. Furthermore, due to the displacement airflow pattern in the slurry pit, the maximum NH_3 concentration in the AOZ was mostly at the sidewall section of the pen in the range of 26 – 54 ppm, exceeding the maximum exposure limit of 25 ppm (CIGR, 1984).

Breum et al. (1990) previously indicated that ventilation systems with the inlet at the floor level (i.e. UFAD systems) provided more effective ventilation at the AOZ than ventilation systems with the inlets at the higher level of the compartment. However, according to Van Wagenberg and Smolders (2002) and Aarnink and Wagemans, (1997) the displacement airflow in UFAD systems create a wide variation in the temperature and contaminant concentrations distribution within the AOZ compared to ventilation systems with the inlets at the higher level of the compartment. In contrast, Botermans and Jeppsson (2008) and Botermans and Jeppsson (2014) found that the ventilation effectiveness in the pig compartment with the UFAD system was high at AOZ but low at HBZ, i.e. 1.5 m above the floor, compared to mixing ventilation systems.

Figure 6.21d compares the average CO_2 concentration while Table 6.4 lists the corresponding minimum and maximum concentrations at the AOZ and the HBZ in the pig compartment. Fig. 6.19c shows the CO_2 concentration contours in the pig compartment. The average CO_2 concentration at the HBZ was lower than at the AOZ by 150 – 350 ppm. The maximum CO_2 concentration in the AOZ falls in the range of

2600 – 3200 ppm (in pen 8) compared to 1990 ppm at the HBZ, which was within the maximum exposure limits of 3000 ppm (CIGR, 1984). Similarly, the lowest CO_2 concentrations in the AOZ were at the section of the pen near the service alley and the maximum concentrations at the other section of the pen near the sidewall (Fig. 6.19c), which agreed with the airflow pattern in the pig compartment (Fig. 6.18).

6.3.2.4. Air exchange rate in the slurry pit

Table 6.3 shows that the air exchange rate (AER_{pit}) in the slurry pit increased with increasing T_H. However, the ratio of the slurry pit to the compartment air exchange rates decreases with increasing VR from 7.0, 4.0, 2.6 and 1.9 at ventilation levels 1 – 4, respectively. This is caused by the greater momentum of the supply air at higher VR, which causes more of the incoming air to flow over the slatted floor in the pen rather than going into the slurry pit. Fig. 6.13 endorses this assumption at sections A-A, B-B and C-C. Nonetheless, the slurry pit air exchange still raises a major concern, as more than 30% of the total NH_3 emissions in pig buildings emanate from the slurry pit and the remainder comes from the pen floor (Hoeksma et al., 1992; Aarnink et al., 1997; Kai et al., 2006, Ni et al., 2000). The proportion of the total NH_3 emissions from the pen floor and the slurry pit depends on several factors such as, the type of ventilation system, the pen floor type, wetted floor area, weight of the pigs, etc. The proposal is that employing the following strategies in future CFD simulations of the developed model could help to minimise the slurry pit air exchange rate, reduce emissions and improve the air quality in the pig compartment.

1. Existing and new UFAD pig barns could install baffles/flaps at the solid pen partitioning beside the slatted floor inlet in the service alley to direct the incoming air away from the slurry pit and promote more mixing and warming up of the incoming air before reaching the AOZ. Botermans et al. (2014) used this approach to reduce the draught on pigs in Sweden. Another approach is the use of porous curtains above the solid pen partitioning at the service alley to encourage air mixing and warming of the incoming air before it is delivered to the AOZ.
2. As discussed in De Paepe et al. (2016) and Ye et al. (2009), airflow deflectors (baffles) could be mounted at the back of the pen to break the airflow that enters the slurry pit and sweeps the NH_3 from the slurry pit to the compartment. Ye et al. (2009) demonstrated that placing the deflectors at an optimal angle could reduce the slurry pit air exchange rate by up to 84% and kept more of the pollutant in the slurry pit. Apart from the airflow deflectors that guided the supply

airflow away from the slurry pit, Ye et al. (2011) also demonstrated compartmentalising the slurry pit using curtains could limit the sweeping distance of the airflow above the slurry surface and consequently reduce the pit air exchange by up to 46% and reduce NH_3 emission by 20% in the pig compartment.

3. Another strategy could be to control the supply air T_H by adjusting the inlet configuration (i.e. opening area, location etc.), air velocity and temperature as an airflow pattern control measure. Furthermore, adjusting the number of exhaust ducts, location and height from the roof depending on the season could be an effective way to regulate the air distribution in the compartment.

6.4. Conclusions

The aim of this study was to develop a three-dimensional CFD model capable of predicting airflow patterns and ammonia emissions in a pig compartment with an Underfloor Air Distribution (UFAD) system. The slatted floor and the pigs in the compartment were modelled as a porous medium and semi-cylinders, respectively. The NH_3 emission sources at both slurry pit and floor level were modelled with a User Defined Function (UDF) applied at the first computational cell zone in connection with the respective emitting surfaces. The modelled air velocity and temperature were validated in the compartment occupied by mock-up pigs at ventilation rates of 11, 34, 62 and 92 $m^3 h^{-1} pig^{-1}$. The modelled airflow pattern, temperature, CO_2 and NH_3 concentrations were validated in the compartment occupied by the real pigs at ventilation rate of 35 $m^3 h^{-1} pig^{-1}$.

There was a good agreement between simulated and measured results. For example, the simulated exhaust NH_3 and CO_2 concentrations were 16.2 ppm and 1981 ppm as compared to measured concentrations of 16.1 ± 0.9 ppm and 2138 ± 169 ppm, respectively. Furthermore, the simulated NH_3 emission rate of 0.40 g $h^{-1} pig^{-1}$compared well with the measured values of 0.38 ± 0.03 g $h^{-1} pig^{-1}$. The simulated results verified NH_3 transport from the slurry pit into the compartment as influenced by the ventilation process in UFAD systems. The air exchange rate of the slurry pit increased with increasing ventilation rate, whereas the ratio of the slurry pit to the compartment air exchange rate decreased at higher ventilation rates. The validated CFD model could be used to predict indoor air quality and emissions of a pig compartment with UFAD systems and to optimise its ventilation performance.

Chapter 7: Effect of ventilation opening configuration on indoor air distribution and NH_3 emission: a CFD modelling approach

7.1. Introduction

In pig buildings equipped with UFAD systems, the underfloor air inlets are often located at the slatted floor in the service alley, and the exhaust duct at the ceiling. Another characteristic of pig buildings with UFAD systems is that the supply air enters the building at very low air speeds (< 1.0 m s^{-1}) due to the large inlet opening area (> 0.014 m^2 pig^{-1}). These design features promote thermal stratification in the building and reduce re-entry (i.e. entrainment) of the displaced old air from the animal area (chapter 6). Therefore, pig buildings with UFAD systems have better air quality and in comparison with mixing ventilation systems effectively remove heat from the animal area (Van Wagenberg and Smolders, 2002; Threm et al., 2012; Adrion et al., 2013; Jeppsson and Botermans, 2014). The drawbacks of UFAD systems, however, are the risk of draught on pigs during winter and the transport of NH_3 and odour from the slurry pit due to the air displacement principle (Botermans and Jeppsson, 2008).

However, information on how to improve the ventilation performance in pig buildings with UFAD system is based on expert advice that shows different recommendations (van der Voorst, 2009; Delva, 2012; Klimaatplatform, 2013). In addition, the different recommendations lack technical information on how they were derived. For instance, while the Klimaatplatform (2013) suggested 70 – 105 cm^2 pig^{-1} as the best total slat gap opening area at the underfloor air inlet, Delva (2012) and Van der Voorst (2009) recommended 60 cm^2 pig^{-1} and 140 cm^2 pig^{-1}, respectively. The Klimaatplatform (2013) also proposed that in order to minimise short-circuiting in pig buildings with UFAD systems, the exhaust duct opening should be positioned at least 3 m from the floor. This suggestion also lacked theoretical information on how the value was derived. Therefore, in this chapter, CFD simulations were performed using the validated CFD model (chapter 6) at different slatted floor inlet configurations and exhaust opening heights. The objectives were to;

1. Test the effects of the inlet and exhaust configurations on the indoor air distribution and NH_3 emissions at different ventilation rates and inlet air temperatures.

2. Assess the impact of the inlet and exhaust configurations on the slurry pit air exchange rate at different ventilation rates and temperatures of inlet air.

7.2. Material and methods

7.2.1. CFD model description

The used CFD model was successfully validated in chapter 6. Detailed description of the ILVO/UGent/HoGent pig building, the experimental measurements and the validation test can be found in chapter 6. The 3D geometry of the pig compartment (Fig. 7.1) was developed using SolidWorks, and ANSYS ICEM CFD 15. Section 6.2.3.1 gives the grid and the numerical methods applied in this chapter of the PhD research.

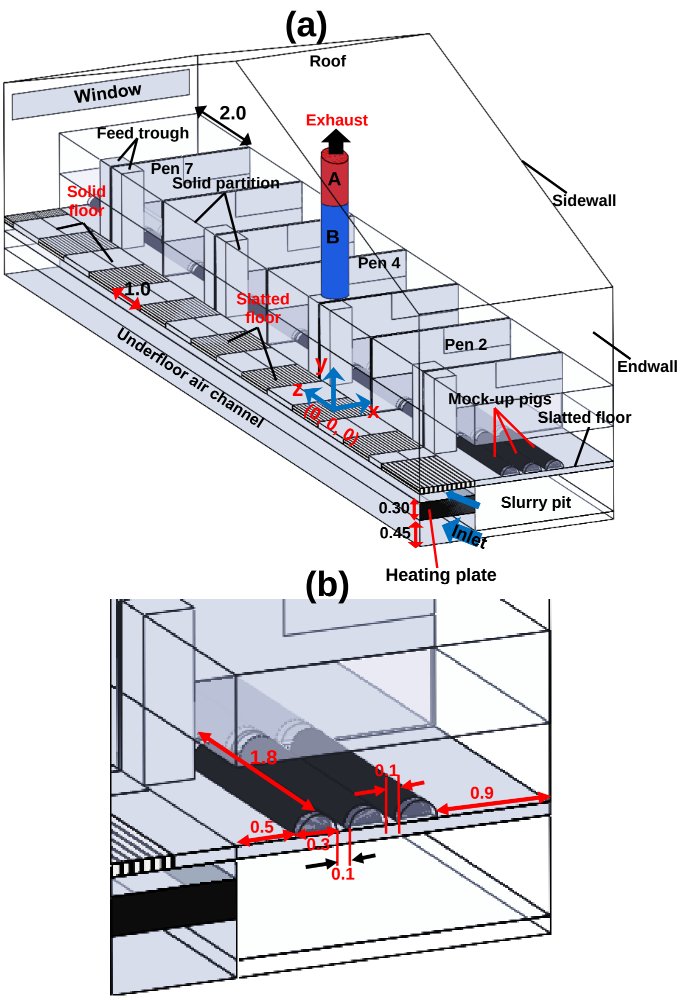

Fig. 7.1 — The geometry of the simulated pig compartment (a) isometric view and (b) the mock-up pig arrangement in the pen (all dimensions are in meters).

The NH_3 and CO_2 emission models were derived from section 6.2.3.3. In the present investigation only the slurry pit was the NH_3 emission source in the pig compartment.

This was because over 60% of the total NH_3 emissions from pig housing emanate from the slurry pit (Aarnink et al., 1996; Hoeksma et al., 1992; Kai et al., 2006). The slatted floor and slotted pen partitioning (Fig. 7.2) were treated as porous media in the CFD model (section 6.2.3.2). The porous media resistance coefficients of the slatted floor and slotted pen partitioning were derived via a virtual CFD wind tunnel (Fig. 6.9a).

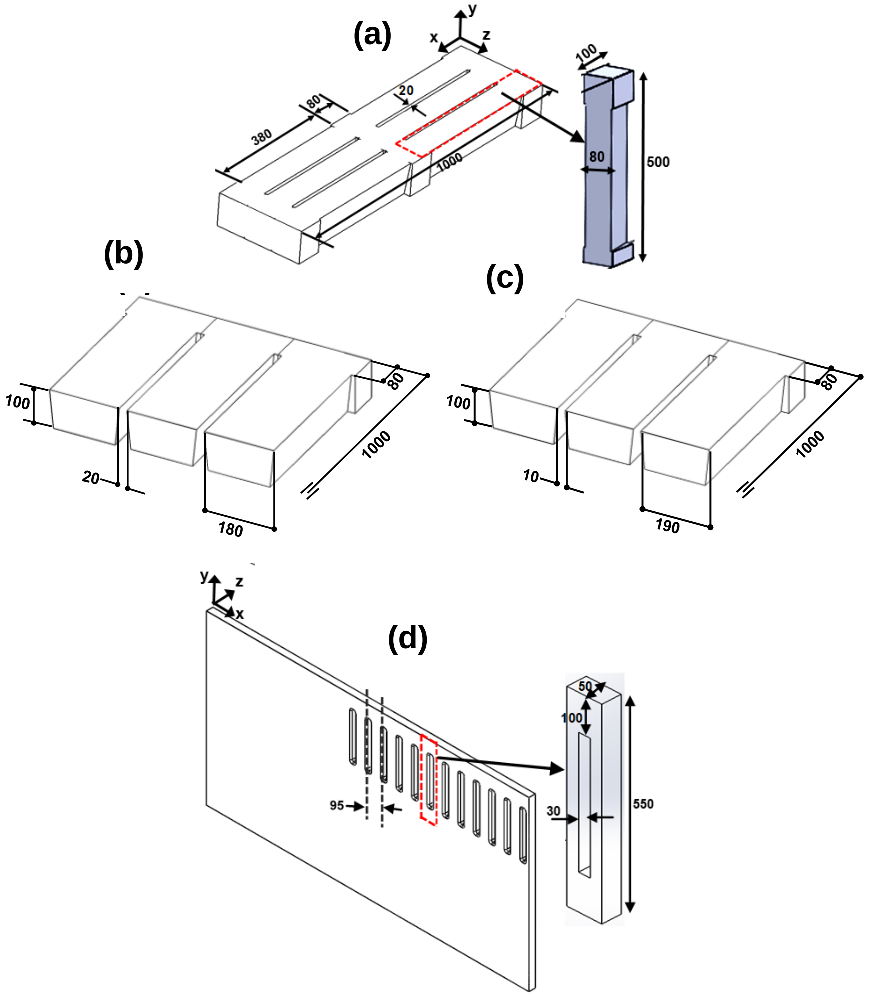

Fig. 7.2 — (a) section of the simulated slatted floor inlet at 15.4% porosity and EOA_{floor} of 0.028 m^2 pig^{-1} (b) 8% porosity and EOA_{floor} of 0.014 m^2 pig^{-1} and (c) 4% porosity and EOA_{floor} of 0.007 m^2 pig^{-1} and (d) pen partition (all dimensions are in mm).

In accordance with the objective of the present study, the porous media resistance coefficients were derived for three slatted floor inlet geometries (Figs. 7.2a - 7.2c) and the slotted pen partitioning (Fig. 7.2d) via a virtual CFD wind tunnel. The slatted floor inlet geometries were selected in accordance with the EU Council Directive (2008) for animal welfare, which require a slat opening width of less than 20 mm and the minimum solid slat width as 80 mm in fattening pig housing.

The virtual wind tunnel simulations were performed at inlet air velocities of 0.05, 0.15, 0.30 and 0.50 m s^{-1} for the slatted floor geometries, and 0.05, 0.10, 0.15 and 0.2 m s^{-1} in the pen partitioning geometries. The inlet air was defined perpendicular to the simulated surfaces in the virtual wind tunnel (Fig. 6.9a). The inlet air velocities in the virtual wind tunnel model matched the measured air velocities in the compartment during field experiments (section 6.2.2.1). The inertial (F, m^{-1}) and viscous resistance coefficients (D, m^{-2}) were then derived by fitting the pressure drop across the virtual wind tunnel and their corresponding inlet velocities in Eq. 6.4. Table 7.1 displays the derived F and D for the three slatted floors and slotted pen partitioning geometries from the virtual wind tunnel simulations. The F and D values were only set in the y-direction of the slatted floor and in the z-direction of the slotted pen partitioning (Figs. 7.2a & 7.2d), respectively. In addition, the F and D in the x and z directions of the slatted floor, and in the x and y directions of the slotted pen partitioning were set at higher values (i.e. $F \times 10^2$ and $D \times 10^2$) compared to the derived F and D values in order to represent obstruction to airflow in these directions (Figs. 7.2a & 7.2d).

Table 7.1 — Derived inertial (F) and viscous resistance coefficients (D) for the slatted floor and pen partitioning geometries from the virtual wind tunnel.

Geometry	EOA (m^2 pig^{-1})	Porosity (%)	F (m^{-1})	D(m^{-2})
Pen partition		19.5	569	95000
Slatted floor 1	0.007	4.0	10335	998323
Slatted floor 2	0.015	8.0	2566	1955460
Slatted floor 3	0.028	15.4	640	29060

7.2.2. Case study simulations and the CFD setup

7.2.2.1. Room temperature, VR and pig sensible heat production

The simulations were performed at UFAC inlet air temperatures of 0, 10, 15, 20 and 30 °C (Tables 7.2). The inlet air temperature of 0 °C represented very cold winter conditions at the pig building without supplementary heating at the central underground air channel (CUAC). Inlet temperature of 10 °C mimicked winter condition with supplementary heating at the CUAC. UFAC inlet temperature of 15 °C represented the yearly average outside temperature in Flanders when the supplementary heating in the CUAC was off, while UFAC inlet temperatures of 20 and 30 °C mimicked warm and very warm outside temperatures respectively.

Table 7.2 — Case studied in this investigation

Case	T_{in} (°C)	VR (m^3h^{-1} pig^{-1})	[a] EOA (m^2 pig^{-1})	[b] Porosity (%)	[c] Exhaust	Purpose
IEC1	0	14.0	0.007	4	A	Effect of inlet floor porosity in winter—No GC heating
IEC2	0	14.0	0.014	8	A	
IEC3	0	14.0	0.028	15	A	
IEC4	10	14.9	0.007	4	A	Effect of Inlet floor porosity in winter—GC heating on
IEC5	10	14.9	0.014	8	A	
IEC6	10	14.9	0.028	15	A	
IEC7	15	22.9	0.007	4	A	Effect of inlet floor porosity—yearly average outdoor temperature in Flanders
IEC8	15	22.9	0.014	8	A	
IEC9	15	22.9	0.028	15	A	
IEC10	20	40.4	0.007	4	A	Effect of inlet floor porosity effect—typical warm summer in Flanders
IEC11	20	40.4	0.014	8	A	
IEC12	20	40.4	0.028	15	A	
IEC13	30	70.0	0.007	4	A	Effect of inlet floor porosity—hot summer
IEC14	30	70.0	0.014	8	A	
IEC15	30	70.0	0.028	15	A	
IEC16	0	14.0	0.014	8	B	Effect of exhaust duct depth in winter
IEC17	0	22.9	0.014	8	A	
IEC18	0	22.9	0.014	8	B	
IEC19	0	14.0	0.007 & 0.028	4 & 8	A	Effect of inlet floor arrangement
IEC20	0	14.0	0.007	8	A	
IEC21	0	40.4	0.014	8	A	Effect of VR on slurry pit AER at T_{in} = 0 °C
IEC22	0	52.1	0.014	8	A	
IEC23	0	70.0	0.014	8	A	
IEC24	20	14.0	0.014	8	A	Effect of VR on slurry pit AER at T_{in} = 20 °C
IEC25	20	14.9	0.014	8	A	
IEC26	20	52.1	0.014	8	A	
IEC27	20	70.0	0.014	8	A	
IEC28	10	22.9	0.014	8	A	Effect of VR on slurry pit AER at T_{in} = 10 °C
IEC29	10	40.2	0.014	8	A	
IEC30	10	52.1	0.014	8	A	
IEC31	10	70.0	0.014	8	A	

T_{in} = UFAC inlet temperature; VR = ventilation rate; [a] EOA = Effective opening area at the slatted floor inlet; [b] The porosity is calculated using only the slatted floor at the service alley; [c] Exhaust duct opening height above the floor, where A = 3.6 m and B = 2.0 m from pen floor. Fig. 7.3 illustrates the different inlet floor arrangements.

The room temperature and ventilation rate (VR) as well as the sensible heat production from the pigs in the compartment were calculated using the steady state simulation model that was developed in chapter 2. The model simulations were performed in the compartment occupied by 48 pigs at 60 kg and a fixed UFAC inlet temperature was taken as the outside air temperature. The steady state simulation model excluded the slurry pit and the UFAC from the total volume of the compartment. Table 7.3 presents the simulated T_i, VR and the pig sensible heat production from the steady state simulation model.

Table 7.3 — Simulated ventilation rate, average room temperature and sensible heat production from the pigs in the compartment using the steady state balance model

T_{inlet} (°C)	VR (m^3 h^{-1} pig^{-1})	T_i (°C)	Sensible heat (W pig^{-1})
0	14.0	14	69
10	14.9	22	62
15	22.9	23	62
20	40.2	24	60
30	70.0	32	52

7.2.2.2. Slatted floor arrangement and the exhaust duct height

The present investigation performed simulations at three different slatted floor inlet arrangements at the service alley. Figure 7.3a illustrates the slatted floor inlet arrangement of the ILVO/UGent/HoGent pig compartment, which consisted of an alternation of slatted and solid floor at the service alley. Fig. 7.3b shows the second slatted floor arrangement in which the first half of the slatted floor inlets at the service alley had total gap opening area of 0.007 m^2 pig^{-1} and the second half had the total gap opening area of 0.014 m^2 pig^{-1}. Figure 7.3c illustrates the third slatted floor inlet arrangement in accordance with the suggestion of Delva (2012), in which half of the slatted floor inlet at the service alley toward the pens was covered in winter.

The Klimaatplatform (2013), also recommended that to minimise short-circuiting of the supply air in summer when the ventilation is operating at the maximum, the minimum exhaust duct height from the floor in the UFAD pig room should be 3 m above the floor. In this study, the exhaust duct height above the floor of 2.0 and 3.6 m (Fig. 7.1a) were performed during the case study simulations.

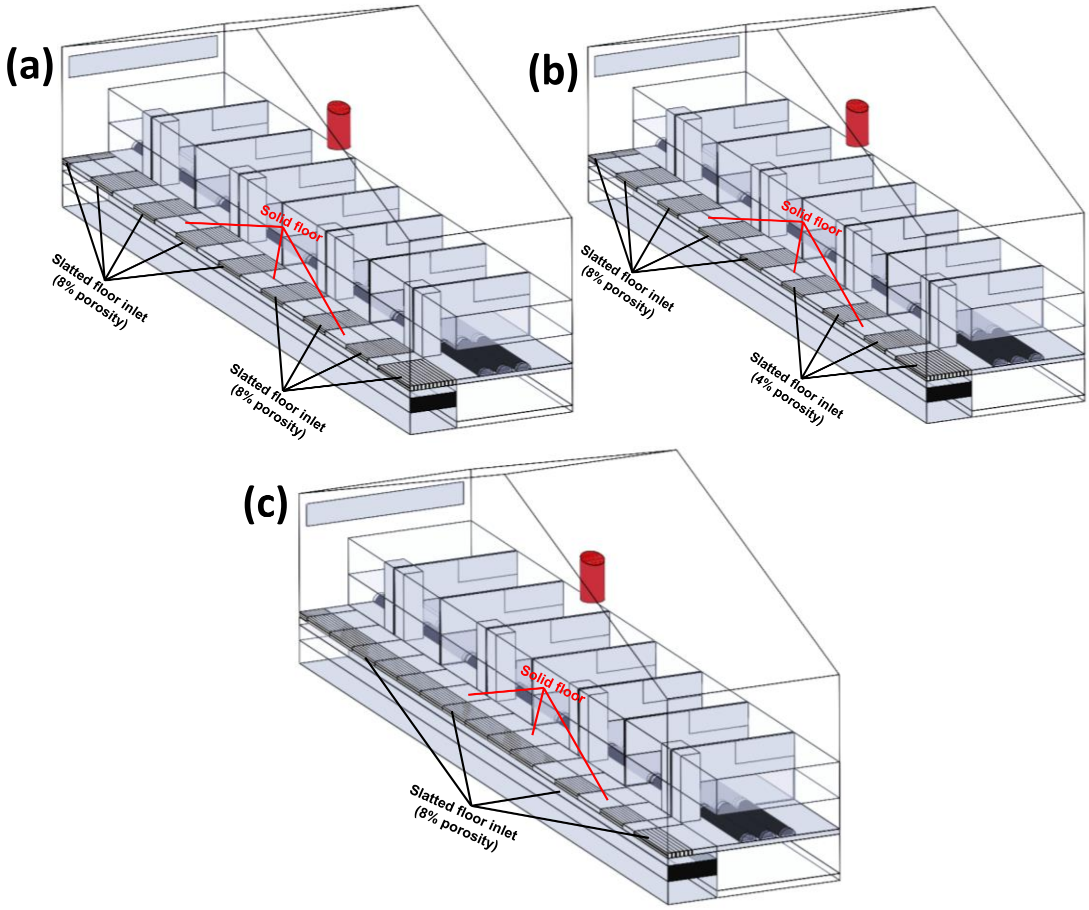

Fig. 7.3 — Slatted floor inlet arrangements in case (a) IEC2, (b) IEC19 and (c) IEC20.

7.2.2.3. Boundary conditions

Table 7.4 illustrates the boundary conditions (BCs) for the different case study simulations. In all the simulations the pressure inlet (0 Pa) BC was selected at the opening of the UFAC, with uniform inlet temperature BC at the hydraulic diameter of 0.95 m and turbulence intensity of 20%. The inlet turbulence boundary condition was derived from the model tuning (chapter 6). In addition, the VR in the room was set as a negative velocity inlet at exhaust opening, which was derived from the ventilation rates; 14.0, 14.9, 22.9, 40.4 and 70.0 $m^3\ h^{-1}\ pig^{-1}$ that correspond with the UFAC inlet air temperatures of 0, 10, 15, 20 and 30 °C, respectively. Note that the simulation at IEC21 – 23, IEC24 – 27 and IEC 28 – 31, were sensitivity tests on the effect of ventilation rate at constant inlet air temperature on the slurry pit air exchange rates (AERs). Therefore, the VR at the T_{inlet} boundary conditions during these simulations did not match the experimental conditions.

Table 7.4 — The CFD boundary conditions for the cases in this investigation

Case	Inlet (°C)	Exhaust velocity (m s^{-1})	Pig heat flux (W m^{-2})
IEC1	0	-1.17	137
IEC2	0	-1.17	137
IEC3	0	-1.17	137
IEC4	10	-1.25	123
IEC5	10	-1.25	123
IEC6	10	-1.25	123
IEC7	15	-1.92	123
IEC8	15	-1.92	123
IEC9	15	-1.92	123
IEC10	20	-3.38	119
IEC11	20	-3.38	119
IEC12	20	-3.38	119
IEC13	30	-5.87	103
IEC14	30	-5.87	103
IEC15	30	-5.87	103
IEC16	0	-1.17	137
IEC17	0	-1.92	137
IEC18	0	-1.92	137
IEC19	0	-1.17	137
IEC20	0	-1.17	137
IEC21	0	-3.38	137
IEC22	0	-4.37	137
IEC23	0	-5.87	137
IEC24	20	-1.17	119
IEC25	20	-1.25	119
IEC26	20	-4.37	119
IEC27	20	-5.87	119
IEC28	10	-1.92	123
IEC29	10	-3.38	123
IEC30	10	-4.37	123
IEC31	10	-5.87	123

In addition, it was assumed in the CFD simulations that all the walls were adiabatic with no-slip wall conditions. The pigs were modelled as semi-cylinders (i.e. 3 semi-cylinders per pen, with one semi-cylinder as two pigs, Fig. 7.1). Thus, the assumption was that each semi-cylinder represented 2 headless 50 kg pigs in sternum lying position (Fig. 7.1). The modelled pig heat production was set as a surface flux per semi-cylinder, which was derived from the sensible heat production, simulated from the indoor temperature in the steady state indoor climate model (chapter 2) and the total exposed surface area of ~1.0 m^2 per semi-cylinder.

The slurry surface TAN concentration was set as 3.14 kg m^{-3}, taken from the field measurement of the bulk slurry concentration (section 6.2.2.2). The slurry pH was assumed as 8.5 after the model tuning from the measured bulk slurry pH of 7.5 (section 6.2.2.2). The assumed slurry surface pH of 8.5 was considered acceptable, since literature suggests at the depth of 5 mm from the top surface, the pH was 1 unit greater than the bulk slurry pH, because of the NH_3 and CO_2 gas loss from the slurry surface (Aarnink and Elzing, 1998; Hafner et al. 2012; Aarnink et al., 2018).

There was 0 ppm incoming air NH_3 concentration. This study calculated the pig CO_2 production using the 0.185 $m^3\ h^{-1}$ per heat production unit (HPU) in CIGR (2002). For the 48 pigs at the weight of 60 kg in the room, the CO_2 production of 6.43×10^{-5} kg $m^{-3}\ s^{-1}$ per pen was then applied to the AOZ of the volume ~1.645 m^3 per pen (Fig. 6.7d). There was no CO_2 production from the slurry, because the slurry pit at the ILVO/UGent/HoGent pig facility was emptied every fortnight and so we did not expect a significant CO_2 production from the pit (Pedersen et al., 2008). In the CFD model, the inlet CO_2 was set at 400 ppm and the volume source of the CO_2 at the AOZ was defined 0.1 m away from all wall surfaces (Fig. 6.7d)._All simulations were performed at slurry depth of 0.14 m and at the same pig arrangement (Fig. 7.1).

7.2.3. Post-processing of the simulated data

The slurry pit and compartment air exchange rates, AER_{pit} and AER_{comp} (h^{-1}), respectively, were calculated using equations 6.15 and 6.16. Detailed description of the assumptions and calculation procedure can be found in section 6.2.6. The homogeneity of the air temperature, air velocity, CO_2 and NH_3 concentrations between the pens in the pig compartment was assessed by volumetrically averaging the simulated parameters over the AOZ in each pen. Spatial distribution of these parameters was evaluated at planes A – D in Fig. 7.4.

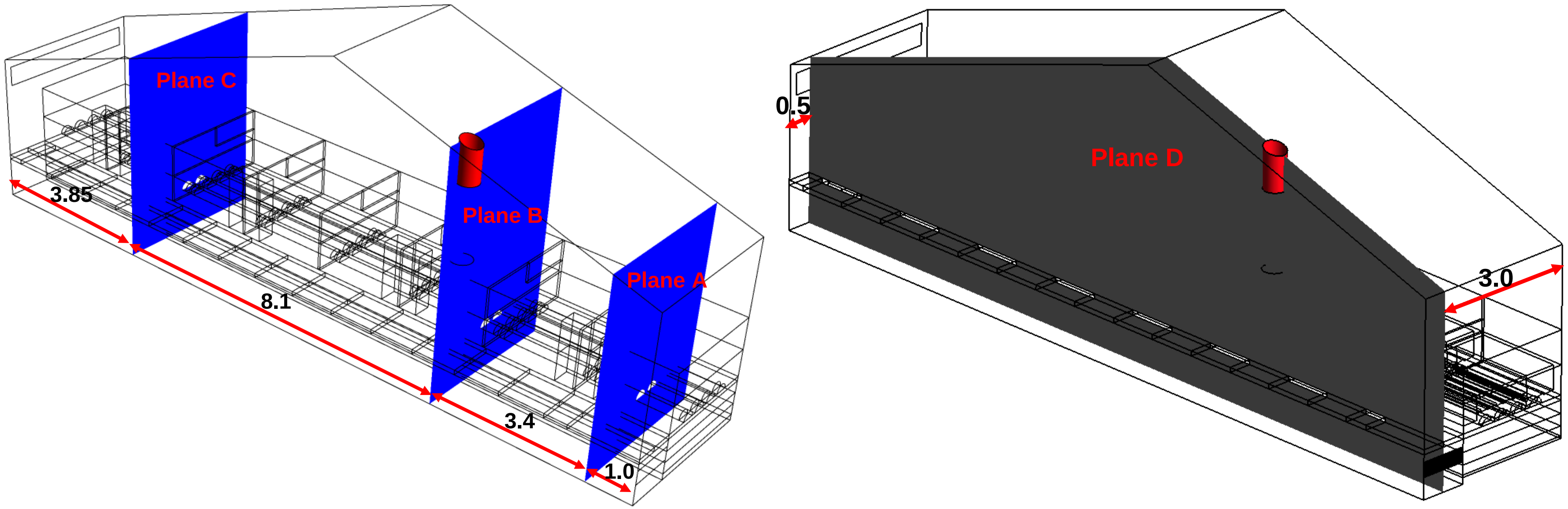

Fig. 7.4 — Locations of plane A–D for illustrating the spatial distribution of the indoor air velocity magnitude and CO_2 concentration.

7.3. Results and discussion

7.2.1. Effect of ventilation rate and inlet temperature on NH_3 emission

Figure 7.5a shows the effect of VR on the NH_3 emission rate in the pig compartment at constant inlet air temperature. At the same inlet air temperature (i.e. 0 °C, 10 °C and 20 °C), the highest NH_3 emissions occurred at the minimum VR of 14.0 m^3 h^{-1} pig^{-1}. Nevertheless, the NH_3 emission remained relatively stable between 22.0 and 52.0 m^3 h^{-1} pig^{-1} VRs, but slightly increased at 70.0 m^3 h^{-1} pig^{-1}. As the inlet air temperature increased, the NH_3 emissions also increased. This result was expected because increasing the inlet temperature increased the temperature of the pit headspace air, which affected the dissociation constant, Henry's law constant and the NH_3 mass transfer coefficient in equations 6.6 – 6.8. As a result the average NH_3 emissions were 1.40, 4.39 and 12.39 g h^{-1}, respectively, at the inlet air temperatures of 0, 10 and 20 °C.

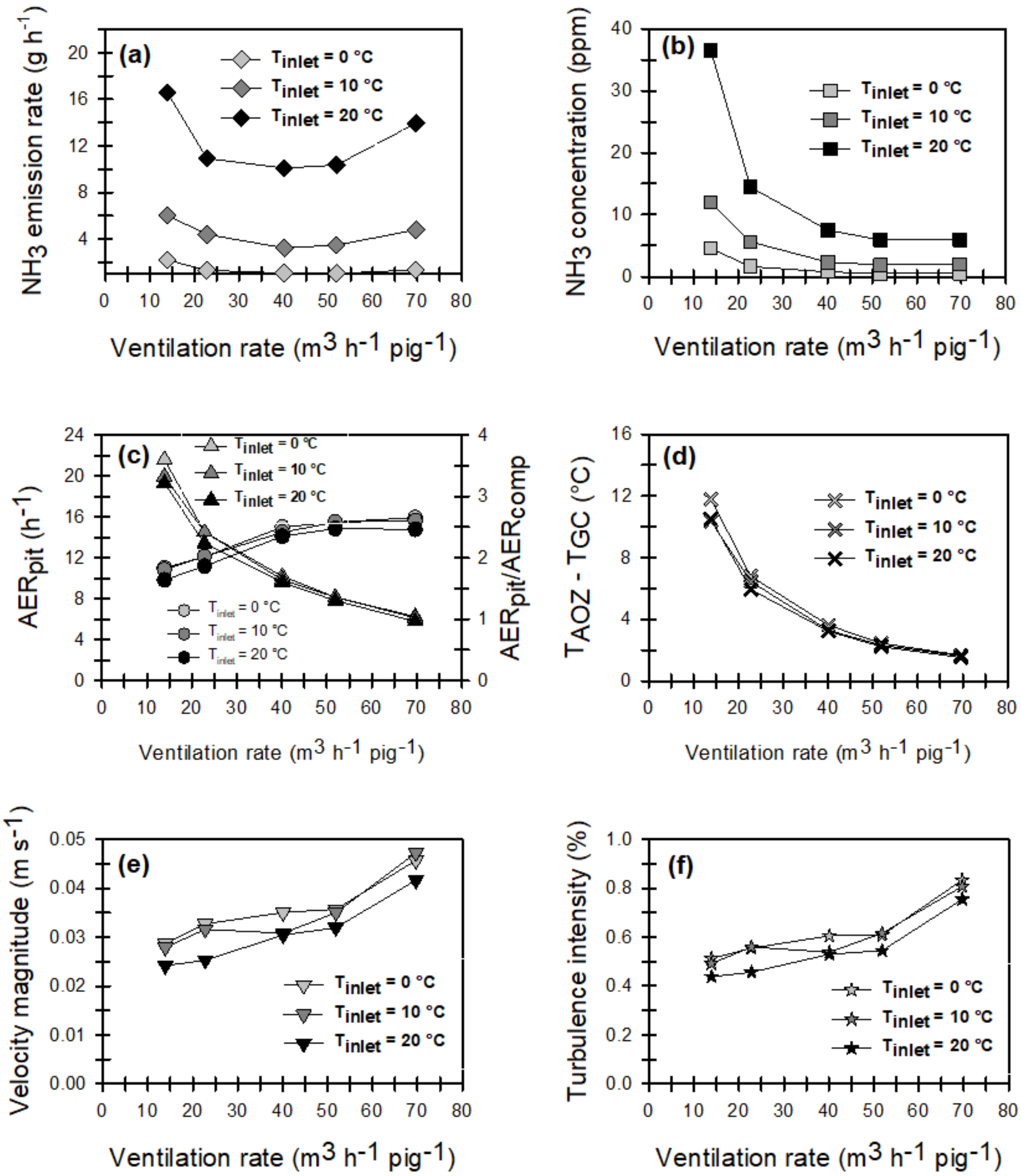

Fig. 7.5 — Effect of ventilation rate at constant T_{inlet} of 0 °C, 10 °C and 20 °C on (a) NH_3 emission (b) exhaust NH_3 (c) slurry pit AER (Circle), AER_{pit}/AER_{comp} (Triangle-up) (d) T_{AOZ} - T_{inlet} (e) air velocity magnitude and (f) turbulence intensity above the slurry surface.

It was indicated in literature that NH_3 emissions in animal housing are positively correlated with VR because increasing VR increases the air velocity at the emitting surface (Table 1.1, Aarnink & Wagemans, 1997; Ni, 1999; Blanes-Vidal et al., 2008). However, the results in Fig. 7.5a are in part contradictory to the literature results. The greater AER_{pit}/AER_{comp} ratio at VR of 14.0 m^3 h^{-1} pig^{-1} (Fig. 7.5c) than the other VRs can explain why the NH_3 emission was highest at the minimum ventilation rate. This phenomenon was previously discussed in chapters 4, 5 and 6 that at higher ΔT and lower VR more of the incoming air entered the slurry pit and transported the NH_3 to the compartment due to the greater buoyancy force coming from the AOZ compared to the momentum force of the inlet air.

The findings in Figs. 7.5a, 7.5c and 7.5d agree with the results in chapters 4, 5 and 6, given that the slurry pit was the only NH_3 emission source in this investigation. In Figs. 7.5e and 7.5f, there was an indication that the air velocity and turbulence intensity above the emitting surface in the slurry pit increased with increasing ventilation rate. This explains the slight increase in the NH_3 emissions at ventilation rates of 70.0 m^3 h^{-1} pig^{-1} compared to 22.0 and 52.0 m^3 h^{-1} pig^{-1}, since both factors affect the NH_3 mass transfer coefficient (Arogo et al., 1999; Rong et al., 2009).

7.2.2. Effect of slatted floor and exhaust configuration on NH_3 emissions

Figure 7.6a compares the effect of the slatted floor inlet effective opening area (EOA) at the service alley on the NH_3 emissions. Reducing the slatted floor inlet EOA from 0.028 m^2 pig^{-1} to 0.007 m^2 pig^{-1} at the service alley had minimal effect on the NH_3 emissions, except at VR of 70.0 m^3 h^{-1} pig^{-1} and T_{inlet} of 30 °C. At this condition, the NH_3 emissions at the EOA of 0.014 m^2 pig^{-1} were greater than the emissions at the EOA of 0.007 m^2 pig^{-1} by 20% and 0.028 m^2 pig^{-1} by 26%. This was because the key factors, which were previously identified to influence the NH_3 volatilisation and the slurry pit air exchange rate remained similar at the different slatted floor inlet EOAs, ventilation rates and T_{inlet} compared to VR = 70.0 m^3 h^{-1} pig^{-1} and T_{inlet} = 30 °C (Figs. 7.6c - 7.6f).

Table 7.5 shows that changing the slatted floor arrangement at the service alley during winter to reduce draught on the pigs increased the NH_3 emissions. The reduction of the slatted floor porosity at the first half of the service alley from 8% in IEC2 (Fig. 7.3a) to 4% in IEC19 (Fig. 7.3b) increased the NH_3 emission by 25%. Covering half of the slatted floor inlet towards the pens at the service alley (Fig. 7.3c), significantly increased the NH_3 emission from 0.57 to 15.34 g h^{-1}. It was obvious that the increase in the NH_3 emission in IEC20 was first due to the significant increase in the air velocity and turbulence intensity above the slurry surface (Table 7.5, Fig. 7.7), which increased the NH_3 mass transfer coefficient. The result in Table 7.5 is supported by the higher exhaust NH_3 concentration in IEC20 (27.1 ppm) than IEC2 (4.6 ppm).

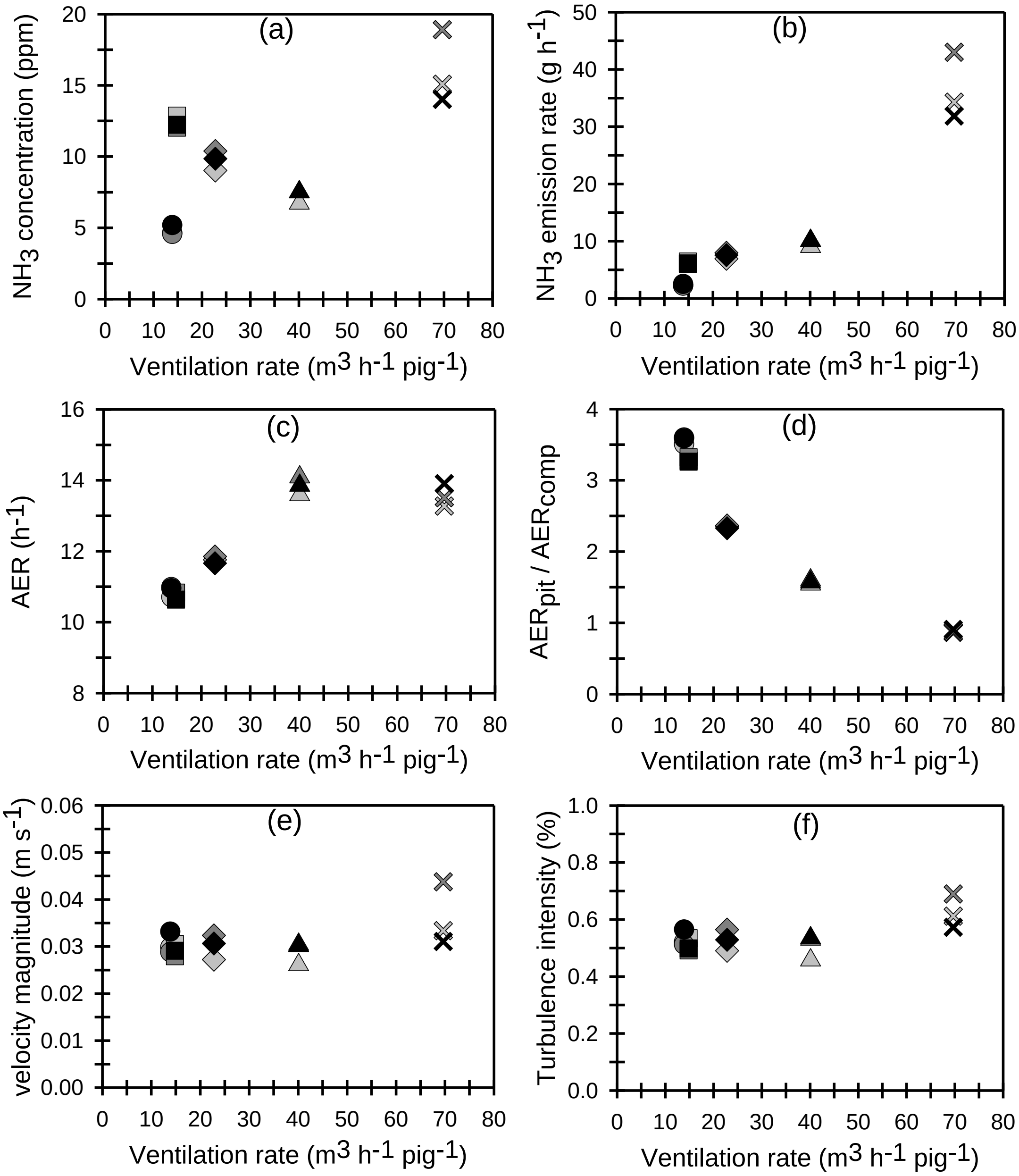

Fig. 7.6 — Effect of ventilation rate at T_{inlet} of 0 °C (Circle), 10 °C (Square), 15 °C (Diamond), 20 °C (Triangle) and 30 °C (×) on (a) NH_3 emission (b) exhaust NH_3 (c) AER_{pit} (d) AER_{pit}/AER_{comp} (e) air velocity and (f) turbulence intensity above the slurry surface. Light grey, dark grey and black are at slatted floor inlet EOA of 0.007, 0.014 and 0.028 m^2 pig^{-1}.

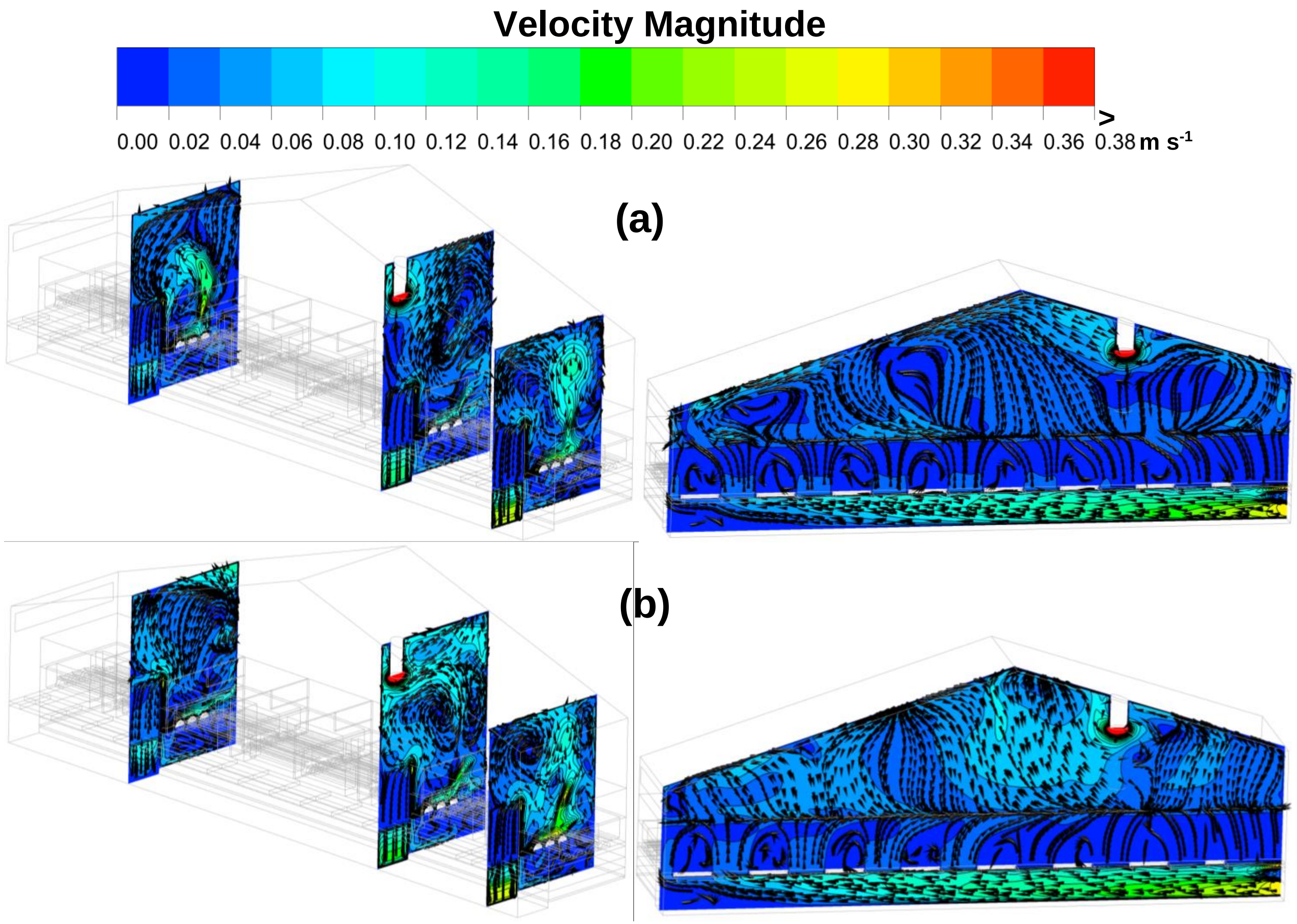

Velocity Magnitude
0.00 0.02 0.04 0.06 0.08 0.10 0.12 0.14 0.16 0.18 0.20 0.22 0.24 0.26 0.28 0.30 0.32 0.34 0.36 > 0.38 m s-1
(a)
(b)

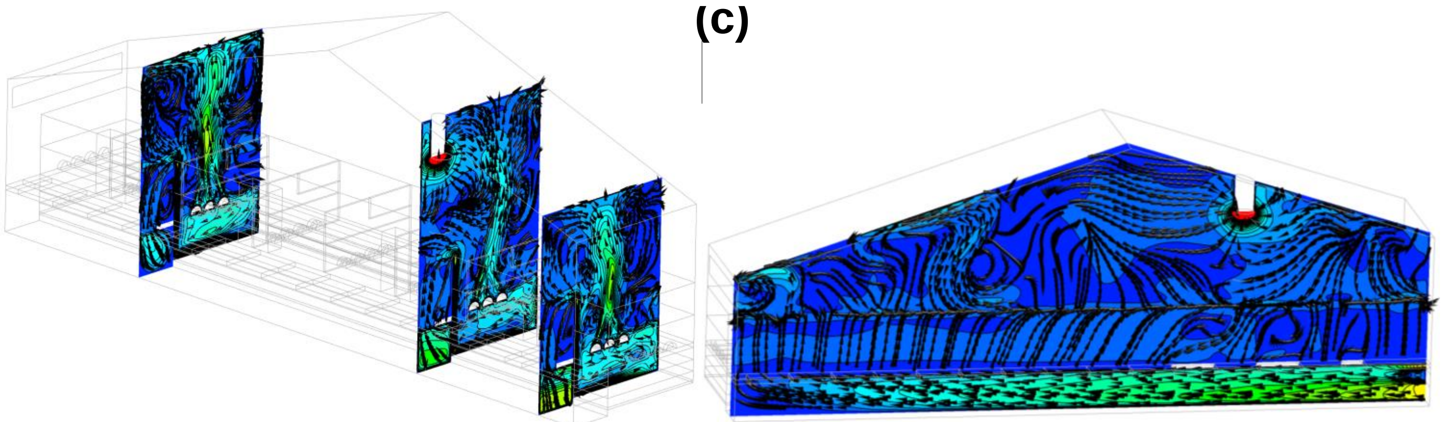

Fig. 7.7 — Predicted air velocity magnitude and airflow streamlines at T_{in} = 20 °C and VR = 14 m^3 h^{-1} pig^{-1} in (a) IEC2 (b) IEC19 and (c) IEC20.

Table 7.5 — Effect of inlet configuration and exhaust duct height on slurry pit air exchange rate, air velocity magnitude, turbulence intensity, exhaust NH_3 concentration and emission rate.

Case	VR (m^3 h^{-1} pig^{-1})	AER_{pit} (h^{-1})	AER_{pit}/AER_{comp}	Velocity (m s^{-1})	TI (%)	Exhaust NH_3 (ppm)	NH_3 ER (g h^{-1})
IEC2[A]	13.9	11.0	3.6	0.029	0.51	4.6	0.57
IEC16[B]	13.9	11.1	3.6	0.033	0.56	5.2	0.65
IEC17[A]	22.8	12.1	2.4	0.033	0.55	1.6	0.13
IEC18[B]	22.8	12.2	2.4	0.035	0.60	1.9	0.15
IEC19	13.9	11.2	3.7	0.035	0.60	5.5	0.71
IEC20	13.9	49.8	16.3	0.242	3.54	27.1	15.34

[A] Exhaust duct opening height is 3.6 m and [B] 2.0 m above the floor.

Another reason was that the slurry pit exchange rate in IEC20 was 5-fold higher than IEC2 (Table 7.5). From Fig. 7.3d, placing the slatted floor inlets at the service alley, 0.5 m away from the pens caused almost all the supply air to enter the slurry pit. This was why the AER_{pit}/AER_{comp} ratio in IEC20 was 16.3 compared to 3.6 in IEC2 (Table 7.5). As described by Lin and Tsai (2014), it appears placing the slatted floor air inlet 0.5 m away from the AOZ increased the gravity current flow of the supply air. Thus, the greater density differences between the inlet air and the AOZ promoted more of the supply air entering into the slurry pit instead of the expected airflow above the pigs and slatted floor in the pen (Fig. 7.7).

The lowering the exhaust opening from 3.6 m to 2.0 m (Fig. 7.1a) at the service alley had a minor effect of the air velocity and turbulence intensity above the slurry surface as well as the slurry pit air exchange rate (Table 7.5, Fig. 7.8). The exhaust opening at 3.6 m from the slatted floor inlet emitted 0.57 g h^{-1} NH_3 compared to 0.65 g h^{-1} at the height of 2.0 m, when the inlet air temperature was 0 °C (Table 7.5).

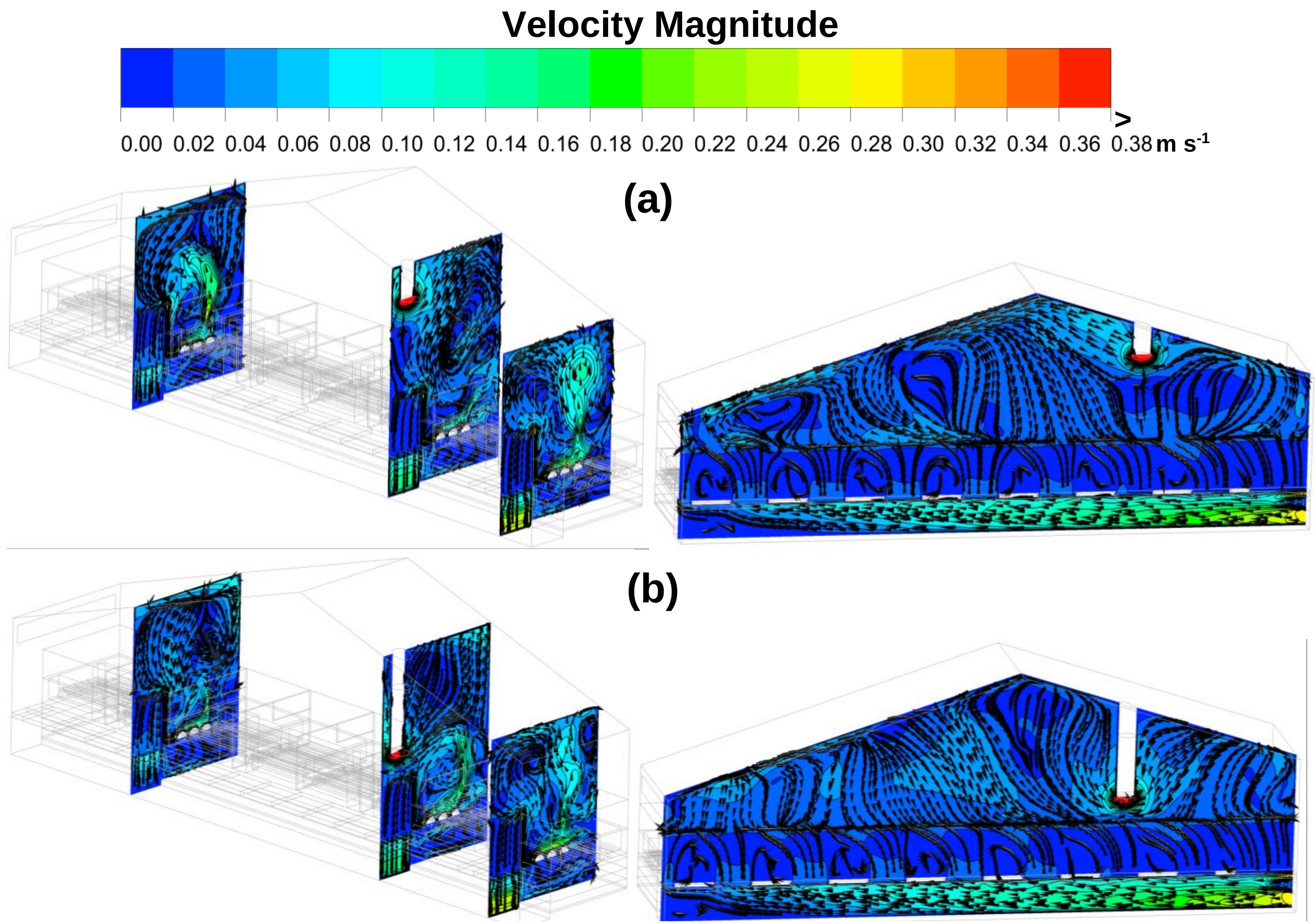

Fig. 7.8 — Predicted air velocity magnitude and airflow streamlines at T_{in} = 20 °C and VR = 14 m^3 h^{-1} pig^{-1} in (a) IEC2 at exhaust duct opening 3.6 m and (b) IEC16 at exhaust duct opening 2.0 m above the slatted floor.

7.2.3. Effect of slatted floor and exhaust configuration on airflow distribution at the AOZ

The air velocity, temperature, CO_2 and NH_3 concentration within the AOZ in each pen were heterogeneously distributed (Fig. 7.9 – 7.12). The higher standard deviation in the calculated air velocity, temperature, CO_2 and NH_3 concentration was due to the displacement airflow pattern and the large volume of the AOZ in the pen (Fig. 6.6). There was less variation in the average air velocity and temperature between the pens compared to the CO_2 and NH_3 concentrations. Increasing the ventilation rate improved the indoor air quality by reducing CO_2 and NH_3 concentration in the pens (Fig 7.9 and 7.10). However, this increased the air velocity and reduced the temperature in the pens. As previously discussed, the slurry pit air exchange rate also increased as ventilation rate increased (Fig. 7.6), which is not suitable for NH_3 emission reduction.

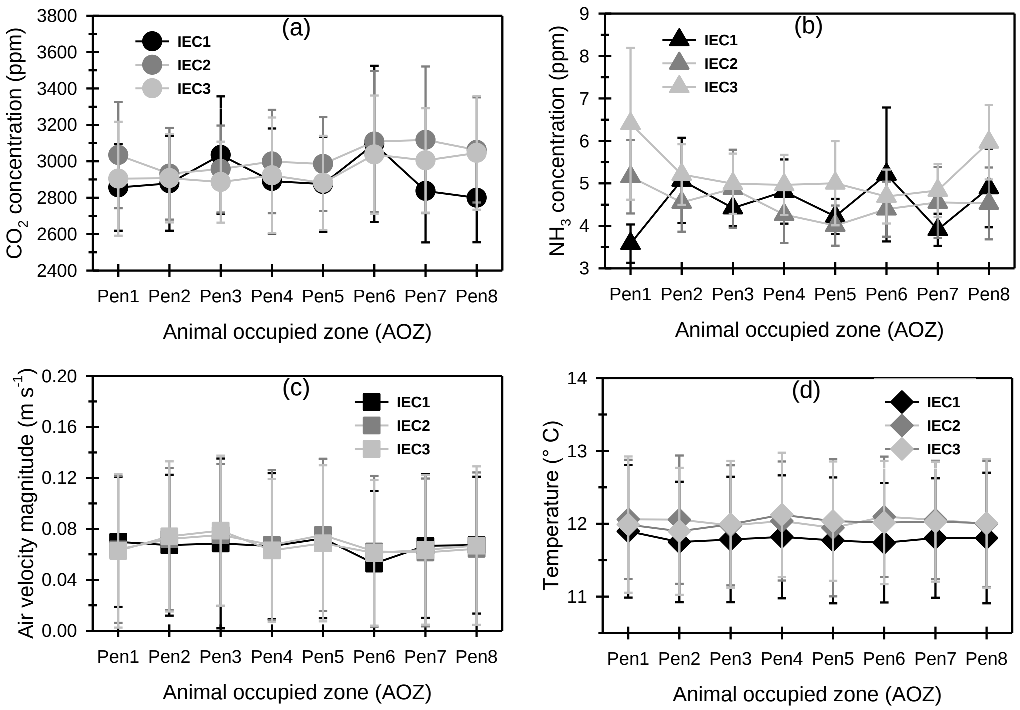

Fig. 7.9 — Effect of effective inlet opening area at 0.007 (black), 0.014 (dark grey).and 0.028 m^2 pig^{-1} (light grey) on the average AOZ (a) CO_2 concentration (b) NH_3 concentration (c) air velocity magnitude (d) air temperature at T_{inlet} = 0 °C and ventilation rate of 14.0 m^3 h^{-1} pig^{-1}.

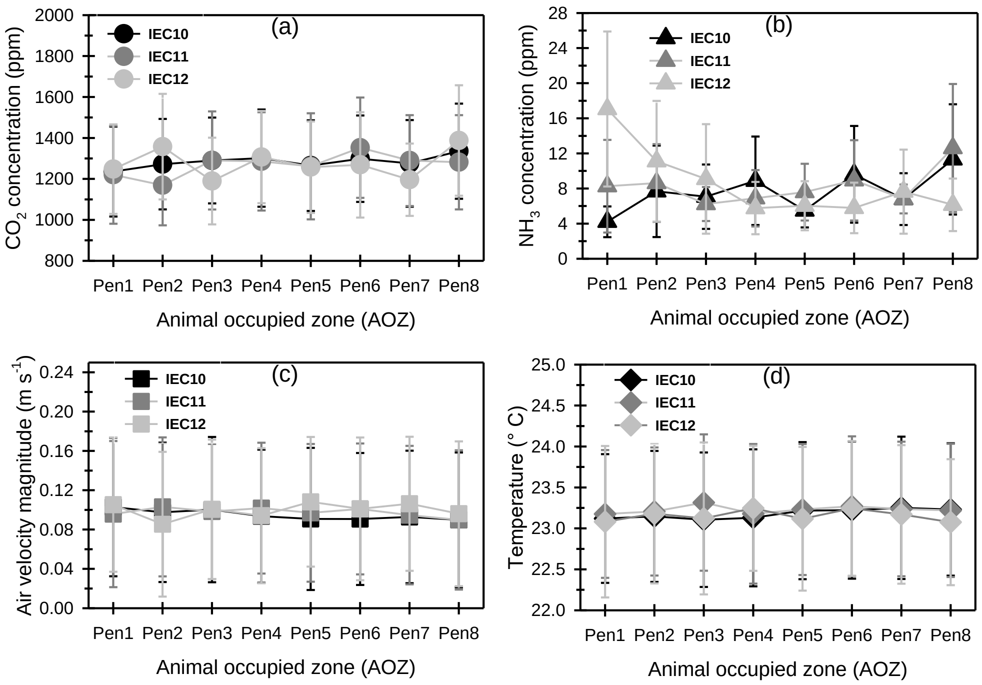

Fig. 7.10 — Effect of effective inlet opening area at 0.007 (black), 0.014 (dark grey).and 0.028 m^2 pig^{-1} (light grey) on the average AOZ (a) CO_2 concentration (b) NH_3 concentration (c) air velocity magnitude (d) air temperature at T_{inlet} = 20 °C and ventilation rate of 40.4 m^3 h^{-1} pig^{-1}.

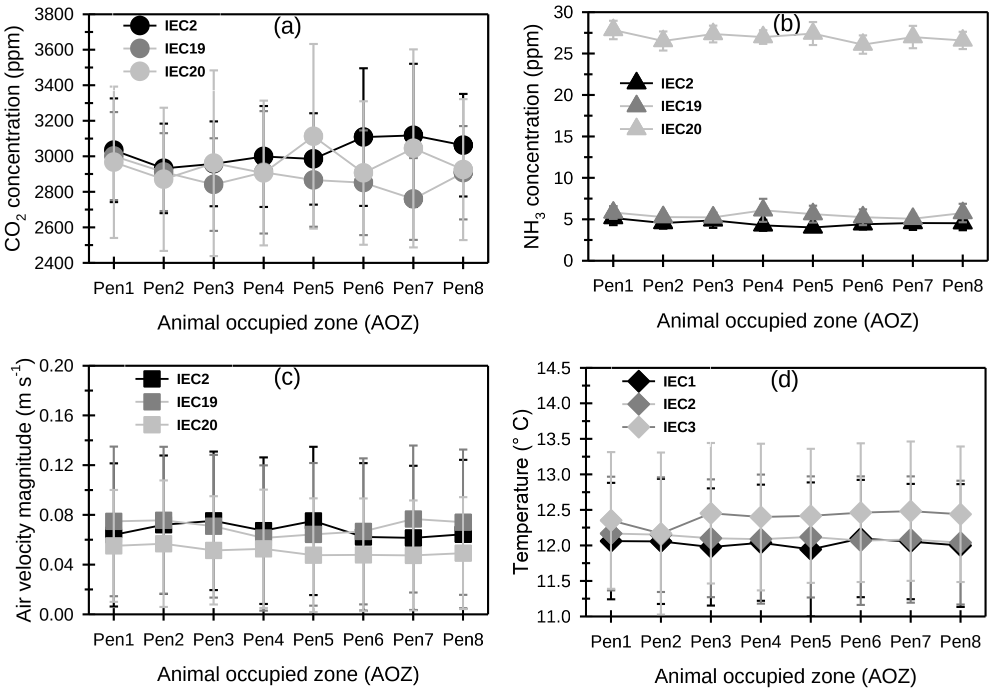

Fig. 7.11 — Effect of slatted floor inlet configuration in case IEC2 (black), IEC19 (dark grey) and IEC20 (light grey) on the average AOZ (a) CO_2 concentration (b) NH_3 concentration (c) air velocity magnitude (d) air temperature at T_{inlet} = 0 °C and ventilation rate of 14.0 m^3 h^{-1} pig^{-1}.

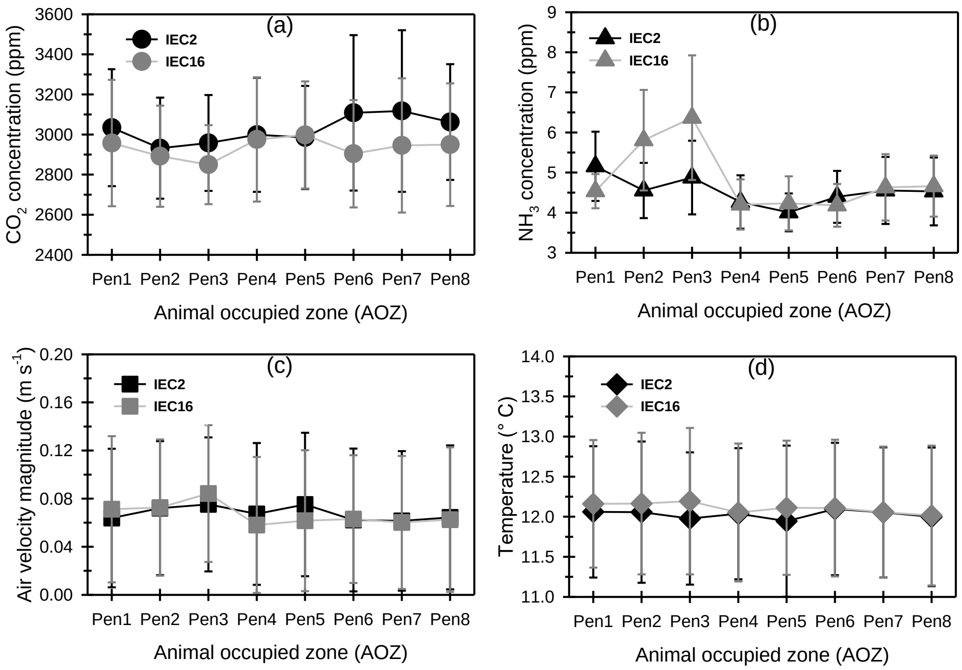

Fig. 7.12 — Effect of exhaust duct opening height at 3.6 m (black) and 2.0 m (dark grey) above the floor on the average AOZ (a) CO_2 concentration (b) NH_3 concentration (c) air velocity magnitude (d) air temperature at T_{inlet} = 0 °C and ventilation rate of 14.0 m^3 h^{-1} pig^{-1}.

Reducing the EOA of the slatted floor inlet from 0.028 to 0.007 m^2 pig^{-1} produced similar average air velocity in the pens at different T_{inlet} and VR (Figs. 7.9c and 7.10c). This strategy produced relatively similar average air temperature in the pens at the different T_{inlet} and VR. However, for T_{inlet} = 0 °C and VR = 14.0 m^3 h^{-1} pig^{-1} the average air temperature was respectively 0.16 – 0.4 °C and 0.1 – 0.3 °C high at EOA = 0.014 and 0.028 m^2 pig^{-1} than at EOA = 0.007 m^2 pig^{-1} (Fig. 7.9d). The heterogeneity in the average CO_2 and NH_3 concentrations between the pens was high compared to the air temperature and velocity at the three EOAs (Figs. 7.9 and 7.10). This was because the air velocity at slatted floor inlets was very low regardless of the slatted floor porosity, causing the temperature difference between the AOZ and the supply air to influence airflow into the pen. Maintaining the same ventilation rate resulted in the same total airflow through the slatted floor inlets regardless the EOA of the slatted floor inlet.

Fig. 7.11 shows the effect of slatted floor arrangement at the service alley on the average air velocity, temperature, CO_2 and NH_3 concentration in the pens. Applying IEC19 lowered the average CO_2 concentration in the pens by 20 – 360 ppm compared to IEC2 (Fig. 13). In six of the pens the average CO_2 concentration at IEC20 was decreased by 60-210 ppm compared to IEC2 (Fig. 13). IEC2 increased the average

CO_2 concentration by 3 and 127 ppm in pens 3 and 5 compared to the same pens at IEC20. The average NH_3 concentration in the pens, at IEC19 was higher than IEC2 by 0.4 – 1.8 ppm. Also, the average NH_3 concentration in IEC20 was greater than IEC2 by 21.7 – 23.4 ppm (Fig. 7.11b). Average air velocities in the pens were low in IEC20 than IEC2 and IEC19 (Fig. 7.11c), with opposite results for the average air temperature (Fig. 7.11d). The higher temperature in the pens at IEC20 than at IEC2 and IEC19 was because more of the incoming entered into slurry pit (Fig. 7.7) rather than flowing over the headed pigs. This increased in slurry pit air exchange rate at IEC20 (49.8 h^{-1}) compared to IEC2 and IEC19 (Table 7.5). Also, the higher NH_3 concentration in the pens at IEC20 than at IEC2 and IEC19 was because of the effect of the slurry pit air exchange rate.

At T_{inlet} = 0 °C and VR = 14.0 m^3 h^{-1} pig^{-1}, lowering exhaust opening height from 3.6 m to 2.0 m (Fig. 7.1a) at the service alley reduced the average CO_2 concentration by 23 – 204 ppm in all the pens, except in pen 5 (Fig. 7.12). Placing the exhaust 2.0 m to the slatted floor inlet reduced the CO_2 concentration at the service alley farther away from the underfloor air channel inlet compared to placing the exhaust opening 3.6 m from the slatted floor air inlet (Fig. 7.14).

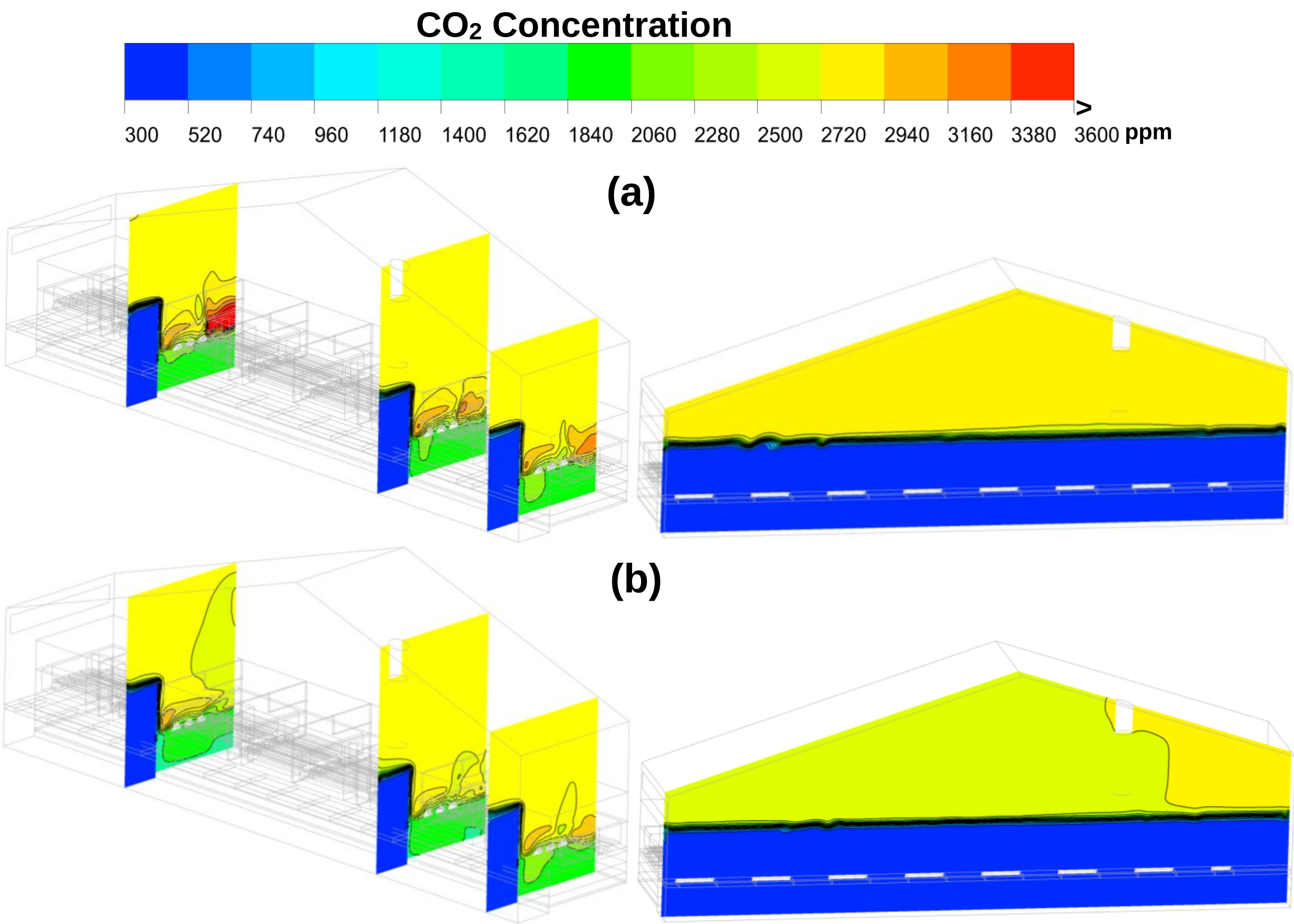
CO2 Concentration
300 520 740 960 1180 1400 1620 1840 2060 2280 2500 2720 2940 3160 3380 3600 ppm
>
(a)
(b)

(c)

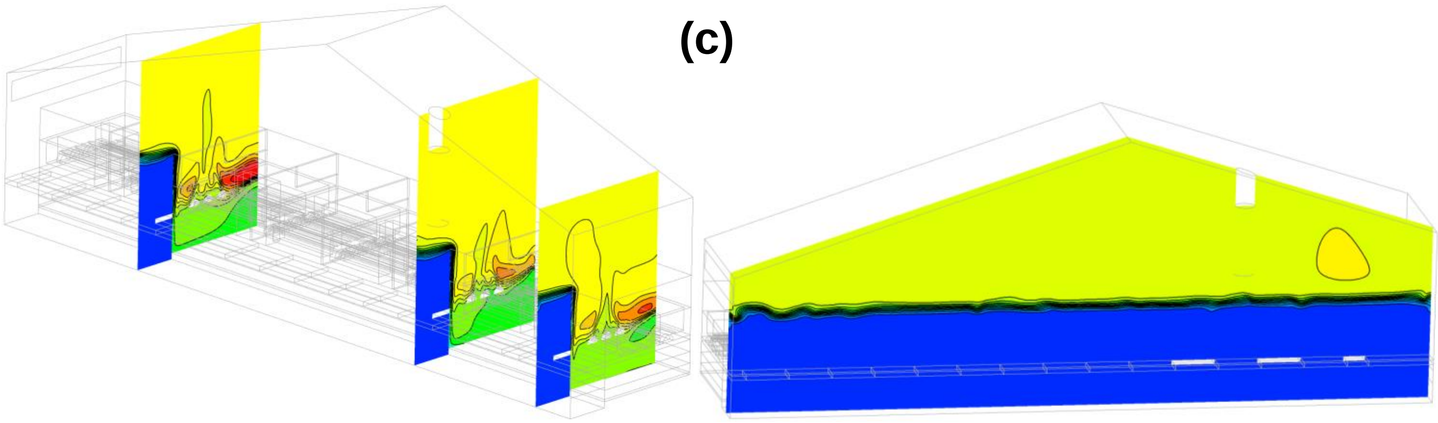

Fig. 7.13 — Predicted CO_2 concentration contours at T_{in} = 20 °C and VR = 14 m^3 h^{-1} pig^{-1} in (a) IEC2 (b) IEC19 and (c) IEC20.

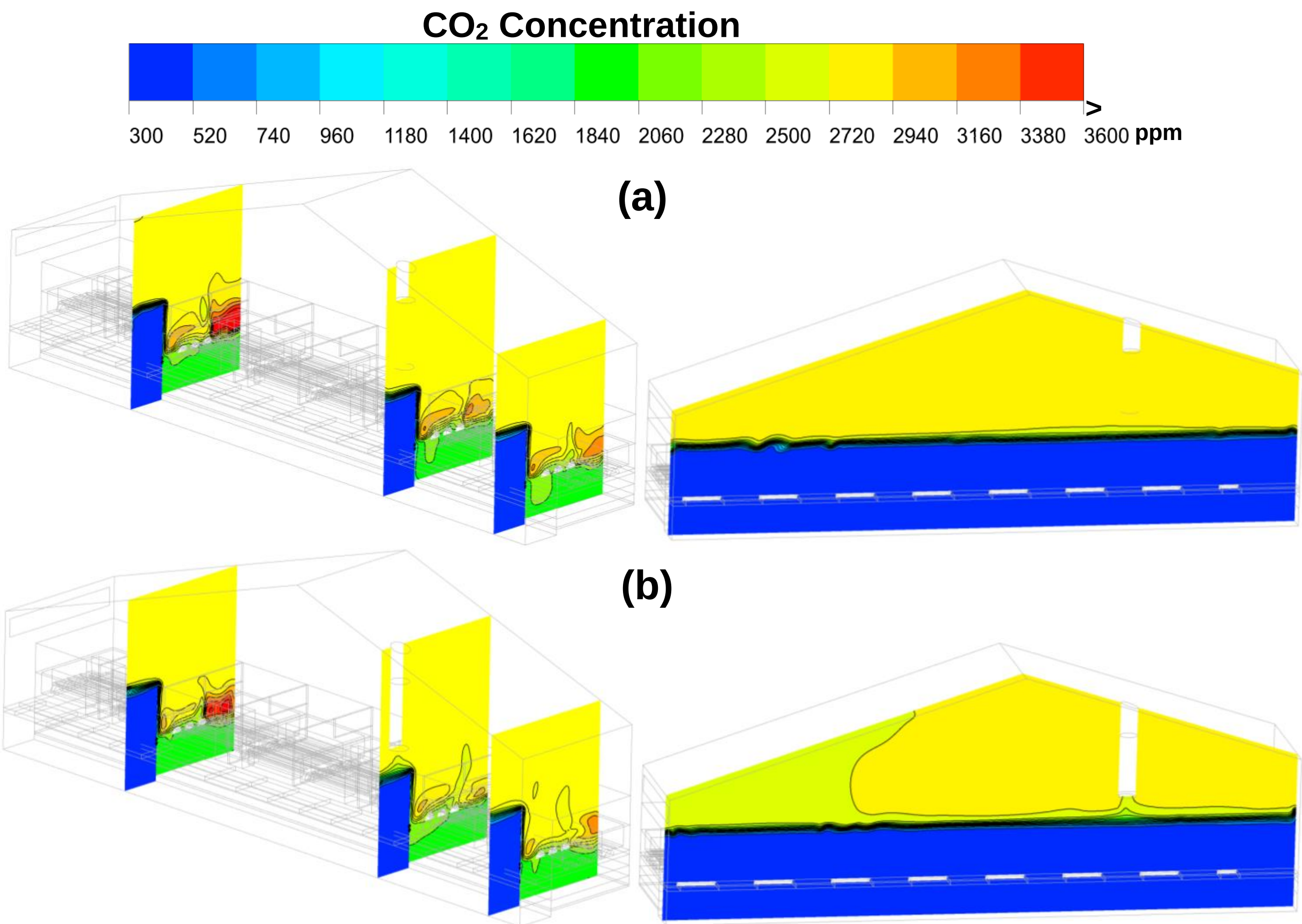

Fig. 7.14 — Predicted CO_2 concentration contours at T_{in} = 20 °C and VR = 14 m^3 h^{-1} pig^{-1} in (a) IEC2 at exhaust duct opening 3.6 m and (b) IEC16 at exhaust duct opening 2.0 m above the slatted floor.

Placing the exhaust opening closer to the slatted floor inlet increased the NH_3 concentration in the pens by 1.3 and 1.5 ppm compared to the higher height, except in pen 2 and pen 3. The average air velocity and temperature at the AOZ in the pens were relatively similar between the two exhaust duct opening heights. However, there was an indication of higher air temperatures at the AOZ in pens 1 – 5 by lowing the exhaust opening closer to the slatted floor air inlet (Fig. 7.12d). This is because placing the exhaust opening closer to the slatted floor inlet extracted more of the cold incoming air and extracted the recirculated CO_2 that was produced at the AOZ (Fig. 7.14). The relatively similar average NH_3 concentrations in pens 4 – 8 was probably due to the difference in the slurry pit air exchange rate in these pens compared to pens 1 – 3. Indeed, Table 7.5 shows that the height of the exhaust opening from the slatted floor air inlet had a minor effect on the slurry pit air exchange rate.

7.4. Conclusions

The results in this chapter showed that at inlet air temperature of 0 °C and VR of 14.0 m^3 h^{-1} pig^{-1}, reducing the slatted floor inlet porosity at the service alley (from 15% to 8% and 4%) did not affect the CO_2 concentration in the pens. However, placing the exhaust duct opening 2.0 m compared to 3.6 m decreased the CO_2 concentration in the pens and improved the air quality at the service alley. Reducing the slatted floor inlet porosity at the service alley had a minor effect on the NH_3 emissions because it produced similar air exchange rate in slurry pit. Applying slatted floor inlet arrangement IEC20 at the service alley increased the NH_3 emissions, since it promoted more pit air exchange and increased the air velocity and turbulence intensity above the slurry surface In the pit.

This chapter also showed that in the pig buildings with UFAD system the animal area and inlet air temperature difference (i.e. ΔT) affect the slurry pit air exchange rate and the NH_3 emission. The highest NH_3 emission occurred when the ΔT was greater than 10 °C and the ventilation rate was at the minimum. This was due to the displacement airflow principle in the building coupled with the fully slatted pen floors that allowed easy access of the supply air into the slurry pit. Thus, in order to reduce NH_3 emissions in fully slatted pig buildings with UFAD systems, new techniques are needed to minimise the supply air going into the slurry

Chapter 8: General discussion, conclusions and future perspectives

8.1. Introduction

The EU and Flemish environmental directives regulate pig production in Flanders in order to reduce the harmful effects of emissions from intensive livestock production. The EU directives on emissions include the National Emission Ceiling (NEC), the Integrated Pollution Prevention and Control (IPPC), and the Habitats and Birds directives. The Flanders ministerial decree on NH_3 emissions for pig and poultry housing is in accordance with the commitments Belgium has made to the NEC directive. The Flanders Programmatic Approach to Nitrogen (PAN) also contributes to the successful implementation of the Habitats and Birds directives. Because of the above environmental regulations, low-cost emission mitigation techniques are increasingly needed to reduce emissions from pig farms and to promote economic activities of the pig industry. The reason is that the emission reduction techniques in the BREF report (Santonja et al., 2017), are capital-intensive to develop, expensive to implement and/or complex to manage, while others have undesirable cross polluting effects. In addition, limiting the reduction of the pollutants (e.g. NH_3 emissions) to only the high-performance techniques such as the approved low-NH_3 emission systems in Flanders alone (Vlaamse Landmaatschappij, 2019) may still be insufficient to achieve the environmental targets, particularly in regions near Natura 2000 sites (Loyon et al., 2016; De Pue and Buysse, 2019).

Therefore, the aim of this PhD research was to identify low-cost and management-based techniques that could complement the high-performance Best Available Techniques (BAT) to reduce NH_3 and odour emissions from Flemish pig buildings. The focus of this PhD research was on ventilation control/design as the emission reduction technique. This is because ventilation rate in livestock housing is typically associated with emissions (Blanes-Vidal et al., 2008; Ngwabie et al., 2011; Schauberger et al., 2013). Furthermore, Vranken (1999) and Zhang et al. (2009) previously demonstrated using computer simulations, that optimal tuning of ventilation control settings (VCS) at the climate computer could reduce NH_3 and odour emissions without additional costs. The hypothesis, therefore, was that lower ventilation levels would minimise NH_3 and odour emissions in pig housing due to the lower air velocities near the emitting surfaces and the reduction in NH_3 and odour displacement from the slurry pit. The general conclusions to this PhD research are as follows:

1. The ground channel temperature (T_{GC}) was a key factor affecting NH_3 emissions from the pig building equipped with the UFAD system. It interacted with the ventilation set-point temperature (T_{set}) to influence NH_3 emission.
2. No significant difference in pig rearing performance was shown for the different ventilation control setting at CON, T1, T2 and T3 (chapter 5).
3. The ventilation setting T1, with an increased $Tset$ by +2 °C compared to CON, significantly reduced the odour emission by 34% compared to the CON. T1, T2 and T3 (chapter 5) did not substantially reduce the hourly average NH_3 emissions compared to CON. However, calculating annual NH_3 emission factors based on the VERA protocol showed the potential of T1 to reduce the annual NH_3 emissions by 11% compared to CON.
4. The lack of the significant difference in the hourly average NH_3 emissions between the tested ventilation control strategies and CON was due in part to the seasonal variation in pig housing airflow patterns. This was caused by the air exchange rate in the slurry pit from the diurnal and seasonal variations in the T_{GC} and the temperature difference between the room and T_{GC}.
5. NH_3 displacement from the slurry pit headspace into the pig compartment positively correlated with the Archimedes number of the incoming air from the slatted floor inlet to the animal occupied zone.
6. The air exchange rate of the slurry pit increased with increasing ventilation rate, whereas the ratio of the slurry pit to the compartment air exchange rate decreased at higher ventilation rates.
7. At inlet air temperature of 0 °C and VR of 14.0 $m^3\ h^{-1}\ pig^{-1}$, reducing the slatted floor inlet porosity at the service alley (from 15% to 4% and 8%) did not affect the CO_2 concentration in the AOZ between the pens in the compartment. However, lowering the exhaust duct opening height (from 3.6 to 2.0 m) decreased the CO_2 concentration at the AOZ and improved the air quality at the service alley.
8. This PhD research evaluated the VERA test protocol's, case-control sampling strategy for calculating the average of NH_3 emission reduction over 1 year from T1, T2 and T3 compared to CON (chapter 5). Thereby 20 different VERA compliant sampling sequences of six 24-hour measurement days were selected. The results showed large variations in the calculated respective yearly average NH_3 emission reductions (T1: -23 to 8%; T2: -6 to 23%; T3: -6 to 14%).

8.2. Significance of the integrated modelling and experimental approach

To achieve the objectives of this PhD work, an integrated mathematical modelling, physical modelling and field measurements approach was applied (Fig. 8.1). The integrated modelling and field measurements methodology included the development of a steady-state indoor simulation model (chapter 2), an experimental test platform (chapter 3) and a CFD model (chapter 6). Takai et al. (2013) previously proposed that new research methodologies on airborne emission from naturally ventilated livestock buildings should explore the advantages of the synergy between mathematical modelling, physical modelling and field measurements to achieve consistent and accurate emission estimates. This PhD research exemplifies the proposed direction of research suggested by Takai et al. (2013), but this PhD work was carried out in a single pig building with mechanically ventilated compartments.

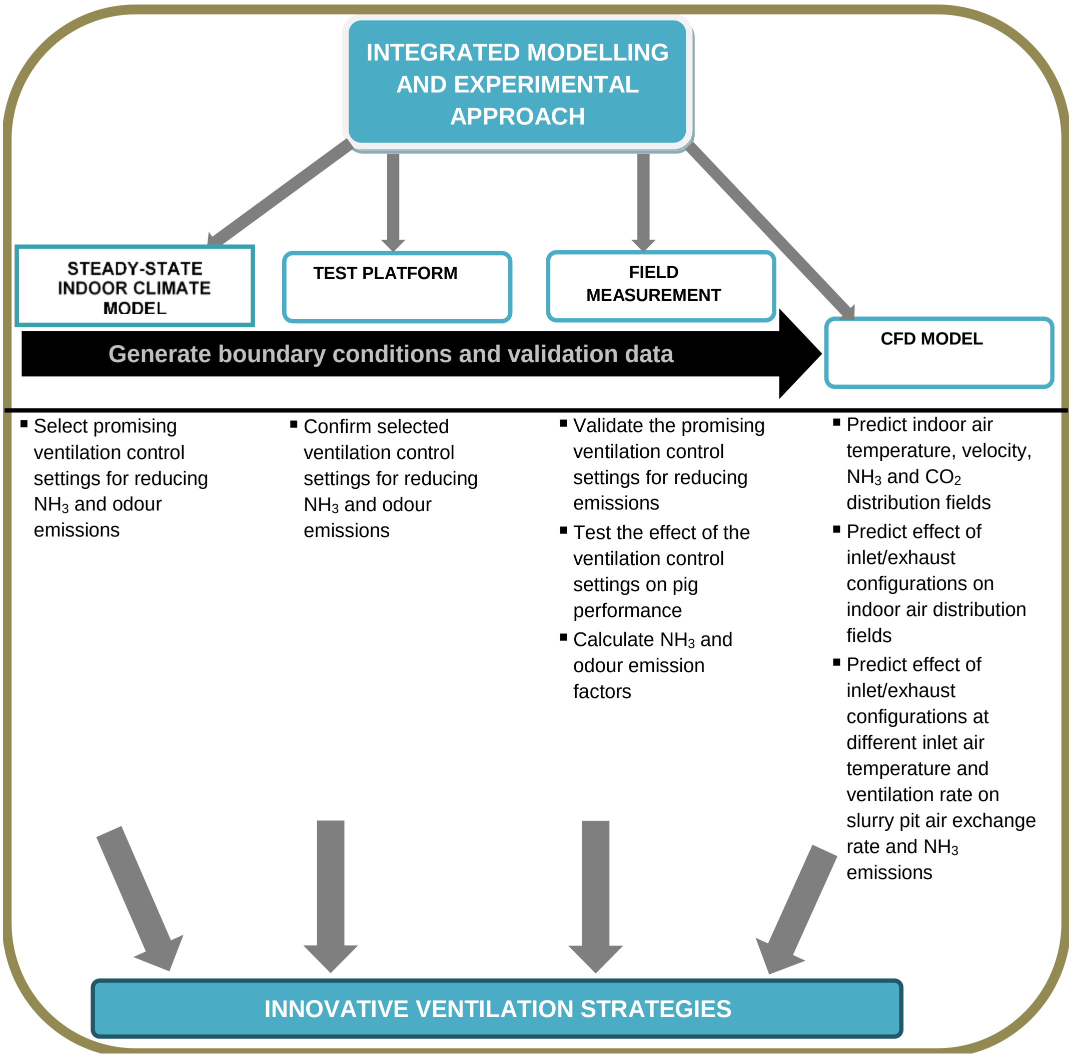

Fig. 8.1. Integrated modelling and experimental approach applied in this PhD research.

The significance of the integrated mathematical modelling, physical modelling and field measurements approach was that it enabled this PhD research to gain detailed knowledge about the pollutants transport behaviour from the emitting source in pig buildings equipped with Underfloor Air Distribution (UFAD) systems. In addition, the integrated approach was used to assess the emission reduction potentials of different ventilation control settings (chapters 4 and 5). The results of field measurements showed acceptable pig performance for the tested ventilation set-points and generated NH_3, odour and GHG emission data for the policy makers. The main drawback of combining the mathematical modelling, physical modelling and field measurements approach is that it is time-consuming, costly and case dependant.

8.3. Potential of adapted ventilation systems on emissions

In this PhD research, changing the set-point temperature by 1 - 2 °C and/or the ventilation requirements in T1, T2 and T3 at the climate computer in the field experiment (Table 5.1) showed no significant difference in the hourly average NH_3 emissions between the three new VCSs and reference strategy (CON) (chapter 5). The hourly average NH_3 emission in T1 decreased by 3%, but the NH_3 emissions increased by 1% in T2 and 3% in T3 compared to the CON. This was contrary to the expected result, as the application of the three new VCSs significantly reduced the hourly average ventilation rates from the CON by 17 – 28%. Nonetheless, it was promising that applying T1 significantly reduced the odour emission by 34% compared to the CON (16 OU_E s^{-1} pig^{-1}). The application of the VCSs in T2 and T3 decreased the odour emission by 22% and 5% compared to the CON respectively; however, the odour emission was not significantly different from CON.

The mock-up pig (chapter 4) and the field (chapter 5) experiments showed that the lack of significant difference in the overall average NH_3 emissions between the three new VCSs and the CON was in part due to the diurnal and seasonal variation in air exchange rate in the slurry pit caused by the T_{GC}, ΔT and their interaction with the VCS that influenced the NH_3 emissions. Particularly, the findings in chapters 4 - 7 showed that a larger proportion of the incoming air flowed into the slurry pit when the incoming air (T_{GC}) was colder than the room and/or the pit headspace temperatures, and the ventilation rate was low. This was because air displacement is the main ventilation principle in the pig building, thus displacing the NH_3 rich headspace air into the compartment. The air displacement coupled with the fully slatted pen floors further promoted the air exchange between the slurry pit and the pig compartment by allowing the easy access of the incoming air into the slurry pit. Thus, this PhD finding indicates that the effect of the indoor airflow pattern on the gaseous release from the slurry pit into the building is equally crucial, despite the importance of the ventilation rate on emissions. Furthermore, as over 50% of the total NH_3 emissions in pig buildings emanate from the slurry pit (Hoeksma et al., 1992; Aarnink et al., 1997; Kai et al., 2005) it is imperative that new strategies are developed to minimise the supply air going into the slurry pit in pig buildings with UFAD systems.

This PhD research (chapter 7) explored the effect of reducing the slatted floor inlet effective opening area (EOA) at the service alley from 0.028 m^2 pig^{-1} to 0.007 m^2 pig^{-1} on the air exchange rate in the slurry pit. However, this strategy had minor effect on the NH_3 emissions and the air distribution at the animal area. Changing the slatted floor inlet arrangements at the service alley compared to the current condition rather increased the NH_3 emissions. This was due to the increase in slurry pit air exchange rate and the increase in the air velocity and turbulence intensity above the slurry surface, which increased the NH_3 mass transfer coefficient. Furthermore, lowering the exhaust duct opening height from 3.6 m to 2.0 m increased the NH_3 emissions. Perhaps, using only a partly slatted pen floor or placing a low porosity slatted floor at the front part of the pen close to the slatted floor inlet could reduce the direct flow of some of the incoming air into the slurry pit. However, there is a higher risk that the pigs would prefer to lay at the opposite and non-draughty section of the pen, thus leaving the solid floor or low porosity section as a dunging area, which is not preferable.

In order to avoid airflows entering the slurry pit, pig barns with UFAD systems which use underfloor air channel systems as geothermal heat exchanger could deliver the incoming air from the underfloor air channel system via alternative inlets at the higher level of the barn, thereby aiming to reduce draught and displacement of emissions from the slurry pit into the compartment. However, delivering the incoming air via the ceiling may reduce the better air quality at the animal occupied zone in pig barns with UFAD systems. Also, existing and new pig barns which use UFAD systems could install baffles/flaps at the solid pen partitioning beside the slatted floor inlet in the service alley to direct the incoming air away from the slurry pit and promote more mixing and warming up of the incoming air before reaching the AOZ. Another approach is the use of porous curtains above the solid pen partitioning at the service alley to encourage air mixing and warming of the incoming air before it is delivered to the AOZ.

The UFAD system in the investigated pig building lowered the hourly average temperature peaks of the supply air to the compartment (i.e. T_{GC}) in summer by 5 – 15 °C compared to the outside air temperature (Fig. 5.8). Similarly, the use of under floor air channel systems as geothermal heat exchanger in Germany, which is similar to the ILVO/UGent/HoGent fattening pig building reduced summer temperature peaks by 7 – 15 °C (Müller et al., 2005; Hessel et al., 2010). This lead to 90% reduction of incoming air temperature fluctuations compared to the diurnal variation of the ambient air temperature, while minimising seasonal variations of the incoming air temperature by 70% compared to the ambient air. Subsequently, Müller et al. (2005) reported about 30% NH_3 emission reduction in summer in the pig barn due to the lowering of the summer ventilation rate. This indicates pig barns with UFAD systems could be an adaptation strategy for combating the impact of climate change on emissions and pig performance. Perhaps, combining the UFAD systems with water sprinkler and/or fogging systems in summer could lead to a further reduction in the NH_3 and odour emissions while reducing pig heat stress, improve the indoor air quality, maintain animal welfare and performance.

For the emission reduction, the sprinkler systems could apply a mixture of additives (e.g. vegetable oils) and water to the floor surface in pig buildings, as Paszek et al. (2001) reported H_2S, NH_3 and odour emission reduction by 17.9%, 36.3% and 27.8% after sprinkling the mixture of soybean oil and water on the pen floor once a day. However, the oils tend to transform into gum and plugs sprinklers in these systems and the sprayed oil in pig housing causes problems during cleaning. Another drawback of water sprinklers is the increase in the water usage as well as the cost of handling the volume of waste water to be treated and disposed, since most of the water ends up in the slurry pit. Table 8.1 shows the emission reduction potential of fogging systems on NH_3 and odour in pig housing, the investment and operational costs and the use of earth to water heat exchangers which reduces the indoor air humidity and does not generate waste water.

Table 8.1 Overview of NH_3 and odour emission reduction potential by fogging, inlet air cooling by Earth-Water-Heat-Exchangers (EWHE) and ventilation control settings.

		Emission reduction (%)		Cost (€ pig^{-1})		
Reference	Technology	NH_3	Odour	Investment	Operational	Comments
[1]	Fogging	22 - 30	12 - 23	3 - 6		Odour and NH_3 emission reduction dues to 14 - 46% dust emission reduction
[2]	Fogging	NS		17.55	0.17	Reduced indoor temperature by 6 °C
[3]	Fogging	NS				Incomplete evaporation of the fogged water increases NH_3 emission by 10 - 14% at T_{out} < 14 °C but reduced indoor temperature by 4 - 5 °C and ventilation rate by 20 - 33%.
[4]	EWHE	11	23		0.13	NH_3 and odour emission reduction only achieved during summer.
[5]	EWHE	8 - 11	33 - 47			The NH_3 and odour emissions reduction only achieved during summer.
This study	Ventilation settings	11	23	None	None	Yearly emission reduction was achieved by increasing in the set-point temperature at the climate controller by +2°C compared to the reference ventilation setting.

[1] Santonja et al. (2017); [2] Lehmann et al. (2011); [3] Haeussermann et al. (2006); [4] Riis et al. (2010); [5] Lyngbye et al. (2006); NS (non-significant);

8.4. Pig performance and indoor conditions

In this PhD dissertation, changing the set-point temperature by 1 - 2 °C and/or the ventilation requirements at the climate computer (i.e. T1, T2 and T3, Table 5.1) compared to the reference strategy in Flanders (CON) did not affect the overall pig performance with respect to the average daily feed intake, daily gain, gain/feed ratio and lean meat percentage (chapter 5). Furthermore, the overall pig performance in all the treatments agree with those reported in commercial piggeries in Flanders (AHDB, 2017). Therefore, in line with the second research question of this PhD dissertation, the above results indicate that the thermal conditions and air quality of the changed VCSs had a negligible effect on the pig performance.

Indeed, the indoor air quality with respect to the CO_2, NH_3 and the relative humidity in the three new VCSs met the recommended indoor exposure limits for both the pigs and the farmer's working environment (Table 1.1). For example, the hourly average room temperature rose in T1, T2 and T3 by only 0.9 - 1.4 °C compared to the CON (23.7 °C), which is within the pigs' thermal requirements (Baxter, 1984; ASAE, 1986). In addition, the hourly average NH_3 and CO_2 concentrations in all the treatments were within the maximum exposure limits of 25 ppm for NH_3 and 3000 ppm for the CO_2 concentration (CIGR, 1984). This is because the hourly average NH_3 and CO_2 concentrations were below 18.0 ppm and 2000 ppm, respectively in all the treatments. The hourly average relative humidity in all the treatments ranged from 61.6 to 62.5%, which is also within the recommended RH value of 40 - 80% for livestock housing (CIGR, 1984).

8.5. Sampling strategies for assessing emission factors

The NEC Directive highlights the importance of EU Member States to report air emission inventories for assessing the progress and to ascertain whether they comply with their commitments to reducing atmospheric emissions. One of the reliable sources of data for reporting the emission inventories is through field measurements of the pollutant’s emission factor. Therefore, determining the emission factor of pollutants for new emission reduction techniques allows researchers to submit to policy makers the abatement efforts of the new techniques for verification.

However, due to the high measurement and labour costs in emission measurements from livestock housing, several protocols with reduced sampling days have been proposed in literature (Vranken et al., 2004; Dekock et al., 2009; Mosquera and Ogink, 2011; Kafle et al., 2018). The VERA measurement protocol (2018) is among the popular emission assessment tools in livestock housing. The experimental design and sampling strategy options in the VERA protocol propose a minimum of six, 24-hour sampling days per farm over the year, taking into account the between and within farm variations, diurnal and seasonal variations and the linear increase of fattening pigs weight to calculate the emission rates.

This PhD research tested the reliability of this aspect of the VERA protocol by comparing the percentage reductions in the NH_3 emission from three new VCSs compared to the CON in the field measurements (chapter 5) by randomly selecting 20 different, six 24-hour measurement days. The NH_3 emission factors for each of the randomly selected six measurement days of each treatment was then compared with the yearly average NH_3 emission calculation with all the measurement days during the entire measurement. The results showed variations in the yearly average NH_3 emission difference between T1, T2, T3 and the CON by 8% to -23%, 23% to -6% and 14% to -6% for the 20 different emission factors. Compared to yearly average NH_3 emission calculation which used all the measurement days, the NH_3 emission difference between T1, T2, T3 and the CON was -11%, 0% and +2%, respectively.

As indicated in chapter 5, the large variations in NH_3 emission difference using the VERA protocol were due to the fact that the T_{GC}, ΔT, V_{phase} and their interactions with the VCS influenced the diurnal and seasonal variations of the NH_3 emissions in the pig barn. To our knowledge, this is one of the first field measurements to explore in detail the impact of VCS as an emission reduction technique and thus applying a similar strategy on a source oriented emission reduction techniques such as slurry acidification may not present a similar result. Nonetheless, the variations in the NH_3 emission from the randomly selected six measurement days confirm the concerns in the recent VERA report that the ‘at least six measurement days’ in their previous VERA report was sometimes misunderstood in practice. Thus, the recent VERA report highlighted the need to increase the number of measurement days from six depending on the test set-up to determine the pollutant emissions appropriately. Nevertheless, there is still a lack of information about the ideal number of days for adequately determining the pollutant emission. Thus, it is imperative in this field of research to develop an ideal protocol for accurately determining the emission factors of pollutant in livestock housing with reduced sampling time and frequency to reduce the measurement costs.

The dataset in this PhD thesis could be used to further explore optimal sampling strategies. For example, the optimal sampling strategies could be explored by increasing the total sampling days from the six 24-h measurement days and varying the total number of the measurement days in the first (i.e. 0 – 50%) and second half (i.e. 50 – 100%) of the fattening period as well as the seasonal distribution of the measurement days within the year. In addition, additional emission measurements should be taken at other farm locations instead of measuring in the single farm to correct the between farm variations and to improve the applicability of the measured emission factors to other farms.

8.6. Future perspectives

The test platform had fixed heat production from the mock-up pigs and the urea solution was applied at a constant frequency every 3 hours. Therefore, it could be interesting in future to optimise the NH_3 emission performance in the test platform compartments by modulating the heat production, urination frequency and the wetted floor area to simulate diurnal pig activity and urination behaviour throughout the day.

The ventilation requirements in pig barns depend on the air inlet type (Klimaatplatform varkenshouderij, 2008, Table 1.2). As a result, the air inlet type affects the indoor air distribution and pollutant emissions (De Praetere & Van Der Biest, 1990; Zong et ql., 2014). Therefore, the effect of the ventilation control settings that was performed in this PhD research should be tested in pig barns with other air inlet types in order to broaden the applicability of the results in the present investigation.

The level of energy use in intensive pig farming is important not only because it contributes to the total operating costs but also to emission of GHG, which contribute to global warming. Therefore, as the new VCSs resulted in 14 - 30% reduction in the hourly ventilation rate compared to the reference strategy (chapter 5), the cost of electricity and pig performance due to the VCSs should be carried out in future experiments to demonstrate the ventilation control strategy holistically as a low-cost management-based technique.

Airflow patterns are difficult to monitor in livestock buildings; therefore, new control algorithms could introduce T_{GC} and ΔT, which are easy to monitor as additional ventilation control parameters in the climate computer. Controlling the airflow in the pig barn at the optimal T_{GC} and ΔT may minimise the slurry pit air exchange rate and pollutant emissions in pig barns with UFAD systems. In addition, the optimal T_{GC} and ΔT could be achieved by pre-conditioning the supply air to the compartment (i.e. T_{GC}) via supplementary heating in winter and by fogging in summer.

The CFD model assumed that all pigs lay fixed in a sternum position and in a regular pattern, which was not the case in the compartment occupied by the real pigs. In addition, the CFD model assumed the same floor fouling area for all pens, located close to the service alley, which was not the case in the compartment with the real pigs. Therefore, it would be interesting in future simulations to examine the effect of pig location, pen fouling area and location on the NH_3 emissions.

Additionally, the porous media assumption at the slatted floor inlet in the CFD model underestimated the air speed exiting the slatted floor, the heat transport in slats, and the air mixing above the slatted floor at the UFAC compared to the experiment. The porous media assumption could also affect the airflow in the slurry pit and the predicted NH_3 emissions in this PhD investigation. Hence, to validate the results of this PhD study, two-dimensional CFD model of the investigated pig compartment with detailed slatted floor geometry could be carried out.

References

Aarnink, A., van de Pas, L., van der Peet-Schwering, C., Hol, A., Binnendijk, G., Le Dinh, P., ... & Ogink, N. (2018). Rekentool voor het bepalen van de effecten van voer-en management-maatregelen op de ammoniakemissie bij varkens: ontwikkeling en validatie (No. 1086). Wageningen Livestock Research.

Aarnink, A. J. (2018). Heat and moisture production in growing-finishing pigs and broilers. *Agricultural Engineering International: CIGR Journal*.

Aarnink, A. J. A., & Elzing, A. (1998). Dynamic model for ammonia volatilization in housing with partially slatted floors, for fattening pigs. *Livestock production science, 53(2),* 153-169.

Aarnink, A. J. A., & Wagemans, M. J. M. (1997). Ammonia volatilization and dust concentration as affected by ventilation systems in houses for fattening pigs. *Transactions of the ASAE, 40(4),* 1161-1170.

Aarnink, A. J. A., Keen, A., Metz, J. H. M., Speelman, L., & Verstegen, M. W. A. (1995). Ammonia emission patterns during the growing periods of pigs housed on partially slatted floors. *Journal of Agricultural Engineering Research*, *62*(2), 105-116.

Aarnink, A. J. A., Schrama, J. W., Heetkamp, M. J. W., Stefanowska, J., & Huynh, T. T. T. (2006). Temperature and body weight affect fouling of pig pens. *Journal of animal science*, *84*(8), 2224-2231.

Aarnink, A. J. A., Swierstra, D., Van den Berg, A. J., & Speelman, L. (1997). Effect of type of slatted floor and degree of fouling of solid floor on ammonia emission rates from fattening piggeries. *Journal of Agricultural Engineering Research*, *66*(2), 93-102.

Aarnink, A. J. A., Van den Berg, A. J., Keen, A., Hoeksma, P., & Verstegen, M. W. A. (1996). Effect of slatted floor area on ammonia emission and on the excretory and lying behaviour of growing pigs. *Journal of Agricultural Engineering Research*, *64*(4), 299-310.

Adrion, F., Threm, J., Gallmann, E., Pflanz, W., & Jungbluth, T. (2013). Simulation of airflow in pig fattening houses with different air supply systems. *landtechnik*, *68*, 2.

Agriculture and Horticulture Development Board (AHDB) (2018). 2017 pig cost of production in selected countries. AHDB Pork, Warwickshire, UK.

Akdeniz, N., Jacobson, L. D., Hetchler, B. P., Bereznicki, S. D., Heber, A. J., Koziel, J. A., ... & Parker, D. B. (2012). Odor and odorous chemical emissions from animal buildings: Part 2. Odor emissions. *Transactions of the ASABE*, *55*(6), 2335-2345.

Albright, L. D. (1989). Slotted inlet baffle control based on inlet jet momentum numbers. *Transactions of the ASAE*, *32*(5), 1764-1768.

Albright, L. D., & Scott, N. R. (1974). An Analysis of Steady Periodic Building Temperature Variations in Warm Weather Part I: A Mathematical Model. *Transactions of the ASAE*, *17*(1), 88-0092.

Albright, L.D. 1990. Environment control for animals and plants. ASAE Textbook Nr. 4, St. Joseph: American Society of Agricultural Engineers.

Alexandratos, N., & Bruinsma, J. (2012). *World Agriculture Towards 2030/2050: The 2012 Revision* (Food and Agriculture Organization of The United Nations, Rome).

American Society of Agricultural Engineers (ASAE). 1986, Revised 2017. Design of Ventilation Systems for Poultry and Livestock Shelters. ASAE EP 270.5 DEC1986 (R2017).

Anderson, J. D. (1995). Computational fluid dynamics: the basics with applications. *Mechanical Engineering Series. McGraw-HILL, Inc*.

Anthony, T. R., Altmaier, R., Park, J. H., & Peters, T. M. (2014). Modeled effectiveness of ventilation with contaminant control devices on indoor air quality in a swine farrowing facility. *Journal of occupational and environmental hygiene*, *11*(7), 434-449.

Arogo, J., Zhang, R. H., Riskowski, G. L., Christianson, L. L., & Day, D. L. (1999). Mass transfer coefficient of ammonia in liquid swine manure and aqueous solutions. *Journal of Agricultural Engineering Research, 73(1),* 77-86.

BAM/deel 3/05, (2015). Sampling and analysis methods for manure, soil and animal feed in the context of the manure decree (in Dutch: Bemonsterings- en analysemethodes voor mest, bodem en veevoeder in het kader van het mestdecreet). https://esites.vito.be/sites/reflabos/2015/Online%20documenten/BAM-deel3-05.pdf (accessed 22 February 2018)

Baxter, S. (1984). *Intensive pig production: environmental management and design*. Granada Technical Books.

Berckmans, D., & Goedseels, V. (1986). Development of new control techniques for the ventilation and heating of livestock buildings. *Journal of Agricultural Engineering Research*, *33*(1), 1–12.

Bilsen, I., Moonen, N., Aerts, W., Baeyens, B., & Van Laer J. (2016). Measurement Campaign for the Determination of Odor Emission Factors for Sows (in Dutch: Meetcampagne Voor De Bepaling Van Geuremissiefactoren Voor Zeugen). VITO NV, Mol, Belgium.

Bittman, S., Dedina, M., Howard, C. M., Oenema, O., & Sutton, M. A. (2014). Options for ammonia mitigation: Guidance from the UNECE Task Force on Reactive Nitrogen. NERC/Centre for Ecology & Hydrology.

Bjerg, B. (2011). CFD Analyses of Methods to Improve Air Quality and Efficiency of Air Cleaning in Pig Production. In *Chemistry, emission control, radioactive pollution and indoor air quality*. IntechOpen.

Bjerg, B., & Andersen, M. (2010, June). Numerical simulation of a pit exhausts system for reduction of ammonia emission from a naturally ventilated cattle building. In XVIIth World Congress of the International Commission of Agricultural and Biosystems Engineering (CIGR), Quebec City, Canada.

Bjerg, B., & Zhang, G. Q. (2013, July). CFD analyses of the influence of ventilation system on the effectiveness of a partial pit exhaust. In Ist International Symposium on CFD Applications in Agriculture 1008 (pp. 143-150).

Bjerg, B., Cascone, G., Lee, I. B., Bartzanas, T., Norton, T., Hong, S. W., ... & Zhang, G. (2013). Modelling of ammonia emissions from naturally ventilated livestock buildings. Part 3: CFD modelling. Biosystems Engineering, 116(3), 259-275.

Bland, J. M., & Altman, D. (1986). Statistical methods for assessing agreement between two methods of clinical measurement. The lancet, 327(8476), 307-310.

Blanes, V., & Pedersen, S. (2005). Ventilation flow in pig houses measured and calculated by carbon dioxide, moisture and heat balance equations. *Biosystems Engineering*, *92*(4), 483-493.

Blanes-Vidal, V., Hansen, M. N., Pedersen, S., & Rom, H. B. (2008). Emissions of ammonia, methane and nitrous oxide from pig houses and slurry: Effects of rooting material, animal activity and ventilation flow. *Agriculture, Ecosystems & Environment, 124(3),* 237-244.

Bliss, P. J., Jiang, K., & Schulz, T. J. (1995). The development of a sampling system for the determination of odor emission rates from areal surfaces: Part II. Mathematical model. Journal of the Air & Waste Management Association, 45(12), 989-994.

Blunden, J., Aneja, V. P., & Westerman, P. W. (2008). Measurement and analysis of ammonia and hydrogen sulfide emissions from a mechanically ventilated swine confinement building in North Carolina. Atmospheric environment, 42(14), 3315-3331.

Bond, T. E., C. F. Kelly, and Hubert Heitman. Hog house air conditioning and ventilation data. (1959): 1-0004.

Botermans, J., & Jeppsson, K. H. (2008). Measurements of the indoor climate during winter time in a pig house with ground channel ventilation. *In Agricultural and biosystems engineering for a sustainable world*. International Conference on Agricultural Engineering, Hersonissos, Crete, Greece, 23-25 June, 2008. European Society of Agricultural Engineers (AgEng).

Braam, C. R., Ketelaars, J. J. M. H., & Smits, M. C. J. (1997a). Effects of floor design and floor cleaning on ammonia emission from cubicle houses for dairy cows. NJAS wageningen journal of life sciences, 45(1), 49-64.

Braam, C. R., Smits, M. C. J., Gunnink, H., & Swierstra, D. (1997b). Ammonia emission from a double-sloped solid floor in a cubicle house for dairy cows. Journal of Agricultural Engineering Research, 68(4), 375-386.

Breum, N. O., Takai, H., & Rom, H. B. (1990). Upward vs. downward ventilation air flow in a swine house. *Transactions of the ASAE*, 33(5), 1-1699.

Brown-Brandl, T. M., Eigenberg, R. A., Nienaber, J. A., & Kachman, S. D. (2001). Thermoregulatory profile of a newer genetic line of pigs. *Livestock production science*, *71*(2-3), 253-260.

Brown-Brandl, T. M., Hayes, M. D., Xin, H., Nienaber, J. A., Li, H., Eigenberg, R. A., Stinn, J.P. & Shepherd, T. (2014). Heat and moisture production of modern swine. ASHRAE Transactions 120 (2014): 469.

Brown-Brandl, T. M., Nienaber, J. A., Xin, H., & Gates, R. S. (2004). A literature review of swine heat production. *Transactions of the ASAE*, *47*(1), 259.

Canh, T. T., Verstegen, M. W. A., Aarnink, A. J. A., & Schrama, J. W. (1997). Influence of dietary factors on nitrogen partitioning and composition of urine and feces of fattening pigs. *Journal of Animal Science, 75,* 700–706.

CEN. (2003). Air Quality. Determination of odour concentration by dynamic olfactometry (EN 13725:2003). *European Committee for Standardization*.

Chepete, H. J., & Xin, H. (2004). Ventilation rates of a laying hen house based on new vs. old heat and moisture production data. *Applied Engineering in Agriculture*, *20*, 835–842.

CIGR. (2002). Report of Working Group Climatization of Animal Houses — Heat and moisture production at Animal and House

Levels. *CIGR Section II, International Commission of Agricultural Engineering*.

Commission Internationale du Genie Rural (CIGR) (1984). Climatization of animal houses. Report of working group, CIGR, Scottish Farm Buildings Investigation Unit, Aberdeen.

Cooper, K., Parsons, D. J., & Demmers, T. (1998). A thermal balance model for livestock buildings for use in climate change studies. *Journal of Agricultural Engineering Research*, *69*(1), 43-52.

Cortus, E. L., Lemay, S. P., Barber, E. M., Hill, G. A., & Godbout, S. (2008). A dynamic model of ammonia emission from urine puddles. *Biosystems Engineering, 99(3),* 390-402.

Craig, B. A., & Schinckel, A. P. (2001). Nonlinear mixed effects model for swine growth. The Professional Animal Scientist, 17(4), 256-260.

De Paepe, M., Pieters, J. G., Cornelis, W. M., Gabriels, D., Merci, B., & Demeyer, P. (2012). Airflow measurements in and around scale model cattle barns in a wind tunnel: Effect of ventilation opening height. *Biosystems engineering*, *113*(1), 22-32.

De Paepe, M., Pieters, J. G., Cornelis, W. M., Gabriels, D., Merci, B., & Demeyer, P. (2013). Airflow measurements in and around scale-model cattle barns in a wind tunnel: Effect of wind incidence angle. *biosystems engineering*, *115*(2), 211-219.

De Paepe, M., Pieters, J. G., Mendes, L. B., Van Weyenberg, S., Merci, B., & Demeyer, P. (2016). Wind tunnel study of ammonia transfer from a manure pit fitted with a dairy cattle slatted floor. *Environmental technology, 37(2),* 202-215.

De Praetere, K., & Van Der Biest, W. (1990). Airflow patterns in piggeries with fully slatted floors and their effect on ammonia distribution. *Journal of Agricultural Engineering Research, 46,* 31-44.

De Pue, D., & Buysse, J. (2019). *Safeguarding Natura 2000 habitats from nitrogen deposition by tackling ammonia emissions from livestock facilities* (No. 2230-2019-1980).

De Pue, D., Roet, D., Lefebvre, W., & Buysse, J. (2017). Mapping impact indicators to link airborne ammonia emissions with nitrogen deposition in Natura 2000 sites. *Atmospheric environment*, *166*, 120-129.

Deglin, D., Van Caenegem, L., & Dehon, P. (1999). Subsoil heat exchangers for the air conditioning of livestock buildings. *Journal of agricultural engineering research*, *73*(2), 179-188.

Dekock, J., Vranken, E., Gallmann, E., Hartung, E., & Berckmans, D. (2009). Optimisation and validation of the intermittent measurement method to determine ammonia emissions from livestock buildings. *Biosystems engineering*, *104*(3), 396-403.

Delva, P. (2012). Aandachtspunten bij kanaalventilatie. Retrieved from http://www.vda-ooigem.be/nl/aandachtspunten-bij-kanaalventilatie-205.htm.

Detchanamurthy, S., & Gostomski, P. A. (2012). Biofiltration for treating VOCs: an overview. *Reviews in Environmental Science and Bio/Technology*, *11*(3), 231-241.

Ding, L., Li, Q., Wang, C., Zhang, G., Jiang, R., Yu, L., ... & Shi, Z. (2020). Determination of the mass transfer coefficient of ammonia emissions from dairy open lots using a scale model. Biosystems Engineering, 190, 145-156.

DLV-Belgium (2014). (Personal communication).

Donham, K. J., Thorne, P. S., Breuer, G. M., Powers, W., Marquez, S., & Reynolds, S. (2002). Exposure limits related to air quality and risk assessment. *Iowa concentrated animal feeding operations air quality study*, 164.

Drewry, J. L., Choi, C. Y., Powell, J. M., & Luck, B. D. (2018). Computational model of methane and ammonia emissions from dairy barns: Development and validation. *Computers and electronics in agriculture*, 149, 80-89.

EC (2017). Commission implementing decision (EU) 2017/302 of 15 February 2017 establishing best available techniques (BAT) conclusions, under Directive 2010/75/EU of the European Parliament and of the Council, for the intensive rearing of poultry or pigs.*Off. J. Eur. Union* 2017, L43, 231–279.

Eça, L., & Hoekstra, M. (2006, October). Discretization uncertainty estimation based on a least squares version of the grid convergence index. In *Proceedings of the Second Workshop on CFD Uncertainty Analysis, Instituto Superior Tecnico, Lisbon, Oct*.

EEA, (2018). European Union emission inventory report 1990-2016 under the UNECE Convention on Long-range Transboundary Air Pollution (LRTAP) (No 6/2018). European Environment Agency, Copenhagen, Denmark.

EN 14793 (2017) Stationary source emissions – Demonstration of equivalence of an alternative method with a reference method.

Erisman, J. W., & Schaap, M. (2004). The need for ammonia abatement with respect to secondary PM reductions in Europe. *Environmental Pollution*, *129*(1), 159-163.

Etheridge, D. W., & Sandberg, M. (1996). *Building ventilation: theory and measurement* (Vol. 50). Chichester: John Wiley & Sons.

Eurostat Database (2019). https://ec.europa.eu/eurostat/data/database, Accessed in August 2019.

Fabrizio, E., Airoldi, G., & Chiabrando, R. (2014). Proceedings of the 8th International Symposium on Heating, Ventilation and Air

Conditioning, 263, 3–11.

Fabrizio, E., Airoldi, G., & Chiabrando, R. (2014). Study of the environmental control of sow farrowing rooms by means of dynamic simulation. In *Proceedings of the 8th International Symposium on Heating, Ventilation and Air Conditioning* (pp. 3-11). Springer, Berlin, Heidelberg.

Faulkner, D., Fisk, W. J., & Sullivan, D. P. (1995). Indoor airflow and pollutant removal in a room with floor-based task ventilation: results of additional experiments. *Building and Environment*, *30*(3), 323-332.

Feilberg, A., Liu, D., Adamsen, A. P., Hansen, M. J., & Jonassen, K. E. (2010). Odorant emissions from intensive pig production measured by online proton-transfer-reaction mass spectrometry. *Environmental Science & Technology*, 44(15), 5894-5900.

Flanders Environment Report (2017). MIRA system balance 2017: Environmental challenges for the energy, mobility and food systems in Flanders. Available: http://milieurapport.be/en/publications/other-reports/mira-system-balance-2017-environmental-challenges-for-the-energy-mobility-and-food-systems.

Galloway, J. N., Townsend, A. R., Erisman, J. W., Bekunda, M., Cai, Z., Freney, J. R., & Sutton, M. A. (2008). Transformation of the nitrogen cycle: recent trends, questions, and potential solutions. *Science,* 320(5878), 889-892.

Gilani, S., Montazeri, H., & Blocken, B. (2016). CFD simulation of stratified indoor environment in displacement ventilation: Validation and sensitivity analysis. *Building and Environment, 95*, 299-313.

Granier, R., Guingand, N., & Massabie, P. (1996). Influence of hygrometry, temperature and airflow rate on the evolution of ammonia levels. *In 28. Journees de la Recherche Porcine 28,* 209–216.

Haeussermann A., Jungbluth T., & Hartung, E. (2006). NH_3 emission from pig husbandry in relation to ventilation control and indoor air cooling. *In Proceedings of The Workshop on Agricultural Air Quality: Washington DC, USA* (pp. 5-8).

Haeussermann, A., Vranken, E., Aerts, J. M., Hartung, E., Jungbluth, T., & Berckmans, D. (2007). Evaluation of control strategies for fogging systems in pig facilities. *Transactions of the ASABE*, *50*(1), 265-274.

Hafner, S. D., Montes, F., & Rotz, C. A. (2013). The role of carbon dioxide in emission of ammonia from manure. *Atmospheric environment, 66*, 63-71.

Hansen, M. J. (2011). Significance of reduced sulphur compunds in relation to odour from pig production (Doctoral dissertation, Aarhus University).

Harmon, J. D., Brumm, M. C., Jacobson, L. D., Pohl, S. H., Stender, D. R., & Stowell, R. R. (2012). Field performance evaluation of a ventilation system: A swine case study. *Applied engineering in agriculture, 28(2),* 251-257.

He, M., Guo, Y., Zhong, Q., & Zhang, Y. (2010). Determination of binary gas diffusion coefficients using digital holographic interferometry. J*ournal of Chemical & Engineering Data, 55(9)*, 3318-3321.

Health and Safety Executive (HSE), (2018). EH40/2005 Workplace Exposure Limits. Third edition, published 2018. Retrieved 18/08/2019, from http://www.hse.gov.uk/pUbns/priced/eh40.pdf.

Herrero, M., Thornton, P. K., Gerber, P., & Reid, R. S. (2009). Livestock, livelihoods and the environment: understanding the trade-offs. *Current Opinion in Environmental Sustainability*,*1*(2), 111-120.

Hessel, E. F., Zurhake, C., & Van Den Weghe, H. F. (2010). Heating and cooling performance of an under floor earth tube air tempering system in a mechanical ventilated farrowing house. In Proceedings of the XVIIth World Congress of the International Commission of Agricultural and Biosystems Engineering (CIGR) (pp. 1-8).

Heyes, E. T., Curran, T. P., & Dodd, V. A. (2006). Odour and ammonia emissions from intensive poultry units in Ireland. *Bioresource technology*, *97*(7), 933-939.

Hoeksma, P., Verdoes, N., Oosthoek, J., & Voermans, J. A. M. (1992). Reduction of ammonia volatilization from pig houses using aerated slurry as recirculation liquid. *Livestock Production Science*, *31*(1), 121-132.

Hoff, S. J., D. Van Utrecht, J. D. Harmon, and D. W. Mangold. 2000. A general purpose laboratory for evaluating livestock ventilation systems. *Applied Engineering in Agriculture*, 16(6): 701.

Hove, N. (2018). Evaluating and optimising dynamic olfactometry for the measurement of odour concentrations in pig house emissions (Doctoral dissertation, Ghent University).

Hu, E., Babcock, E. L., Bialkowski, S. E., Jones, S. B., & Tuller, M. (2014). Methods and techniques for measuring gas emissions from agricultural and animal feeding operations. *Critical reviews in analytical chemistry*, *44*(3), 200-219.

Huynh, T. T. T., Aarnink, A. J. A., Gerrits, W. J. J., Heetkamp, M. J. H., Canh, T. T., Spoolder, H. A. M., ... & Verstegen, M. W. A. (2005a). Thermal behaviour of growing pigs in response to high temperature and humidity. Applied animal behaviour science, 91(1-2), 1-16.

Huynh, T. T. T., Aarnink, A. J. A., Verstegen, M. W. A., Gerrits, W. J. J., Heetkamp, M. J. W., Kemp, B., & Canh, T. T. (2005b). Effects of increasing temperatures on physiological changes in pigs at different relative humidities. Journal of Animal

Science, 83(6), 1385-1396.

Jeppsson, K. H., & Botermans, J. (2014). Dust levels depending on ventilation system in buildings for growing finishing pigs. *In Proceedings International Conference of Agricultural Engineering (AgEng). Zurich, Switzerland* (pp. 1-6).

Juska, A. (2010). "Profits to the Danes, for us–hog stench?" The campaign against Danish swine CAFOs in rural Lithuania. *Journal of rural studies, 26(3)*, 250-259.

Kafle, G. K., Joo, H., & Ndegwa, P. M. (2018). Sampling Duration and Frequency for Determining Emission Rates from Naturally Ventilated Dairy Barns. *Transactions of the ASABE*, 61(2): 681-691.

Kai, P., Kaspers, B., & Van Kempen, T. (2006). Modeling sources of gaseous emissions in a pig house with recharge pit. *Transactions of the ASABE*, *49*(5), 1479-1485.

Kang, G., Kim, J. J., Kim, D. J., Choi, W., & Park, S. J. (2017). Development of a computational fluid dynamics model with tree drag parameterizations: Application to pedestrian wind comfort in an urban area. *Building and Environment*, *124*, 209-218.

Kavolelis, B. (2003). Influence ventilation rate on ammonia concentration and emission in animal house. Polish Journal of Environmental Studies, 12(6), 709-712.

Kearney, J. (2010). Food consumption trends and drivers. *Philosophical transactions of the royal society B: biological sciences*, *365*(1554), 2793-2807.

Kelly, T. G., Dodd, V. A., & Ruane, D. J. (1986). Ventilation and air flow patterns in climatic calf houses. *Journal of Agricultural Engineering Research*, *33*(3), 187-203.

Kim, K. Y., Ko, H. J., Kim, H. T., Kim, Y. S., Roh, Y. M., & Kim, C. N. (2007). Effect of ventilation rate on gradient of aerial contaminants in the confinement pig building. *Environmental research*, *103*(3), 352-357.

Klimaatplatform varkenshouderij (2008). Richtlijnen klimaatinstellingen.

Klimaatplatform varkenshouderij (2013). Leaflets klimaatsystemen.Grondkanaalventilatie via controlegang

Klimaatplatform varkenshouderij. (2006). *Leaflets klimaatsystemen. Grondkanaalventilatie via controlegang*.

Kool, D. M., E. Hoffland, S. P. Abrahamse, and J. W. Van Groenigen. 2006. What artificial urine composition is adequate for simulating soil N2O fluxes and mineral N dynamics? *Soil Biology and Biochemistry*, 38(7): 1757-1763.

Krishnan, P. V. (1965). Spacing of buildings for natural ventilation. *Transactions of the American Society of Agricultural Engineering*, *8*, 208-215.

Krommweh, M. S., Rösmann, P., & Büscher, W. (2014). Investigation of heating and cooling potential of a modular housing system for fattening pigs with integrated geothermal heat exchanger. *Biosystems Engineering*, *121*, 118-129.

Kuczyński, T., & Przybyła, K. (2002). Porous ceiling air inlet as a potential source of uncontrolled air exchange at nurseries with exhaust mechanical ventilation. *Agricultural Engineering*, *5*(1), 02.

Kwon, K. S., Lee, I. B., Zhang, G. Q., & Ha, T. (2015). Computational fluid dynamics analysis of the thermal distribution of animal occupied zones using the jet-drop-distance concept in a mechanically ventilated broiler house. *Biosystems Engineering*, 136, 51-68.

Labussière, E., S. Dubois, J. van Milgen, and J. Noblet. 2013. Partitioning of heat production in growing pigs as a tool to improve the determination of efficiency of energy utilization. *Frontiers in Physiology*, 4: 146.

Lee, K., Zhang, T., Jiang, Z., & Chen, Q. (2009). Comparison of airflow and contaminant distributions in rooms with traditional displacement ventilation and under-floor air distribution systems. *ASHRAE Transactions*, *115*(2), 306-321.

Leen F., Van den Broeke A., Aluwé M., Ampe B., Lauwers L., Van Meensel J., & Millet S. (2016). Performance curves for growing finishing pigs: evaluation of published growth models. European Federation of Animal Science Annual Meeting, Belfast, UK.

Lehmann, B., Baumeister, J., & Klindtworth, K. (2011). Use of a high-pressure water spraying system for cooling fattening pig houses. *Landtechnik*, *66*(3), 191-193.

Leonard, J. J., & McQuitty, J. B. (1986). Archimedes number criteria for the control of cold ventilation air jets. *Canadian Agricultural Engineering*, *28*(2), 117-123.

Lin, Y. J. P., & Tsai, T. Y. (2014). An experimental study on a full-scale indoor thermal environment using an Under-Floor Air Distribution system. *Energy and Buildings, 80*, 321-330.

Loyon, L., Burton, C. H., Misselbrook, T., Webb, J., Philippe, F. X., Aguilar, M., & Bonmati, A. (2016). Best available technology for European livestock farms: Availability, effectiveness and uptake. *Journal of Environmental Management, 166*, 1-11.

Lu, Y., Hayes, M., Stinn, J. P., Brown-Brandl, T., & Xin, H. (2017). Evaluating ventilation rates based on new heat and moisture production data for swine production. *Transactions of the ASABE*, *60*(1), 237-245.

Lyngbye, M., Riis, A. L., & Feilberg, A. (2006). Luftskiftets betydning for lugt-og ammoniak emission fra slagtesvinestalde (In Danish). The significance of air change on odor and ammonia emission from growing pig units) Meddelelse, 756.

Mackie, R. I., Stroot, P. G., & Varel, V. H. (1998). Biochemical identification and biological origin of key odor components in livestock waste. *Journal of Animal Science*, *76*(5), 1331-1342.

Maghirang, R. G., Jerez, S. B., & Predicala, B. Z. (2001). Relative ventilation effectiveness in a mechanically ventilated airspace under isothermal conditions. *Transactions of the ASAE*, *44*(3), 691.

Maghirang, R. G., Manbeck, H. B., & Puri, V. M. (1994). Numerical simulation of particle transport in slot-inlet ventilated airspaces. *Transactions of the ASAE*, *37*(5), 1607-1612.

Marquer, P., Rabade, T., & Forti, R. (2014). *Pig farming in the European Union: considerable variations from one Member State to another. Pig farming sector—statistical portrait*.

Meisinger, J. J., & Jokela, W. E. (2000). Ammonia volatilization from dairy and poultry manure. Proceedings from Managing Nutrients and Pathogens from Animal Agriculture, 334-354.

Menconi, M. E., Grohmann, D., & Borghi, P. (2014). Dynamic thermal simulation on retrofitting scenarios for semi-extensive sheep farms. *Journal of Agricultural Engineering*, 45(2), 80.

Mendes, L. B., Pieters, J. G., Snoek, D., Ogink, N. W., Brusselman, E., & Demeyer, P. (2017). Reduction of ammonia emissions from dairy cattle cubicle houses via improved management-or design-based strategies: A modeling approach. *Science of the Total Environment*, *574*, 520-531.

Mol, G., & Ogink, N. W. M. (2003). The effects of three pig housing systems on odor emission. *In Air Pollution from Agricultural Operations-III (p. 1). American Society of Agricultural and Biological Engineers.*

Montes, F., Rotz, C. A., & Chaoui, H. (2009). Process modeling of ammonia volatilization from ammonium solution and manure surfaces: a review with recommended models. Transactions of the ASABE, 52(5), 1707-1720.

Morsing, S., Strøm, J. S., Zhang, G., & Kai, P. (2008). Scale model experiments to determine the effects of internal airflow and floor design on gaseous emissions from animal houses. *Biosystems Engineering, 99(1)*, 99-104.

Mosquera, J., & Ogink, N. W. M. (2011). Reducing the sampling periods required in protocols for establishing ammonia emissions from pig fattening buildings using measurements and modelling. *Biosystems engineering*, *110*(2), 90-96.

Müller, H. J., Stollberg, U., &Venzlaff, F W. (2005). Geothermal Heat Exchanger in Sow Breeding Houses: A Possibility to Improve the Climate Parameters in Pig Houses and Reduce Emissions. landtechnik, *60*, 4.

Ngwabie, N. M., Jeppsson, K. H., Nimmermark, S., & Gustafsson, G. (2011). Effects of animal and climate parameters on gas emissions from a barn for fattening pigs. *Applied engineering in agriculture, 27(6)*, 1027-1037.

Ni, J. (1999). Mechanistic models of ammonia release from liquid manure: a review. Journal of Agricultural Engineering Research, 72(1), 1-17.

Ni, J. Q., & Heber, A. J. (2001). Sampling and measurement of ammonia concentration at animal facilities – A review. ASAE Paper No. 01-4090. St. Joseph, Mich.: ASAE.

Ni, J. Q., Hendriks, J., Vinckier, C., & Coenegrachts, J. (2000). Development and validation of a dynamic mathematical model of ammonia release in pig house. Environment international, 26(1-2), 105-115.

Ni, J. Q., Vinckier, C., Coenegrachts, J., & Hendriks, J. (1999). Effect of manure on ammonia emission from a fattening pig house with partly slatted floor. Livestock production science, 59(1), 25-31.

Ni, J. Q., Vinckier, C., Coenegrachts, J., & Hendriks, J. (1999b). Effect of manure on ammonia emission from a fattening pig house with partly slatted floor. *Livestock production science*, *59(1)*, 25-31.

Ni, J. Q., Vinckier, C., Hendriks, J., & Coenegrachts, J. (1999a). Production of carbon dioxide in a fattening pig house under field conditions. II. Release from the manure. *Atmospheric Environment, 33(22)*, 3697-3703.

Nielsen, P. V. (2000). Velocity distribution in a room ventilated by displacement ventilation and wall-mounted air terminal devices. *Energy and Buildings*, *31*(3), 179-187.

Nienaber, J. A., Hahn, G. L., & Eigenberg, R. A. (1997a). Development of an upper temperature threshold for livestock. *ASAE Paper*, *974010*.

Nienaber, J. A., Hahn, G. L., Eigenberg, R. A., Korthals, R. L., Yen, J. T., & Harris, D. L. (1997b). Genetic and heat stress interaction effects on finishing swine. *Livestock environment V*, *2*.

Nimmermark, S., & Gustafsson, G. (2005). Influence of temperature, humidity and ventilation rate on the release of odour and ammonia in a floor housing system for laying hens. *Agricultural Engineering International: the CIGR Ejournal.* Vol. VII. Manuscript BC 04 008.

Norton, T., Grant, J., Fallon, R., & Sun, D. W. (2009). Assessing the ventilation effectiveness of naturally ventilated livestock buildings under wind dominated conditions using computational fluid dynamics. *Biosystems Engineering*, *103*(1), 78-99.

Norton, T., Grant, J., Fallon, R., & Sun, D. W. (2010). Improving the representation of thermal boundary conditions of livestock during CFD modelling of the indoor environment. *Computers and Electronics in Agriculture, 73(1),* 17-36.

Norton, T., Sun, D. W., Grant, J., Fallon, R., & Dodd, V. (2007). Applications of computational fluid dynamics (CFD) in the modelling and design of ventilation systems in the agricultural industry: A review. *Bioresource technology, 98(12)*, 2386-2414.

Ogink, N. W. M., & Groot Koerkamp, P. W. G. (2001). Comparison of odour emissions from animal housing systems with low ammonia emission. *Water Science and Technology, 44(9)*, 245-252.

Olesen, J. E., & Sommer, S. G. (1993). Modelling effects of wind speed and surface cover on ammonia volatilization from stored pig slurry. Atmospheric Environment. Part A. General Topics, 27(16), 2567-2574.

O'Neill, D. H., & Phillips, V. R. (1991). A review of the control of odour nuisance from livestock buildings: Part 1, influence of the techniques for managing waste within the building. *Journal of Agricultural Engineering Research*, *50*, 1-10.

O'Neill, D. H., & Phillips, V. R. (1992). A review of the control of odour nuisance from livestock buildings: Part 3, properties of the odorous substances which have been identified in livestock wastes or in the air around them. *Journal of Agricultural Engineering Research*, *53*, 23-50.

Panagakis, P., & Axaopoulos, P. (2004). Comparison of two modeling methods for the prediction of degree-hours and heat-stress likelihood in a swine building. *Transactions of the ASAE*, *47*(2), 585-590.

Panagakis, P., & Axaopoulos, P. (2006). Simulation comparison of evaporative pads and fogging on air temperatures inside a growing swine building. *Transactions of the ASABE*, *49*(1), 209-215.

Panagakis, P., & Axaopoulos, P. (2008). Comparing fogging strategies for pig rearing using simulations to determine apparent heat-stress indices. *Biosystems engineering*, *99*(1), 112-118.

Park, H. J., & Holland, D. (2001). The effect of location of a convective heat source on displacement ventilation: CFD study. *Building and environment*, *36*(7), 883-889.

Park, J. H., Peters, T. M., Altmaier, R., Sawvel, R. a., & Renée Anthony, T. (2013). Simulation of air quality and cost to ventilate swine farrowing facilities in winter. *Computers and Electronics in Agriculture*, 98, 136–145.

Paszek, D. A., Jacobson, L. D., Johnson, V. J., & Nicolai, R. E. (1998). Design and management of an oil sprinkling system to control dust, odor, and gases in and from a curtain-sided pig finishing barn. In *2001 ASAE Annual Meeting* (p. 1). American Society of Agricultural and Biological Engineers.

Pedersen, P., & Jensen, T. L. (2010). A new design for highly efficient partial pit ventilation. *XVIIth World Congress of the International Commission of Agricultural and Biosystems Engineering (CIGR).* Québec City, Canada June 13-17, 2010.

Pedersen, S., Blanes-Vidal, V., Jørgensen, H., Chwalibog, A., Haeussermann, A., Heetkamp, M. J. W., & Aarnink, A. J. A. (2008). Carbon dioxide production in animal houses: A literature review. *Agricultural Engineering International: CIGR Journal. Manuscript BC 08 008,* Vol. X.

Pedersen, S., Takai, H., Johnsen, J. O., Metz, J. H. M., Koerkamp, P. G., Uenk, G. H., ... & White, R. P. (1998). A comparison of three balance methods for calculating ventilation rates in livestock buildings. *Journal of Agricultural Engineering Research*, *70*(1), 25-37.

Petersen, S. O., Hutchings, N. J., Hafner, S. D., Sommer, S. G., Hjorth, M., & Jonassen, K. E. (2016). Ammonia abatement by slurry acidification: A pilot-scale study of three finishing pig production periods. *Agriculture, Ecosystems & Environment*, *216*, 258-268.

Philippe, F. X., & Nicks, B. (2015). Review on greenhouse gas emissions from pig houses: production of carbon dioxide, methane and nitrous oxide by animals and manure. *Agriculture, Ecosystems & Environment*, *199*, 10-25.

Philippe, F. X., Laitat, M., Canart, B., Vandenheede, M., & Nicks, B. (2007). Comparison of ammonia and greenhouse gas emissions during the fattening of pigs, kept either on fully slatted floor or on deep litter. *Livestock Science*, *111*(1-2), 144-152.

Phillips, V. R., Lee, D. S., Scholtens, R., Garland, J. A., & Sneath, R. W. (2001). A review of methods for measuring emission rates of ammonia from livestock buildings and slurry or manure stores, Part 2: monitoring flux rates, concentrations and airflow rates. *Journal of Agricultural Engineering Research*, *78*, 1-14.

Platteau, J., Lambrechts, G., Roels, K. & Van Bogaert, T. (reds.) (2018). Uitdagingen voor de Vlaamse land- en tuinbouw. Landbouwrapport 2018, Departement Landbouw en Visserij, Brussel.

Portejoie, S., Dourmad, J. Y., Martinez, J., & Lebreton, Y. (2004). Effect of lowering dietary crude protein on nitrogen excretion, manure composition and ammonia emission from fattening pigs. Livestock Production Science, 91(1-2), 45-55.

Pouliot, F., Dufour, V., Belzile, M., Feddes, J., Lemay, S., Morin, M., & Godbout, S. (2011). Impact of temperature control strategies on animal performance, gas emissions and energy requirements for grower-finisher pigs. *Journées de la Recherche Porcine en France*, *43*, 193-197.

Puma, M. C., Maghirang, R. G., Hosni, M. H., & Hagen, L. (1999). Modeling of dust concentration distribution in a simulated swine room under non-isothermal conditions. *Transactions of the ASAE*, *42*(6), 1823-1832.

R Core Team. R: A language and environment for statistical computing. R Foundation for Statistical Computing, Vienna, Austria. (2017).

Radon, K., Weber, C., Iversen, M., Danuser, B., Pedersen, S., & Nowak, D. (2001). Exposure assessment and lung function in pig and poultry farmers. *Occupational and Environmental Medicine*, *58*(6), 405-410.

Randall, J. M. (1975). The prediction of airflow patterns in livestock buildings. *Journal of Agricultural Engineering Research*, *20*(2), 199-215.

Randall, J. M., & Battams, V. A. (1979). Stability criteria for airflow patterns in livestock buildings. *Journal of Agricultural Engineering Research*, *24*(4), 361-374.

Renaudeau, D., Kerdoncuff, M., Anais, C., & Gourdine, J. L. (2008). Effect of temperature level on thermal acclimation in Large White growing pigs. *Animal, 2(11)*, 1619-1626.

Riis, A. L., Jensen, T. L., & Pedersen, P. (2010). Reducing odour and ammonia emission by cooling inlet air in a farrowing facility. *XVIIth World Congress of the International Commission of Agricultural and Biosystems Engineering (CIGR)*, Québec City, Canada.

Roache, P. J. (1994). Perspective: a method for uniform reporting of grid refinement studies. *Journal of Fluids Engineering*, *116(3)*, 405-413.

Rom, H. B., & Zhang, G. Q. (2010). Time delay for aerial ammonia concentration measurements in livestock buildings. *Sensors*, *10*(5), 4634-4642.

Romain, A. C., Nicolas, J., Cobut, P., Delva, J., Nicks, B., & Philippe, F. X. (2013). Continuous odour measurement from fattening pig units. *Atmospheric Environment, 77*, 935-942.

Rong, L., & Aarnink, A. J. A. (2019). Development of ammonia mass transfer coefficient models for the atmosphere above two types of the slatted floors in a pig house using computational fluid dynamics. Biosystems Engineering, 183, 13-25.

Rong, L., Bjerg, B., & Zhang, G. (2015). Assessment of modeling slatted floor as porous medium for prediction of ammonia emissions–Scaled pig barns. *Computers and Electronics in Agriculture*, *117*, 234-244.

Rong, L., Nielsen, P. V., & Zhang, G. (2009). Effects of airflow and liquid temperature on ammonia mass transfer above an emission surface: experimental study on emission rate. *Bioresource technology*, *100*(20), 4654-4661.

Rong, L., Nielsen, P. V., & Zhang, G. (2010). Experimental and numerical study on effects of airflow and aqueous ammonium solution temperature on ammonia mass transfer coefficient. *Journal of the Air & Waste Management Association*, 60(4), 419-428.

Rong, L., Nielsen, P. V., Bjerg, B., & Zhang, G. (2016). Summary of best guidelines and validation of CFD modeling in livestock buildings to ensure prediction quality. *Computers and Electronics in Agriculture, 121*, 180-190.

Saha, C. K., Feilberg, A., Zhang, G., & Adamsen, A. P. S. (2011c). Effects of airflow on odorants' emissions in a model pig house—A laboratory study using Proton-Transfer-Reaction Mass Spectrometry (PTR-MS). *Science of the Total Environment*, *410*, 161-171.

Saha, C. K., Wu, W., Zhang, G., & Bjerg, B. (2011b). Assessing effect of wind tunnel sizes on air velocity and concentration boundary layers and on ammonia emission estimation using computational fluid dynamics (CFD). *Computers and electronics in agriculture*, *78*(1), 49-60.

Saha, C. K., Zhang, G., & Ni, J. Q. (2010). Airflow and concentration characterisation and ammonia mass transfer modelling in wind tunnel studies. *Biosystems engineering*, *107*(4), 328-340.

Saha, C. K., Zhang, G., Ni, J. Q., & Ye, Z. (2011a). Similarity criteria for estimating gas emission from scale models. *Biosystems engineering*, *108*(3), 227-236.

Sällvik, K., & Walberg, K. (1984). The effects of air velocity and temperature on the behaviour and growth of pigs. Journal of Agricultural Engineering Research, 30, 305-312.

Santonja, G. G., Georgitzikis, K., Scalet, B. M., Montobbio, P., Roudier, S., Sancho; L. D. (2017). Best Available Techniques (BAT) Reference Document for the Intensive Rearing of Poultry or Pigs; EUR 28674 EN; doi:10.2760/020485.

Sapounas, A. A., Campen, J. B., Smits, M. C. J., & Van Dooren, H. J. C. (2009, July). Simulating the effect of forced pit ventilation on ammonia emission from a naturally ventilated cow house with CFD. In 4th European Conference on Precision Livestock Farming (pp. 81-89).

Schauberger, G., Lim, T. T., Ni, J. Q., Bundy, D. S., Haymore, B. L., Diehl, C. A., & Heber, A. J. (2013). Empirical model of odor emission from deep-pit swine finishing barns to derive a standardized odor emission factor. *Atmospheric environment, 66*, 84-90.

Schauberger, G., Piringer, M., & Petz, E. (2000). Steady-state balance model to calculate the indoor climate of livestock buildings, demonstrated for finishing pigs. *International Journal of Biometeorology*, *43*(4), 154–162.

Scheepens, C. J. M., Hessing, M. J. C., Laarakker, E., Schouten, W. G. P., & Tielen, M. J. M. (1991a). Influences of intermittent daily draught on the behaviour of weaned pigs. *Applied Animal Behaviour Science, 31(1-2)*, 69-82.

Scheepens, C. J. M., Tielen, M. J. M., & Hessing, M. J. C. (1991b). Influence of daily intermittent draught on the health status of weaned pigs. *Livestock Production Science*, *29(2-3)*, 241-254.

Seedorf, J., Hartung, J., Schröder, M., Linkert, K. H., Pedersen, S., Takai, H., ... & Phillips, V. R. (1998). A survey of ventilation rates in livestock buildings in Northern Europe. *Journal of Agricultural Engineering Research*, *70*(1), 39-47.

Seedorf, J., Hartung, J., Schröder, M., Linkert, K. H., Pedersen, S., Takai, H., & Phillips, V. R. (1998). Temperature and moisture conditions in livestock buildings in Northern Europe. *Journal of Agricultural Engineering Research*, *70(1)*, 49-57.

Seo, I. H., Lee, I. B., Moon, O. K., Hong, S. W., Hwang, H. S., Bitog, J. P., & Lee, J. W. (2012). Modelling of internal environmental conditions in a full-scale commercial pig house containing animals. *Biosystems Engineering*, *111*(1), 91-106.

Smith, P., Crabtree, H., & Bird, N. (2009). *Perfecting the pig environment*. Nottingham University Press.

Sommer, S. G., Zhang, G. Q., Bannink, A., Chadwick, D., Misselbrook, T., Harrison, R., Hutchings, N.J., Menzi, H., Monteny, G.J., Ni, J.Q. & Oenema, O. (2006). Algorithms determining ammonia emission from buildings housing cattle and pigs and from manure stores. *Advances in Agronomy*, *89*, 261-335.

Srebric, J., Vukovic, V., He, G., & Yang, X. (2008). CFD boundary conditions for contaminant dispersion, heat transfer and airflow simulations around human occupants in indoor environments. *Building and Environment*, *43(3)*, 294-303.

Stamou, A., & Katsiris, I. (2006). Verification of a CFD model for indoor airflow and heat transfer. *Building and Environment*, *41(9)*, 1171-1181.

Sun, G., Guo, H., & Peterson, J. (2010). Seasonal odor, ammonia, hydrogen sulfide, and carbon dioxide concentrations and emissions from swine grower-finisher rooms. *Journal of the Air & Waste Management Association*, *60*(4), 471-480.

Sun, H., Keener, H. M., Deng, W., & Michel Jr, F. C. (2004). Development and validation of 3-d CFD models to simulate airflow and ammonia distribution in a high-rise™ hog building during summer and winter conditions. *Agricultural Engineering International: CIGR Journal*. *Manuscript BC 04 004.* Vol. VI.

Tan, Z., & Zhang, Y. (2004). A review of effects and control methods of particulate matter in animal indoor environments. *Journal of the Air & Waste Management Association*, *54*(7), 845-854.

Threm, J., Gallmann, E., Pflanz, W., & Jungbluth, T. (2012). Comparison of different air supply and cooling systems in pig fattening houses. *In 2012 IX International Livestock Environment Symposium (ILES IX)* (p. 3). American Society of Agricultural and Biological Engineers.

Tong, X., Hong, S. W., & Zhao, L. (2019). Using CFD simulations to develop an upward airflow displacement ventilation system for manure-belt layer houses to improve the indoor environment. *Biosystems engineering*, *178*, 294-308.

United States Department of Agriculture (USDA) (2019). *Livestock and Poultry: World Markets and Trade. http://www.fas.usda.gov/data/livestock-and-poultry-world-markets-and-trade.*

Vaddella, V. K., Ndegwa, P. M., Ullman, J. L., & Jiang, A. (2013). Mass transfer coefficients of ammonia for liquid dairy manure. Atmospheric Environment, 66, 107-113.

Van Buggenhout, S., Van Brecht, A., Özcan, S. E., Vranken, E., Van Malcot, W., & Berckmans, D. (2009). Influence of sampling positions on accuracy of tracer gas measurements in ventilated spaces. *Biosystems Engineering*, *104*(2), 216-223.

Van der Voorst, P. (2009). Op allerlei manieren frisse lucht bij de dieren. Retrieved from http://www.pigbusiness.nl/huisvesting/kennisdocumenten/113/op-allerlei-manieren-frisse-lucht-bij-de-dieren.

Van Gansbeke, S., Van den Bogaert, T., Vettenburg, N. (2009). Ventilatie en klimaatbeheersing bij varkensstallen.

Van Langenhove, H., & De Bruyn, G. (2001). Development of a procedure to determine odour emissions from animal farming for regulatory purposes in Flanders. *Water Science and Technology, 44(9)*, 205-210.

Van Ransbeeck, N., Van Langenhove, H., & Demeyer, P. (2013). Indoor concentrations and emissions factors of particulate matter, ammonia and greenhouse gases for pig fattening facilities. *Biosystems engineering, 116(4)*, 518-528.

Van Wagenberg A., Bjerg B., & Bot G (2004). Measurement and Simulation of Climatic Conditions in the Animal Occupied Zone in a Door Ventilated Room for Piglets. Agricultural Engineering International: *the CIGR Journal of Scientific Research and Development*. *Manuscript BC 03 020*.

Van Wagenberg, A. V., & de Leeuw, M. T. J. (2003). Measurement of air velocity in animal occupied zones using an ultrasonic anemometer. *Applied engineering in agriculture*, *19*(4), 499.

Van Wagenberg, A. V., & Smolders, M. A. H. H. (2002). Contaminant and heat removal effectiveness of 3 ventilation systems in nursery rooms for pigs. *Transactions of the ASAE, 45(6)*, 1985.

Van Wagenberg, A.V., 2005. Measurement, evaluation and control of the microclimate in rooms for weaned piglets. Ph.D. Thesis, Wageningen University and Applied Research Division of Animal Sciences Group, Lelystad, The Netherlands

VERA. (2018). VERA Test Protocol for Livestock Housing and Management Systems – Version 3:2018-09. Available at: http://www.vera-verification.eu/en/test-protocols/ (accessed Junuary 2019).

Versteeg, H. K., & Malalasekera, W. (2007). *An introduction to computational fluid dynamics: the finite volume method*. Pearson education.

Vlaamse Landmaatschappij, (2019). Lijst van ammoniak-emissiearme stalsystemen (AEA-lijst).https://www.vlm.be/nl/themas/Mestbank/mest/emissiearme%20stallen/Paginas/default.aspx (Assessed August 2019).

Vranken, E. (1999). *Analysis and optimisation of ventilation control in livestock buildings* (Doctoral dissertation, K.U. Leuven).

Vranken, E., Claes, S., & Berckmans, D. (2003). Reduction of ammonia emission from livestock buildings by the optimization of ventilation control settings. *In the proceedings of Air Pollution from Agricultural Operations III*, North Carolina, USA (pp 167-173). ASAE Publication Number 701P1403.

Vranken, E., Claes, S., Hendriks, J., Darius, P., & Berckmans, D. (2004). Intermittent measurements to determine ammonia emissions from livestock buildings. *Biosystems engineering*, *88*(3), 351-358.

Wan, M. P., & Chao, C. Y. (2005). Numerical and experimental study of velocity and temperature characteristics in a ventilated enclosure with underfloor ventilation systems. *Indoor air*, *15(5)*, 342-355.

Wang, X., & Zhang, Y. (2005). Experimental study of effect of ventilation on animal environment in a swine building. In *Livestock Environment VII-7th International Symposium* (pp. 7-12).

Willers, H. C., R. W. Melse, and N. W. M. Ogink. 2003. Concentration of urine from fatteners combined with ammonia removal by scrubbing exhaust air of a pig house. In *Proc. Ninth International Animal, Agricultural and Food Processing Wastes Symposium,* 584-589. Research Triangle Park, North Carolina, 12-15 October.

Wing, S., Horton, R. A., Marshall, S. W., Thu, K., Tajik, M., Schinasi, L., & Schiffman, S. S. (2008). Air pollution and odor in communities near industrial swine operations. *Environmental health perspectives, 116(10)*, 1362.

Wu, W., Zhai, J., Zhang, G., & Nielsen, P. V. (2012). Evaluation of methods for determining air exchange rate in a naturally ventilated dairy cattle building with large openings using computational fluid dynamics (CFD). *Atmospheric Environment, 63*, 179-188.

Yang, Z., Greisen, S. K., Hansen, J. R., Pedersen, N. A., & Jensen, M. R. (2009, August). On the single-zone modeling for optimal climate control of a real-sized livestock stable system. In *2009 International Conference on Mechatronics and Automation* (pp. 3849-3854). IEEE.

Ye, Z., Saha, C. K., Li, B., Tong, G., Wang, C., Zhu, S., & Zhang, G. (2009). Effect of environmental deflector and curtain on air exchange rate in slurry pit in a model pig house. *Biosystems engineering*, *104*(4), 522-533.

Ye, Z., Zhang, G., Li, B., Strøm, J. S., & Dahl, P. J. (2008a). Ammonia emissions affected by airflow in a model pig house: effects of ventilation rate, floor slat opening, and headspace height in a manure storage pit. Transactions of the ASABE, 51(6), 2113-2122.

Ye, Z., Zhang, G., Li, B., Strøm, J. S., Tong, G., & Dahl, P. J. (2008b). Influence of airflow and liquid properties on the mass transfer coefficient of ammonia in aqueous solutions. *Biosystems Engineering*, *100*(3), 422-434.

Ye, Z., Zhang, G., Seo, I. H., Kai, P., Saha, C. K., Wang, C., & Li, B. (2009). Airflow characteristics at the surface of manure in a storage pit affected by ventilation rate, floor slat opening, and headspace height. Biosystems Engineering, 104(1), 97-105.

Ye, Z., Zhu, S., Kai, P., Li, B., Blanes-Vidal, V., Pan, J., ... & Zhang, G. (2011). Key factors driving ammonia emissions from a pig house slurry pit. *Biosystems engineering*, *108*(3), 195-203.

Yin, S., van't Ooster, B., Ogink, N. W., & Koerkamp, P. W. G. (2016). Assessment of porous media instead of slatted floor for modelling the airflow and ammonia emission in the pit headspace. *Computers and Electronics in Agriculture*, *123*, 163-175.

Yu, H., Hou, C. H., & Liao, C. M. (2002). Scale model analysis of opening effectiveness for wind-induced natural ventilation openings. *Biosystems Engineering*, *82*, 199-208.

Zhang, G., & Strøm, J. S. (1999). Jet drop models for control of non-isothermal free jets in a side-wall multi-inlet ventilation system. *Transactions of the ASAE*, *42*(4), 1121.

Zhang, G., B. Bjerg, J. S. Strøm, S. Morsing, P. Kai, G. Tong, and P. Ravn. 2008. Emission effects of three different ventilation control strategies—A scale model study. *Biosystems Engineering*, 100(1): 96-104.

Zhang, G., Bjerg, B., Strøm, J. S., & Kai, P. (2009). Reducing odor emission from pig production buildings by ventilation control. In *Livestock Environment VIII, 31 August–4 September 2008, Iguassu Falls, Brazil* (p. 99). American Society of Agricultural and Biological Engineers.

Zhang, G., Bjerg, B., Strøm, J. S., Morsing, S., Kai, P., Tong, G., & Ravn, P. (2008). Emission effects of three different ventilation control strategies—A scale model study. *Biosystems Engineering*, *100*(1), 96-104.

Zhang, G., Morsing, S., & Strøm, J. S. (1996). Modeling jet drop distances for control of a nonisothermal, flap-adjusted ventilation jet. *Transactions of the ASAE*, *39*(4), 1-1431.

Zhang, K., Zhang, X., Li, S., & Jin, X. (2014). Experimental study on the characteristics of supply air for UFAD system with perforated tiles. *Energy and buildings*, *80*, 1-6.

Zhang, R. H., Day, D. L., Christianson, L. L., & Jepson, W. P. (1994). A computer model for predicting ammonia release rates from swine manure pits. J*ournal of Agricultural Engineering Research, 58(4),* 223-229.

Zhang, R. H., Day, D. L., Christianson, L. L., & Jepson, W. P. (1994). A computer model for predicting ammonia release rates from swine manure pits. Journal of Agricultural Engineering Research, 58(4), 223-229.

Zhang, R., Rumsey, T. R., Fadel, J. G., Arogo, J., Wang, Z., Mansell, G. E., & Xin, H. (2005). A Process-Based Ammonia Emission Model for Confinement Animal Feeding Operations—Model Development. *Agricultural and Biosystems Engineering Conference Proceedings and Presentations*. 219.

Zhang, Y., & Barber, E. M. (1993). Variable ventilation rate control below the heat-deficit temperature in cold-climate livestock buildings. *Transactions of the ASAE*, *36*(5), 1473-1482.

Zhang, Y., & Barber, E. M. (1995). An evaluation of heating and ventilation control strategies for livestock buildings. *Journal of Agricultural Engineering Research*, *60*(4), 217-225.

Zhang, Y., Barber, E. M., & Sokhansanj, S. (1992). A model of the dynamic thermal environment in livestock buildings. *Journal of agricultural engineering research*, *53*, 103-122.

Zhang, Z., Zhang, W., Zhai, Z. J., & Chen, Q. Y. (2007). Evaluation of various turbulence models in predicting airflow and turbulence in enclosed environments by CFD: Part 2—Comparison with experimental data from literature. *Hvac & R Research, 13(6)*, 871-886.

Zhao, Y., Xin, H., Shepherd, T. A., Hayes, M. D., & Stinn, J. P. (2013). Modelling ventilation rate, balance temperature and supplemental heat need in alternative vs. conventional laying-hen housing systems. *Biosystems Engineering*, *115*(3), 311–323.

Zong, C., & Zhang, G. (2014). Numerical modelling of airflow and gas dispersion in the pit headspace via slatted floor: Comparison of two modelling approaches. *Computers and electronics in agriculture*, *109*, 200-211.

Zong, C., Feng, Y., Zhang, G., & Hansen, M. J. (2014). Effects of different air inlets on indoor air quality and ammonia emission from 2 experimental fattening pig rooms with partial pit ventilation system–Summer condition. *Biosystems engineering, 122*, 163-173.

Zong, C., Li, H., & Zhang, G. (2015). Ammonia and greenhouse gas emissions from fattening pig house with two types of partial pit ventilation systems. *Agriculture, Ecosystems & Environment*, *208*, 94-105.

Zong, C., Zhang, G., Feng, Y., & Ni, J. Q. (2014). Carbon dioxide production from a fattening pig building with partial pit ventilation system. *Biosystems engineering*, *126*, 56-68.

Appendix

Assessing the effect of inlet the temperature boundary conditions

To derive an appropriate inlet thermal boundary condition, sensitivity tests were performed with respect to 3 different underfloor air channel (UFAC) inlet temperature boundary conditions in the CFD model. The simulations were performed at ventilation rate of 62 m^3 h^{-1} pig^{-1} (level 3) using the field experiment data in the compartment with the mock-up pigs (section 6.2.2.1). Table 6.1 in the paper presents the boundary conditions used during the test. During the test, all simulation parameters and boundary conditions remained unchanged, except inlet temperature boundary condition in each simulated case. The tested temperature profiles (Table B) were derived from the 4 temperature sensors at cross-section A-A (z = -3.0 m) in Figs. 6.2 and 6.3:

Table B. Coordinates and temperature values of the tested UFAC inlet temperature profile (T_{Prof}) boundary conditions.

x (m)	y (m)	z (m)	Inlet T_{Prof} 1 (°C)	Inlet T_{Prof} 2 (°C)	Inlet T_{Prof} 3 (°C)
0.20	-0.8	-4.5	11.4	10.5	9.6
-0.25	-0.8	-4.5	11.4	10.5	9.9
0.20	-0.5	-4.5	11.4	10.5	11.9
0.20	-0.3	-4.5	11.4	14.1	14.1

T_{Prof} refers to the interpolated temperature profile at the UFAC inlet using the constant interpolation method in ANSYS Fluent from the coordinates and their corresponding temperature in Table 6.2.

(1) Inlet temperature profile 1 (inlet T_{Prof} 1): a uniform inlet temperature boundary condition at the UFAC inlet derived from the average temperature of all the 4 temperature sensors.
(2) Inlet temperature profile 2 (inlet T_{Prof} 2): two uniform average temperatures at the UFAC inlet from the 3 and 1 temperature sensors at the bottom and the top of the heating plate, respectively.
(3) Inlet temperature profile 3 (inlet T_{Prof} 3): an inlet temperature profile derived from the interpolation of the 4 temperature sensors at the UFAC. Figure A compares the effect of the inlet temperature boundary conditions on the temperature profile at the UFAC.

Assessing the effect of inlet turbulence boundary conditions

At the UFAC inlet opening, we applied a uniform turbulence boundary condition in the CFD model. The study initially applied turbulence intensity (Tu) of 5% and a viscosity ratio of 10 for the inlet velocities from 0.1 to 1.0 m s^{-1} corresponding to inlet Reynolds numbers of 6.0×10^3

to 6.0 × 10^4, which is in the range of low to medium turbulence level according to the ANSYS Fluent users' guide. A preliminary comparison of the simulated result with experimental data at this inlet turbulent condition showed the model could not accurately predict the UFAC temperature farther away from the UFAC inlet (Fig. B). This was probably because of the lack of air mixing at the UFAC inlet due to the exclusion of the underground air channel upstream of the UFAC inlet. Subsequently, a hydraulic diameter and turbulence intensity boundary condition was applied, and the turbulence level adjusted from 5 to 20% at a fixed inlet hydraulic diameter of 0.95 m (Table C) to increase the air mixing in the UFAC. These simulations were also performed at ventilation rate of 62 m^3 h^{-1} pig^{-1} (level 3) using the field experiment data in the compartment with the mock-up pigs (section 2.2.1). During the test, all simulation parameters and boundary conditions remained unchanged, except inlet turbulence boundary condition in each simulated case. Table 6.1 presents the boundary conditions applied during the test.

Table C. Tested inlet turbulence boundary conditions.

Inlet parameter	**Inlet Tu 1**	**Inlet Tu 2**	**Inlet Tu 3**	**Inlet Tu 4**
Hydraulic Diameter (m)	-	0.95	0.95	0.95
Turbulence intensity (%)	5	5	10	20
Turbulent viscosity ratio	10	-	-	-

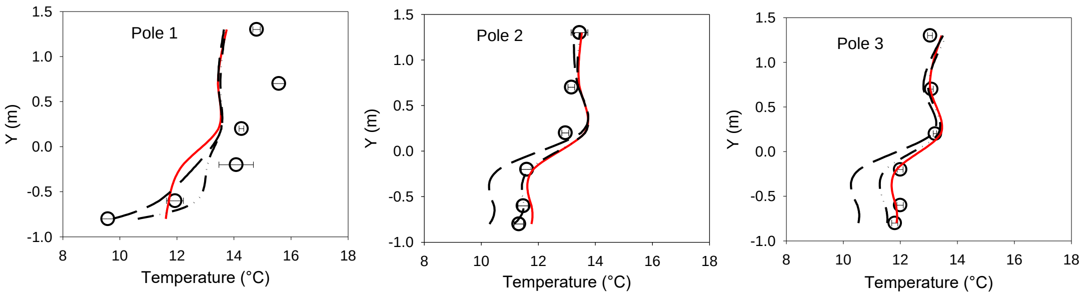

Fig. A. The effect of the different inlet thermal boundary condition on air temperature at the UFAC with (O; error bars are standard deviations): experiment; (——): inlet TP 1; (— —): inlet TP 2; and (—· ·—): inlet TP 3.

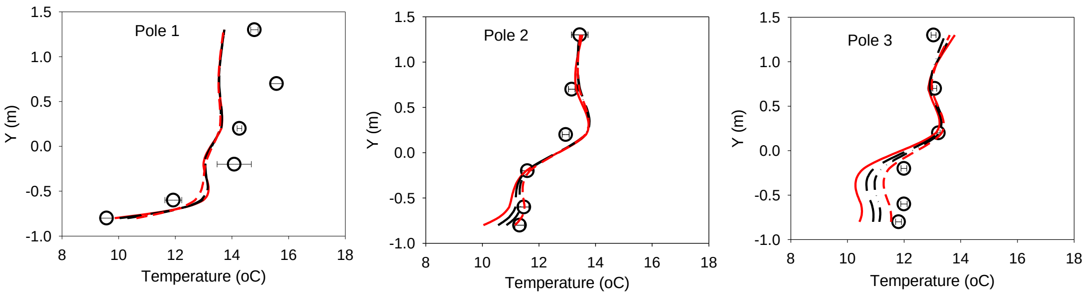

Fig. B. Effect of the inlet turbulence level on the air temperature at the UFAC with (O; error bars are standard deviations): experiment; (——): inlet Tu 1; (— —): inlet Tu 2; (—· ·—): inlet Tu 3 and (— —): inlet Tu 4.

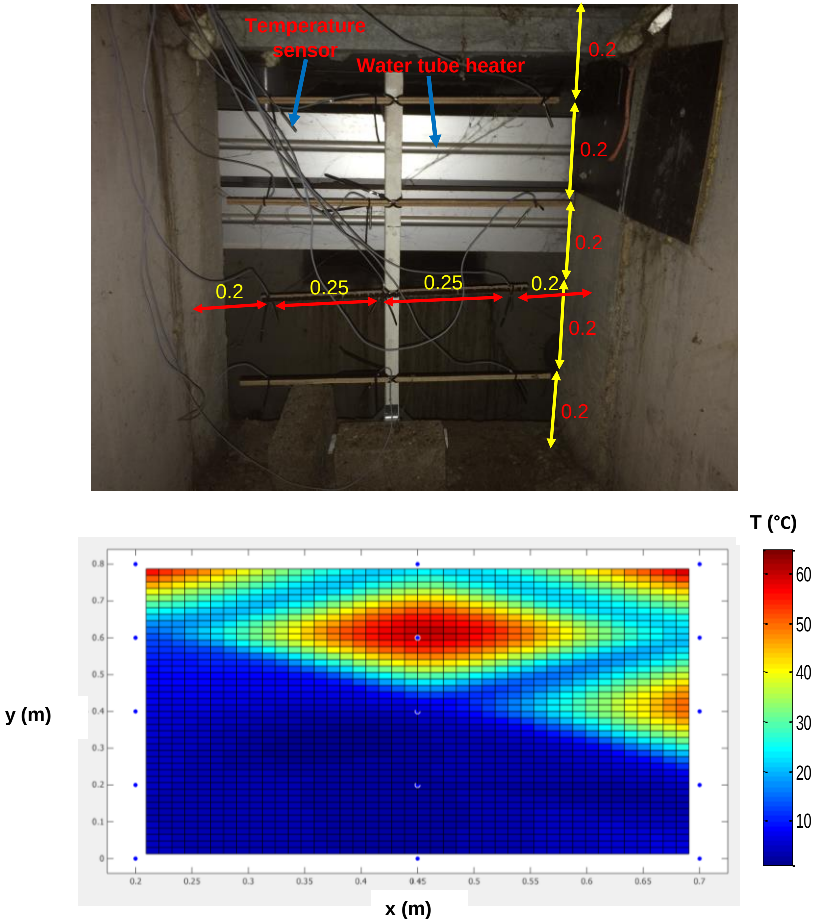

Fig. C. Measurement of air temperature at the inlet of the UFAC (top) experimental set-up with 12 temperature sensors, with (bottom) interpolation of the air temperature at the inlet of the UFAC based on 12 temperature measurement points. The measurement was taken in the compartment with the mock-up pigs at ventilation rate of 27 m^3 h^{-1} pig^{-1}, room and outside temperatures of 19.3 °C and 10.3 °C, respectively.

Curriculum vitae

EDUCATION

April 2015 – Present	Doctoral School of Bioscience Engineering, Ghent University (Belgium)
24 August 2009 – 29 August 2011	MSc. Biosystems Engineering (Environmental Technology option) Aarhus University (Denmark)
18 August 2003 – 09 June 2007	BSc. Agricultural Engineering, Kwame Nkrumah University of Science and Technology (Ghana)

PROFESSIONAL CAREER

January 2020 – Present	Postdoctoral Research Fellow Nord University (Norway)
February 2014 – September 2019	Researcher Flanders Research Institute for Agriculture, Fisheries and Food (ILVO) (Belgium)
September – December 2011	Research Assistant Department of Engineering, Aarhus University (Denmark)
October 2008 – August 2009	Teacher Bongo Senior High Secondary School (Ghana)
October 2007 – August 2008	Teaching Assistant Agricultural Engineering Department, University of Ghana (Ghana)

List of publications

1. **Tabase, R. K.,** Liu, D., & Feilberg, A. (2013). Chemisorption of hydrogen sulphide and methanethiol by light expanded clay aggregates (Leca). *Chemosphere*, 93(7), 1345-1351.

2. **Tabase, R. K.,** Millet, S., Brusselman, E., Ampe, B., Sonck, B., & Demeyer, P. (2018). Effect of ventilation settings on ammonia emission in an experimental pig house equipped with artificial pigs. *Biosystems Engineering*, 176, 125-139.
3. **Tabase, R. K.,** Millet S., Brusselman E., Vangeyte J., Sonck B., & Demeyer P. (2019). Mimicking indoor climate dynamics and ammonia emission in a pig housing compartment using artificial pigs and an automatic urea spraying installation. *Agricultural Engineering International: CIGR Journal*, *21*(1), 40-50.
4. **Tabase, R. K.,** Millet, S., Brusselman, E., Ampe, B., De Cuyper, C., Sonck, B., & Demeyer, P. (2020). Effect of ventilation control settings on ammonia and odour emissions from a pig rearing building. Biosystems Engineering, 192, 215-231.
5. **Tabase, R. K., Van** linden V., Aarnink A. J. A., Bagci, O., De Paepe, M., & Demeyer, P. (2020). CFD simulation of airflows and ammonia emissions in a pig compartment with underfloor air distribution system: Model validation at different ventilation rates. Computers and Electronics in Agriculture, 171, 105297.

CONFERENCES

1. **Tabase, R. K.,** Van linden V., Sonck, B.,, Vierendeels J., & Demeyer P. (2016). Air distribution in an underground air supply channel of a ground channel ventilated pig house. *International Conference on Agricultural Engineering—CIGR (Aarhus):* 26 - 29 June 2016: (Oral presentation).
2. **Tabase, R. K.,** Millet S., Brusselman E., Sonck B., & Demeyer P. (2017). Effect of set-point temperature on ammonia emission in a ground channel ventilated pig house equipped with artificial pigs and automatic Spraying installation. Emission of Gas and *Dust from Livestock Conference (Saint-Malo, France)*: 21 - 24 May 2017: (Poster presentation).
3. **Tabase, R. K.,** Van linden V., & Demeyer P. (2018). Development of a computational fluid dynamics (CFD) based ammonia emission model for a ground channel ventilated pig house. *European Society of Agricultural Engineers—AgEng (Wageningen)*: 08 - 11 July 2018.

OTHER SCIENTIFIC ACTIVITIES

Visiting researcher, COST Action—LivAGE, Wageningen University and Research, Host Scientist: Dr Andre Aarnink

Acknowledgements

My gratitude goes to Flanders Research Institute for Agriculture, Fisheries and Food (ILVO) and Flanders Agency for Innovation and Entrepreneurship (VLAIO), who funded this PhD research. Their interest in sustainable agriculture research gave me the opportunity to pursue my PhD at Ghent University, one of the most prestigious universities in the world. The following people have also contributed to my PhD work: Special thanks to my ILVO and Ghent University PhD promoters, Dr. Peter Demeyer and Prof. Bart Sonck for their expert scientific advice and guidance on ventilation and emission measurement in livestock buildings. By their patience, attention and encouragement, I was able to grow in the same scientific way as they did during this PhD research. I also extend my appreciation to Prof. Michel De Paepe, my co-promotor at Ghent University. I acknowledge the expert advice on CFD provided by the late Prof. Jan Vierendeels, my former promotor, who is dearly missed.

I am thankful to the members of the Examination Board; Prof. Wim Soetaert, Prof. Jan Pieters, Prof. Stefaan De Smet, Prof. Tomas Norton, Dr. Andre Aarnink and Prof. Guoqiang Zhang who thoroughly examined this PhD dissertation. I find your comments very relevant and constructive, these have improved the story in this PhD thesis. Without the assistance of the staff at the Varkenscampus", odour lab, odour panellist and technicians at ILVO, including Dr. Jürgen Vangeyte this PhD work would not have also been possible. Also, my thanks go to Dr. Bart Ampe and Dr. Carolien De Cuype for their statistical assistance. I appreciate Dr. Eva Brusselman and Prof. Sam Millet for their assistance before the experimental start-up of the field measurements and their comments on my manuscripts. Eva also organised the pig farm visits at West Flanders in the first year of this project work. This allowed me to comprehend the pig husbandry conditions in Flanders that was useful throughout my PhD research. I appreciate the comments and suggestions from Dr. Wentao Wu from the Harvard Centre for Green Buildings and Cities, Harvard University, Dr. Veerle Van linden and Dr. Ozer Bagci at ILVO during the CFD model development and the manuscript preparation. Later during my PhD work, Dr. Andre Aarnink hosted me as a visiting researcher at Wageningen University and Research through the aid of the COST-Action project. It was a pleasant stay and your expertise in emission modelling in livestock housing improved my PhD work.

It was great working in the same office with Dr. Gerlinde De Vogeleer and Dr. Philippe Van Overbeke during my PhD—you are great people 😊. Whenever I needed assistance, you helped delightfully, whether it was administrative, technical or language translation. It helped me to settle into ILVO and Belgium. Furthermore, Gerlinde volunteered as a companion driver to teach me how to drive and I really appreciate your efforts. I thank Dr. Se-Woon Hong and

Dr. Luciano Mendes who I shared the same office with during the start of my PhD. I benefited from your CFD advice and tips. Dr. Raphael Ane Atanga also read through my PhD thesis and helped me to improve it. In order not to leave out any person, I would like to thank every person who has contributed to my stay in Belgium, study and the successful completion of this PhD work.

Finally, I would like to express my heartfelt gratitude to my partner, Ingrid Vancoppenolle for her support and love in the last period of my PhD work, which has motivated me. I also appreciate family and friends for their prayers and thought throughout this PhD work. They hoped that one day I would complete this PhD research.

I dedicate this work to my parents Mr. Edward and Mrs. Beatrice Tabase who brought me forth and their continuous sacrifice.